Università degli Studi di Padova
DIPARTIMENTO DI GEOSCIENZE

University of Tasmania
CODES - ARC
Centre of Excellence in Ore Deposits

SCUOLA DI DOTTORATO DI RICERCA IN:
SCIENZE DELLA TERRA
CICLO XXVI

Jurassic magmatism in Patagonia, Mauritania and Mali: Examples of silicic and basaltic Large Igneous Provinces

Direttore della Scuola: Ch.mo Prof. Massimiliano Zattin
Supervisore: Ch.mo Prof. Andrea Marzoli
Co-supervisore: Ch.mo Prof. Vadim Kamenetsky

Dottorando: Lina Maria Serrano Duran

ABSTRACT

At the end of the Triassic and during Jurassic times, the Central Atlantic Magmatic Province (CAMP) with a dominant mafic composition, and the mainly felsic Patagonian Province (PA) were formed in the context of Pangea break-up. CAMP basaltic to basaltic-andesitic dykes and sills from Hank and Hodh, in Mauritania, and Kaarta, in Mali, were emplaced at ca. 197 Ma yielding a signature defined by low to high TiO_2-values (0.39 - 2.29 wt.%), Nb-Ta troughs, Pb spikes and enriched Nd-Sr-Pb compositions ($^{143}Nd/^{144}Nd_{201Ma}$: 0.51224 - 0.51241, $^{87}Sr/^{86}Sr_{201Ma}$: 0.70572 - 0.70795, $^{207}Pb/^{204}Pb_{201Ma}$: 15.61 – 15.68 $^{208}Pb/^{204}Pb_{201Ma}$: 38.44 – 38.07 and $^{206}Pb/^{204}Pb_{201Ma}$: 18.11 – 18.48). Nb/U ratios (= 12 – 15), tracers of recycled material, combined with enriched isotopic signatures suggest the contribution of continental crust in the origin of these magmas. Differences in the ratios of La/Yb of the whole set suggest the existence of an enriched group in Kaarta (La/Yb_N>4.3) coupled to increasing ratios of Nb/Zr and Th/Y, probably reflecting lower degrees of partial melting in these rocks. Geochemical compositions revealed in this region indicate a strong affinity to the Taoudenni and Marocco CAMP rocks. As a first approach, a possible distribution of the geochemical signatures in regional districts is here suggested, but should be explored by further studies.

A thick sequence of Jurassic magmatic rocks of bimodal composition represents the volcanism of the Patagonia Province (PA). It consists of rhyolitic lava flows and ignimbrites of the Marifil (~189-177 Ma) and Chon Aike (~170 – 153 Ma) Formations (Fm), with a minor andesitic component represented by the Bajo Pobre (BP) (~166 – 154 Ma), Cañadón Asfalto (~179 – 176 Ma) and Lonco Trapial Fm, which in total record a period of magmatic activity of at least 38 Ma. New U-Pb ages on zircons for the Marifil Fm confirm that the first felsic pulse partially coincided with the Karoo-Ferrar magmatic event (~184-174Ma). However, observed differences in the life span of the two Provinces (Karoo 10 Ma, PA: 38Ma) and the geochemical contrast of their products (PA: intermediate-felsic, mainly, Karoo: mafic, mainly) argue against a genetic relation between the two provinces, and thus with a common mantle plume origin. Mafic to intermediate Jurassic volcanism represented by the Cañadon Asfalto (CA) and Bajo Pobre Fm are synchronous to the felsic PA events and display the closest evidence of little evolved mantle-derived melts of the Province. Analysis of Cr-spinel inclusions in Opx-rich rocks with

occasional anhedral olivine crystals, show compositions (Mg# 62 - 36; Cr# 46 - 32) in the most primitive Cr-spinel grains, which in terms of Al_2O_3 (22 – 31 wt.%) and TiO_2 (1.3 – 1.3 wt.%) are similar to Cr-spinel from MORBs. Geochemical evidences of the whole set of PA indicate a signature typical of arc magmatism characterized by calc-alkaline affinity, Nb-Ta troughs, LILE enrichment and peraluminous character. Particularly, a group of mafic rocks display high Al_2O_3 (>16 wt.%) accompanied by high Sr (>400ppm), absence of Eu anomaly, high Sr/Y (86-30) and Gd/Yb (3-1.8) which resemble adakitic magma compositions.

Geocheochronological evidences strongly suggest that continuous processes should have ruled the origin of PA more than by sporadic events, whereas geochemical data imply the possible contribution of the oceanic subducted crust and continental material in the production of large amounts of silicic magma. Here we propose an alternative model in which the origin of the PA could be the result of a hybrid tectonic setting derived from the subduction of the young and hot Phoenix plate coupled with extensional regime and continental rift formation caused by the break up of Gondwana.

RIASSUNTO

Alla fine del Triassico e durante il Giurassico si sono formate le grandi province magmatiche (LIP) della Central Atlantic Magmatic Province (CAMP) e della Patagonia (PA) contemporanee con la rottura della Pangea. Dichi e sills di composizione basaltica e basaltica-andesitica d'età e composizione affine alla CAMP, sono stati riportati nelle regioni di Hank e Hodh, in Mauritania, e di Kaarta in Mali, che sono oggetto della prima parte di questa tesi. I dati geochimici indicano che i campioni sono caratterizzati da variabili contenuti di TiO_2 (0.39 - 2.29 wt.%) e da anomalie negative di Nb-Ta e anomalie positive di Pb, accompagnati da una firma arricchita negli isotopi di Nd-Sr-Pb ($^{143}Nd/^{144}Nd_{201Ma}$: 0.51224 - 0.51241, $^{87}Sr/^{86}Sr_{201Ma}$: 0.70572 - 0.70795, $^{207}Pb/^{204}Pb_{201Ma}$: 15.61 – 15.68 $^{208}Pb/^{204}Pb_{201Ma}$: 38.44 – 38.07 e $^{206}Pb/^{204}Pb_{201Ma}$: 18.11 – 18.48). I bassi rapporti di Nb/U (= 12 – 15) sono indicatori dell'apporto di materiale crostale, possibilmente riciclato. Questi valori di Nb/U suggeriscono, insieme alle composizioni isotopiche arricchite, un contributo della crosta continentale nella origine dei magmi CAMP in Mauritania e Mali. Variazioni nei rapporti di La/Yb mostrano l'esistenza di un gruppo arricchito tra le rocce di Kaarta (La/Yb_N> 4.3). Questa osservazione è anche supportata dalle correlazione positive con Nb/Zr e Th/Y e probabilmente riflette minori gradi di fusione parziale del mantello. Le composizione geochimiche osservate in Hank, Hodh e Kaarta, mostrano una forte affinità con le rocce intrusive del bacino di Taoudenni e le colate CAMP del Marocco. La correlazione fra queste regioni, fa pensare a una possibile distribuzione geografica oppure alla presenza di domini geochimici all'interno della CAMP. Comunque, quest'osservazione è basata su una stima qualitativa e per verificarla son necessari ulteriori studi.

Il vulcanismo della Provincia è rappresentato da un'importante sequenza di età Giurassica ed è a composizione bimodale. Comprende infatti lave e ignimbriti riolitiche denominate come Formazione Marifil (~189-177 Ma) e Chon Aike (~170 – 153 Ma). Altre formazioni meno voluminose ma non meno importanti sono rappresentate dall'andesite della Formazione Bajo Pobre (BP) (~166 – 154 Ma), e daii basalti di Cañadón Asfalto (~179 – 176 Ma) e Lonco Trapial. L'attività magmatica registrata per questa Provincia dura al meno per 38 Ma. Nuove datazioni U-Pb ottenute in questo progetto, confermano l'età delle rioliti di Marifil, che rappresentano quindi l'attività più antica della Provincia, comparabile

solo parzialmente con le età conosciute per la LIP del Karoo (~184 – 174 Ma**)**. Le differenze geochimiche e di durata fra queste due LIP (Karoo: ca. 10 Ma e un magmatismo mafico, PA: 38 Ma e un magmatismo dominante acido) non appoggiano l'ipotesi d'un origine comune eventualmente da un mantle-plume unico. Lo studio del vulcanismo mafico – intermedio, rappresentato dalle Formazione Cañadon Asfalto (CA) e Bajo Pobre (BP), è stato sviluppato in questa tesi con l'obiettivo di conoscere le caratteristiche dei magmi meno evoluti che potrebbero portare informazioni sull'ambiente tettonico in cui si è formata la provincia. Con questo fine sono stati realizzati analisi di cromiti incluse in cristali di ortopirosseno e olivina. Le composizioni trovate nei cristali più primitivi (Mg# 62 – 36 e Cr# 46 – 32) di queste formazioni sono quasi identiche anche se sono geograficamente distanti. Il loro contenuto di Al_2O_3 (22 – 31 wt.%) e TiO_2 (1.3 – 1.3 wt.%) è simile alla composizione di Cr-spinelli nei MORB. I dati geochimici in queste rocce, evidenziano una firma d'arco magmatico caratterizzata da una composizione calco-alcalina, anomalie negative di Nb-Ta, arricchimento di LILE e un'affinità peraluminosa. In particolare, alcune rocce mafiche mostrano alti valori di Al_2O_3 (>16 wt.%) e di Sr (>400ppm), assenza dell'anomalia di Eu e alti rapporti di Sr/Y (86-30) e Gd/Yb (3 - 1.8) comparabili alle composizione di magmi adakitici.

La continua attività magmatica registrata dalla PA suggerisce che l'origine di queste rocce sia stato relazionata a processi costanti per almeno 38 Ma, più che ad eventi sporadici e di corta durata. Le evidenze geochimiche qui sposte suggeriscono il contributo di crosta oceanica e materiale continentale nell'origine di questa LIP. Perciò si propone un modello alternativo per l'origine della PA chesarebbe il risultato di un ambiente tettonico ibrido tra la subduzione di una placca giovane e calda che fonde (la placca Pheonix) e un regime distensivo relazionato alla disgregazione della Gondwana.

Index

INTRODUCTION

Large Igneous Provinces and continental break-up

Large Igneous Provinces or LIPs, represent exceptionally high volumes of magmatic rocks formed in short periods of the Earth history. The term, initially proposed by Coffin and Eldholm (1992) described the emplacements of predominantly mafic (Mg-Fe rich) extrusive and intrusive rocks whose origins lie in processes other than *normal* seafloor spreading. However, later works have recognized a more varied character and included as integral parts of the LIPs different compositions including substantial felsic components (Bryan et al., 2002; Bryan, 2007; Sheth, 2007). In a revisited definition, Bryan and Ernst (2008) described the LIPs as "magmatic provinces with areal extents >0.1 Mkm^2, igneous volumes >0.1 Mkm^3 and maximum lifespans of ~50 Ma that have *intraplate* tectonic settings or geochemical affinities, and are characterized by igneous pulse(s) of short duration (~1–5 Ma), during which a large proportion (>75%) of the total igneous volume has been emplaced." Although the new definition is more precise defining volume, origin or length of the LIPs, many questions still remain about the tectonic setting involved in the LIPs origin.

Based on the thought that anomalously high magma production rates represent major mantle melting processes caused by other than plate boundary processes (ie: subduction or seafloor spreading), the intraplate magmatism ascribed to the LIPs has been considered as a predictable consequence of mantle plumes. In spite of this, multiple models have contemplated alternative hypothesis in which the intraplate character of the LIPs is revisited and the mantle plume origin is unnecessary. Some of them included decompression melting in a rift setting (White and McKenzie, 1989, 1995), slab breakoff, delamination and back-arc extension (Carlson and Hart, 1987; Rivers and Corrigan 2000; Long et al., 2012), convection (Anderson, 1996, 1998; King and Anderson, 1998) or meteorite impact as triggering mechanisms of melting (Jones et al., 2002; Ingle and Coffin, 2004; Hagstrum, 2005).

Clearly, deciphering the tectonic setting in which the LIPs were formed is a matter of great debate in the literature, but also an opportunity to contribute with new data to understand its influence in the production of large volumes of magma.

During the Late Triassic–Early Jurassic three major continental LIPs were formed: 1) Tholeiitic basaltic magmatism of the Central Magmatic Atlantic Province (CAMP), (10 x 10^6 km^2) spanning only a few million years, with peak activity at ca. 201 Ma (Marzoli et al., 2011); 2) Southern African Karoo basalts (2.5 x $10^6 km^3$), Antarctic Ferrar gabbro and Kirkpatrick basalts (0.5 x 106 km^3), emplaced between ca. 184 and 174 Ma and peak activity at ca. 184-179 Ma (Storey & Kyle, 1997; Riley & Knight, 2001; Jourdan et al., 2007, 2005, 2004); and (3) the silicic magmatic province (2.35 x 10^5 km^3) of South America and the Antarctic Peninsula, formed between ca. 189 and 151 Ma ago (Pankhurst and Rapela, 1995; Feraud et al., 1999.; Riley et al., 2001). Outburst of the three Provinces occurred during the break-up of the Pangea supercontinent (fig. 1) and coincide with two major mass extinction events at ca. 201Ma (end-Triassic; Tanner et al., 2004; Marzoli et al., 2004) and ca. 183 Ma (Pliensbachian-Toarcian; Aberhan and Fursich, 2000).

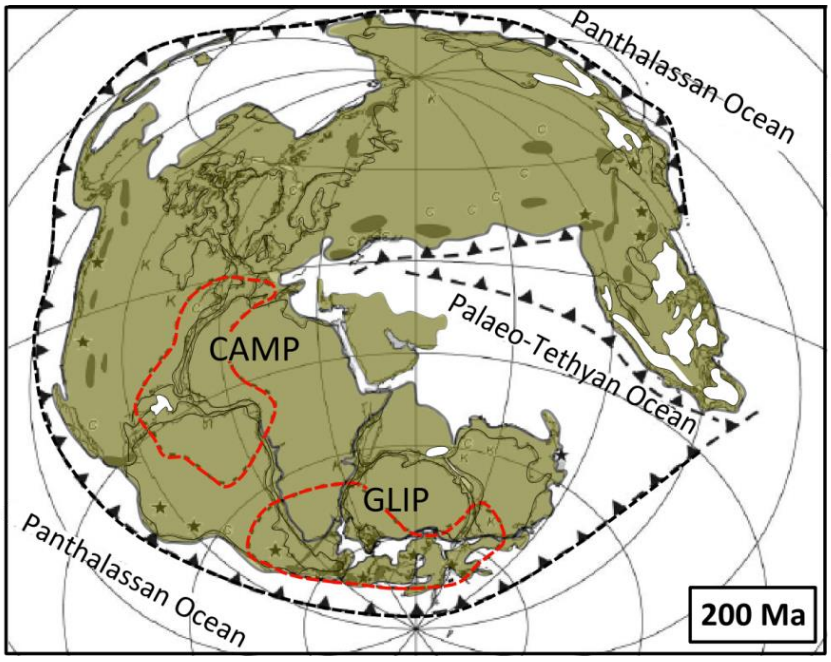

Figure 1. Plate tectonic reconstruction for Pangea in Early Jurassic times, redrawn after Vaughan and Storey (2007). Dashed lines indicate the areas where Large Igneous Provinces occurred. Central Atlantic Magmatic Province (CAMP) area after Marzoli et al. (1999) and **Bertrand** et al. (2013). Gondwana break-up magmatism (Gondwana Large Igneous Province; GLIP) area after Storey & Kyle (1997) and Pankhurst et al. (2000). Subduction zones modified after Metcalfe (1996).

In this research, two examples of basaltic and felsic Large Igneous Provinces were considered as representative of the great heterogeneity that comprise the LIPs: 1) Mafic dykes and sills part of the Central Atlantic Magmatic Province (CAMP), from the regions of Hank and Hodh in Mauritania and

Kaarta in Mali, and 2) the mainly silicic Patagonia Province in Argentina. Despite the fact that the two LIPs were formed in the frame of continental break up, they display clear differences in terms of duration and compositions. Their study gives insights into the petrogenetic aspects and the triggering role of the tectonic setting in the origin of their magmas.

Accordingly, this thesis was divided in two parts consistent with the two studied LIPs:

Part I: we report new geochemical data (major and trace elements, Sr, Nd, Pb isotopes) and geochronological evidence ($^{40}Ar/^{39}Ar$ dating) of the mafic intrusive bodies from Mauritania and Mali with the aim of characterizing these rocks and their comparison with different CAMP locations.

Part II: Include petrographic analysis, mineral chemistry, geochemistry of major and trace elements as well as radio-isotopic dating (LA-zircon U/Pb dating) of the mafic and felsic rocks from the Patagonia Province in order to unravel the tectonic setting and its role in the petrogenesis of this Province.

The results from this project contribute to portray basaltic and silicic Large Igneous Provinces and understand the relation between magmatic processes and tectonic settings in the origin of the LIPs.

PART I: Dykes and Sills from Hank, Hodh and Kaarta

1. Earlier Studies

1.1 The Central Atlantic Magmatic Province

Composed by tholeiitic basaltic and basaltic-andesitic dykes, sills and lava flows, the Central Atlantic Magmatic Province (CAMP) extends up to 7 x 10^6 km^2 along West-Africa, eastern North America, north eastern South America and South western Europe (Marzoli et al., 1999). The widespread activity recorded by the CAMP span a brief magmatic event with the main peak of activity at 201 Ma (Marzoli et al., 2011). Such episode coincides with the Triassic – Jurassic (Tr-J) boundary and is associated with the breakup of Pangea and the precursory stages of the Central Atlantic opening (Marzoli et al., 1999., Marzoli et al., 2004).

In a general way, most of the CAMP products are low in Ti (TiO_2< 2.0 wt.%), show negative mantle normalized Nb anomalies (relative to K and La), and moderate to strong enriched rare earth elements (REE) patterns (Marzoli et al., 2004). In terms of the Ti content (TiO_2wt%), three groups can be recognized in the CAMP. A first one with low Ti O_2 (0.6 – 0.9 wt.%), high MgO (7 - 14 wt.%) and low alkalis, present in the Southeastern U.S.A. A moderate-Ti type (0.9 -1.4 wt.%) common in northeastern North America (Greenough and Dostal., 1992; Merle et al., 2013; Callegaro et al., 2013) Brazil (Fodor et al., 1990; Marzoli et al., 1999), Iberia (Caroff et al., 1995; Jourdan et al., 2003), Guinea and much of West Africa (Bertrand, 1991; Bertrand and Villeneuve, 1989). A third group with high-Ti (1.6 - 3 wt.%) and high alkalis, is only documented in single localities of Northern Brazil, French Guiana, Surinam, and Liberia (Dupuy et al., 1988; De Min et al., 2003; Merle et al., 2011; Nomade et al., 2003). Low Ti tholeiites record an enriched isotopic signature while high Ti ones a more restricted and depleted composition (Alibert, 1985; Dupuy et al., 1988; Greenough et al., 1989; Mauche et al., 1989; Heatherington and Mueller., 1991; De Min et al., 2003; Jourdan et al., 2003; Deckart et al., 2005; Verati et al., 2005; Merle et al., 2011, 2014; Callegaro et al., 2013, 2014; Bertrand et al., 2014). Despite several geodynamic models attribute the magmatism of the CAMP to a large mantle plume (eg: May, 1971; De Boer and Snider, 1979; Hill, 1991; Wilson, 1997), a (methasomatized) lithospheric origin has been alternatively proposed (eg., Pegram, 1990; Heatherington and Mueller, 1999,

McHone, 2000) and a limited influence of a mantle plume, which maybe acted only as a heat supplier triggering the volcanism of the CAMP (Cebria et al., 2003; Merle et al., 2011).

The age of the CAMP has been constrained by multiple radio-isotopic ^{40}Ar-^{39}Ar dating on samples from central Brazil, French Guyana, Carolinas and Newark basins, Morocco, West Africa, France and Portugal pointing out a period of magmatic activity between ca. 190 Ma and ca. 203 Ma.(eg: Deckart et al., 1997; Marzoli et al., 1999; Hames et al., 2000; Knight et al., 2004; Marzoli et al., 2004; Verati et al., 2005, 2007; Nomade et al., 2007; Jourdan et al., 2009; Marzoli et al., 2011; Merle et al., 2011). The entire set of available ^{40}Ar-^{39}Ar ages has been recalculated by Marzoli et al (2011) after Renne et al., 2010) , defining the main peak of CAMP volcanism at c. 201.5 Ma and addressing a relation with the climatic changes and biotic disruption that define the T-J boundary (U/Pb: 201.58 ± 0.17 Ma; Schaltegger et al., 2008; 201.31 ± 0.43 Ma, Schoene et al., 2010).

1.2 Dykes and sills of West Africa

Extrusive basalts of CAMP are found in the circum-Atlantic region and as far as the central Brazil (Marzoli et al., 1999) and subandean area in southern Bolivia (Bertrand et al., 2013). They were emplaced in fault bond basins and widespread dykes which fed fissure eruptions and evidence the Pangean tectonic events during the Early Mesozoic (Olsen, 1997). A much larger flood basalt province that has been mostly removed by erosion (Rampino and Stothers, 1988). is documented by enormous dykes swarms along eastern North America, northern South America, West Africa, SW Europe (Fig. 2) (Bertrand, 1991; McHone, 1996; Marzoli et al., 1999; McHone, 2000; Marzoli et al., 2004; Verati et al., 2005; Chabou et al., 2010).

In West Africa, numerous dykes and sills are distributed as large accumulations of tubular magma piles of fissural origin intruding different levels of Precambrian and Paleozoic sedimentary rocks (Bertrand, 1991). Typically, CAMP dykes do no show a radial pattern and their emplacement is mainly controlled by inherited pre-existing crustal structures with multiple orientation (Bertrand, 1991, McHone, 2000; Verati et al., 2005; Beutel, 2009).

A few major dykes of more than 100 km length (Ksi-Ksou in Algeria and Foum-Zguid in Morocco) are present in the Northern part of the continental margin of Africa (Bertrand, 1991; Deckart et al., 1996). In contrast, several swarms of generally shorter dykes with variable thickness (5 to 300 m) form dense networks Southward, as those from the Taoudenni basin in Northern Mali (Verati et al., 2005), Regurbat in Mauritania and Western Senegal (Bertrand, 1991).

Similar to the dykes, Sills also are highly variable in thickness and surface. The most important are tabular and are widespread in Guinea, Southwest Mali (Diallo et al., 1976; Dars, 1961) or in South East Mauritania (Hodh area). The Kaarta sill, at the South West of Mali, is one of the best exposed with a surface of over 7000 km^2 (Rossi, 1982; Bertrand and Coffrant, 1986). Some others exhibit numerous secondary ramifications or are cut by associated dyke swarms. Several of these bodies are dyke-like elongated, such as Touirist and Azlaf sills in the Hank region in Mauritania (Villemur, 1967) and the dolerite sills and dykes of Tindouf, Reggane, in the Hank basins (Chabou et al., 2010).

In addition to the sills, some layered complexes are also documented as those in Freetown in Sierra Leona and Kokoulima in Guinea (Bertrand, 1991). Exceptionally, mafic and ultramafic intrusive cumulitic bodies from the Fouta Djalon sills and the Kakoulima laccolith in Guinea are also documented (eg., Deckart et al., 2005).

Sills and dykes from the North West Africa have been described as dolerites and microdolerites of uniform textural and mineralogical features along all over the area in which they occur (Bertrand, 1991; Youbi et al., 2011). Compositionally, West African sills and dykes are SiO_2-oversaturated quartz normative basaltic to basaltic andesitic tholeiites. In general they have been described as high SiO_2, low TiO_2, except for the Ti-rich basalts from Liberia (eg., Dupuy et al., 1988). Comparable with the secular depletion observed by Marzoli et al. (2004) on lava piles from Moroccan basalts, Bertrand (1983) suggested that in northern Mali, two generations of dykes are suspected to correspond to high and low La/Yb_N (normalized to chondrite) types.

The age of these rocks has been defined based on $^{40}Ar/^{39}Ar$ radio-isotopic ages on mafic intrusive rocks from Mauritania that also reflect CAMP magmatism (Usui et al., 2010; Callegaro, pers. comm., 2011). Recalculated $^{40}Ar/^{39}Ar$ data by Marzoli et al (2011) (after Renne, 2010), show ages of 197.5 ±

1.9 Ma to 204.6 ± 2.1 Ma for the dykes and sills of the Taoudenni basin (Verati et al, 2005) comparable to those obtained on Guinea sills (192.3 ± 1.2 Ma, 203.5 ± 0.4 Ma and 197.8 ± 1.0; Deckart et al., 1997).

1.3 Geology of Hank-Hodh-Kaarta

The Hank basin, located in the middle part of the West African craton, In Northern Mali, Maurtiania, and South West Algeria, is considered an extension of the Taoudenni basin in Mali, about 1000 km from the western African margin (fig. 2). The basement, composed by Paleoproterozoic rocks (2.21-2.07 Ga) of the Yetti-Eglab massif, in the Reguibat shield (Peucat et al., 2005) is covered by the Neoproterozoic to Carboniferous sedimentary sequences and intruded by a dense and complex mafic dyke swarm and related sills. Most of such intrusions were injected in sandstones and claystones forming raised portions which are covered by Quaternary deposits (Girard, 1984; Verati et al., 2005; Chabou et al., 2010).

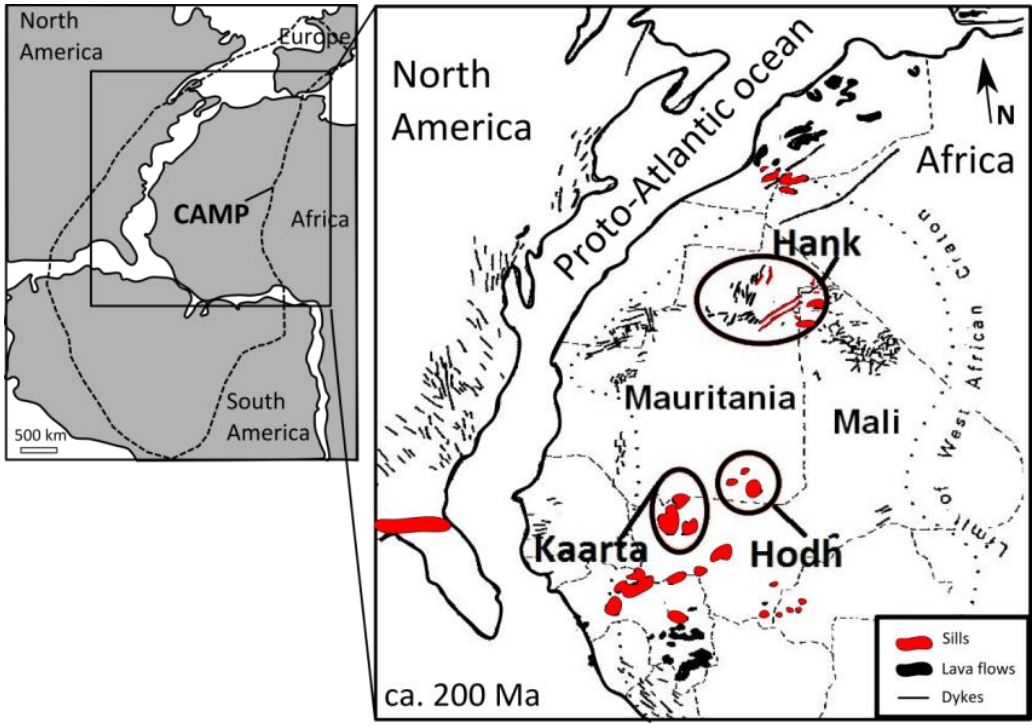

Figure 2. Location of dykes and sills of Hank, Hodh and Kaarta. Modified from Bertrand et al (1991) and Marzoli et al (2011).

Hank dykes intrude in NS, NW-SE and E-W preferential planes, being most of them thick bodies of more than 20m thickness, except for those NW-SE oriented which do not exceed 3 m thickness. In general, all preferred directions coincide with the main trends of dykes from the Taoudenni Basin (Bertrand, 1991; Verati et al., 2005). Described as dolerites and microdolerites, these bodies have been characterized as consisting of calcic plagioclase, augite, pigeonite and minor amounts of titanomagnetite with locally common microphenocrysts of altered olivine resembling the typical paragenesis of the CAMP tholeiites in West Africa (Bertrand (1991) and Chabou et al., 2010).

Available geochemical data for this region have shown that Hank rocks are quartz normative tholeiitic basalts with silica content ranging from 50.9 wt.% to 51.9 wt.%, high MgO (7.25-8.25 wt.%) and low TiO_2 (1-1.1 wt.%). Samples are also slightly enriched in LILE and LREE relative to HREE and HFSE, and display a negative Nb anomaly and a $(La/Yb)_N$ (normalized to chondrite) ratio of about 2.18. Their compositional range is similar to that of other low-Ti CAMP tholeiites, in particular to those from Morocco and Ksour Mountains (Saharan Atlas, Algeria) and Taoudenni dyke swarm (Mali) (Bertrand, 1991). One Ar-Ar weighted mean age of 197.1 ± 0.6 Ma (Chabou et al., 2010) is available for the Hank basin in Algeria. This date is also consistent with the Ar-Ar ages obtained on the Low-Ti group of the Taoudenni basin which range from 197.5 ± 1.9 Ma to 204 ± 2.1 Ma (Verati et al., 2005).

Both sills and dykes are also present in the region of Hodh, South East Mauritania. They intrude Superior Nerman Formation and consist of N-S dykes of variable size which vary from 3 to 25 m length.

Sills from the Hodh basin, in South East Mauritania, as well the Kaarta sill, exposed over more than 7000 km^2 in South West Mali (fig. 2), have been barely studied. A few petrographical and chemical analyses made by Bertrand (1991) indicate a great diversity of textures as a function of cooling history on these rocks. Microdolerites (grain size <1 mm) with microporphyritic texture appear at the margins of the intrusive bodies, while intergranular and ophitic ones are more common through the center and the inner parts. Gabbro dolerites, are also recognized but only at the core of thick dykes. The mineral associations consist of ± olivine, plagioclase, clinopyroxene, opaques, micropegmatite and apatite. Microphenocrysts of olivine (Fo_{78}-Fo_{75}) in Kaarta sill, are exceptionally documented. The short

available data from these regions, suggest compositions akin to those described for the Hank dykes. No radio-isotopic ages have been performed for none of these bodies.

2. Petrography

A collection of 71 samples, consisting of 26 rocks from Hank, 16 from Hodh and 28 from Kaarta, was considered in this study. The samples were provided by Professor Herve Bertrand thanks to an academic collaboration.

Samples from the three locations resemble the petrographic characteristics described for the West African tholeiites (Bertrand, 1991). They display typical features of hypoabyssal intrusive bodies that do not vary from one to the other region. They are typically characterized by a porphyritic texture with an intersertal matrix defined by fine acicular plagioclase intergrowth with allotriomorphic clinopyroxene and occasionally devitrified glass (palagonite). Pilotaxitic groundmass is also common defining a flux texture with a poor orientation of the phenocrysts. Glomeroporfiric texture is common and occur as clusters of idiomorphic phenocrysts of plagioclase and clinopyroxene (augite) seated in microfelsitic or brownish glassy matrix (fig. 3c). Despite the predominance of the porfidic textures the occurrence of samples with phaneritic textures is also common, especially in Kaarta. They consist of holocrystalline, hipidiomorphic-granular textured rocks of fine (0.8 – 1 mm) to medium grain size (1-2mm) composed of plagioclase, and clinopyroxene. In particular, some of them present phenocrysts of pyroxenes enclosing euhedral laths of plagioclase defining an ophitic texture (fig. 3a). The inverse assemblage is, also common even in the same samples, defining subofitic textures (Fig. 3b). Ondulatory extinction in both pyroxenes and plagioclase is also common. It is remarkable that all samples are olivine-free. Fine and acicular apatite embedded in the groundmass is frequent as an accessory phase in all samples. The alteration is in general moderate and scarce, mainly affecting the matrix. The most frequent secondary phases are sericite and chlorite.

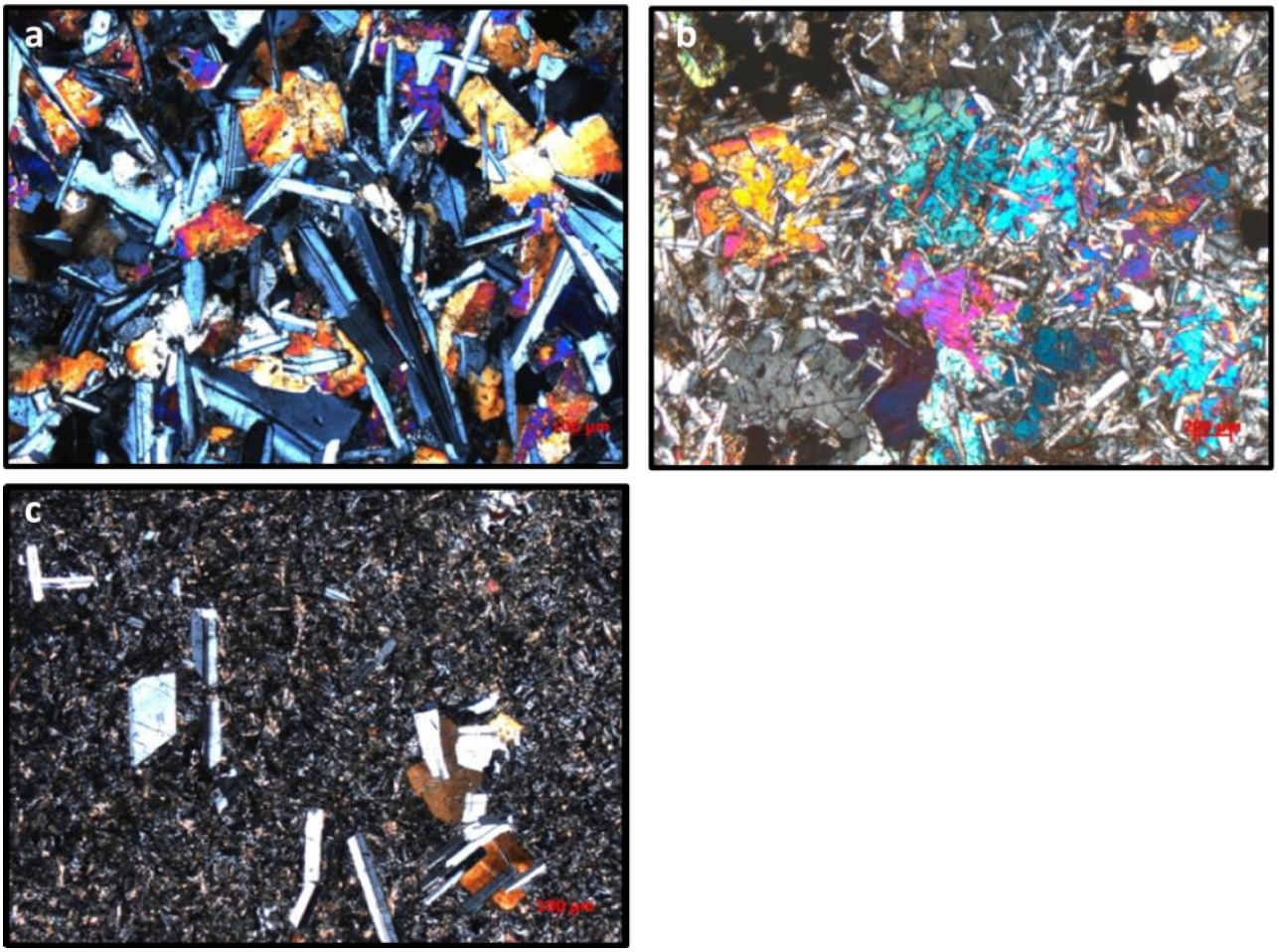

Figure 3. Petrographic features of Hank, Hodh and Kaarta rocks. (a) Subophitic texture in Kaarta (MO 8) , (b) ophitic arrangement in Hodh (HD 44) and (c) glomeroporphiric texture in Hank (HA 52).

3. Geochronology

Furnace step heating ^{40}Ar-^{39}Ar dating was performed on plagioclase separates at the Curtin University, Perth, Australia. In order to achieve high quality data, three samples were prepared according with rigorous proceedings. Fractions were prepared after crushing with a press and geologic hammer, washing with de-ionized water and splitting the phases using the magnetic separator Frantz at the University of Padova. Hand picking of pure crystals of plagioclase was completed at the University of Bonn during a research stay.

Sample MO 3, from Kaarta, yielded a saddle shaped age spectrum with increasing ages at low and high temperature steps, producing an apparent old age of 228.44 ± 1.36 Ma (fig xa). The excess argon, suggested from these features, cannot be explained by impurity or alteration of plagioclase (cf. the observed constant Ca/K ratio, fig 4) but by slow cooling in old basement (Deckart et al., 1997). Four concordant age steps at intermediate temperatures (38.9% of total ^{39}Ar released), define a range between 197.39 ± 1.79 and 193.00 ± 2.87 Ma, considered the most representative age estimate for this rock.

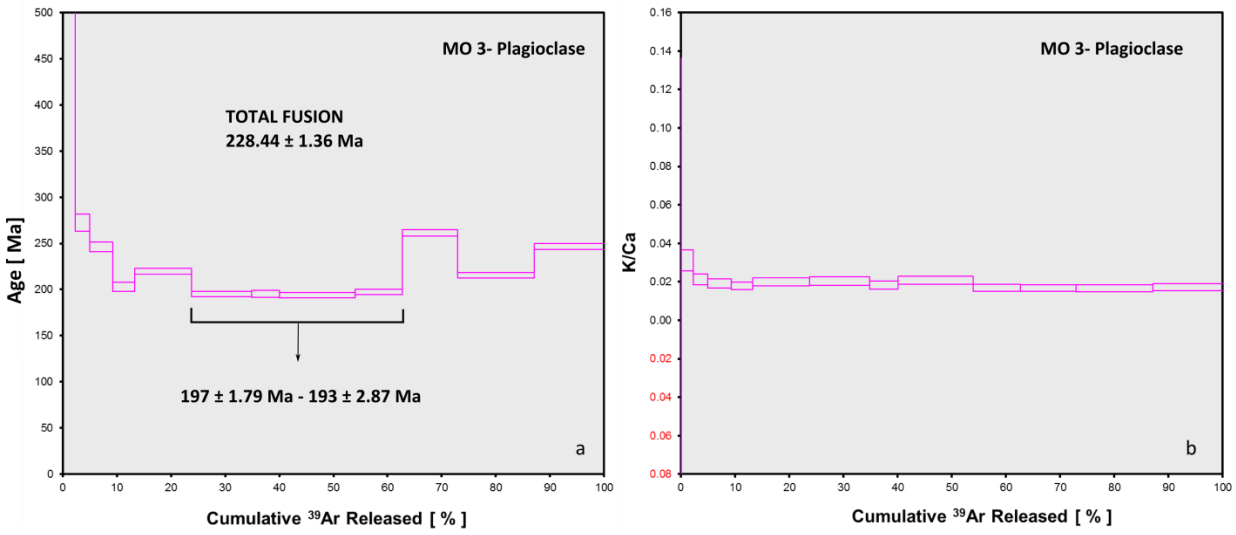

Figure 4. Apparent $^{40}Ar/^{39}Ar$ age and Ca/K (calculated from $^{37}Ar/^{39}Ar$) spectra of the plagioclase separates versus the cumulative percentage of ^{39}Ar released. Errors are quoted as 2σ.

4.Geochemistry

Selected samples for geochemical analysis from Hank, Hodh and Kaarta (HHK), were prepared at the University of Padova. The rocks were crushed with a hammer and sieved in a Cr-steel ring to a grain size <500 micron. All samples were washed in distilled water in an ultrasonic bath, dried at 50°C in a furnace and pulverized with an agate mill.

In order to compare the obtained data with the previous studies, I compiled a database with major, trace elements and isotopic compositions of CAMP locations around the Province (North America, South America, Africa and Europe). Comparative plots using these data are presented along this chapter.

4.1 Major elements composition

27 samples from Kaarta, 16 from Hodh and 25 from Hank were analyzed for geochemistry of major elements by X-Ray fluorescence at ENS-Lyon. According with their alkalis and silica content, they classify as basalts, basaltic andesites and andesites (Le Maitre et al., 1989) (fig. 5). Particularly, Hodh rocks show a more fractionated character with respect to Hank and Kaarta, being enriched in silica and alkalis (fig. 5). More homogenous and less evolved compositions are observed in Hank and Kaarta samples. On a AFM plot (A: $Na_2O + K_2O$; F: $FeO + Fe_2O_3$; and M: MgO), most of the samples are clearly discriminated as tholeiites with a few exceptions close to the calc-alkaline field (Kaarta samples: MO31a- MO27, Hank: HA 102, Hodh: HD 8, HD 48) (fig. 6)

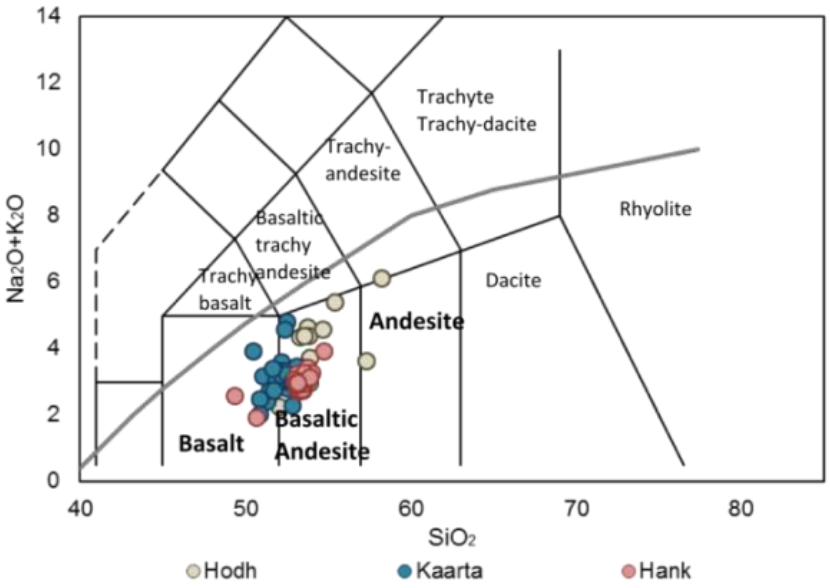

Figure 5. Total alkali vs silica (TAS) classification diagram (Le Maitre et al., 1989) for samples from Hank, Hodh and Kaarta. Different lithological fields are separated by continuous black lines; the gray line discriminate alkaline and subalkaline compositions after Irvine and Baragar (1971).

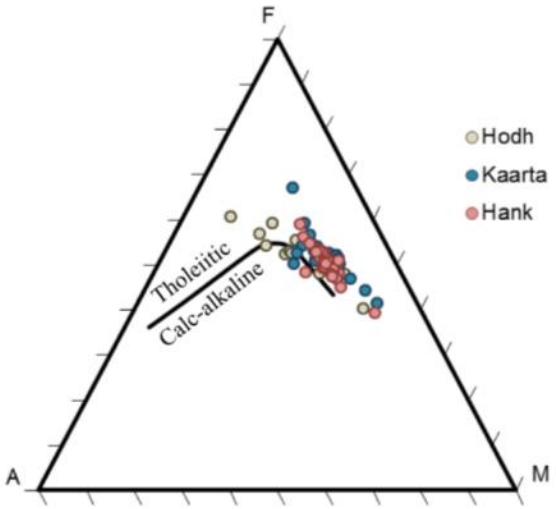

Figure 6. AFM diagram expressing contents of alkalis (A), total Iron (F) and magnesium (M) of Hank, Hodh and Kaarta samples. Continuous line represent differentiate tholeiitic and calc-alkaline fields; after Irvine and Barigar (1971). *(FeO calculated as FeO*= Fe_2O_3*0.8889).

Mg numbers [Mg = 100*Mg/(Mg+0.85*·Fe_t)] confirm that Hodh rocks can be more fractionated (Mg#= 67.98 - 22.64) than those from Kaarta (68.25 - 34.28) or Hank (69.74 - 43.28). Normative quartz in Hodh rocks as well as normative olivine observed only in Kaarta and Hank is in agreement with this feature (fig. 7). A positive correlation between the Ti-content and normative quartz is also recognized. Particularly, TiO_2 varies in a large range with the more depleted values belonging to Hank rocks (0.39 wt.%) and the more enriched to Hodh (2.29 wt.%). Three groups can be then recognized with respect to the content of TiO_2. Two of them, the low TiO_2 (0.39 - 0.86 wt.%) and intermediate TiO_2 (0.93 - 1.62 wt.%) match with the ranges observed for the CAMP in Marocco (Marzoli et al., 2004) and with the Taoudenni dyke swarm (Verati et al., 2005) (fig. 8). The third group, characterized by high TiO_2 (1.71 - 2.29 wt.%) is only comparable to some CAMP dykes from Liberia(Group I: 1.43 - 2.22 wt.%; Dupuy et al., 1988) and northern Brazil (eg:~ 2 wt.% in Maranhão; Merle et al., 2011). Moreover, a negative correlation defined by the lower Mg # and higher TiO_2 of Hodh and given compositions of Hank and Kaarta, is also recognized in other regional sets of CAMP after plotting available geochemical data from the literature. Particularly, it is notable that compositions of HHK span the heterogeneities of all the different CAMP locations (fig. 8). A positive correlation from the bivariate plots using Mg# as a differentiation index, is also observed in HHK with respect to CaO and Al_2O_3 whereas inverse correlations are displayed by SiO_2, Na_2O, K_2O probably ruled by the fractionation of plagioclase during the differentiation. Increasing contents of FeO at lower Mg# are typical of these rocks, as it is expected for tholeiitic magmas (fig. 9).

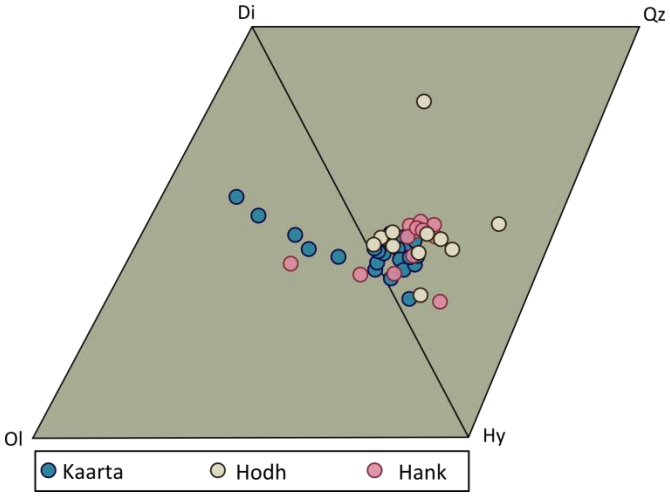

Figure 7. CIPW normative composition of the samples from Hodh, Hank and Kaarta. Ol: Olivine, Di: Diopside, Hy: Hyperstene, Qz: Quartz.

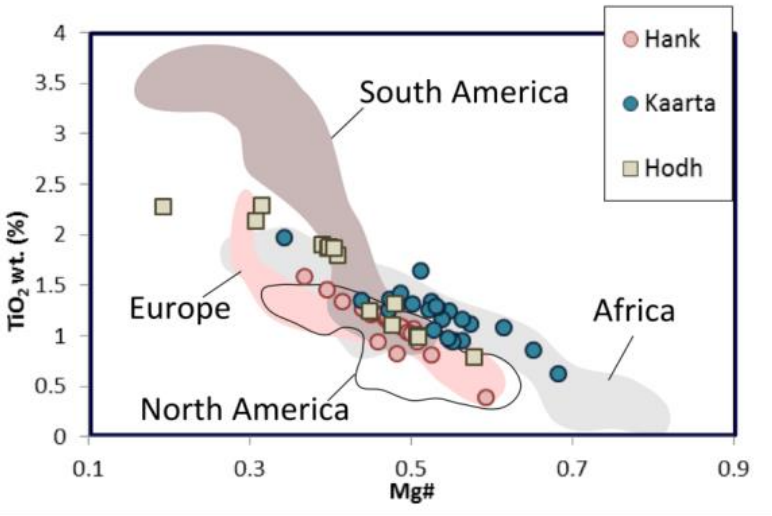

Figure 8. TIO_2 vs Mg # [Mg/(Mg+0.85·Fe_t)]. Fields corresponding to values of the CAMP in South America, Europe, Africa and North America from); Cebria et al. (2003); Callegaro et al. (2013, 2014); Deckart et al. (2005); Merle et al. (2011, 2014) Verati et al. (2005); Marzoli et al. (2004); Chabou et al. (2010).

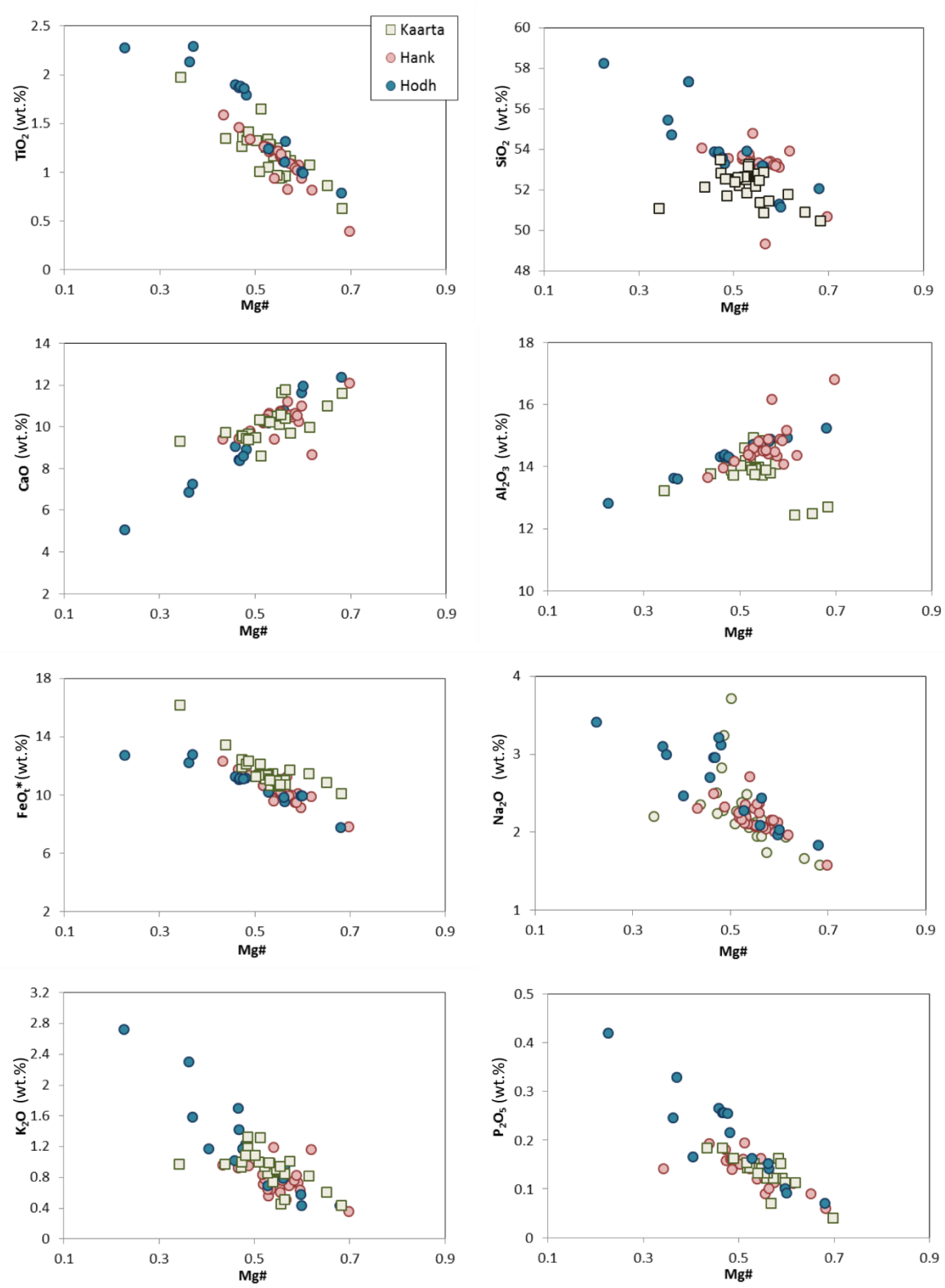

Figure 9. Bivariate diagrams of major elements against Mg# of HHK samples. Mg# calculated using: [(MgO/MgO + FeO*)].

4.2 Trace elements composition

Trace element abundances of 10 samples from Kaarta and 13 from Hank were obtained by ICP-MS at Brest University. An enrichment of large ion lithophile elements (LILE) and light rare earth elements (LREE) is in general recognized with respect to the heavy rare earth elements (HREE) in all samples (fig 10). Negative anomalies of Nb-Ta, Sr, and slightly of Eu are typical of both regions as well as a positive anomaly of Pb. Samples from Hank exhibit homogeneous compositions whereas those from Kaarta display a larger range, with a more enriched character. Despite this, most of the rocks agree in similar trends that only differ in the contents of Ba. Kaarta rocks typically present troughs of Ba (89 – 239 ppm) whereas those from Hank display Ba-spikes (189 – 898 ppm), being the highly enriched values, probably an effect of secondary alteration. The observed differences in LREE with respect to HREE are reflected by La/Yb_N ratios (normalized to primitive mantle) which vary from 4.54 to 2.48 in Hank and from 3.64 to 3.19 in Kaarta.

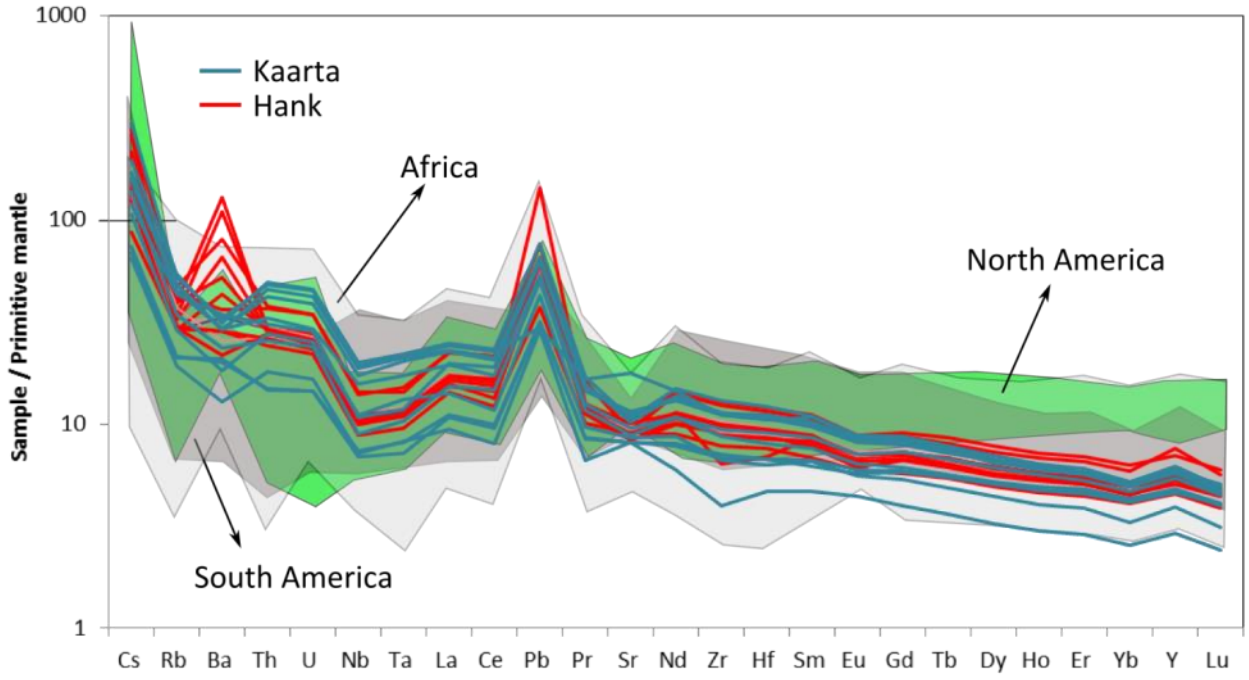

Figure 10. Trace elements composition of Hank and Kaarta rocks and fields corresponding to CAMP compositions in North America, South America and Africa (data from Callegaro et al., 2013; Deckart et al., 2005; Merle et al., 2011; Verati et al., 2005; Marzoli et al., 2004; Charaf et al., 2010). Values normalized to primitive mantle from Sun and McDonough (1989).

Trace element compositions and patterns similar to those of Hank and Kaarta are also recognized in the rest of the CAMP. The most heterogeneous and the most depleted compositions in HREE are displayed by samples from Africa, only comparable to two samples from Kaarta by Kaarta rocks. Flatter patterns of REE in North America (representative of Eastern North American dykes –ENA-) contrast with the more fractionated character of the other locations (fig 11).

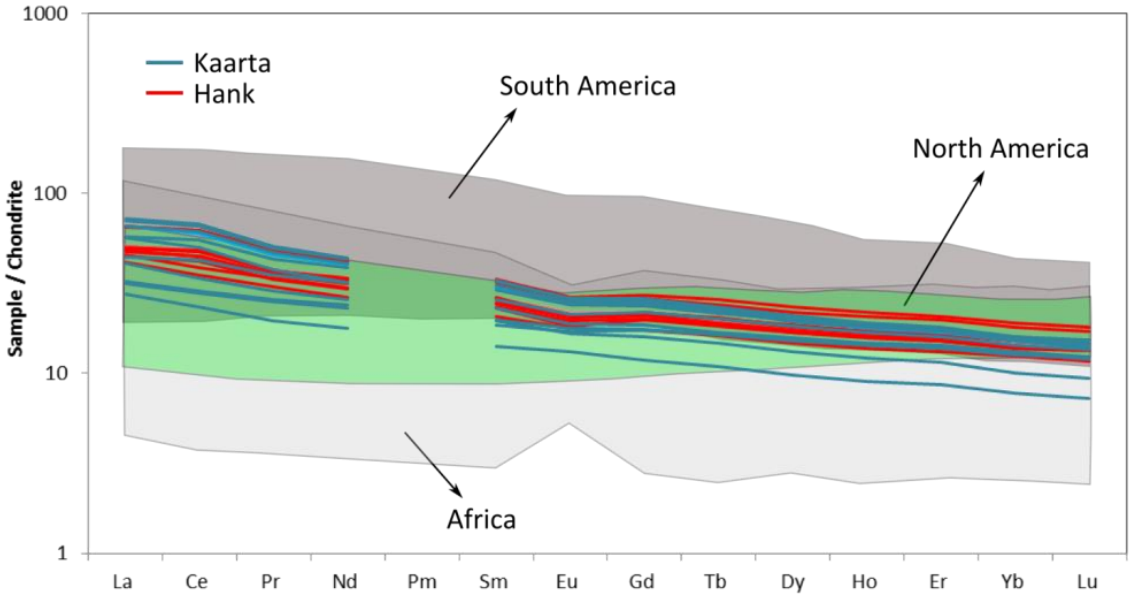

Figure 11. Chondrite normalized rare earth elements (REE) diagram from Hank and Kaarta samples and CAMP locations in North America, South America and Africa (data from Callegaro et al., 2013); Deckart et al., 2005); Merle et al., 2011; Verati et al., 2005; Marzoli et al., 2004); Charaf et al., 2010). Chondrite values from McDonough and Sun (1995).

Ratios of La/Yb >6 in Kaarta suggest the presence of an enriched group also recognized in samples from Taoudenni and Morocco. The more depleted La/Yb from Hank are comparable to reported compositions of CAMP in Europe and Maranhão basin in Brazil. Variations in the ratios of La/Yb in both regions (Hank and Kaarta) are not correlated with TiO_2 since the enriched La/Yb group in Kaarta, occur at equivalent moderate-TiO_2 contents as those displayed by Hank and the rest of samples from Kaarta (fig 12a). However, high ratios of Nb/Zr (> 0.1 in Kaarta) and of Th/Y (>0.11), sensitive to partial

melting, are positively correlated with La/Yb (fig 12b). Large variations in terms of these ratios are described only by Kaarta samples contrasting with homogeneous compositions of the Hank rocks. These compositions resemble the CAMP locations, being those from Kaarta in the range observed for Africa (Morocco and Taoudenni) whereas samples from Hank display compositions like rocks from Europe.

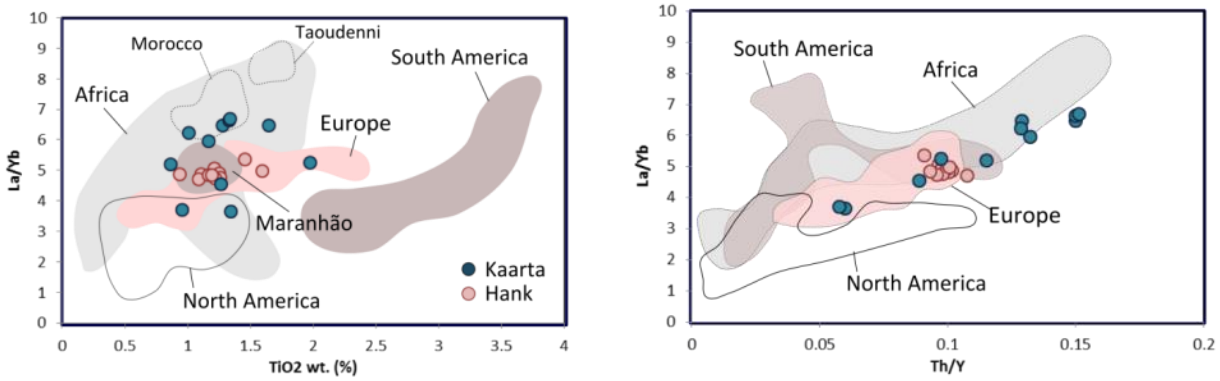

Figure 12. a)La/Yb vs TiO_2 content and b) La/Yb vs Th/Y plots for Hank, Kaarta and CAMP locations (North America, Europe, South America and Africa; data from Callegaro et al., 2013; Deckart et al., 2005; Merle et al., 2011; Verati et al., 2005; Marzoli et al., 2004; Charaf et al., 2010).

Trace element ratios such as Nb/U, with almost identical partition coefficient tend to be useful in identifying source differences and petrogenetic processes. According with the rational proposed by Hofmann (2003), this ratio is considered as a tracer of mantle source compositions as well as of the recycled continental material. Obtained results show almost constant values that only vary from 15 and 13 in the two regions of Hank and Kaarta, also comparable to Nb/U data for Europe and Africa (Taoudenni and Marocco) and the mean continental crust (Nb/U= 8). More enriched compositions are displayed by South America, North America and Africa (Liberia) in agreement to enriched-Ti regions and isotopically different sources discussed in the next section.

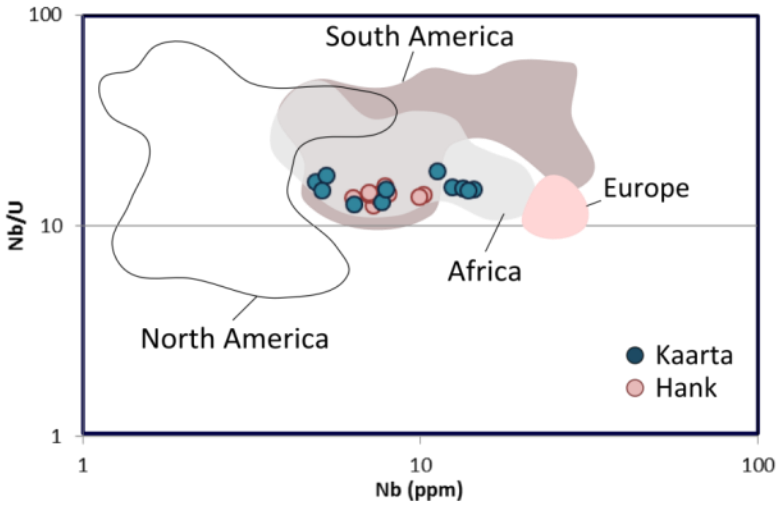

Figure 13. Nb/U ratio vs Nb content (ppm) of Kaarta and Hank rocks and CAMP locations (North America, Europe, South America and Africa; data from Callegaro et al., 2013; Deckart et al., 2005; Merle et al., 2011; Verati et al., 2005; Marzoli et al., 2004; Charaf et al., 2010).

4.3 Sr-Nd-Pb isotopes

Nd, Sr and Pb isotopes were measured on 9 samples from Kaarta, 1 from Hodh and 7 from Hank. The analysis were performed at the Laboratory of Radiogenic Isotopes, University of Geneva. The preparation of the samples followed the same proceedings described for major and trace elements analysis in the previous chapters. Samples were further hand-picked to eliminate altered portions. Results are reported in the Appendix .

Isotope compositions available from the literature were compiled from the four described CAMP rocks per continents. North America: Northern North America (Sherlbourne, Caraquet dykes in Canada) (Dostal and Durning, 1998; Puffer, 1992 ; Southern North America)Southeastern coast of the U.S.A.) (Callegaro et al., 2012). South America: Guyana, Brazil (Roraima, Amazonia, Anari, Tapirapuà, Maranhão) (Merle et al., 2011; De Min et al., 2003; Deckart et al., 2005; Heartherington and Mueller, 1999). Africa: Morocco, Mali, Liberia, Guinea (Marzoli et al., 2004; Verati et al., 2005; Deckart et al., 2005; Dupuy et al., 1988). Europe: Portugal, Spain, and France (Rapaille et al., 2003 Alibert, 1985; Jourdan et al., 2003; Cebria et al., 2003).

Initial $^{87}Sr/^{86}Sr_i$ and $^{143}Nd/^{144}Nd_i$ ratios (recalculated to 201 Ma) vary in Kaarta from 0.70590 to 0.70812 and from 0.51228 to 0.51247, respectively. In contrast, Hank rocks display distinctively more radiogenic $^{87}Sr/^{86}Sri$ (0.70693 - 0.70984) and lower $^{143}Nd/^{144}Ndi$ (0.51224 - 0.51228) (fig 14). Only one sample from Kaarta reaches more depleted Nd compositions than Hank. Moreover, a negative correlation is observed after plotting Nd and Sr initial isotopic ratios of all the different regional sets of CAMP, where similar compositions occur only at moderate Ti-values (1.7 - 0.7 wt.%). Most of the CAMP samples (including Hank and Kaarta) vary in terms of $^{143}Nd/^{144}Nd_i$ and $^{87}Sr/^{86}Sr_i$ between 0.5124 and 0.5122 and 0.7079 to 0.7051, respectively. Exceptional high values in $^{143}Nd/^{144}Nd$ (0.5127 – 0.5125) and the lowe in $^{87}Sr/^{86}Sr_i$ (0.7043 – 0.7029) coincide with the highest values of along to high-Ti basalts and gabbros from Liberia, Guyana, and NE-Brazil (Deckart et al., 2005; Dupuy et al., 1988; De Min et al., 2003; Merle et al., 2011). Only one sample from Kaarta displays low $^{143}Nd/^{144}Nd$ and high $^{87}Sr/^{86}Sr_i$ (0.51226; 0.7098), just comparable to rocks from the Roraima region, in Brazil, and to some

Guinea dolerites. However, given the great differences with the rest of samples from that group, it is possible that the enrichment is due to secondary alteration.

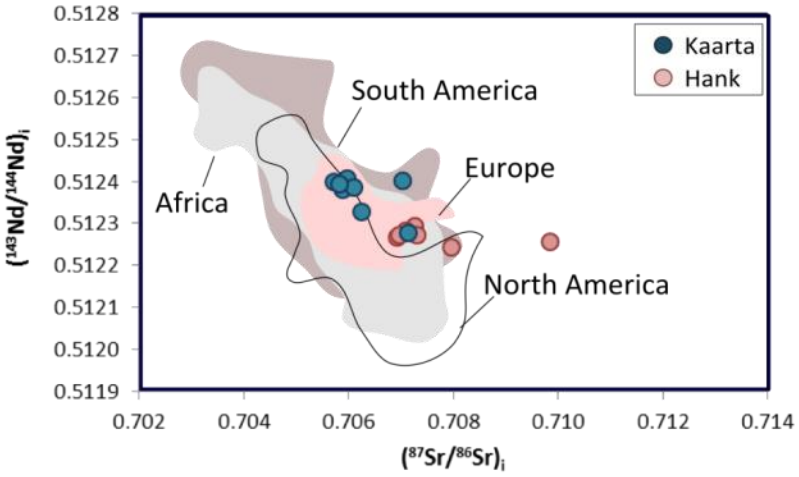

Figure 14. Initial Sr and Nd isotopic compositions of Kaarta and Hank rocks and of CAMP basalts from South America, Europe, Africa and North America CAMP. All data recalculated to 201 Ma. CAMP fields plotted from (Dostal and Durning, 1998; Puffer, 1992; Callegaro et al., 2013; Alibert, 1985; Cebria et al., 2003; Rapaille et al., 2003; Callegaro et al., 2014; Deckart et al., 2005; Verati et al., 2005; Mauche et al., 1989; Dupuy et al., 1988; Heartherington and Mueller, 1999; Merle et al., 2011, 2014).

In general, CAMP rocks display initial $^{87}Sr/^{86}Sr$ ratios inversely correlated to values of Nb/U. Enriched Sr isotopic compositions and progressively depleted Nb/U may be due to the influence of the continental crust (Nb/U= 8; Hoffman, 2003). However, scarce variations in the Nb/U ratio in Kaarta and Hank (Nb/U= 15 – 12) contrast with larger variations in isotopic composition of Sr suggesting a homogenous process of partial melting but a more enriched source for Hank than for Kaarta rocks. Similar compositions are shown by samples from Morocco and Taoudenni in Africa. In contrast, depleted $^{87}Sr/^{86}Sr$ ratios and higher Nb/U are only typical from North America (eg: Callegaro et al., 2013) and Guyana samples (Deckart et al., 2005).

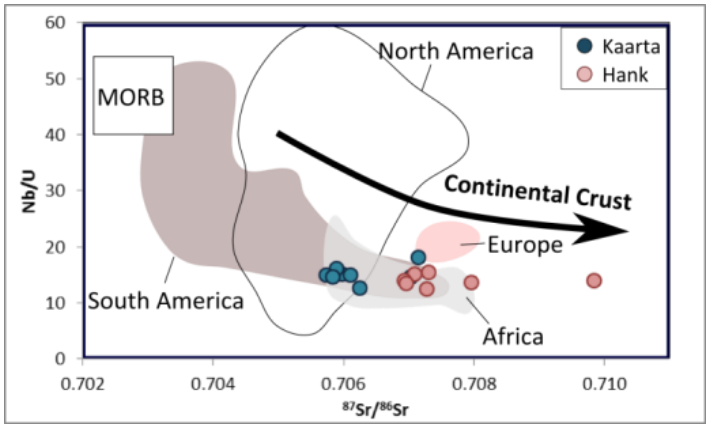

Figure 15. Nb/U vs Initial ratios of $^{87}Sr/^{86}Sr$ (recalculated to 201 Ma) for Kaarta, Hank rocks and for various CAMP locations (Data from Callegaro et al., 2012; Cebria et al., 2003; Deckart et al., 2005; Verati et al., 2005; Merle et al., 2011, 2014).

Available lead isotopes for Kaarta and Hank show a relatively restricted signature in terms of $^{206}Pb/^{204}Pb_i$, $^{207}Pb/^{204}Pb_i$ and $^{208}Pb/^{204}Pb_i$. Particularly, Hank samples display more homogenous compositions ($^{206}Pb/^{204}Pb_i$:18.45 - 18.24; $^{207}Pb/^{204}Pb_i$: 15.68 - 15.63; $^{208}Pb/^{204}Pb_i$: 38.53 - 38.22) than Kaarta rocks (18.69-18.06; 15.68-15.62; 38.79-38.08). A positive correlation is observed for the initial ratios (also recalculated to 201 Ma) of $^{206}Pb/^{204}Pb_i$ vs. $^{207}Pb/^{204}Pb_i$ (fig 17a) and $^{208}Pb/^{204}Pb_i$ (fig 17b). Contrasting with this well-defined trends, only two samples from Kaarta reach more enriched $^{206}Pb/^{204}Pb$ (18.78 and 18.69) with moderate and high $^{208}Pb/^{204}Pb$ (38.30 and 38.79). All samples and the general CAMP fields plot to the right of the Geochron (fig 17) and to the left of the Northern Hemisphere Reference Line (NHRL) and in general trend to the EMI and EMII components (fig 16) (Zindler and Hart, 1986). Data from Guinea are the only available to compare with CAMP samples in Africa, displaying slightly depleted $^{207}Pb/^{204}Pb$ (15.62-15.57) with respect to Kaarta and Hank samples. The less radiogenic $^{206}Pb/^{204}Pb$, $^{207}Pb/^{204}Pb$, and $^{208}Pb/^{204}Pb$ are recorded by the Maranhão basin and South Eastern North America dykes (18.11- 17.70; 15.51-15.47; 37.95 - 37.46, respectively).

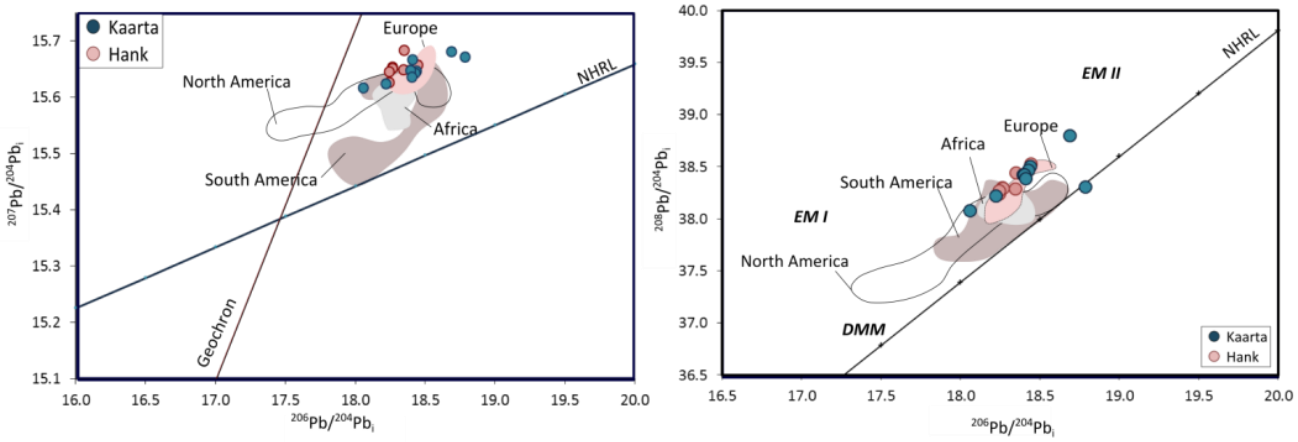

Figure 16. Initial Pb composition back calculated to 201 Ma. A) Plot $^{207}Pb/^{204}Pb$ vs $^{206}Pb/^{204}Pb$ and $^{208}Pb/^{204}Pb$ vs $^{206}Pb/^{204}Pb$. Mantle end-member values from Zindler and Hart (1986) also recalculated to 201 Ma.

PART II: The Patagonia Province

5. Earlier studies

A revised definition of Large Igneous Provinces by Bryan and Ernst (2008) considers that substantial volumes of silicic magmatism are often an integral part of continental LIPs; and that a few of them are mainly silicic. A thick sequence of Late Jurassic magmatic rocks extends from the Atlantic to the Andes and covers about $1x10^6$ km^2 of the Patagonian region in Argentina. Despite the presence of minor mafic rocks, this Province is dominated by a felsic affinity and represents one of the few silicic LIPs on Earth (Pankhurst et al., 1995).

The Jurassic volcanism in Patagonia was firstly reported by Feruglio (1949). Since then, a confusing use of different terms loose an unclear consensus about the name and formations comprised by the Province. Some of them included “Tobifera” (Bruhn et al, 1978); “Mid-Jurassic volcanic rocks” (Gust et al., 1985), “Jurassic volcanic Province” (Pankhurst and Rapela, 1995) or Chon Aike Province (Kay et al., 1989). The last one, is probably the most common denomination used in the literature even if Chon Aike is also one of the constituent formations of the Province. In order to avoid the conflict between the nomenclature and the stratigraphy, the Jurassic magmatic rocks of Patagonia are called in this study *the Patagonia Province (PA).*

The PA crops out along the Andean and extra-Andean areas of the Patagonian region. Descriptions in the literature, have considered the political division (Rio Negro, Chubut and Santa Cruz) and the main physiographic features of the region to name and locate the geologic units of PA. The most representative locations include the North Patagonian Massif, which comprise the Somuncura Massif and the Cañadón Asfalto Basin, in the Chubut area, The Cordilleran and Pre-Cordilleran region in the Andean zone, and the Deseado Massif, in Santa Cruz (fig. 17).

In general terms, the robust silicic volcanism of the PA comprises thick sequences of ignimbrites, rhyolites, debris flows, fallout and epiclastic deposits from geographically separated formations, comparable to those from the Antarctic Peninsula (Kay et al. 1989; Storey and Alabaster 1991; Pankhurst et al., 1998). The main outcrops are located in the Somuncura Massif (Chubut Area), the

Deseado Massif and the Cordilleran region of Chile and Argentina. Despite the discrepancies about the name and the forming units, it is in general well accepted that at least Marifil and Chon Aike represent the felsic magmatism in the extra-Andean zone, and that the tilted altered rocks from the Ibáñez and El Quemado Formation are the equivalents in the Cordilleran region (Uliana, 1985; Pankhurst et al., 1995, Bryan et al., 2002). A minor basaltic to andesitic component is displayed by Bajo Pobre (BP) and Lonco-Trapial Formations which are possibly cogenetic to the felsic magmatism of Chon Aike(fig. 18). A contemporaneous extensional back arc basin in the Central Chubut Province, yield basaltic- andesitic magmas known as Cañadon Asfalto (CA) Formation that overlap the composition of BP and the volcanic period of the PA (fig. 18). Previous K-Ar , Ar-Ar, Rb-Sr and U-Pb ages evidence a period of magmatic activity that also spans the middle and late Jurassic (table 1). Exceptionally, ultramafic rocks of the Cresta de los Bosques Formation, are the only described plutonic Jurassic rocks of the Province.

Exposed along graben and hemigraben structures (Uliana et al., 1985; Feraud et al., 1999), rocks from the PA have been traditionally related to the break-up of Gondwana and the effects of the Karoo mantle plume (Pankhurst et al., 1995, 1998, 2000; Riley et al., 2001). However, a more complex geodynamic setting where a general extensional regime was favored by the continental break-up, the opening of the Weddell Sea and the back-arc basins formed by the subduction of the Phoenix plate, should also be considered. A bibliographic review, presented below, attempts to constrain the geological record and tectonic setting related to this Province.

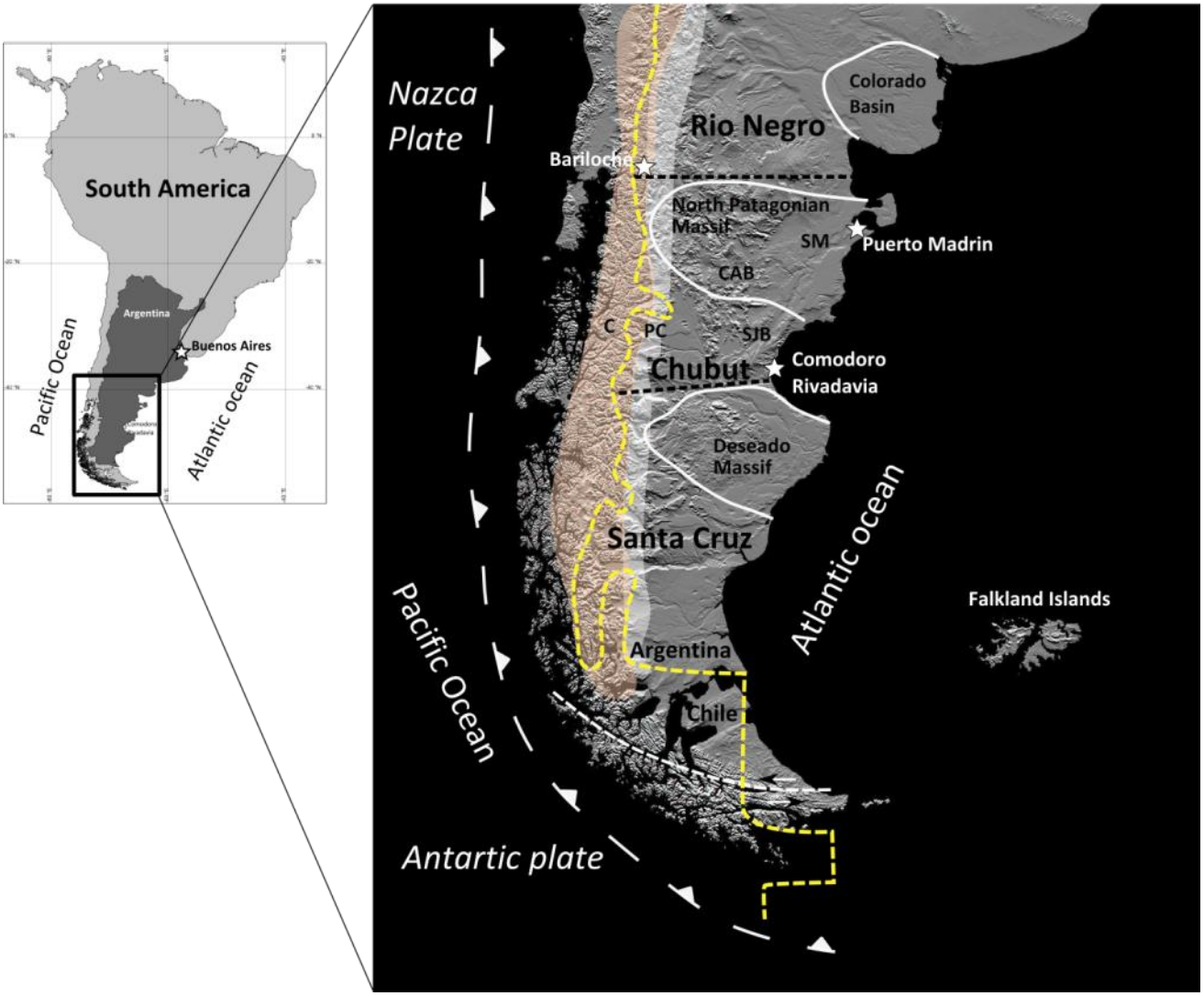

Figure 17. Location of the Patagonian Province. Notice the main physiographic features and the political division. C: Cordilleran; PC: Pre-Cordilleran; SJB: San Jorge Basin, CAB: Cañadón Asfalto Basin; SM: Somuncura Massif. Image of South America from http://photojournal.jpl.nasa.gov/

5.1 Regional geology

5.1.1 Pre-Jurassic basement

The basement in the Patagonian Province has been hardly recognized due the large extent, thickness and volume of the Jurassic magmatic cover. However, a few outcrops are exposed as relatively small areas within the Patagonian massifs and the Andean Cordillera (Pankhurst et al 1998). The oldest stable area of continental basement in the Patagonian region is considered the Northward Río de la Plata Craton (ca. 2-2.2 Ga) (Santos et al., 2003; Ramos, 2008). A Paleozoic sedimentary sequence known as Sierras Australes de Buenos Aires, o Sierra de la Ventana (Northward of Colorado basin), crops out Southward of the Craton overlying a younger (Neoproterozoic) crystalline basement with crustal anatectic granite at 607±5 Ma and I/A-type granites at 531±4 and 524±5 Ma (Rapela et al., 2003) (fig. 18).

In Northern Patagonia, two different metamorphic and magmatic belts have been described: the Northern and the Western belts (Caminos and Llambías, 1984; Rapela and Llambías, 1985; Rapela and Caminos, 1987; Dalla Salda et al., 1992a,b, 1994;Von Gosen, 2002, 2003; Varela et al. 2005, 2007; and Pankhurst et al., 2006, Ramos 2008). The northern metamorphic and magmatic belt is preserved along the Río Limay valley from the city of Bariloche, in the west up to the Sierra Grande region, to the Atlantic coast (Varela et al., 1998a; Basei et al., 1999). It consist of granitoids and low grade metamorphic rocks yielding U-Pb ages of ca. 470 Ma (Pankhurst et al., 2006). The inherited zircons of these rocks have an important Neoproterozoic contribution (570-540 Ma), indicating a Brazilian–Panafrican source, and possibly a para-autochthonous origin within Gondwana for the Somúncura Massif (Ramos, et al., 2008). The western metamorphic and magmatic belt crosses central Patagonia with a NNW trend and continues into the Deseado Massif and further south (Ramos, 2008). It has been described as an assemblage of magmatic and metamorphic rocks exposed in San Martin de Los Andes – Bariloche to Paso de Indios, along the Rio Chico Valley, in Central Chubut. They consist of metamorphic rocks in greenschists to amphibolite facies associated with foliated tonalities and granodiorites, mylonites and granitic cataclasites, formed in a collisional setting. Its age was assumed as Precambrian or Early Paleozoic, however an U-Pb age of 345 ± 4.3 Ma (Basei et al., 1999) has been interpreted as the result of a metamorphic event during the Late Paleozoic times. The origin of this

event has been related to a collision setting in the Mid Carboniferous prior to the emplacement of peraluminous S-type garnet-bearing leucogranites of Paso del Sapo (Canadon Asfalton Basin) and Sierra de Pichiñanes which yielded 314 ± 2 Ma and 318 ± 2 Ma crystallization ages (Ramos, 2008). Despite the great conflicting nomenclature in the area, the metamorphic and igneous rocks are grouped as Cushamen (330-365 Ma?; Pankhurst et al.,2006) and Mamil Choique Formation (281 ± 2 Ma; Pankhurst et al., 2006). Sedimentary sequences of presumed Early Jurassic age are represented by the pale sediments of Las Leoneras and Osta Arena, which underlie the volcanics of Lonco Trapial and host the gabbros of Cresta de los Bosques, respectively (Page and Page, 1993, Cúneo et al., 2013).

Further south, in the Deseado Massif, the basement is composed by scarce micaceous and amphibolitc schists possibly of very late Precambrian or Cambrian age according with a K-Ar age of 549 Ma for an amphibolite (Pezzuchi, 1978, Pankhurst et al., 1998), granitoids and metamorphic rocks with the same NW trend of the Western belts (Giacosa and Márquez, 2002). Available U–Pb zircon ages of the granitoids yielded Early Paleozoic (472 and 454 Ma; Loske et al., 1999) as well as Devonian and Middle Carboniferous ages (Pankhurst et al., 2003). Based on the continuity of the magmatic belt with dominant NW structures and the range of U–Pb ages, it is assumed that the igneous and metamorphic Western belt is connected through the San Jorge Basin with the Deseado Massif. Conglomerates of Permo-Triassic age fill small basins and represent the oldest evidence of an extensional regime during the Triassic, with the regional formation of NNW-SSE trending graben through Patagonia (Uliana et al., 1985; Uliana and Biddle, 1987).

5.1.2 Jurassic magmatic units

Chubut area

5.1.2.1 Marifil Formation

Named by Malvicini and Llambías (1974) and described in more detail as the 'Marifil Complex' by Cortés (1981) and Haller et al (1990), it comprises the silicic volcanic sequences from the Eastern Somuncura Massif (fig. 18) (Uliana et al., 1985; Pankhurst and Rapela 1995; Pankhurst et al., 1998). It consists of flat lying, rhyolitic ignimbrites with associated volcaniclastic deposits and lava flows. Pyroclastic deposits predominate over tuffs and lavas, although the latter are volumetrically significant. Ignimbrites form cooling units up to 100 m thick, in which welding is often strong, and commonly have a massive red– brown aspect. They cover an area of over 50,000 km^2 in the east of the Marifil Formation, where flat lying ignimbrite sheets predominate and are believed to have been erupted from large (100 km diameter) calderas (Aragon et al., 1996). However, evidences of remnant eruptive centers are not observed in the field and in most of the cases the volcanism seems to be related to the tectonic structures (Marquez et al., 2010). The thickness of this units is estimated up to 600–900 m. Although the stratigraphic contacts are hardly visible, this unit has been described by Iglesia-Llanos et al (2003) as unconformably overlying Precambrian and Palaeozoic rocks and covered by Cretaceous continental sediments and Cenozoic marine and continental deposits. Strong geochronological evidence suggest that Marifil Formation represent the oldest pulse of the Province. Five Rb-Sr whole rock isochron dating (Rapela and Pankhurst, 1993) and twelve results by $^{40}Ar/^{39}Ar$ dating (Feraud *et al.,* 1999; Alric et al., 1996 not recalibrated due to missing data on the used age monitor), agree in a magmatic activity period from ~189 Ma to ~179 Ma. Only three ages differ from this range. Two Rb-Sr ages of 169 ± 3 (MSDW= 7.9 and high $^{87}Sr/^{86}Sr$ =0.7127), and 174±1 Ma (MSDW= 0.5 and low Rb/Sr) (Pankhurst and Rapela., 1995), and one $^{40}Ar/^{39}Ar$ age of 176.9 ± 0.5 Ma (recalculated data from Feraud et al., 1999). All errors are given to 1σ.

5.1.2.2 Lonco Trapial Formation

In the Central Chubut area, near the valley of the Chubut River, a volcano-sedimentary sequence is composed by a large alternation of agglomerates, volcanic breccias, andesitic and basaltic dykes and lavas. A sedimentary member intercalated has been associated also associated. It is composed of volcaniclastic conglomerates, sandstones and lahar deposits with significant lateral lithofacies variations. The differentiated volcanic and sedimentary facies have been alternatively called as Tequetren Formation, Cerro Carnerero Formation or Cañadón Puelman beds, collectively grouped under the so-called Lonco Trapial Formation (Lesta y Ferello, 1972) or (Nullo y Proserpio, 1975) or Lonco Trapial Group. Overlaying the sediments of La Leonera Formation, and transitional to Cañadón Asfalto, the cumulative thickness of the Lonco Trapial Formation is estimated in 500–800 m. A broadly defined Middle to Late Jurassic (176–146 Ma) age has been suggested based on K–Ar geochronology (Nullo, 1983). A maximum age of 188.95 ± 0.10 Ma (Cuneo et al., 2013) is probable from the U-Pb single zircon dating on the sediments of Las Leoneras.

5.1.2.3 Cañadón Asfalto Formation

The Cañadón Asfalto Formation (Stipanicic *et al.*, 1968), has been historically described as an assemblage of lacustrine and fluvial deposits, pyroclastic intercalations, and olivine-rich basalt flows at its base, outcropping in the Medium Valley of the Chubut River (Stipanicic et al., 1968; Nullo, 1983; Turner, 1983; Cabaleri et al., 2010, 2013, Figari, 2005). The basin, known by the same name, is characterized by a great diversity of environments represented mainly by lakes, rivers, ponds, and wetlands, which suffered dry and wet intervals affected by magmatic activity (Lizuain and Silva Nieto, 1996; Cabaleri and Armella, 1999; Cabaleri et al., 2010a; Gallego et al., 2011, Cabalieri et al., 2013). Three depocenters have been considered within the basin, named as Cerro Cóndor, Cañadón Calcáreo and Fossati, which served as micro-basins in response to the driving tectono-sedimentary processes (Silva Nieto et al., 2007). Some authors have divided this Formation in two members: a lower lacustrine/tuffaceous (Las Chacritas), and an upper siliciclastic fluvial (Puesto Almada) member (Cabaleri et al., 2010a,b). In the Cerro Cóndor area, the Lonco Trapial–Cañadón Asfalto transition is marked by several distinct basalt flows interlayered with fossiliferous lacustrine strata. The age of the basal Cañadón Asfalto is constrained by one K-Ar age of 170.9±4.4 Ma (Salani, 2007) and three U-Pb

zircon dates of 176.15 ± 0.12 Ma, 177.62 ± 0.53 Ma and 178.77 ± 0.092 Ma (Cúneo et al., 2013), from which the last one represents the maximum deposition age of the Lower Cañadón Asfalto. Significantly younger U-Pb and K-Ar ages of 161±3 Ma, and 147.1±3.3 Ma, respectively, were obtained on what is described as upper Puesto Almada Member. However, Cuneo et al (2013) suggested that this member could correspond to the Cañadón Calcáreo Formation. Two more U-Pb ages in this latter unit of 157.387±0.045 Ma agree this interval (Cuneo et al., 2013).

Deseado Massif

5.1.2.4 Chon Aike

Covering an area of about 100.000 km^2 in the Deseado Massif (fig. 18), the Chon Aike Formation is probably the largest expression of the robust felsic volcanism in Patagonia. Historically, this rocks were described as one of the two volcanic series of Bahia Laura Group (Feruglio, 1949), but was not only until Archangelsky (1967), that received the name of Chon Aike Formation.

The main plateau consists of volcanic and volcaniclastic rocks cut by dykes and overlain by rhyolitic domes. Pyroclastic rocks predominate and ignimbrites form ca. 85% of the outcrop (<300 m thick), with subordinate epiclastic deposits, air-fall tuffs and intercalated felsic lavas. In general, individual flows vary in thickness from tens of cm to tens of meters, exceptionally reaching 100 m or more, like at Río Pinturas. The degree of welding varies from a predominant poorly welded and highly altered ignimbrite to perlitic vitrophyres. The better-welded ignimbrites are massive and frequently show coarse columnar jointing. Some features suggest emplacement over wet sediments or subaqueous emplacement , associated with lacustrine epiclastic rocks referred to as La Matilde Formation. Rhyolitic dykes up to 20 m wide cross-cut the pyroclastic and epiclastic sequences of the formation. The pyroclastic and lava facies are petrographically similar. Modally, the ignimbrites are phenocryst-poor rhyolites or leucocratic dacites. Devitrification is a common phenomenon and results in a variety of textures: axiolitic, spherulitic, micro- and crypto-crystalline. The vitrophyres are characterized by perlitic texture. The proportions of ash and pumice vary, although ash-rich deposits predominate. The

principal minerals are quartz, K-feldspar, plagioclase and biotite; accessories are magnetite, ilmenite, apatite and zircon with associated monazite. The alteration assemblage is quartz, sericite, calcite, albite and clay minerals. Alteration is widespread and often obvious from the pervasive pink to dark red colour of the rocks. Silicification and vein-like deposits of Fe and Mn oxides are common, especially in the rhyolite domes. Locally, hydrothermal alteration was succeeded by bleaching along joints and fractures (Pankhurst et al., 1998). Lithological characteristics from different localities have been described in detail by Sruoga and Palma (1984, 1986); Sruoga and Irigoyen (1987); Sruoga (1989, 1994).

Radio-isotopic dating by ^{40}Ar-^{39}Ar (Alric et al., 1996; Feraud et al., 1999; Pankhurst et al., 2000), U-Pb (Pankhurst et al., 2000) and Rb-Sr (Pankhurst et al., 1993) (table 1) constrain the length of this unit in a range between 170.3 ± 0.4 Ma and 153.0 ± 0.5 Ma. Only one age of 177.6 ± 1.4 Ma obtained by Alric et al. (1996) is considerably older and just comparable to the youngest ages from Marifil. Analytic data supporting such older age for Chon Aike are missing from the literature.

5.1.2.5 Bajo Pobre

Volcanic rocks from the Bajo Pobre Formation (Lesta and Ferello, 1972) (Guido et al., 2006) consist of subhorizontal altered basaltic andesite and volcanic agglomerates intercalated with sandstones and tuffs (de Barrio *et al.* 1999; Panza, 1995; Guido et al., 2006; Pankhurst et al., 1998). Disperse outcrops in an area of more than 300 km^2 in the Central part of the Deseado Massif, are the only known locations where this unit is exposed (fig. 18). They are represented by lava flows from 7 m to 30 m of thickness, of aphanitic to slightly porphyritic basaltic andesites with plagioclase phenocrysts, highly altered. Mafic clastic deposits interbedded with the lavas are up to 100 m thick and are dominated by locally palagonitized epiclastic debris-flow units. The upper parts of some sections are formed of coarse agglomerates, with 0.5 m blocks of pyroxene andesite. Some coarser-grained mafic to intermediate intrusive bodies, occur as at Cerro Leon (Guido, 2002; Guido et al., 2004). Most of the rocks of the Bajo Pobre Formation are hydrothermally altered and they occasionally exhibit disseminated sulphide mineralization. The total length of the unit is unknown since most of their contacts are not observed. However, De Giusto et al. (1980) suggested a thickness of about 200 m, and 600 m for the latter partly tectonically thickened. Although the base of the formation is rarely

exposed, in the central part of the massif it is unmasked by an anticline structure, where it overlies the epiclastic and pyroclastic Toarcian-Aalenian rocks of the Roca Blanca Formation (Stipanicic and Bonetti, 1970). Although the stratigraphic relations are dubious in this unit, BP has been traditionally considered as discordantly covered by the Chon Aike Formation (Pankhurst et al., 1998). However, Guido (2006) described the volcanics from Bajo Pobre as intercalated with the felsic flows from Bahia Laura Group, including the Chon Aike Formation in the coastal zone of the Deseado Massif. Geochronological evidence support this hypothesis. Three $^{40}Ar/^{39}Ar$ ages of 165.7 ± 0.3, 154.2 ± 1.2, and 154.3 ± 2.6 Ma obtained by Feraud et al. (1999) (recalculated data after Renne et al., 2010) are within the errors (at 1 σ) of one $^{40}Ar/^{39}Ar$ age at 156.7 ± 4.6 Ma obtained by Alric et al. (1996) (not recalibrated data due to missing data on the used age monitor) and one Ar-Ar isochron at 150.6 ± 2.0 Ma from Pankhurst et al. (2000) (table 1). A maximum age of 174 Ma is suggested by the Toarcian–Aalenian fossil flora found in the Roca Blanca Formation.

Cordilleran and Pre-Cordilleran Region

5.1.2.6 El Quemado, Ibáñez and Lago la Plata Formation

Jurassic volcanic outcrops in the Andean region are exposed along a narrow belt mainly parallel to the Cordillera, and are composed by the El Quemado, Ibáñez and Lago la Plata Formations (fig. 18). Comparable to those of the Chon Aike Formation, volcanic silicic sequences of El Quemado, and Lago La Plata northward, have been faulted, tilted and thrust as a result of the Andean deformation (Uliana et al., 1985; Pankhurst et al., 1998, Marquez et al., 2011). On the Western Andes, in Chile, the Ibáñez Formation has been usually regarded as a direct equivalent. Both of them comprise rhyolitic ignimbrites associated with epiclastic deposits, air fall tuffs and breccias of various origins. The ignimbrites have a high content of Plagioclase and Fe-rich biotite. In general, the degree of hydrothermal alteration, propylitic and chloritic is significantly higher than in the Chon Aike (Pankhurst et al., 2000). Minor andesitic lava flows and volcaniclastic rocks are also present, similar to those from Bajo Pobre. The more or less felsic character of the sequences has been interpreted as the result of the increasing influence of the subduction at the Pacific margin (Gust et al., 1985; Sruoga, 1989). The age of this volcanism is defined by U-Pb ages of 154.5 ± 1.4 and 154.1 ± 1.5 Ma and ^{40}Ar-

^{39}Ar ages of 144.6 ± 1.4 and 169.5 ± 2.0 Ma (Pankhurst et al., 2000). Together, these ages, span the period of magmatic activity recorded by Chon Aike but also comprise the youngest record of the PA.

5.1.2.7 Cresta de los Bosques

Ultramafic intrusive rocks from Cresta de los Bosques are exposed mainly in the Tecka and Tepuel basins, in the Pre Cordillera region. They occur mainly as discontinuous elongated intrusive bodies of variable dimensions, but reaching 14 km of length and 7 km of thickness in the Tecka Range. In most cases, they appear like sills, lacolites and less frequent as dykes. They consist of stratified layered gabbros characterized by cumulitic textures and layering defined by oikocrystals. Mineralogically, they are composed by coexistent phenocrysts of olivine, orthopyroxene, clinopyroxene and plagioclase. Some sulphides like pyrite are common, as well as traces of metallic elements. The age of this unit is poorly constrained and no radio-isotopic dating is available. However, a Middle Jurassic age has been suggested from the stratigraphic relations given by the intrusive contact with the Early Jurassic sediments of Osta Arena (Marquez et la., 2001).

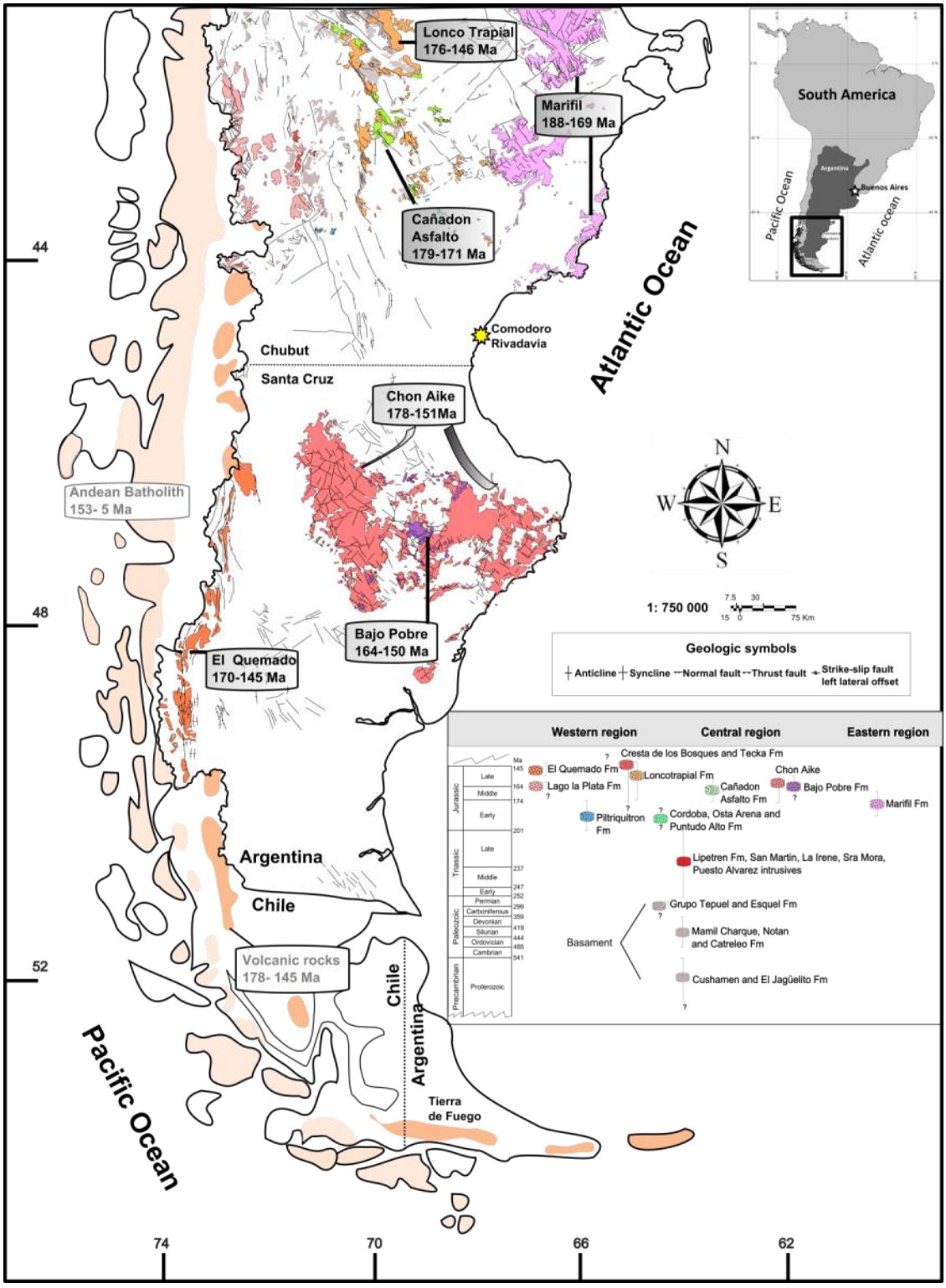

Figure 18. Geological map of the Jurassic magmatic units and basement of the Patagonia Province. A summary of the Formations and available ages from the literature and this study, is presented together to remarkable Jurassic features in Chile. After Mapa geologico de la Provincia de Santa Cruz (1994) and Mapa geologico de la Provincia del Chubut (1995). Geochronological intervals based on Rapela and Pankhurst (1993); Pankhurst and Rapela (1995); Alric et al. (1996); Feraud et al. (1999); Pankhurst et al. (1993); Cuneo et al. (2013).

Table 1. Radio-isotopic ages available in the literature for the Patagonian Province.

Formation	Age	Method	Citation	Formation	Age	Method	Citation
Cañadón A.	178.7 ± 0.046	U-Pb	1	Marifil	188 ± 0.5	Rb-Sr	5
Cañadón A.	176 ± 0.06	U-Pb	1	Marifil	174 ± 1	Rb-Sr	5
Cañadón C.	157.4 ± 0.023	U-Pb	1	Marifil	169 ± 1	Rb-Sr	5
Cañadón C.	157.5 ± 0.025	U-Pb	1	Marifil	169 ± 3	Rb-Sr	5
El Quemado	154.5 ± 1.4	U-Pb	2	Marifil	182.6 ± 0.75	Rb-Sr	6
El Quemado	154.1 ± 1.5	U-Pb	2	Marifil	181.4 ± 3.55	Rb-Sr	6
El Quemado	144.6 ± 1.4	Ar-Ar	2	Marifil	180.8 ± 2.15	Rb-Sr	6
El Quemado	171.2 ± 2	Ar-Ar	2	Marifil	178 ± 0.65	Rb-Sr	6
El Quemado	145.6 ± 0.4	Ar-Ar	3	Bajo Pobre	165.7 ± 0.3	Ar-Ar	3
El Quemado	148.6 ± 0.5	Ar-Ar	3	Bajo Pobre	154.2 ± 1.2	Ar-Ar	3
Ibañez	153 ± 1	U-Pb	2	Bajo Pobre	154.3 ± 2.6	Ar-Ar	3
Tobifera	178.4 ± 1.4	U-Pb	2	Bajo Pobre	152.1 ± 2	Rb-Sr	2
Tobifera	171.8 ± 1.2	U-Pb	2	Bajo Pobre	156.7 ± 2.3	Ar-Ar	4
Marifil	187.2 ± 0.3	Ar-Ar	3	Chon Aike	168 ± 1	Rb-Sr	7
Marifil	189.1 ± 0.3	Ar-Ar	3	Chon Aike	169.1 ± 1.6	Ar-Ar	2
Marifil	188.1 ± 1.5	Ar-Ar	3	Chon Aike	168.4 ± 1.6	U-Pb	2
Marifil	183.4 ± 0.3	Ar-Ar	3	Chon Aike	162.7 ± 1.1	U-Pb	2
Marifil	184.5 ± 0.3	Ar-Ar	3	Chon Aike	165.2 ± 1.8	U-Pb	2
Marifil	180.3 ± 0.9	Ar-Ar	3	Chon Aike	170.3 ± 0.4	Ar-Ar	3
Marifil	180.3 ± 0.3	Ar-Ar	3	Chon Aike	154.9 ± 0.3	Ar-Ar	3
Marifil	178.8 ± 0.8	Ar-Ar	3	Chon Aike	179.6 ± 0.4	Ar-Ar	3
Marifil	176.9 ± 0.5	Ar-Ar	3	Chon Aike	156.1 ± 0.5	Ar-Ar	3
Marifil	186.2 ± 1.5	Ar-Ar	4	Chon Aike	153.0 ± 0.5	Ar-Ar	3
Marifil	187.4 ± 0.6	Ar-Ar	4	Chon Aike	160.0 ± 0.3	Ar-Ar	3
Marifil	178.7 ± 0.2	Ar-Ar	4	Chon Aike	159.5 ± 0.5	Ar-Ar	3
Marifil	178.5 ± 0.6	Ar-Ar	4	Chon Aike	177.6 ± 0.7	Ar-Ar	4
				Chon Aike	151.5 ± 0.5	Ar-Ar	4

*All errors were recalculated to 1σ level. 1: Rapela and Pankhurst, 1993; 2: Pankhurst and Rapela, 1995; 3: Alric et al., 1996; 4: Feraud et al 1999; 5 : Pankhurst et al., 1993; 6 : Cuneo et al., 2013. Cañadón A: Cañadón Asfalto; Cañadón C: Cañadón Calcáreo.Ages from Feraud et al., 1999 were recalculated after Renne (2010).

5.2 Geodynamic context

The geology of the Patagonian region document a complex and long history of processes driven by major changes in the geodynamic evolution. Formed at the Southwestern margin of Gondwana, the PA was inexorably influenced by the geologic history of this supercontinent. A long history of magmatic events connected with tectonic processes has been broadly discussed without fully explaining all the existing data. Nevertheless, a description that include the most remarkable episodes during the Paleozoic and the Jurassic in Patagonia, should contribute to understand the problematic geologic history of this region.

5.2.1 Pre-Jurassic tectonic setting

After the final configuration of Gondwana, at 570 Ma (Cordani et al., 2003), several episodes of collision have been proposed to explain the origin of the igneous and metamorphic belts in Patagonia (Ramos, 1984, 1986; 2002, 2004; Pankhurst et al., 2006). Ramos (1988), considered that allocthonous terranes (Chilenia, Cuyania, Pampia, Patagonia and Deseado Massif, (fig. 19) were accreted to the proto-margin of Gondwana since the Early Ordovician to the Late Carboniferous, and that ophiolitic sequences in this region, correspond to the last pieces of the oceanic domain between the Proto-Gondwanian margins and the terranes (Ramos, 2000).

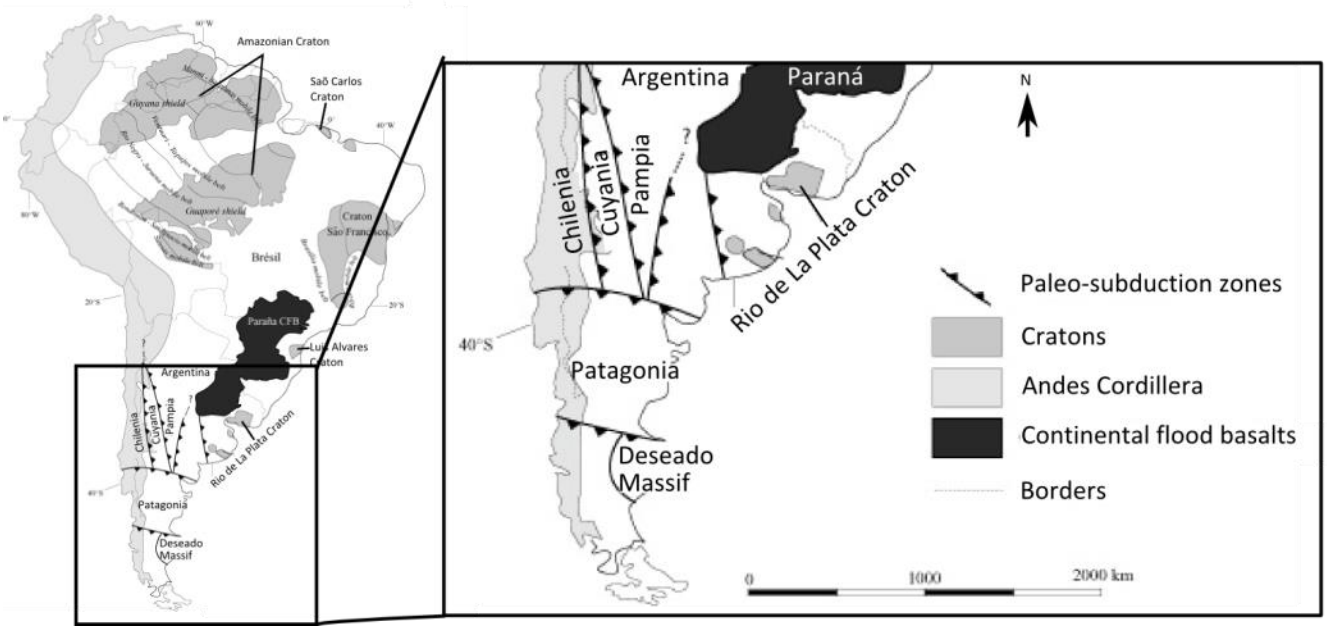

Figure 19. Allocthounous terranes distribution, proposed by Ramos (1988), paleo-suture zones and craton areas of South America. After Ramos (1988) and Dantas (2003).

The collision phases, fold belts and provenance of the "terranes" were revisited by Pankhurst et al. (2006), who concluded that the Patagonian basement was not exotic to Gondwana. A tectonic analysis later presented by Ramos (2008) partially supported this hypothesis. Accordingly, the Patagonian basement or continental crust would be represented by the North Patagonian and the para-authoctonous Deseado Massif, this last being one separated from the continental margin by a rift during the Cambrian. The accretion of this block, dated as mid Carboniferous, interrupted an exceptional magmatic arc and generated a compressive regime that lasted up to the Early Permian

(Pankhurst et al., 2006). A successive event called the "Gondwanian Orogenic Cycle" at the end of the Permian, was characterized by an important widespread felsic magmatism recorded by the *Choiyoi Province* (Kay et al., 1989) and extensional events precursory of the Gondwana break-up. This volcanism was originally interpreted as the product of crustal extension (Zeil, 1979), but Mpodozis and Kay (1990) proposed that it was related to large-scale crustal melting as a result of slab breakoff. Later studies by Ramos (2000) have interpreted this period as an early cycle of subduction followed by acid-non-orogenic magmatism associated with active extensional faulting. A Triassic rift system with a general NW-SE trend was heavily controlled by basement fabrics. An important magmatic episode of calc-alkaline affinity and bimodal compositions accompanied also the extension during the Triassic-Jurassic times in Central and Western Patagonia. This event was interpreted as the result of subduction influence, also coeval to a marginal basin in Northwest Patagonia (Neuquen basin). The mechanical interaction between different lithospheric plates at the Pre-Andean (Pacific) continental margin would be followed by slab detachment during the terminal stage of a long lived subduction zone (Pysklywec et al., 2000; Wortel and Spakman, 2000), playing an essential role in the Tr-J extension (Franzese and Spalletti, 2001).

5.2.2 Jurassic Tectonic setting

Before and during the initial rifting episodes of fragmentation of Gondwana, the supercontinent was bounded on the Pacific side by an active subduction margin (Storey et al., 1992). Three main episodes at ca. 180 Ma, 130 Ma and 100 - 90 Ma have been documented in the disintegration of the Gondwanaland continent. Particularly, the first rifting stage led to the seaway between West (South America and Africa) and East Gondwanaland (Antarctica, Australia, India and New Zealand), and the subsequent sea-floor spreading in the Somali, Mozambique and possibly Weddell Sea basins, around 155 Ma (Storey, 1995).

As well as the subduction, the early stages of rifting in Gondwana at the first fragmentation episode, were contemporaneous with the formation of a large intraplate magmatism. A long belt that stretched from southern Africa (Karoo Province) (Cox, 1992), through Antarctica (Ferrar Province)

(Elliot, 2004; 1992), to Australia (Tasman Province) (Hergt, 1989), was related to a mantle plume beneath Gondwana (Ernst and Buchan, 2001; Vaughan and Storey, 2007; Golonka and Ocharova, 2000, Storey, 1995) (fig. 20).

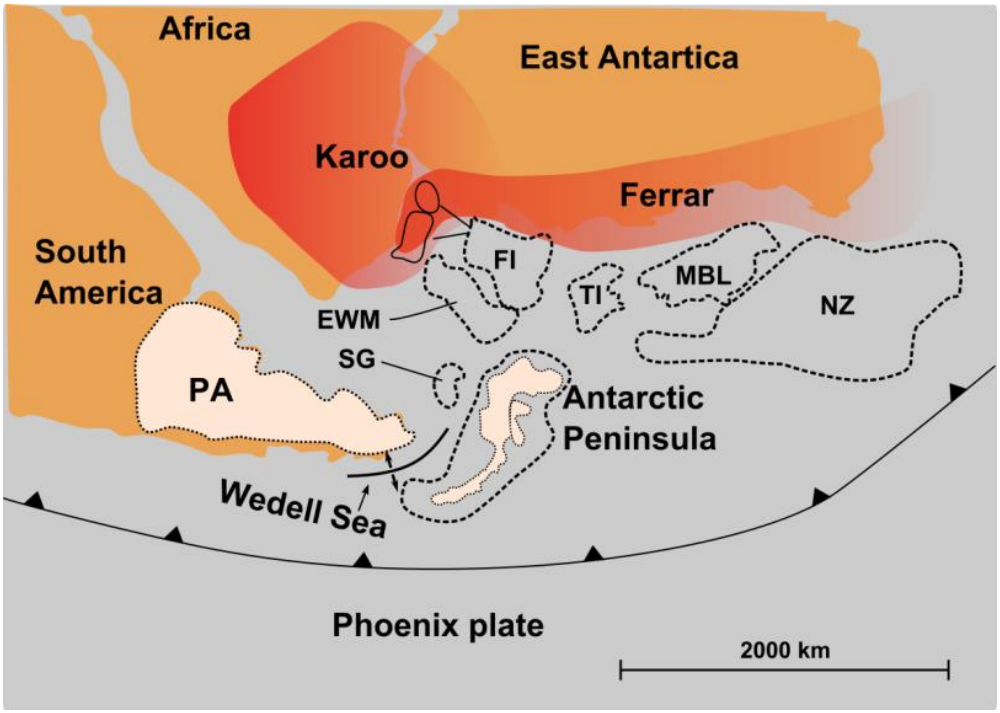

Figure 20. Tectonic configuration and main magmatic products at the formation of the Patagonian Province. Dotted lines enclose microplates whose limits are not well defined. EWMs: Ellsworth–Whitmore mountains, SG: South Georgia, FI: Malvinas-Falkland Islands, TI: Thurston Island, MBL: Marie Byrd Land, NZ: New Zealand continental platform. Modified from Pankhurst et al., 1998; after Storey et al., 1992, Vaughan and Storey (2007) and Seton et al (2012).

In the first regional studies, Pankhurst and Rapela (1995) and Pankhurst et al. (1998) considered the PA as an extensional province result of a complex tectonic configuration mainly dominated by the break-up of Gondwana. Nevertheless, later works suggested the synchrony of the first pulses of PA (188- 169 Ma) and the Karoo-Ferrar Province (184 Ma – 178 Ma; Jourdan et al., 2005, 2007) as well as a possible common origin related to a plume event. Based on a set of ^{40}Ar-^{39}Ar ages, Feraud et al. (1999) proposed that the magmatism in PA occurred with a regular decreasing pattern of the ages from the ENE (187 Ma) to the WSW (144 Ma) through NNW-SSE oriented half grabens (fig. 21). Such event would culminate with the opening of the Rocas Verdes marginal basin in the SSW of the Province. In this model, the progression of the volcanism is interpreted as the result of physical variations in a subduction zone and the thermal effect of the Karoo-Ferrar plume. A set of U-Pb, Rb-Sr

and ^{40}Ar-^{39}Ar ages were presented by Pankhurst et al. (2000), defining three main pulses of activity in Patagonia and the Antarctic Peninsula: V1 at 188 Ma -178 Ma; V2 at 172 Ma – 162 Ma and V3 at 157 Ma – 153 Ma. Based on these data, the authors argued that the magmatism migrated away from the Karoo mantle plume towards the Proto-Pacific margin during the break-up of Gondwana. Additionally, geochemical constrains for upper crustal incorporation on V1 was interpreted as an evidence of anatexis in the origin of PA. In this scenario, a plume-head would have been the heat supplier and the crustal thinning due the break-up setting should have facilitated the anatexis. Riley et al. (2001), supported this hypothesis also adding that mafic underplating could had place associated with the Discovery-Shona-Bouvet group of plumes thought to have originated the Karoo Province.

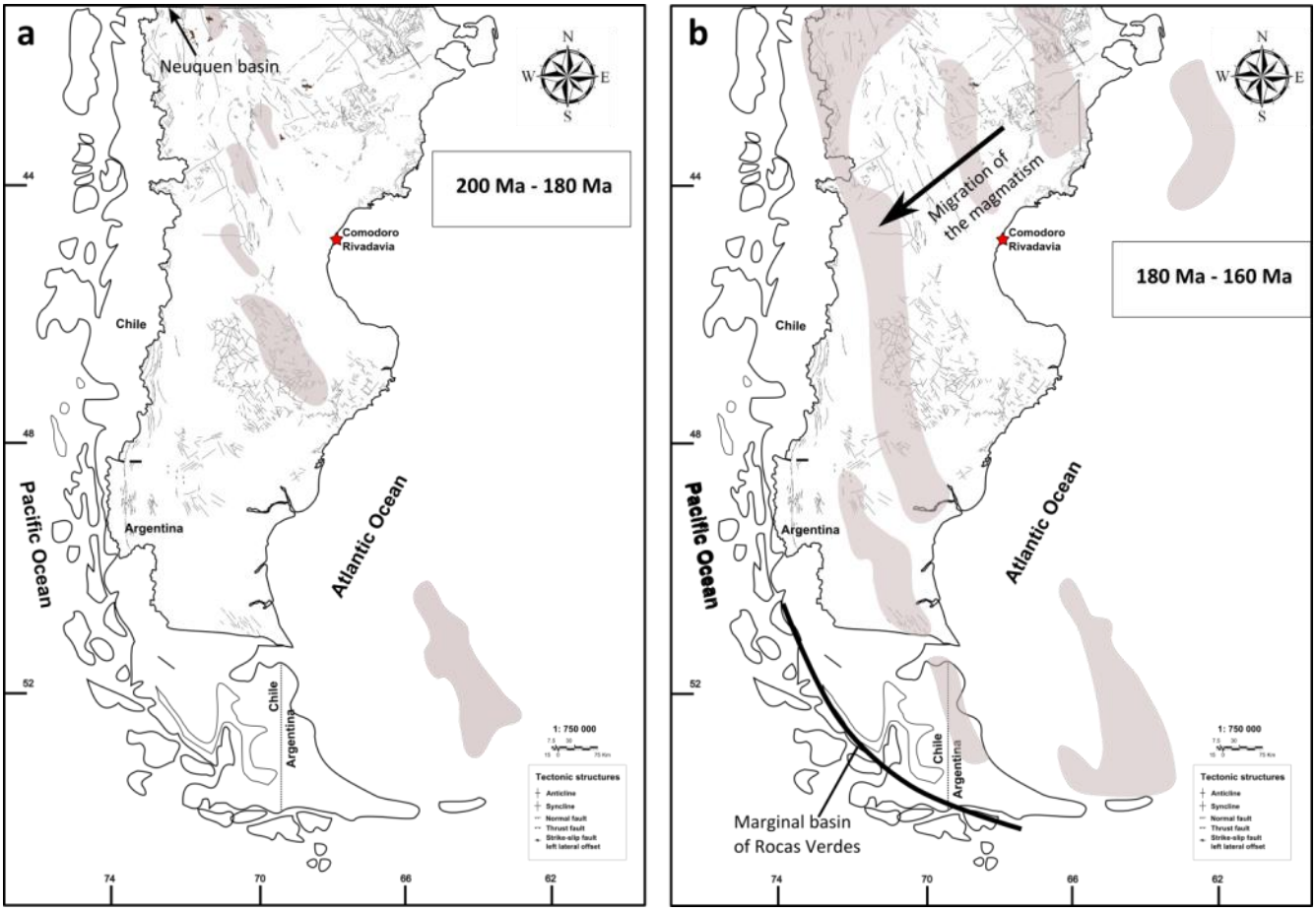

Figure 21. Illustration of the half graben structures (shaded zones, after Uliana and Biddle, 1988) and migration of the magmatism at Early Jurassic (A) and Middle (B) Jurassic times. Modified from Feraud et al (1999). Location of the Neuquen basin is shown according to MPodozis and Ramos (2008).

6. Field work and sampling

A collection of 337 samples of different Jurassic magmatic units spread along the Patagonian Province was considered is this study. Three sets of samples compose this collection. One of them consists of 57 samples collected for this research in 2012 during an E-W transect in the Chubut Province (northern Patagonia). A second and a third set were previously sampled by Prof. Giuliano Bellieni in the Macizo del Deseado (Central Patagonia), and by Prof. Herve Bertrand from northern to southern Patagonia. These samples were included in this project thanks to an academic collaboration with the researchers.

The study area was divided in two major regions: The Chubut area and the Deseado Massif. Samples from the first area correspond to 4 major physiographic zones recognized in the Province: 1) The Cordilleran region, 2) Pre-Cordillera, 3) the Cañadon Asfalto basin and 4) The Somuncura Massif. Accordingly, rocks correspondent to Loncotrapial, Cresta de los Bosques, Lago la Plata and Piltriquitron Formation were acquired in the regions 1 and 2. Samples from Cañadon Asfalto were collected in the region 3 whereas those from Marifil were obtained in the region 4. Samples from Chon Aike and Bajo Pobre Formation were collected in the Deseado Massif. The location of the total samples and the physiographic regions are shown in the fig. 22.

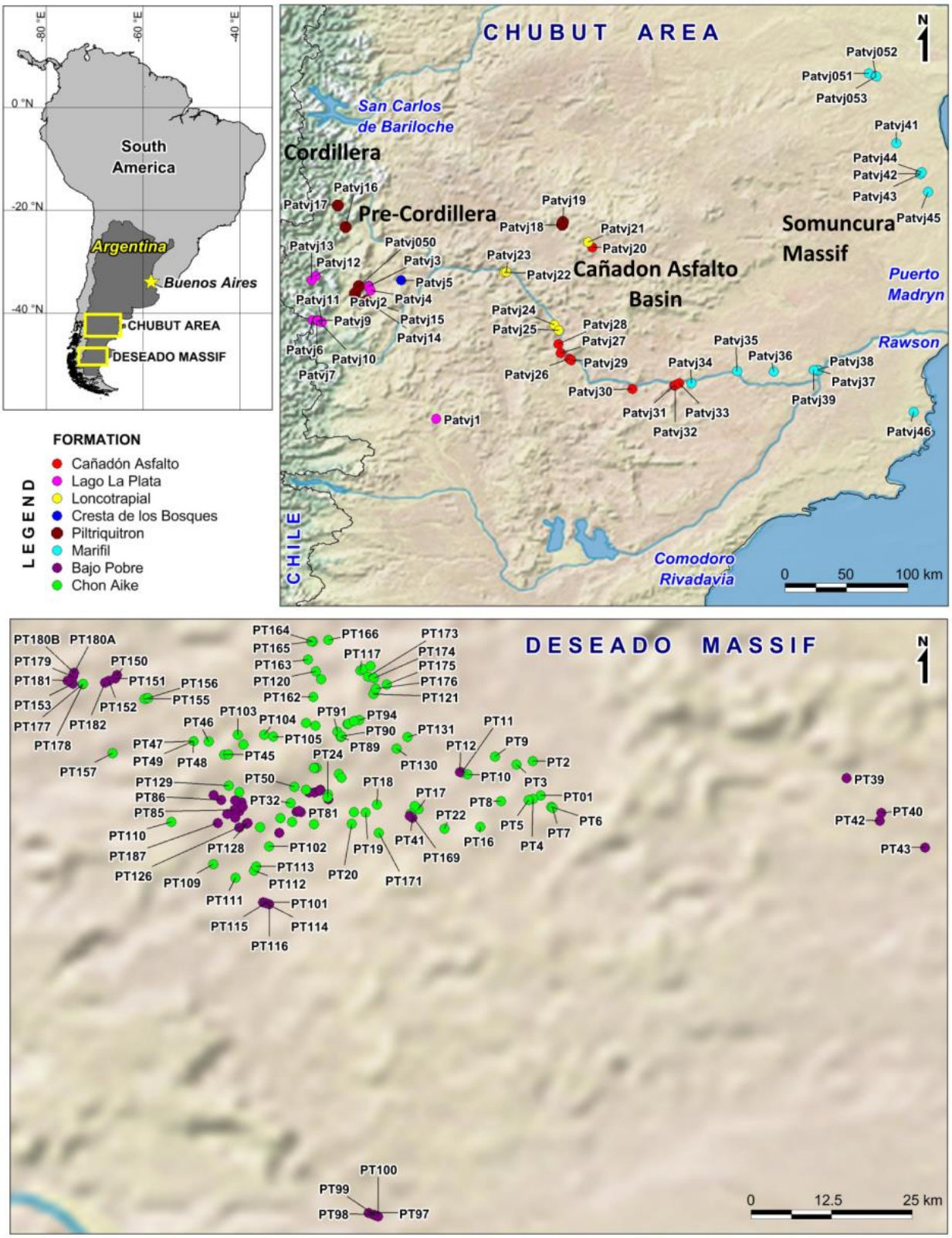

Figure 22. Sample location map. Jurassic magmatic rocks collected in the Chubut area and Deseado Massif in the Patagonian Province, Argentina.

7. Petrography

A collection of 337 samples of different Jurassic magmatic units spread along the Patagonian Province is considered is this study. It consists of samples obtained in a E-W transect in the Chubut Province (northern Patagonia) during this project; and a second and third set previously collected by Prof. Giuliano Bellieni in the Macizo del Deseado (Central Patagonia), and by Prof. Herve Bertrand along the Province (northern to southern Patagonia). Previous collections were included in this study thanks to an academic collaboration with the researchers.

After a careful examination of all samples, 36 rocks were selected as the most representative and well preserved to perform the different analysis carried out in this study. A petrographical analysis done on these selected rocks is described below in two main sections called *Mafic and felsic rocks* in agreement with the bimodal composition of the Province. In order to complement the phase/mineralogical identification, the petrographic analysis was combined with the use of the MLA electron microscope (FEI Quanta 600 MLA ESEM) and the electron microprobe CAMECA SX 100 at the University of Tasmania, Hobart, Australia, as well as with the electron microprobe microanalyser (EPMA) JEOL 8200 Superprobe at the Steinmann Institut, University of Bonn. The analysis were assisted by Dr. Karsten Goemann and Dr Sandrin Feig, University of Tasmania, and by Prof. Thorsten Nagel and the PhD candidate Sacha Sandmann at the University of Bonn. Mineral proportions were calculated based on grain-counts of each sample and an estimated average for each unit.

7.1 Mafic rocks

In the Patagonian Province, mafic volcanic rocks are represented by basaltic and andesitic lavas and some dykes of the Cañadon Asfalto, Loncotrapial and Bajo Pobre Formations. Mafic plutonic rocks are scarce and only reported for the Cresta de los Bosques Formation.

7.1.1 Cresta de los Bosques Formation

This unit consists of discontinuous lateral intrusions propagated as sills along a ca. NS direction, in the East margin of Sierra de Tepuel and Sierra de Tecka, Cordilleran region of the Chubut Province. Regionally, it crops out as a discontinuos cumulitic gabbro intruding the volcanosedimentary sequence of Osta Arena Formation, of Toarcian age (Musacchio and Riccardi, 1971; Blasco *et al.,* 1979; Ploszkiewicz, 1987).

Lateral intrusions from this unit are holocrystalline, hipidiomorphic-granular textured rocks of medium size grain (1-2mm) composed of plagioclase ($_{An88-84}$), augite ($Wo_{39-33}En_{59-51}$) enstatite (Wo_4En_{21-15}) and olivine (Fo_{81-76}) mainly. As a characteristic feature, anhedral and subhedral phenocrysts of orthopyroxene and clinopyroxene enclose allotriomorphic olivine forming a poikilitic texture (fig. 23). Subhedral intercumulus plagioclase fill part of the spaces between the mafic phases. Ondulatory extinction and zonation in both pyroxenes are also common and suggest deformation events during the crystallization process. Accessory and fine minerals spread along the rock were identified with the electron microscope and comprise phlogopite with ilmenite inclusions or intergrowth with orthopyroxene and plagioclase; fine phenocrysts of apatite, badaleyite, zirconolite and pirrotine as well as primary chalcopyrite and pentlandite as inclusions in olivine. Carbonate crowns surrounding olivine phenocrysts (Fig. 1) and serpentine veins in the same phase are the most common secondary association followed by epidote. Nonetheless, the rocks are well preserved and alteration is considered as negligible. No melt inclusions were identified in phenocrysts. According with the mineral proportions, the rocks was classified as *poikilitic olivine gabbro.*

Mineral proportions:

Cpx (%)	Opx (%)	Pl (%)	Ol (%)
23	18	23	36

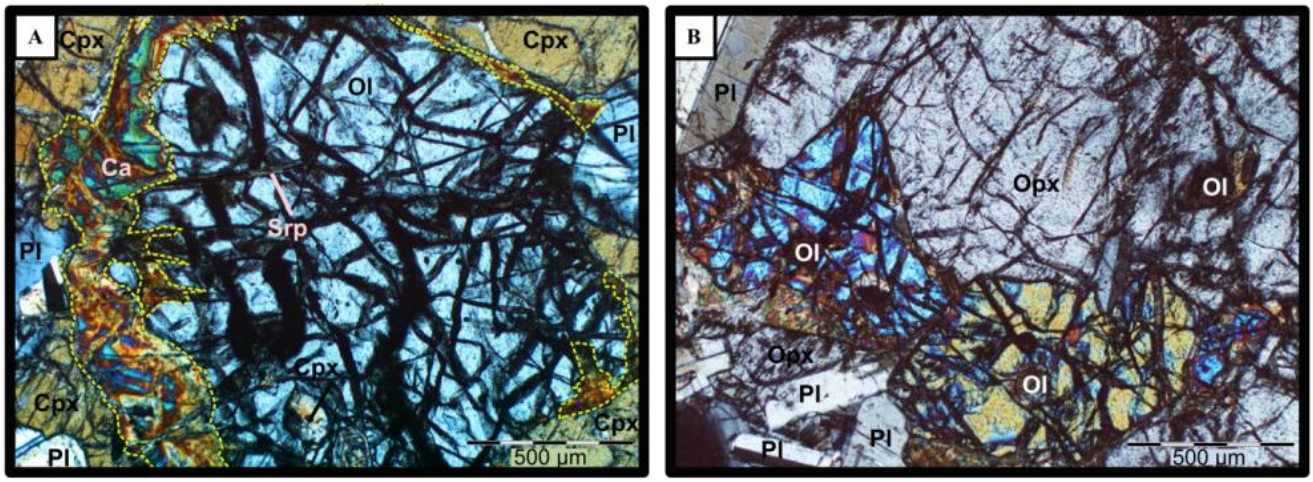

Figure 23. Cross polarized light images of Olivine (Ol) with rims of carbonates and serpentine (Srp) veins and enclosed by clinopyroxene (Cpx) (A) and orthopyroxene (Opx)(B).

7.1.2 Cañadón Asfalto Formation

Lavas of the Cañadon Asfalto Formation crop out in the homonymous basin , in the northen-central part of the Chubut Province. They are brown pilotaxitic and pale intersertal textured rocks with idiomorphic plagioclase (An_{69-50}) and allotriomorphic – inequigranular augite ($Wo_{40}En_{47}$) and enstatite (En_{74-64}). Fresh olivine (Fo_{84-76}) is scarce but present in some samples. It consists of fine grains (≤0.5mm) intergrown with ortho- and clinopyroxene, fractured, sometimes zoned, with overgrowth of chromite, ilmenite and crystallized melt inclusions (fig. 24a). Anhedral resorbed olivine grains are more frequent, they have cores of serpentine or carbonates with preserved inclusions of chromite and rims of iddingsite and are sometimes also replaced by opaques (magnetite) (fig. 25b). Olivine-free rocks show clusters of pyroxenes forming a glomeroporphiric texture and enclose euhedral laths of plagioclase in ophitic texture. Subhedral tabular augite and euhedral prismatic enstatite are commonly zoned and exhibit inclusions of ilmenite, titanomagnetite and magnetite. Sieve texture with dissolution of the non-equilibrium center of the crystal and zonation in plagioclase is a common feature in most samples of this unit (fig. 25c) either due to decompression, change of water content or magma mixing. Accessory minerals include fine apatite and less frequent zircon. Abundant crystallized melt inclusions in pyroxenes and plagioclase are characteristic of the Canadon Asfalto fm. (Fig. 25d). Based on their mineral proportions, lavas of this unit are classified as *olivine basalt and basalt.*

Mineral proportions:

Mtx (%)	Cpx (%)	Opx (%)	Ol (%)	Pl (%)
51	11	9	14	14

Mtx (%)	Cpx (%)	Opx (%)	Pl (%)
49	17	12	22

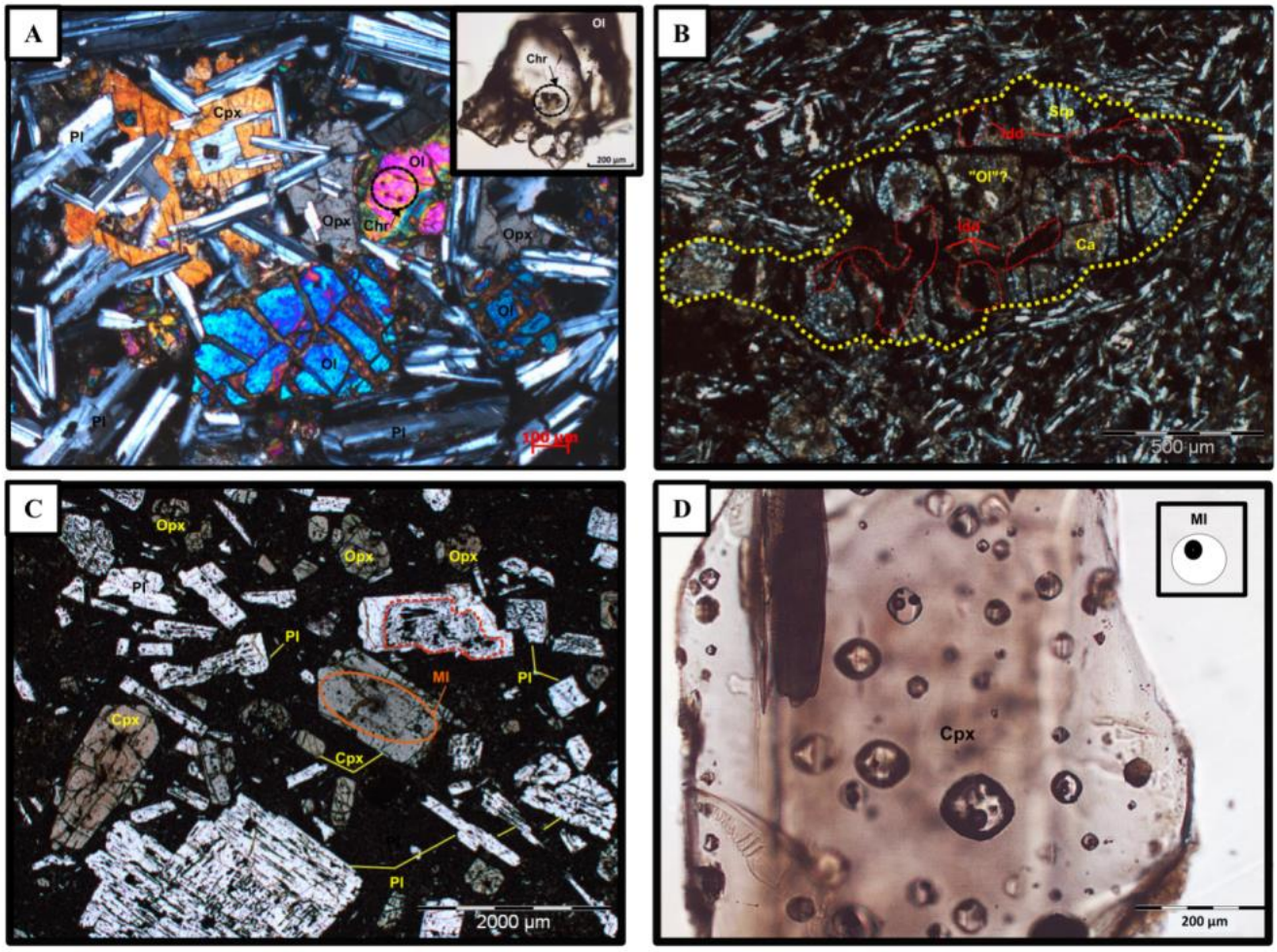

Figure 24. A) Clinopyroxene (CPx), orthopyroxene (Opx) and olivine (Ol) (Fo_{84}) with chromite (Chr) inclusions in intersertal groundmass. B) Olivine replaced by carbonates (Ca) and serpentine (Srp) in intersertal matrix. C) Clino and orthopyroxene with melt inclusions (MI), corroded plagioclase (Pl) with sieve texture coated by euhedral growths as forming during magma mixing. D) Melt inclusions in clinopyroxene. A, B, C: Cross polarized light. D: Plane polarized light.

7.1.3 Bajo Pobre Formation

Volcanic rocks from Bajo Pobre Formation were collected in the Macizo del Deseado, Santa Cruz Province. They consist of brownish pilotaxitic and intersertal groundmass textured with allotriomorphic phenocrysts of plagioclase (An_{83-73}), orthopyroxene (En_{56-73}), clinopyroxene ($Wo_{44-37}En_{47-39}$) and ocassional xenocrysts of anhedral mafic phenocryst resorbed (olivine?). Disequilibrium features like zonation and exsolution textures are frequent in the main phases. Orthopyroxene phenocrysts are often zoned. At the electron microscope such variation was recognized as normal and reverse zoning which varies from Mg-rich rims to more evolved cores (fig. 25a). Fresh orthopyroxene crystals enclose resorbed olivine with discontinuous rims and fresh euhedral chromite inclusions in the cores (fig. 25b). Olivine is frequently replaced by carbonates and/or serpentine. Olivine free rocks show clusters of euhedral-subhedral tabular clinopyroxene, prismatic twined orthopyroxene and plagioclase in glomeroporphiric texture (fig. 25c). Fine clinopyroxene overgrown in ferro-augite form crowns and simplectitic texture. Plagioclase is often zoned and presents sieve texture with spongy rims. Accessory minerals identified with the electron microscope comprise apatite in the groundmass and as inclusion in pyroxenes, lamellar natural iron probably related to exsolution from olivine, and titanomagnetite as inclusion in pyroxenes and resorbed olivine. Melt inclusions are usually crystallized, with irregular rims and altered were recognized in pyroxenes and plagioclase (fig. 25d). According with the mineralogy, mafic rocks of the Bajo Pobre Formation are classified as *andesitic basalts.*

Mtx (%)	Cpx (%)	Opx (%)	Pl (%)
43	19	12	26

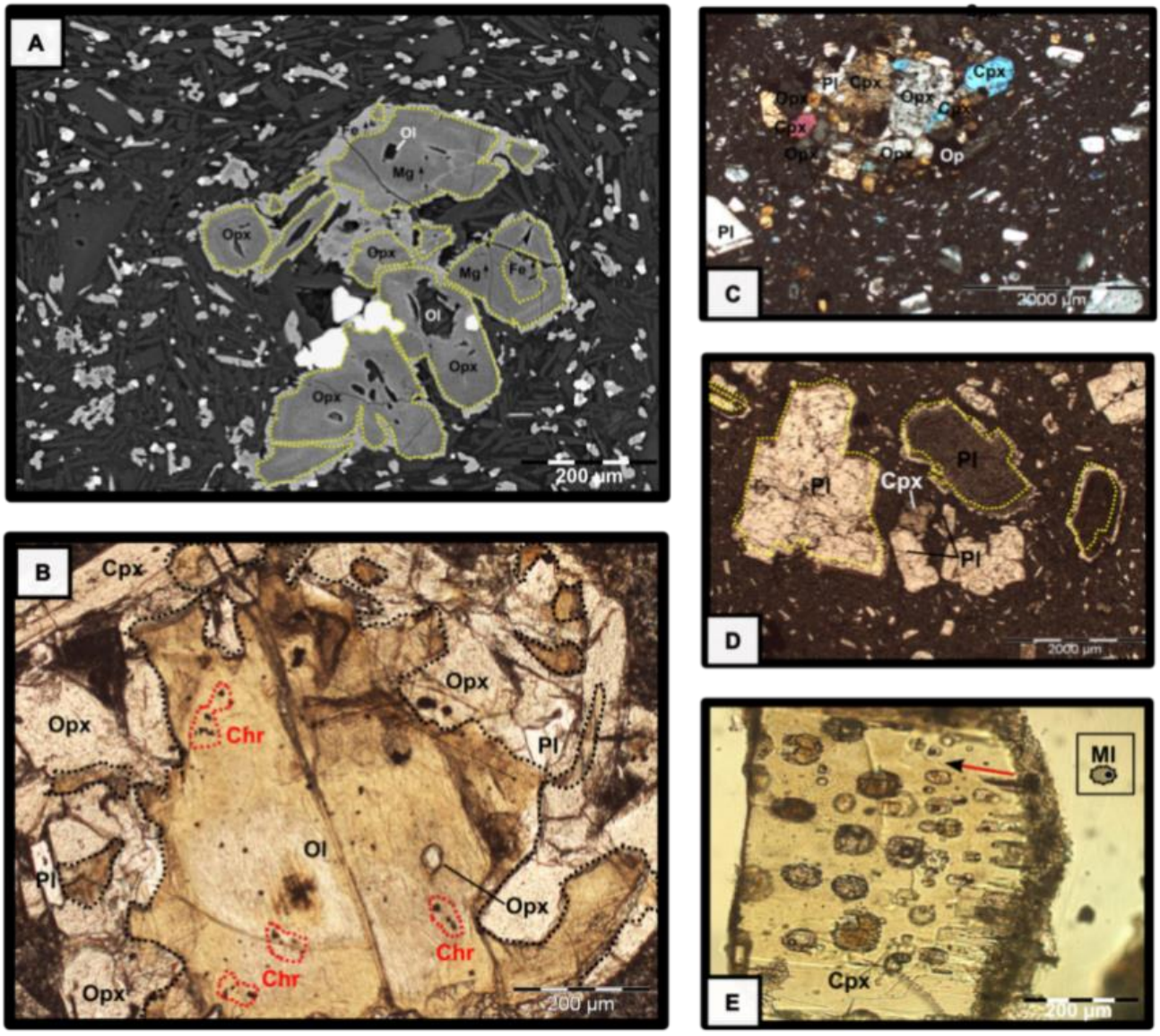

Figure 25. A) **Backscattered** electron **image of n**ormal and reverse zoning in Orthopyroxene (Opx) embedded in intersertal groundmass. B) Resorbed olivine (Ol) with chromite (Chr) inclusions enclosed by Opx. C) Glomeroporphiric texture. D) Zoned and resorbed plagioclase (Pl) in pilotaxitic matrix. E) Crystallized, fractured, altered and oriented melt inclusions (MI) in clinopyroxene (CPx). (B, D, E:plane polarized light; C:cross polarized light).

7.1.4 Loncotrapial Formation

Rock samples from this unit were collected in the Cañadón Asfalto basin, in the Chubut Province. They represent mafic lava flows, dykes and autobreccias of extrusion. Lava flows are porphiric with a dark gray microlitic-glassy flux oriented groundmass. Differing from the other units, phenocrysts of these rocks consists exclusively of amphibole (probably hornblende) and plagioclase (fig.26a). Amphibole is

inequigranular, with fine to medium grain size (<1mm-2mm), idiomorphic, hexagonal and pleocroic ranging from light to dark green. Fractures in amphibole occur mainly along the cleavages. Zoning and pseudo simplectitic textures with lamellar feldspar (fig. 26b) are also frequent as well as opaques replacing the rims. Plagioclase is fine grained, subhedral and tabular with corroded aspect and spongy rims. Apatite is present as accessory phase. According with the mineral proportions the rock is classified as *andesite.*

Mtx (%)	Amp (%)	Pl (%)
59	18	23

Dark rimmed, subangular, inequigranular and oligomictic fragments of oxidized andesitic lava are embedded in fine fragments of microlitic plagioclase and devitrified glassy groundmass (fig 26b). Idiomorphic hexagonal phenocrysts of amphibole, highly fractured with well-developed rims of opaques are less frequent but present. Minor subhedral plagioclase shows pervasive sieve texture.

Based on field and petrographic observations, this rock is named andesitic autobreccia.

Mtx (%)	Clasts (%)	Pl (%)	Amp (%)
31	38	15	19

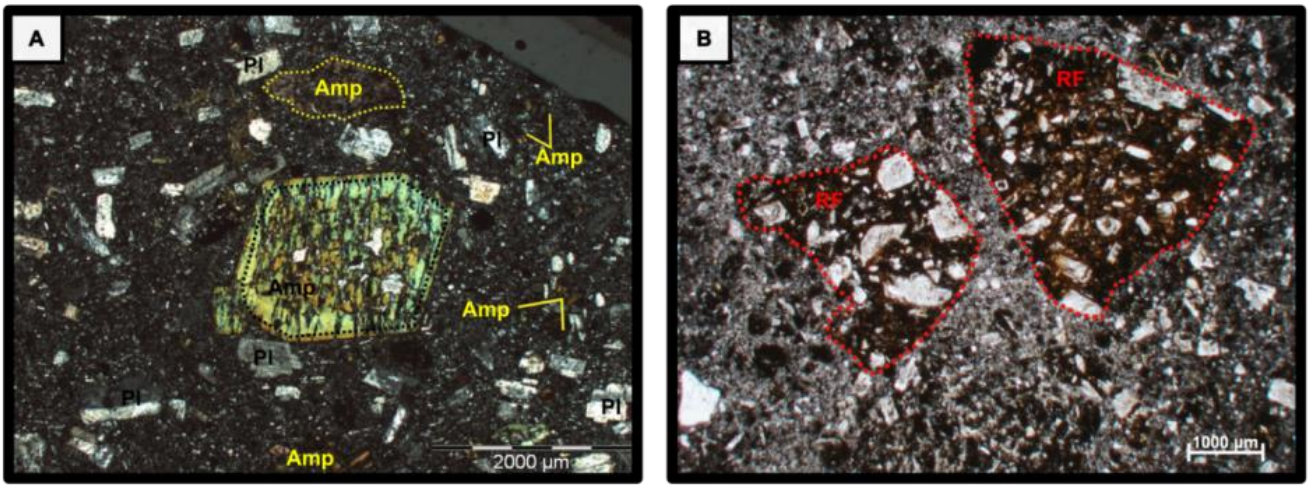

Figure 26. A) Amphibole (Amp) and plagioclase (Pl) phenocrysts in trachytic groundmass. Zoned and simplectitic amphibole at the center. B) Lithoclasts of andesitic rock in autobreccia. RF: Rock fragments. A: Cross polarized light. B: Plane polarized light.

7.2 Felsic rocks

Jurassic felsic rocks of the Patagonian region are present as thick levels of volcanoclastic deposits and rhyolitic lava flows of the Marifil and Chon Aike Formations.

7.2.1 Marifil Formation

Samples from ignimbritic deposits and less frequent rhyolitic lava flows from the Macizo de Somuncura characterize this Formation.

Ignimbritic depositis of the Marifil Formation comprise dark brown reddish groundmass of glass, shards and pumice fragments (fig. 27a). Vitroclastic texture and granophyric mosaics of quartz and feldspar are also common as groundmass. In all cases, sampled ignimbrites were crystal rich with phenocrysts of coarse (1mm-2mm) bipyramidal and anhedral quartz, fine (<1mm) sheet-tabular brown biotite and less frequent microcline feldspar. Devitrified and recrystallized welded shards, fiammae as well as fractured and deformed quartz, evidence deformation of the rock. Resorbed amphibole and mafic xenocrysts are embedded in the matrix, oxidized and replaced by opaques (fig. 27b). Accessory minerals include apatite and zircon as single grains or overgrown in crystal-rims. Glassy and crystallized melt inclusions are hosted by quartz phenocrysts, sometimes related to secondary fracturing (Fig. 27g).

Glass levels intercalated with the ignimbritic deposits are red colored, lightly devitrified with scarce phenocrysts of anhedral quartz.

Pale brown oligomictic breccias of devitrified pumiceous matrix and microlitic feldspar and quartz enclose inequigranular blobs of alotriomorphic plagioclase, quartz and minor fine biotite.

Felsic lavas of the Marifil Formation present in thin section a brownish foliated and colorless perlitic texture. Coarse (1mm-2mm) phenocrysts of bipyramidal (beta) quartz, feldspar, plagioclase and less frequent brownish alotriomorphic biotite are commonly embedded in the groundmass (Fig. 27b, 27e). Foliated rhyolites include fine xenocrysts of resorbed mafic minerals. Rhyolites with perlititic texture comprise arcuate, overlapping and intersecting cracks. Quartz with vermicular resorption and

deformed biotite are affected by the perlitic fracturing (Fig. 27E). High contents of water (to 4 wt.%) are related to the formation of the perlitic texture. Coarse, altered and internally cracked melt inclusions are hosted in quartz.

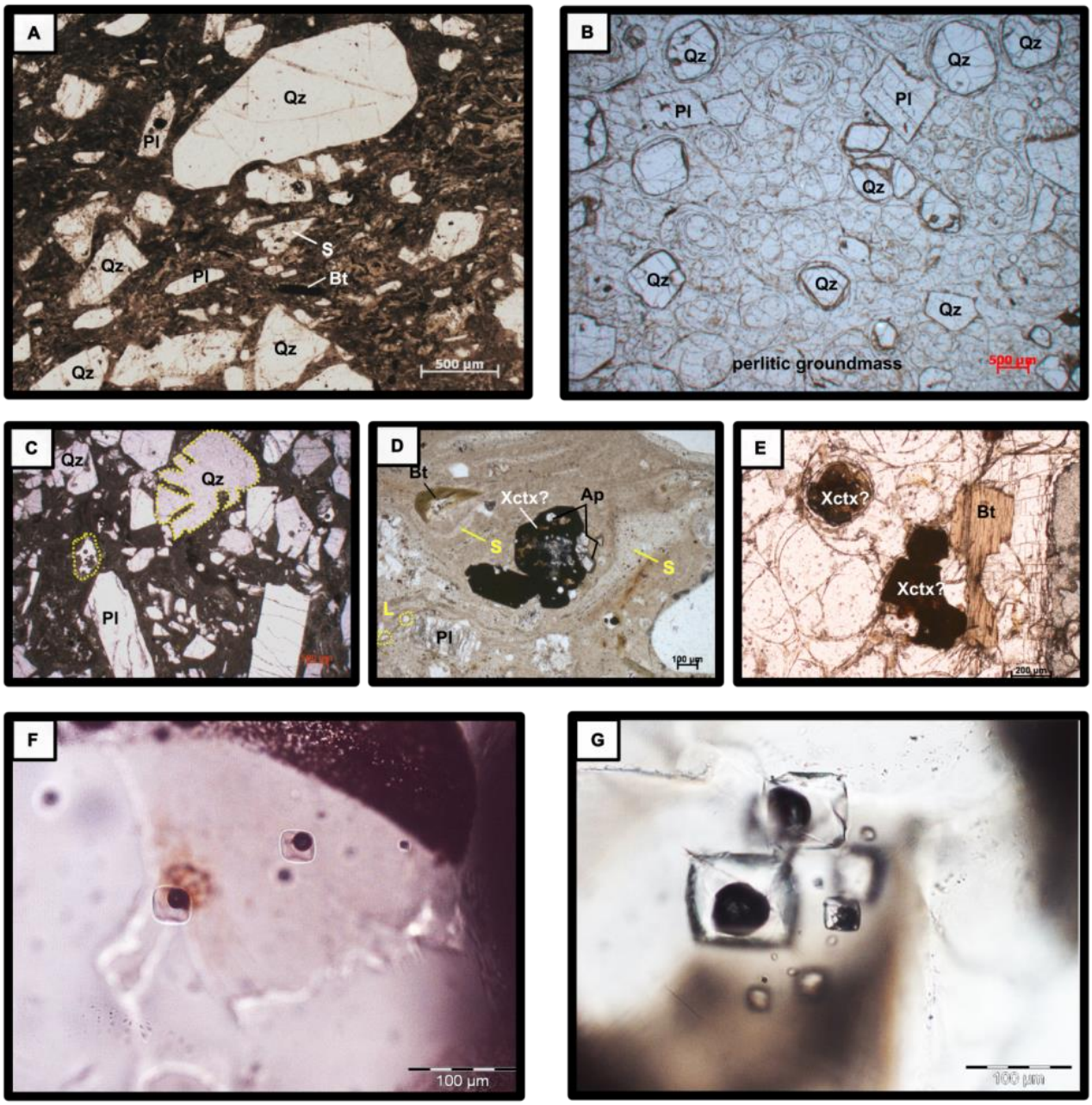

Figure 27. A) crystal rich ignimbrite with deformed and compacted welded shards. B) Perlitic texture enclosing phenocrysts of quartz (Qz) and plagioclase (Pl). C) Poor sorted ignimbrite with vermicular quartz resorption. D) Ferromagnesian xenocrysts (xctx) embedded in glassy matrix with lapilli (L) and welded shards (S). E) Ferromagnesian xenocrysts and biotite embedded and deformed by perlitic matrix. F) Glassy melt inclusions (MI). G) Cubic crystallized MI.

7.2.2 Chon Aike Formation

Samples from the Chon Aike Formation represent mainly series of ignimbritic deposits from the Macizo del Deseado, Santa Cruz Province. They consist of crystal rich ignimbrites that comprise coarse bipyramidal, colorless and smoky quartz, inequigranular subhedral plagioclase, sanidine and pleocroic (from greenish to reddish) biotite in a brown matrix composed of glass shards (Fig. 28a). Cuspate, platy and recrystallized shards are often stretched, flattened and deformed around the phenocrysts evidencing compaction and primary emplacement. Stretched brown eutaxitic textured rocks are also common. They enclose welded and deformed lapilli tuff with recrystallized internal vesicular microstructure and local axiolitic devitrification (Fig 28b). Apatite and zircon are the main accessory minerals. Random broken and resorbed ferromagnesian phases are replaced by opaques and embedded in the matrix by flux textures with rotational structure around the grains. Lithophysaes in quartz and occasional organic matter are also present. Pervasive fracturing in all present phases, myrmekitic textures in plagioclase, oxidation in biotite and devitrification are regular secondary features. Glassy and crystallized melt inclusions are hosted in quartz (Fig 28c). Some of them might be related or affected by strong fracturing in quartz (Fig 28d).

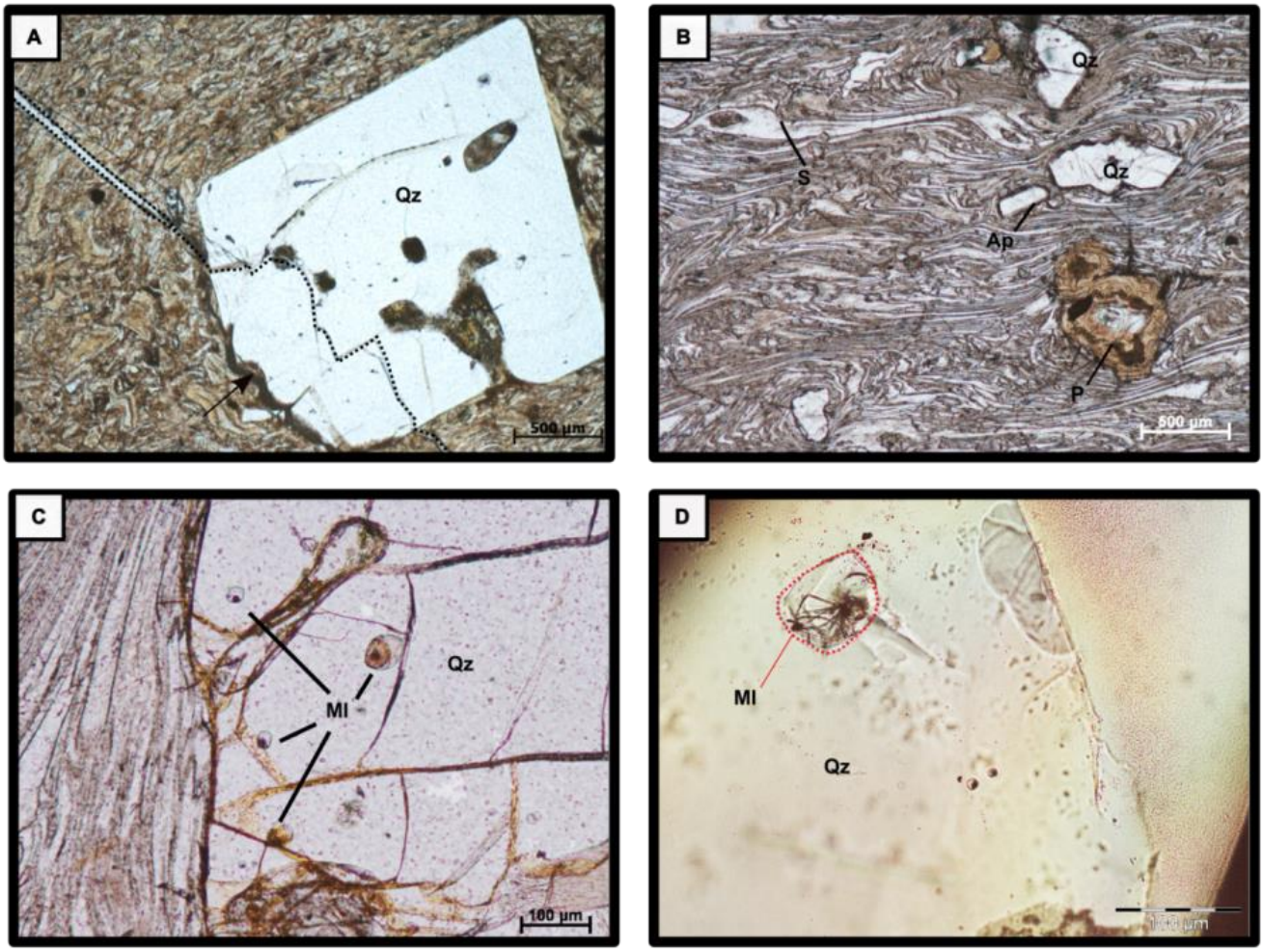

Figure 28. A) Ignimbrite with welded shards, stretched and deformed borders of large quartz (Qz) affected by secondary vein. B) Banded obsidian with undeformed shards, lapilli (P) with axiolitic texture affected by rotational structure. C) Melt inclusions (MI) related to fracturing. D) Internal fracturing in melt inclusion maybe related to fast quenched in crystal rich ignimbrite.

8. Mineral chemistry

Compositional analyses on the main mineral phases present in the volcanic rocks of the Patagonian Province are described in this chapter. Data on olivine and chromite were acquired with an electron microprobe (Cameca SX100 (TCP/IP Socket)) equipped with 5 tunable wavelength dispersive spectrometers, at the University of Tasmania, Hobart, Australia. Compositions of orthopyroxene, clinopyroxene and plagioclase were obtained by electron probe microanalyser (EPMA) JEOL 8200 Superprobe of the Steinmann Institut, University of Bonn. The measurements were assisted by Dr. Karsten Goemann and Dr Sandrin Feig at the University of Tasmania, and by Prof. Thorsten Nagel and Sascha Sandmann, PhD candidate, at the University of Bonn. Unpublished analysis provided by Giuliano Bellieni performed at the University of Padova are also included in this chapter.

8.1 Olivine

The abundance of olivine phenocrysts in the Patagonian Province is scarce. Normative and fresh modal olivine occurs only in the poikilitic gabbros of Cresta de los Bosques Fm (patvj 005) and in one sample of basalt from Cañadon Asfalto Formation (patvj 027). Both samples are also normative in hyperstene and diopside. Rare, resorbed and replaced by orthopyroxene and altered to carbonates, iddingsite and serpentine are the common forms of olivine in most of the mafic units. 16 unzoned crystals from patvj 005 and 38 from patvj 027 samples were analyzed on thin section and grain mount, respectively (Appendix 1). Obtained compositions are relatively low in forsteritic component (Fo) and vary from Fo_{81} to Fo_{76} in patvj 005, and in a large range between Fo_{84} and Fo_{63}, in patvj 027 (fig. 29). At a given MgO (or Fo), patvj 005 olivine are slightly enriched in SiO_2 abundances (43.54 to 39.62 wt.%) compared to patvj 027 (42.80 - 31.31 wt.%), and are depleted in CaO (0.18-0.05 vs. 0.28 - 0.14 wt.%) (not shown).

Similar forsterite contents (Fo_{84-75}) in the two samples occur despite significantly different whole-rock compositions in terms of Mg# (Mg# [100*Mg/(Mg+Fe)]), an effect may be related to MgO poor melts in the case of patvj 27 (Li and (Li and Ripley, 2010) and mineral accumulation in patvj 005. Considering

a bulk distribution coefficient (K_D) of Fe-$Mg^{Ol/liq}$ of 0.30 ± 0.03 (Roeder and Emslie, 1970; Ulmer, 1989), olivine crystals from rock patvj 027 range from Fo higher than expected at equilibrium to Fo below equilibrium. In contrast, patvj 005 olivine phenocrysts (below the equilibrium curves) suggest a re-equilibration process of the crystals or accumulation of mafic mineral, common features in slow cooling faneritic rocks (fig 29).

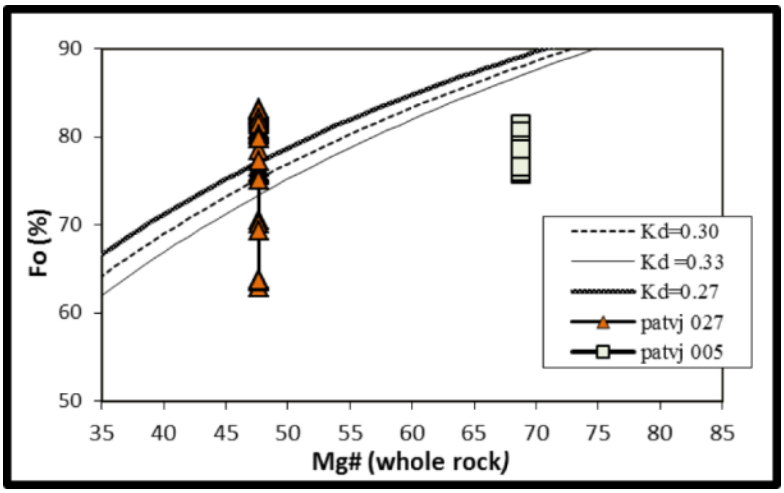

Figure 29. Forsterite (Fo) content (%) of patvj 027 and pat vj 005 against Mg# in the whole rock.

Mn and Ni contents show linear trends with Fo changes (Simkin and Smith, 1970). In particular, Mn is negatively correlated with Fo and shows values that vary from 1624 ppm to 5390 ppm in patvj 027, and from 1688 ppm to 3013 ppm in patvj 005 (fig 30b). On the contrary, a positive trend is described by Ni vs Fo variations for patvj 027 (Ni = 126 ppm to 1764 ppm) (fig 30a), while Ni contents in patvj 005 range from 660 ppm to 1603 ppm and are not correlated with Fo variations. Being relatively enriched in Mn and depleted in Ni, both samples differ from MORB or LIP - OIB rocks (Sobolev et al., 2007) probably (also) as an effect of quite evolved compositions of the analyzed olivine crystals (O'Hara, 1968). Overall variations of Mn (patvj 027: 1764 – 126 ppm; patvj 005: 1603- 660 ppm) and Ni (0.22- 0.01 and 0.20- 0.08) in both samples contrast with remarkable differences in terms of the rock compositions (patvj 027, Mg#=~48; patvj 005 (Mg#= ~69) and reflect the more differentiated character of patvj 027.

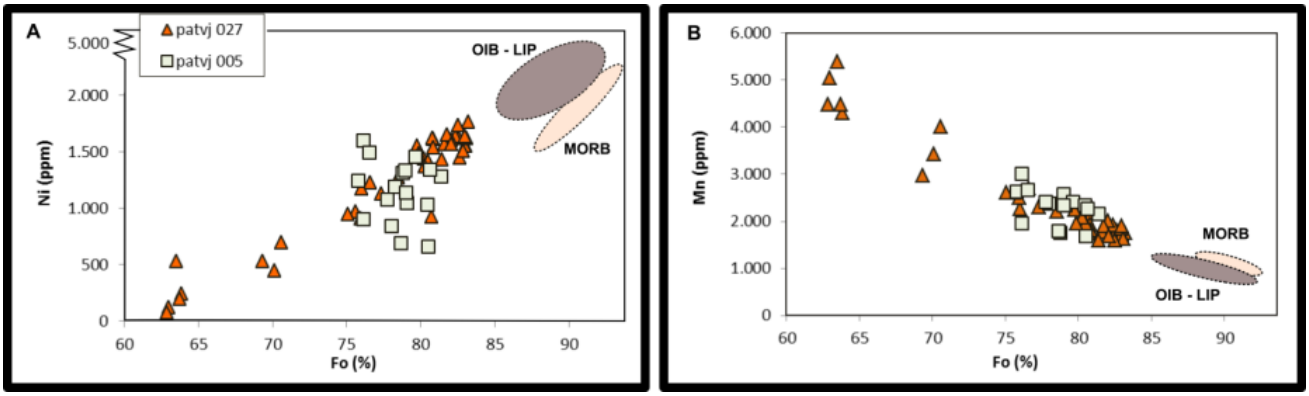

Figure 30. Ni (A) and Mn (B) concentrations (ppm) plotted against forsterite content (%) in olivine from Cañadon Asfalto Formation (patvj 027) and Cresta de los Bosques Formation (patvj 005). Fields of MORB and OIB – LIP, correspondant to within plates magmas of thin and thick lithosphere from Sobolev et al (2007).

Ratios of Ni/Mg/Fe and Ca/Fe (fig 31a and 31b), in the most forsteritic grains (Fo_{84-80}) of the two units, do not show any trend with respect to Mn/Fe. Depleted values of Ni/Mg/Fe overlap all fields plotted by Sobolev et al. (2007) in a restricted range. Unlike Ni and Mn, Ca is not strongly dependent of Mg content but of depth of crystallization (Simkin and Smith, 1970). The observed low Ca/Fe ratio is then in agreement with the iron-enriched whole-rock compositions and the differentiated character of the rocks. Despite the large effect that the degree of olivine fractionation and the low forsteritic compositions could have on the described ratios, Mn/Fe is the parameter less dependent on them (Sobolev et al., 2007). Large variations of Mn/Fe from 1.62 to 1.18 in patvj 005 and from 1.55 to 1.17 in patvj 027 are comparable to those from MORB and within plate basalts.

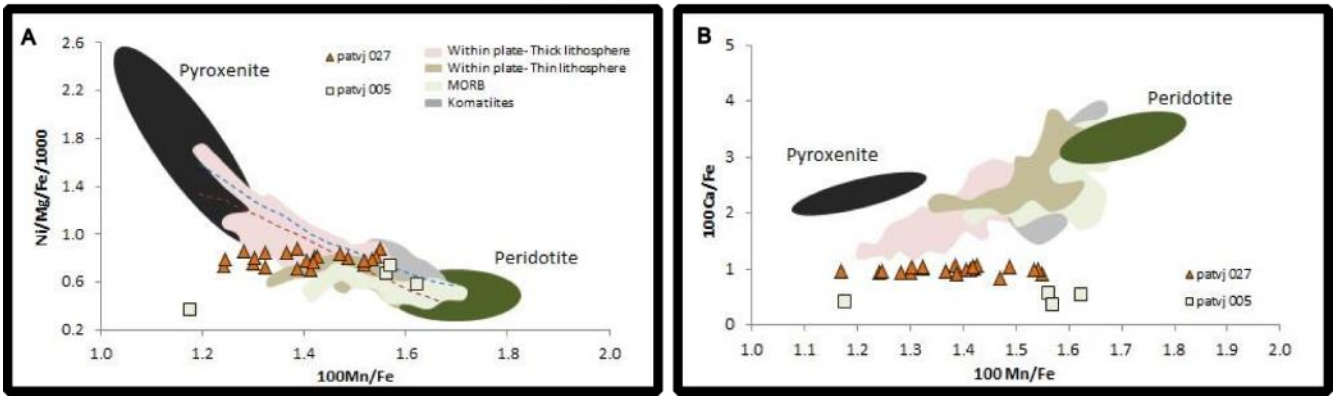

Figure 31. Composition of Ni/Mg/Fe (a) and Ca/Fe (b) against Mn/Fe in olivine from Cañadon Asfalto Formation (patvj 027) and Cresta de los Bosques Formation (patvj 005) compared with different tectonic settings (Modified from Sobolev et al 2007). Blue and red dotted lines correspond to MIX Herzberg (Herzberg and O'Hara, 2002) and MIX Kinzler (Kinzler et al., 1990).

8.2 Chromium-spinel

Chromium spinel is present in some of the mafic volcanic rocks from the Patagonian Province as inclusion in phenocrysts of fresh (patvj 027) and resorbed olivine (pt40, geo8, pt101) or orthopyroxene (patvj 020). Commonly host olivine is replaced by carbonates and presents crowns of orthopyroxene (pt 40). Despite the strong alteration, fresh chromium-spinel is present within the olivines as very fine grains (1 µm - 20 µm) of cubic shape and dark brown colour (fig. 32).

The inclusions were identified by MLA electron microscope (FEI Quanta 600 MLA ESEM) of the University of Tasmania and measured by EPMA at the same institution. The calibration was monitored using the international standard USNM117075. A beam focused was used, and operating conditions were 40 degrees take-off angle, and a beam energy of 15 keV. The beam current was 30 nA.

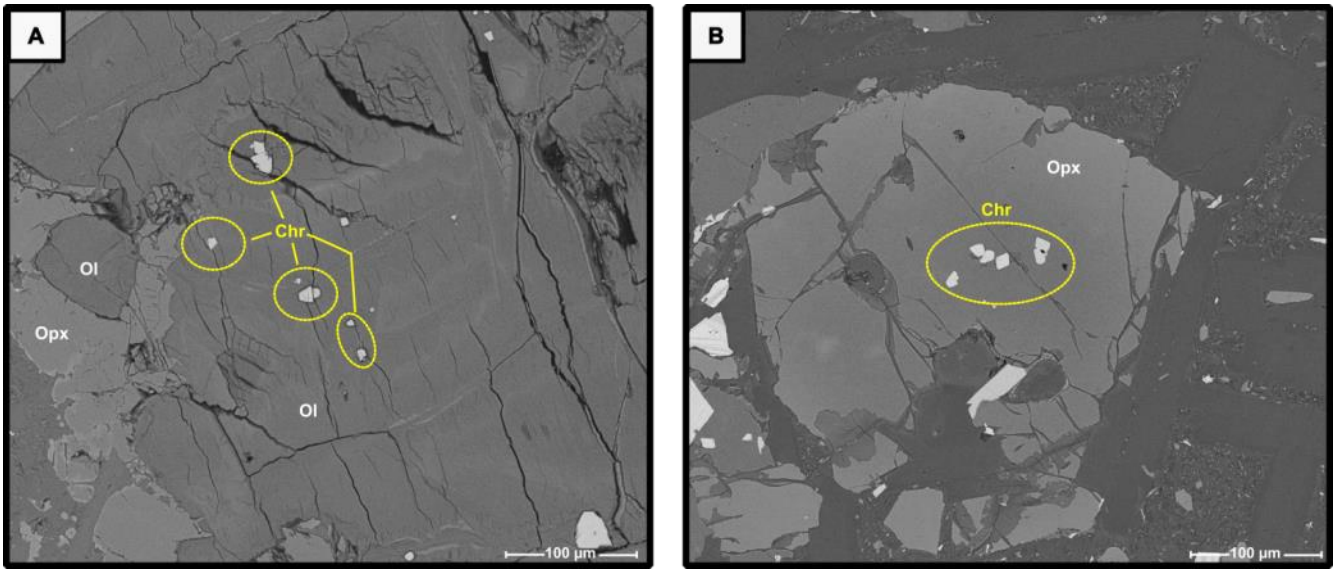

Figure 32. Backscattered *electron* image of chromite in resorbed olivine with orthopyroxene rims (A: pt40) and fresh orthopyroxene (B: geo8).

Obtained compositions on four analysed samples from Bajo Pobre (BP) Formation (geo8, pt 40, pt 101) and two from Cañadon Asfalto (CA)(patvj 020, patvj 027) show Cr# [100*Cr/(Cr+Al)] ranging from 61 to 32 and from 52 to 6 at Mg# [100*Mg/(Mg+Fe)] of 83 - 36 and 52–10, respectively (fig. 33). The most primitive chromite compositions in highest Mg olivines in the Patagonian Province show Cr# of

46- 32 at Mg# 62- 36 in the two formations. Highly evolved compositions from both sets of samples were discarded for discriminative diagrams considering that these are constructed for primitive rocks (Hart and Davis, 1978). Consistent with this, more depleted values in Mg# show a less clear pattern with respect to Cr# whereas high-Mg# compositions correlate negatively with Cr#. Although olivine on pt 40 was resorbed, compositions of Fo_{84-80} were inferred assuming that the almost identical chromite, like those observed in both samples, should also occur in host compositionally akin (fig. 33).

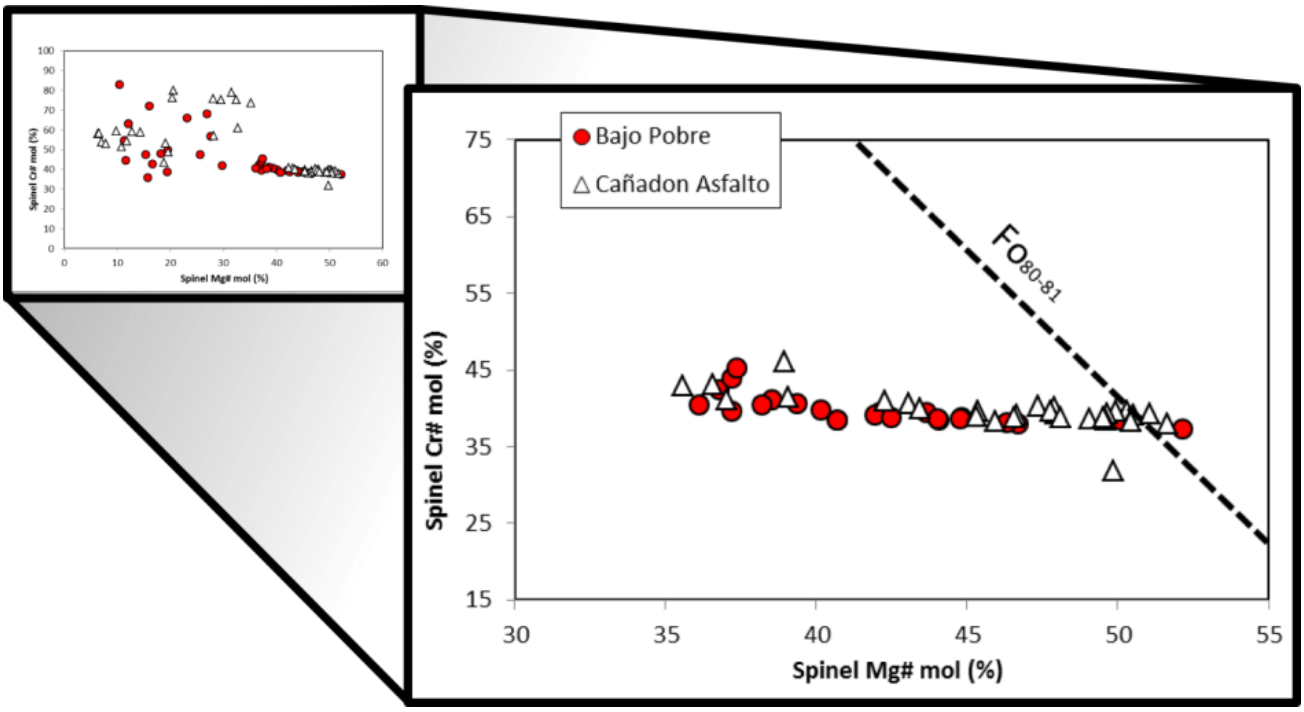

Figure 33. Calculated values of Mg# and Cr# on chromium-spinel MgO>8.5 wt (%) of Bajo Pobre and Cañadon Asfalto Formation.

Positive correlations overall set of samples are observed from the Cr_2O_3 and Al_2O_3 vs MgO diagrams (fig 34). Cr_2O_3 and Al_2O_3 compositions vary between 30.4 - 6.7 wt.% and 47.9 - 15.4 wt.% in Bajo Pobre, and like 25.2 - 4.0 wt.% and 30.9 - 5.0 wt.% in Cañadon Asfalto, respectively. Similar compositions in terms of MgO are observed, ranging from 11.7 to 2.0 wt.% in BP and from 11.4 to 1.2wt.% in CA. A negative trend described by increasing values of FeO (~35.1- 19.2wt% in the two units) at decreasing Al_2O_3 is in agreement with the regular substitution of Al by Fe during the differentiation. Large variations in Mg#, even observed in the most primitive chromite inclusions

(Mg#~52-35), contrast with more homogenous values of Cr# (~46-38). According to Ballhaus (1991), such differentiation trends occur under oxidizing conditions and drift toward ferrite and ulvouespinel enrichment. Different contents in NiO (0.04 - 0.22 and 0.20 - 0.11 wt.%) and ZnO (0.22-0.1 and 0.24-0.08 wt.%) in Cañadón Asfalto and Bajo Pobre Formation, occur at constant Cr# and span Ni and Zn values from host olivine (0.22-0.12) (fig. 35).

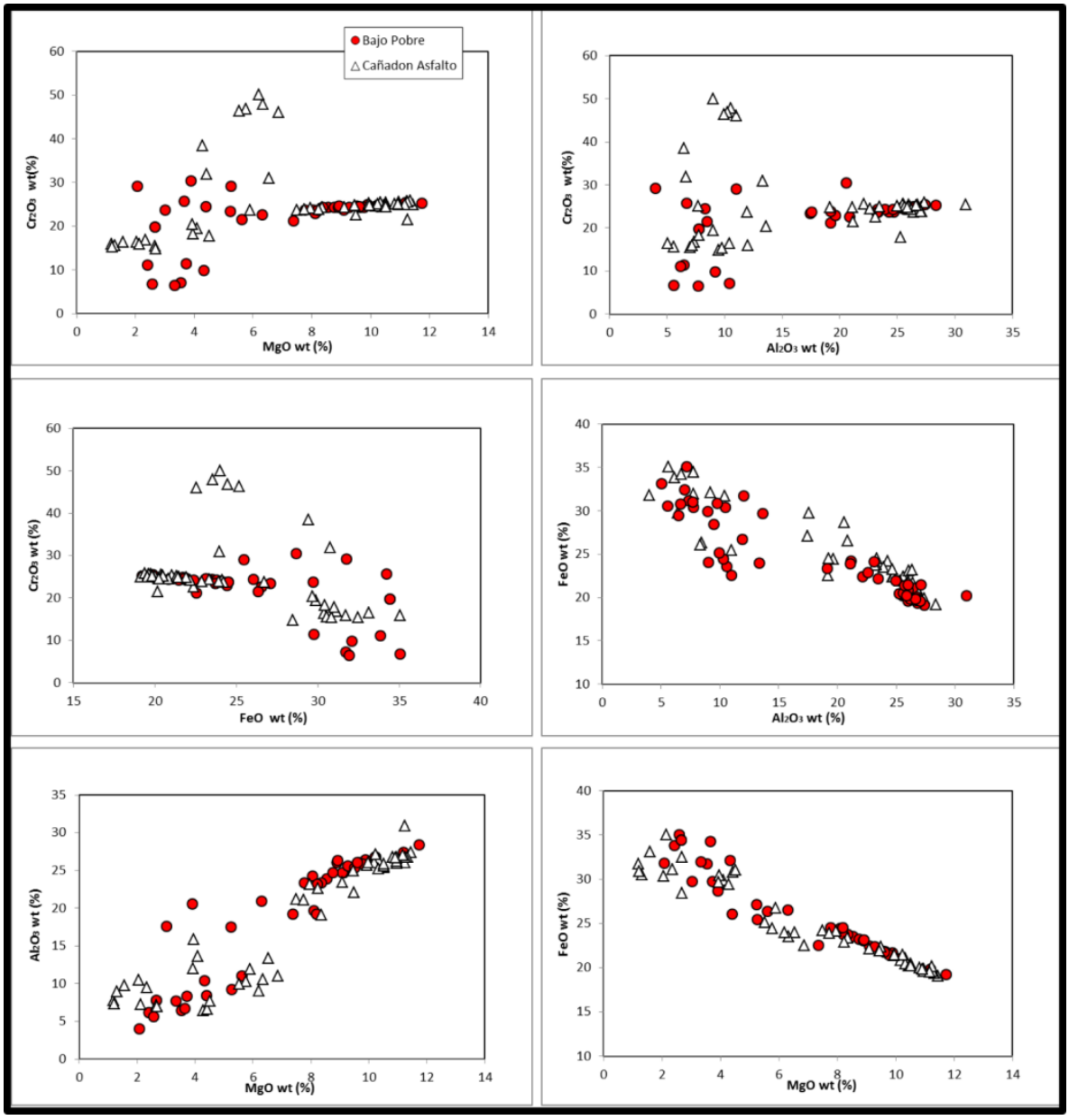

Figure 34. Graphic relations between different content of major elements and compositional parameters of chromium-spniel of Bajo Pobre and Cañadon Asfalto Formation.

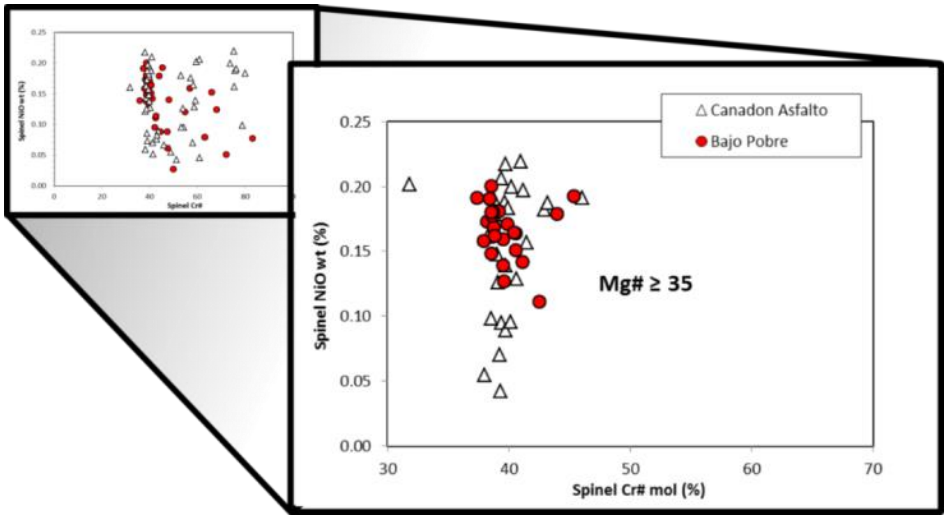

Figure 35. NiO (wt.%) content against calculated values of Cr# on primitive chromium spinel (Mg# >35) of Bajo Pobre and Cañadon Asfalto Formation.

Spinel composition is sensitive to pressure, temperature and fO_2, i.e. to the oxidation state (Ballhaus, 1991; Poustovetov and Roeder, 2000). Increasing values of Cr# at rising $Fe^{3+}/\sum Fe$ (BP: 054-0.38; CA: 0.45-0.36) (fig 36a) as well as the inverse correlation of $Fe^{3+}/Al+Cr+Fe^{3+}$ (BP: 0.70-0.15; CA: 0.6-0.12) and Mg# are in agreement with oxidized conditions where low normative chromite and large compositional variations are common (fig. 36b). Trends in the two analyzed Formations claim for a similar evolution that also reflects the history of Fe-Mg exchange with the host olivine. Higher compatibility of Ni in olivine and the decreasing NiO contents at lower Mg# support this observation (fig. 37b). Negative correlations of MnO (Fig10a) and less clear of TiO_2 (fig. 37c), occur also with respect to Mg#. MnO ranges from 0.42 wt.% to 0.18 wt.% and ZnO from 8.38 wt.% to 0.42 wt.% in CA, while concentrations in BP are 9.91-1.04 wt.% and 0.46 – 0.23 wt.%, respectively.

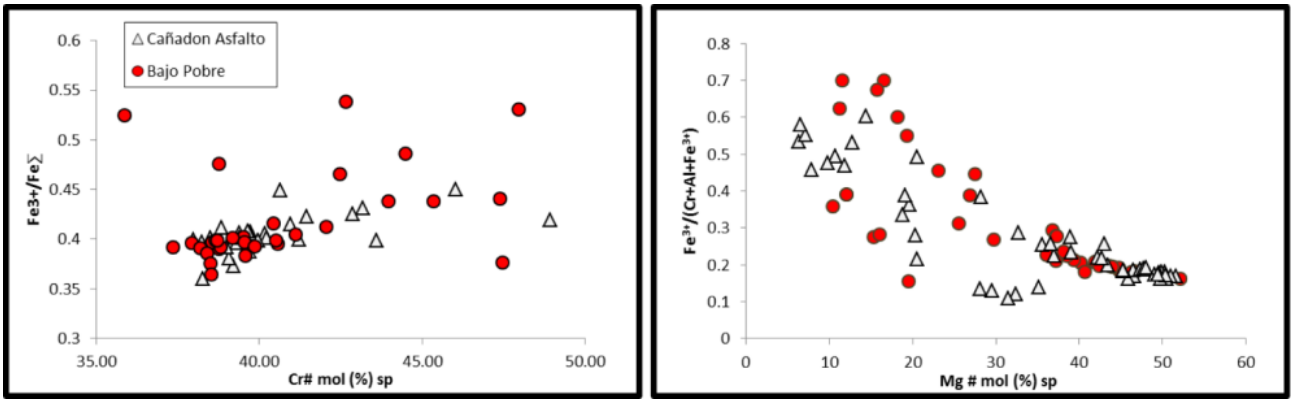

Figure 36. Calculated ratios of $Fe^{3+}/Fe\sum$ and $Fe^{3+}/Cr+Al+Fe^{3+}$ with respect to Cr and Mg#, respectively. Data from Bajo Pobre and Cañadon Asfalto Formation.

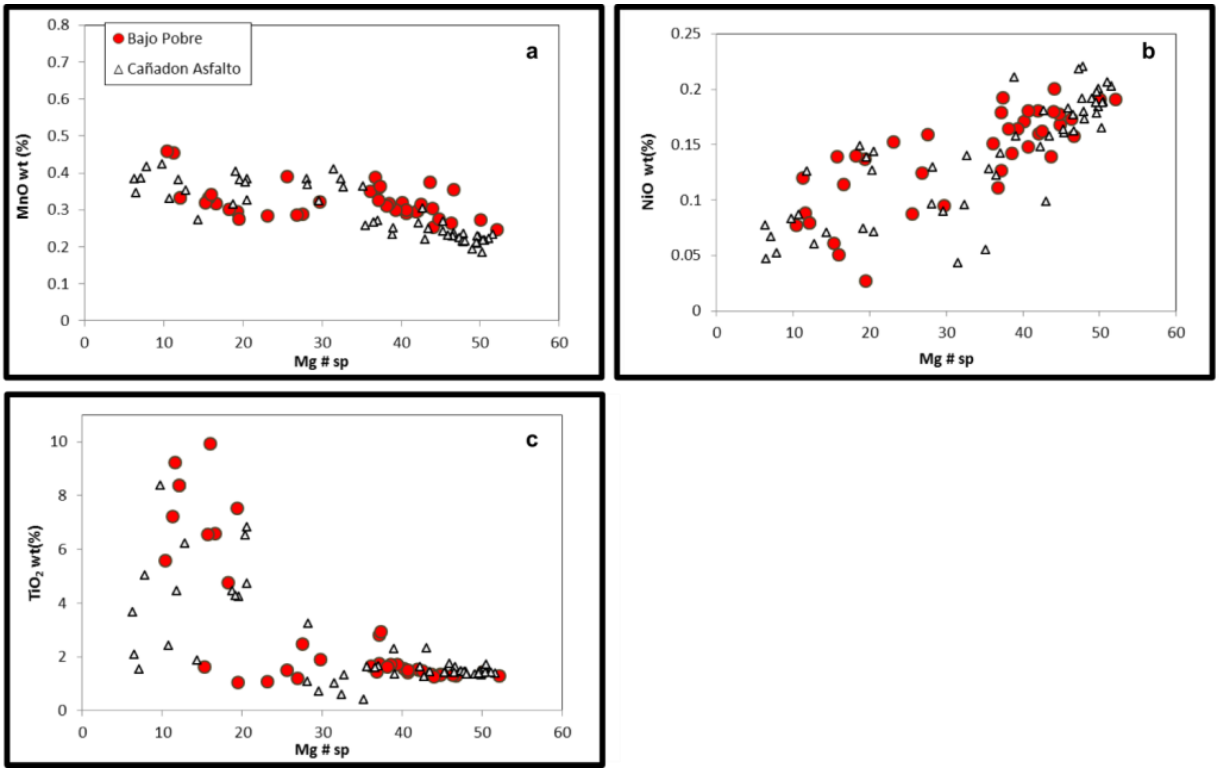

Figure 37. Calculated Mg number against MnO (a), NiO (b) and TiO2 (c) concentrations in chromium-spinel inclusions from Bajo Pobre and Cañadón Asfalto Formation.

Enriched concentrations in Al_2O_3 (28.3-24.67 wt.% in BP, and 30.9-22.1 in CA) and moderate in TiO_2 (1.5 -1.29 wt.% and 2.33 - 1.34 wt.%, respectively) are typical of the two samples, plotting in the MORB field in the tectonic classification diagram of Kamenetsky et al (2001) (Fig 38). .

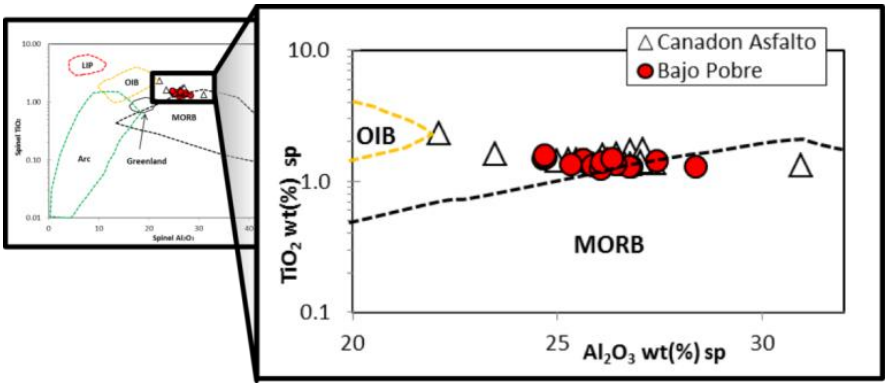

Figure 38. Contents of Al_2O_3 and TiO_2 in chromium-spinel of Bajo Pobre and Cañadon Asfalto Formation plotted with different tectonic settings. Modified from (Kamenetsky et al., 2001).

Decreasing spinel Mg# at calculated contents of forsterite ($Fo_{\sim 84\text{-}80}$) on Cañadon Asfalto evidence the effect of fractional crystallization processes and overlap the fields of MORB and back-arc settings (fig. 39) from Kamenetsky *et al* (2001). A similar trend should be also described by Bajo Pobre Formation according to the assumption that similar compositions yielded by the two units and the Fo content inferred from fig. 33.

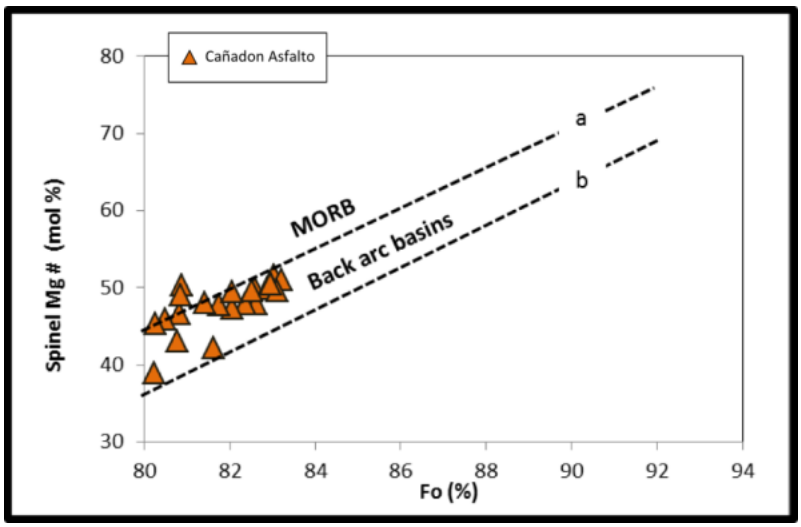

Figure 39. Mg# of spinel inclusions and olivine Fo host composition of Patvj 027 Cañadon Asfalto Formation. Dashed lines correspond to olivine and spinel compositional ranges from different geographic locations and tectonic settings. a: Lamont Seamount EPR (Allan et al., 1988); b: North Fiji Basin (Sigurdsson et al 1993). Modified from Kamenetsky et al (2001).

Obtained data from the most primitive chromite-olivine association display almost identical compositions between the two analyzed samples, even if they correspond to different, geographically distant stratigraphic units. These data, sensitive to the different tectonic setting in which they were

formed, differ clearly from the typical compositions described for LIPs and OIBs (fig 38). the affinity observed to the MORB and back arc settings, recognized from the classification diagrams of Kamentsky (2001), have remarkable implications for the petrogenesis of these magmas.

8.3 Piroxene

Mafic rocks of the Patagonian Province are in all cases pyroxene rich. Normative in hyperstene and diopside (fig. 40a), most of the samples contain also modal orthopyroxene and clinopyroxene. Only those from Loncotrapial Formation are pyroxene-free and enriched in amphibole. EMPA analysis on pyroxene cores of 21 samples from Bajo Pobre (BP), Cresta de los Bosques (CB), Lago la Plata (LP), Cañadon Asfalto (CA) and Chon Aike Formation are presented in the (Appendix 1) and are next described.

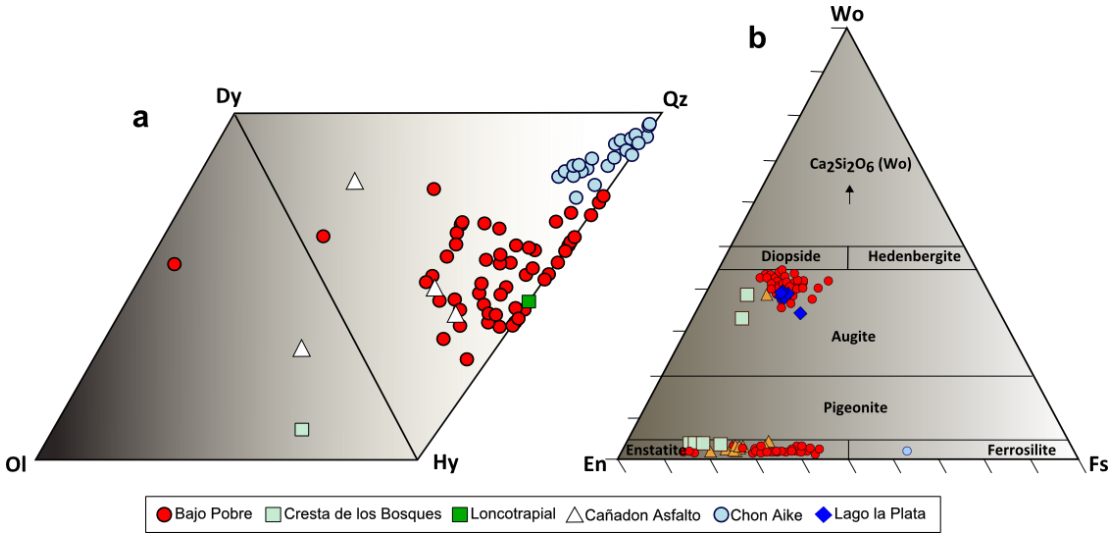

Figure 40. a) CIPW-normative compositions of the Patagonian rocks. b) Pyroxene composition of Patagonian samples and end-member classification. En: Enstatite; Wo: Wollastonite; Fs: Ferrosilite. Modified from Morimoto et al (1988).

Clinopyroxenes are of augitic composition (fig. 40b); Wo_{45-37} and En_{51-32} in Bajo Pobre, Wo_{40} En_{47} in Cañadon Asfalto, Wo_{39-33} En_{55-51} in Cresta de los Bosques and Wo_{39-20} En_{43-41} in Lago la Plata). Commonly, augite coexists with Mg-rich orthopyroxene (enstatite) which varies from En_{84} to En_{64} and

very En-poor composition limited to Chon Aike rocks (En_{34}). En content in orthopyroxene is not correlated with whole-rock MgO composition. Particularly, En-rich crystals (En_{84-82}) occur in whole-rocks with very different MgO contents (Cresta de los Bosques: 17 wt.%; Bajo Pobre: 2.4 wt.%) with the most magnesian orthopyroxens occurring in the most evolved (low MgO) rocks exsolution textures and crystal-zonation previously described on pyroxenes from this unit (Chapter 7), evidence a long evolution history of their host rocks and is consistent with the compositional heterogeneities here reported. Magma mixing or interaction with a silicate melt during the fractionation of these magmas is suggested from these data and supported by exceptional ferrosilitic orthopyroxene on a rhyolitic ignimbrite from the Chon Aike Formation. Its presence, together with mafic xenocrysts observed in other ignimbrites and rhyolites of this unit allow to infer the influence of a mafic component in the petrogenesis of the felsic magma types.

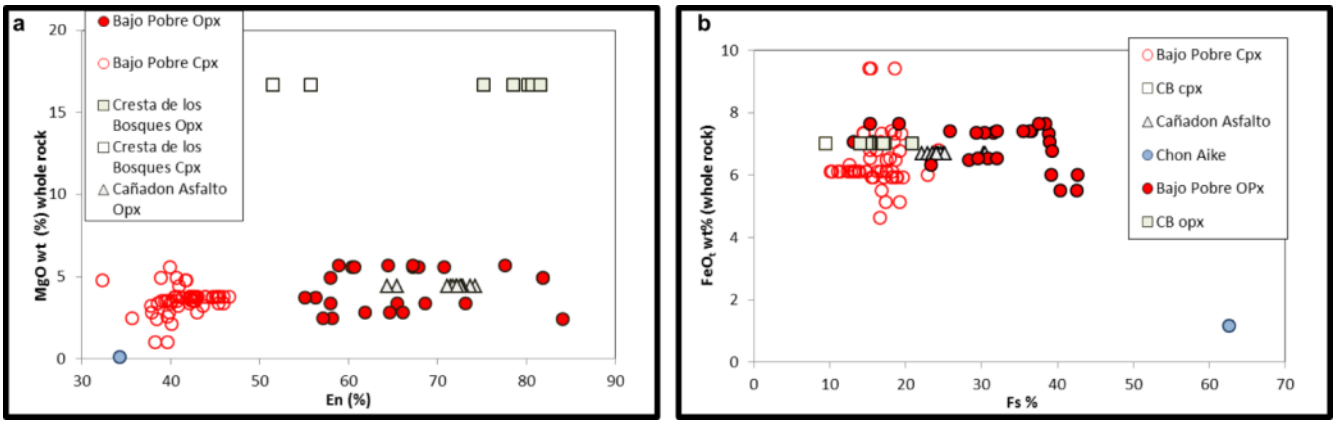

Figure 41. Enstatite (En) (a) and ferrosilite (Fs) (b) contents against MgO wt% and FeO_t of their respective whole rocks.

TiO_2 abundances in all pyroxenes are positively correlated with their Mg# (fig. 42a) whereas Cr_2O_3 barely display a positive trend (fig 42b). Samples pt 180 from BP and patvj 005 from CB, only, show higher TiO_2 augites (BP: 2.14 – 0.56 wt.% and CB: 0.62-0.12 wt.%) despite being low-Ti rocks (BP: 1.38 and CB: 0.14 wt.%). Late crystallization of augite from a more evolved melt (richer in Ti) could explain this trend.

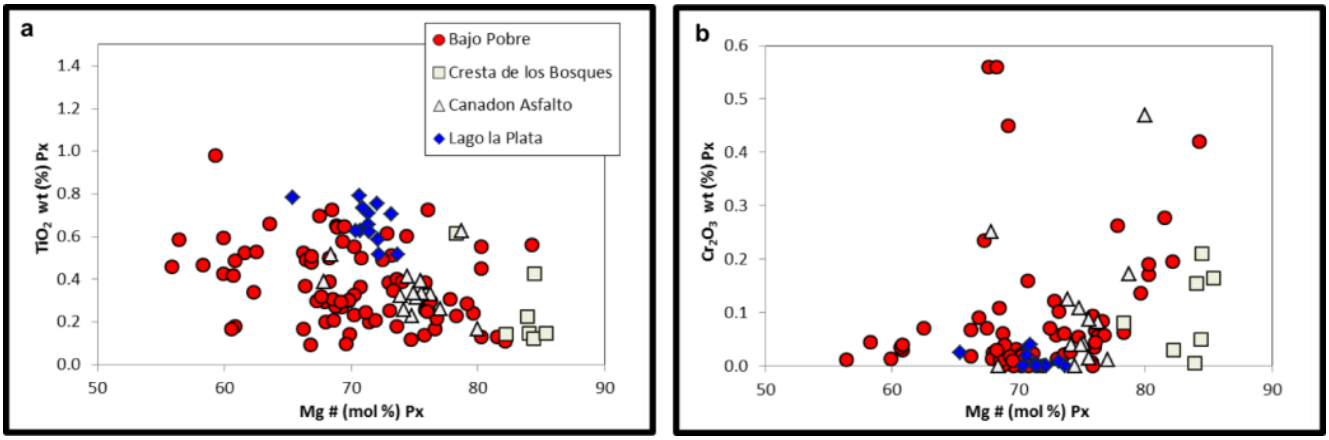

Figure 42. TiO_2 wt% (a) and Cr_2O_3 wt% (b) of all pyroxenes against their correspondent Mg#.

In order to achieve indicative crystallization conditions, some estimates of pressure and temperature were made on the Patagonian samples using the two pyroxene thermobarometer of Putirka (2008). Rhodes diagrams for both pyroxenes were also plotted to evaluate the equilibrium of the crystals with the bulk rocks (fig. 43a). Most of the augites from Bajo Pobre (pt 43, geo 8, pt 42, pt 182, pt 24, pt 84) plot above the calculated equilibrium lines (for $K_D\,(Fe\text{-}Mg)^{px/liquid}$ of 0.20-0.30, i.e. at 2 Kbar and 3 wt.% H_2O at the NNO buffer; (Gaetani and Grove, 1998). Only augites from pt 40 (Mg# 69), appear in equilibrium with the host rock. Also most orthopyroxenes are out of equilibrium with the host-rock. However, samples pt 39, pt 43 and geo 8 from Bajo Pobre and patvj 033 from Canadon Asfalto, appear in equilibrium (for $K_D\,(Fe\text{-}Mg)^{px/liquid}$ of 0.20). In contrast, Pt 40, pt 182 and pt 153 are in equilibrium with their host rock for $K_D = 0.30$ (fig. 43b).

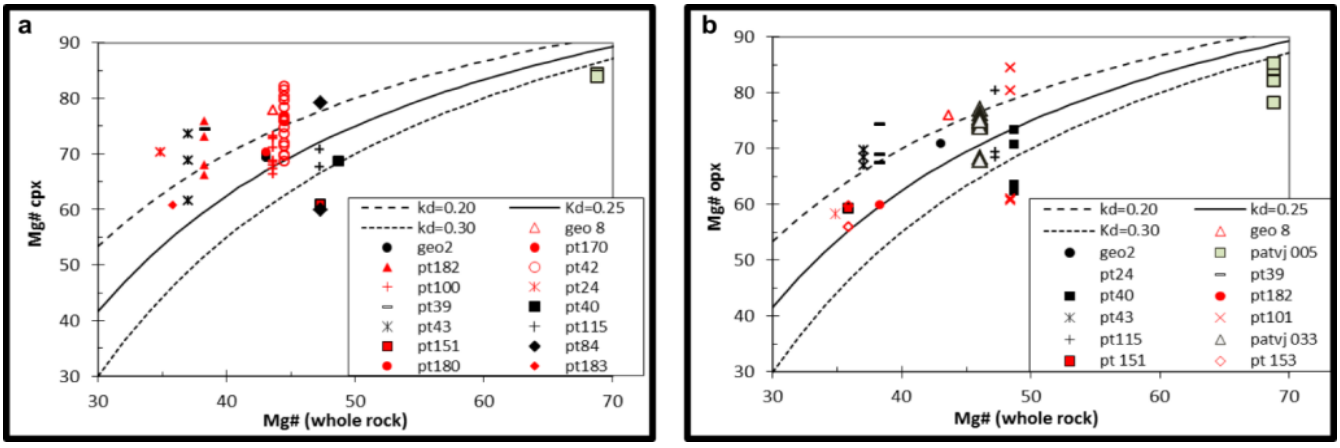

Figure 43. Rhodes diagrams for clinopyroxene (a) and orthopyroxene (b) with melt equilibrium lines at $K_D\,(Fe\text{-}Mg)^{px/liquid}$ of 0.20, 0.25 and 0.30. *Samples on red and black symbols correspond Bajo Pobre Formation, white triangles to Canadon Asfalto and gray cubes to Cresta de los Bosques. Mg# =100* [Mg/Mg+Fe^{2+}].

Given the multiple evidences of disequilibrium, temperatures and pressures obtained from the present calculations should be taken only as indicative. In attempt to get the most accurate results, only the four samples (from sixteen calculated) which approach equilibrium with their whole-rock were considered. For these samples, crystallization temperatures of 987°C - 1172°C in BP, 1172°C in CB and 1096°C in CA were obtained (table 2). Calculated crystallization pressures are variable between the units, with moderate values of ~8 kbar - 8.9 kbar in BP and lower pressures of 5.6 kbar in CB. In general, pressures are consistent with the observed mineral assemblage (opx+cpx+pl±ol) in the studied rocks, which, according to Elton & Scarf (1984) requires a P of 10 kbar and a T of 1170°C.

Table 2. Obtained results of P-T conditions after Putirka (2008). In black the values con

sample	T°(C)	P(kbar)	K_D(Fe-Mg) (obs.)
geo8_m9	1040.2	5.5	0.897
geo2_m2	**1010.9**	**8.0**	**1.044**
PTvj005_2	1080.3	3.7	0.849
PTvj005_10	**1172.5**	**5.6**	**1.014**
PT24_m1	1004.0	20.7	0.594
PT182_m5	1056.5	21.5	0.552
PT 39	972.7	10.9	0.717
PT 40	981.9	15.2	0.757
PT 43	1046.1	11.3	1.338
PT 43	**987.3**	**8.9**	**1.035**
PT 43	1023.7	9.3	0.724
PT 115	1011.8	3.7	2.177
PT 115	1047.1	3.6	3.060
PT 151	991.2	18.4	0.734
PT 153	**996.3**	**19.7**	**0.953**
patvj024_2	**1094.7**	**5.6**	**1.081**

8.4 Plagioclase

EPMA analysis on fresh and unzoned plagioclase cores were performed on 35 samples from Bajo Pobre, Cañadon Asfalto, Cresta de los Bosques and Chon Aike Formation (Appendix 1). Compositions are shown in the triangular classification diagram for feldspars (averaged end members expressed as: Anorthite, An ($CaAl_2Si_2O_8$)= 100×Ca/(Ca+Na+K), Albite, Ab ($NaAlSi_3O_8$)=100×Na/(Ca+Na+K) and Orthoclase, Or ($KAlSi_3O_8$)= 100×K/(Ca+Na+K)) (fig. 44). As a main characteristic, most of the plagioclases from the Patagonian Province display calcium rich compositions. Crystal-cores from BP

range from An_{93} in pt84 to An_{48} in pt30, whereas some exceptional albitic compositions (An_{1}) coexist with An_{84} on sample pt100. Large variations in the center of the grains are evident also in pt43 (An_{87-63}) and pt39 (An_{86-68}). CA sample patvj 033 yields An_{78-45} plagioclase, whereas patvj 005 (CB) contains only bytownite (An_{89-84}). Plagioclase from the felsic rocks of the Chon Aike Formation span the crystal compositions of the CA and BP varying from labradorite (An_{58}) in pt111, to oligoclase (An_{20}). Scarce alkali feldspars are identified in some Chon Aike (Or_{74-65}) and CA rocks (Or_{28-26}).

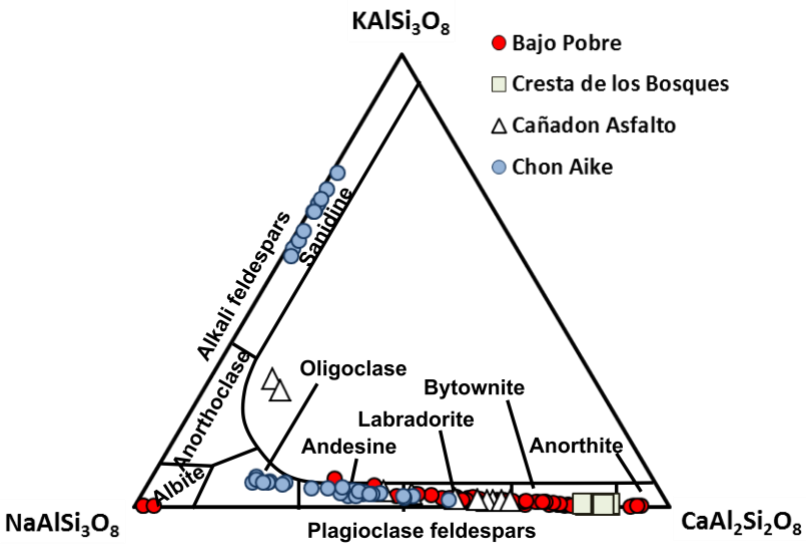

Figure 44. Ternary classification of feldspars from Bajo Pobre, Cresta de los Bosques and Cañadón Asfalto.

Compositions in terms of TiO_2 show roughly rising values with depletion of An in the mafic BP and CA (fig. 45a). However, the contents are so low (0.08 wt.% - 0.01 wt.%), that is hard to differentiate from theanalytic effect on them. In contrast, anomaly high contents of TiO2 are observed on CB ranging from 0.24wt.% to 0.49 wt.% at An_{87}. A more evident negative trend is observed from BP and Chon Aike on the FeO *vs* An diagram (fig. 45b) with values that change from 0.01 wt.% at An93 to 0.23 wt.% at Ab_{99}, respectively. On the other hand, compositions of CA are higher in Fe with values from0.49 wt.% to 0.24 wt.% at An_{65} – An_{45} whereas those from CB change like 1.64 - 0.67 wt.% at An_{88-87}. In all cases, rising concentrations of FeO are correlated with less anortitic compositions as it would be normaly expected during the differentiation process.

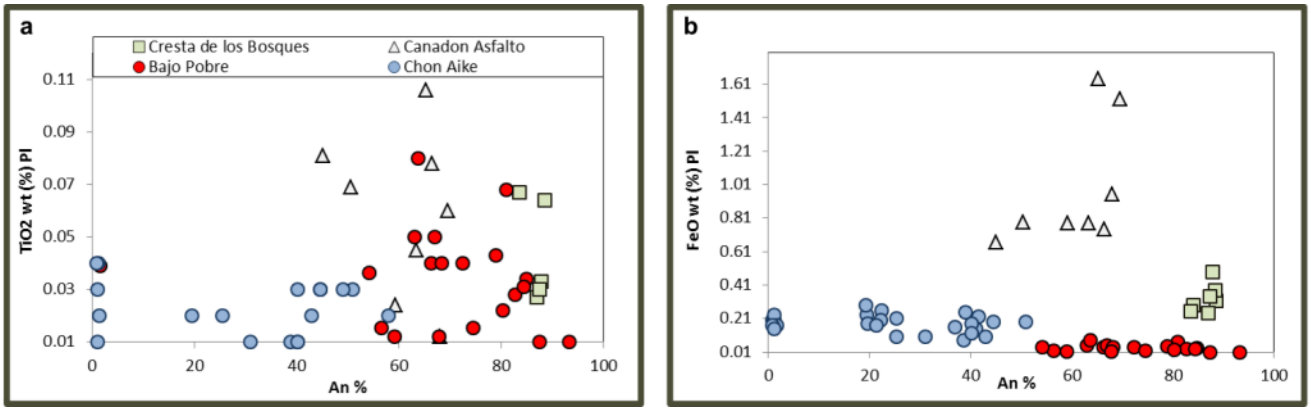

Figure 45. TiO_2 wt% (a) and FeO wt% (b) compositions against anortitic content (An %) measured on plagioclase from Bajo Pobre, Canadon Asfalto and Cresta de los Bosques Formation.

Anorthitic values are well coupled to the Ca# (100*C/(Ca+Na)) of the whole rock (fig 46). In particular, Bajo pobre samples plot close to the Kd(Ca-Na) curve of 3, whereas Chon Aike and Cañadón Asfalto samples are close to the KD= 1 line.

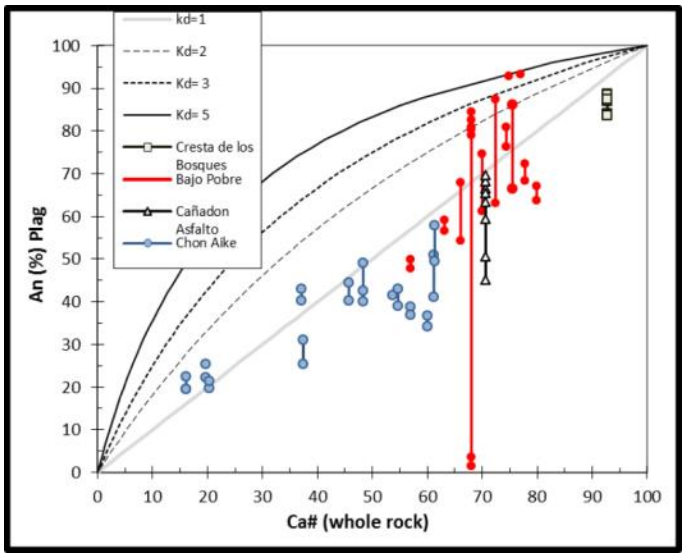

Figure 46. Anortitic values (An %) against calculated Ca# in the whole rock in Chon Aike, Bajo Pobre, Cañadon Asfalto and Cresta de los Bosques Formation.

High-An plagioclases like those from Patagonia (BP in particular), are typical of subduction zone magmatic rocks (ie: Pearce, 1995; Panjasawatwong and Danuyshevsky, 1995). Earlier described dusty, resorbed, spongy and sieve-like plagioclase crystals are in agreement with this and furthermore suggest magma mixing (Tsuchiyama, 1985). Calcium enrichment with respect to the bulk-rock composition can be explained by long residence in an evolving magma, water effect on the plagioclase

liquidus or crystallization of calcic pyroxene (Pearce et al., 1995). The influence of an extremely refractory magma (high Ca/Na), mixing with more felsic magmas or Al_2O_3 rich melt is evaluated from the geochemistry in the next chapters.

9. Geochemistry

9.1 Major elements compositions

Major element abundances were determined on whole rocks by X-Ray fluorescence at the University of Bonn and at the University of Tasmania. Unpublished analysis performed by Giuliano Bellieni at the University of Padova by the same method, are also considered in this chapter. Samples collected during this project were prepared at the Steinmann Institute and CODES by crashing the rocks with an hydraulic press and pulverizing with a tungsten mill. Results are presented in the Appendix.

9.1.1 Mafic units

In general terms, rocks from the Patagonian Province are subalkaline spanning from basalt to rhyolite in a TAS (Total Alkalis silica) diagram (fig. 47). A group of mafic to intermediate rocks (50-69 wt.% SiO_2) represented by 4 samples from Cañadon Asfalto, one from Loncotrapial (LT), one from Cresta de los Bosques and 58 from Bajo Pobre, is described in this section. Displaying the less evolved compositions, lavas from CA are classified as basalt, basaltic andesite and andesite, ranging in terms of silica and alkalis from 50 to 58 wt.% and from 6.2-4.0 wt.%, respectively. Rock analysis on BP are more abundant and clearly more heterogeneous. They change from basalts with ~51 wt.% SiO_2 to dacites at ~69 wt.% SiO_2. The only sample from Loncotrapial is an andesite (52 wt.% SiO_2) and is comparable to the intermediate rocks from BP. The olivine gabbro from Cresta de los Bosques shows a less evolved composition (SiO_2 49 wt.%) with respect to the volcanic rocks.

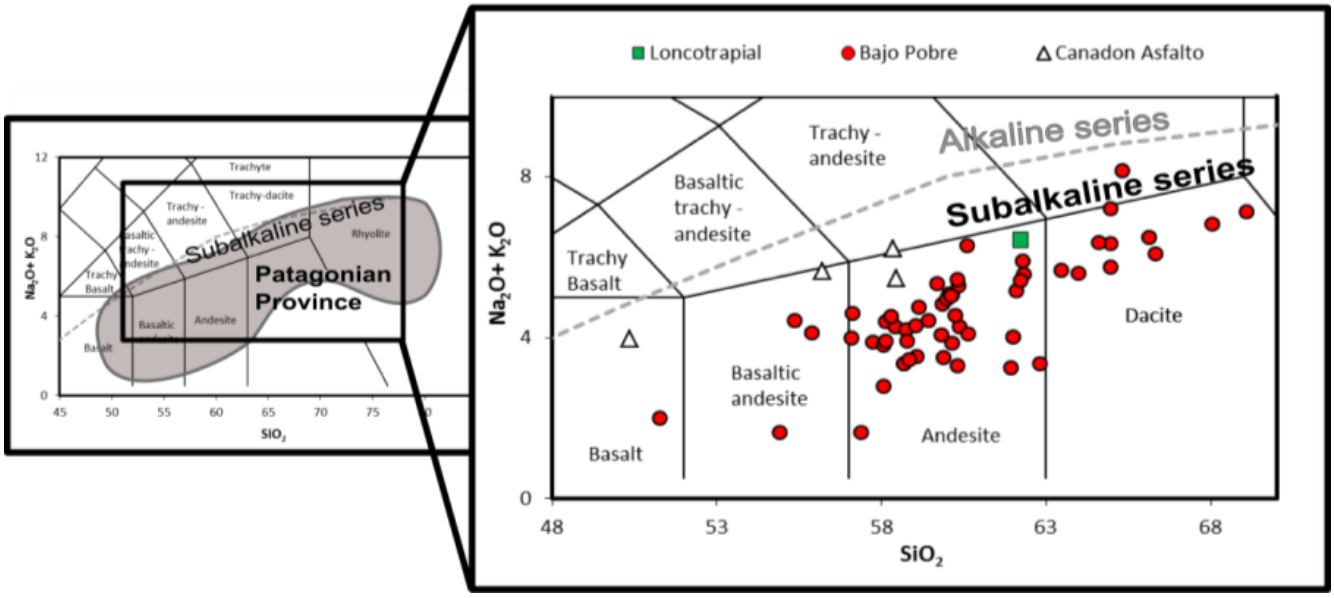

Figure 47. Total alkalis versus silica (TAS) classification diagram of the 64 samples from the mafic units of the Patagonian Province. Compositional fields are from LeMaitre et al (1989). The dashed line separates the alkaline and subalkaline field, after Irvine & Baragar (1971).

Most of the subalkaline rocks do not show iron enrichment during differentiation processes, plotting within the calc-alkaline field on an AFM diagram (A: $Na_2O + K_2O$; F: $FeO + Fe_2O_3$; and M: MgO) (fig. 48a). Values on BP (pt26, pt180, pt116, pt86, pt114) show a slight evolution trend with increasing Fe-contents at alkalis enrichment whereas CB is Mg-rich and extremely alkalis depleted. Large K-variations are observed in the SiO_2 versus K_2O diagram (fig 48b). Samples from BP show high to low-K, while those from CA span the high to medium-K fields where also the only sample from LT plots. A minority of six rocks composed by five samples from BP and the one from CB, display tholeiitic affinities.

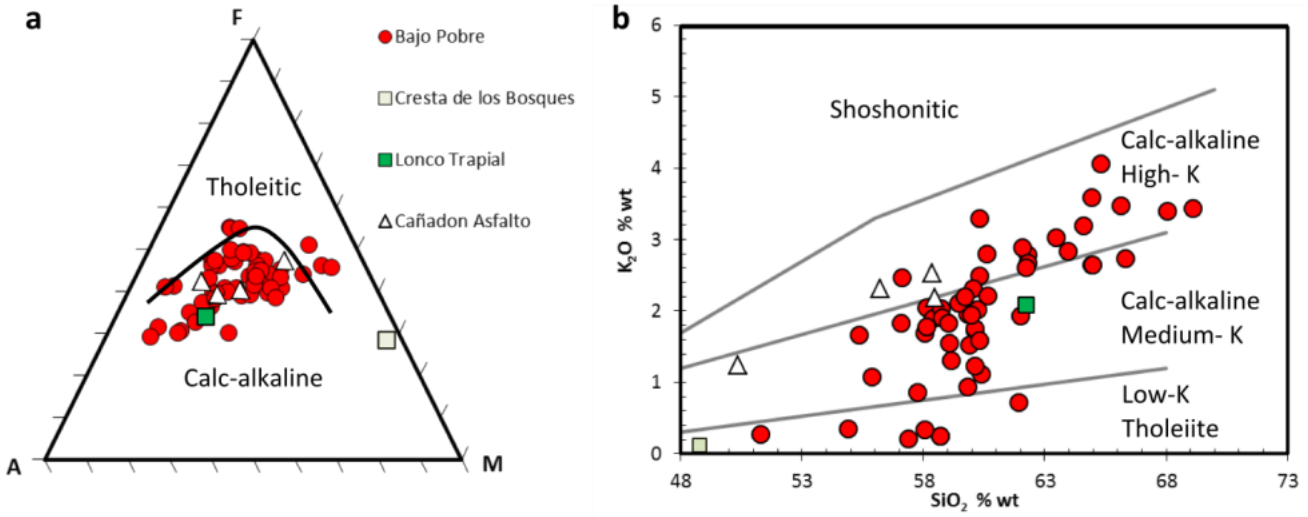

Figure 48. a) AFM diagram (A: $Na_2O + K_2O$; F: $FeO + Fe_2O_3$, and M: MgO) with compositions of Bajo Pobre, Loncotrapial, Cañadon Asfalto and Cresta de los Bosques Formation, after Irvine & Baragar (1971). FeO calculated = $0.8998 \cdot Fe_2O_3$. b) K_2O-SiO_2 classification diagram for the same samples in A, after Peccerillo and Taylor (1976).

With a vast major majority of Qz-normative samples, mafic to intermediate rocks from the Patagonian Province are characterized by moderate to enriched values of SiO_2, widely variable MgO, high Al_2O_3 and CaO, and low TiO_2 (fig. 49). As a typical feature, these samples display a peralouminous character defined as $Al_2O_3 > Na_2O+K_2O+CaO$. Increasing $SiO_2$is correlated with decreasing MgO (9-1 wt.%) in all samples. Only the olivine gabbro from CB yields very high MgO (16.7 wt.%). Mg# [$100*Mg/(Mg+0.85 \cdot Fe_t)$] in Qz-normative rocks ranges from 54 to 22 while only the rare Ol-normative samples display consistently higher Mg# (CB: 69; CA: 48). Constant high Al_2O_3 contents (16-20 wt.%) at variable MgO are typical of all formations. Variable but notably enriched CaO compositions reach values of ~14 wt.% in BP and 10 wt.% in CA, being in all cases positive correlated to MgO. Low TiO_2 (0.14-1.49 wt.%) is characteristic of all samples. As it is expected in calc-alkaline rocks, variations in terms of FeO_t occur without correlating with MgO, resembling the early fractionation of magnetite. FeO_t contents change from 9.12 to 3.49 wt.% in BP and from 9.97-5.85 wt.% in CA, while values of 4.90 wt.% and 7.0wt% are observed in CB and LT at given Mg#, respectively. In contrast, increasing K_2O and Na_2O (BP: 4.10-1.28; CA: 2.72-2.53; CB:4.34 LT: 0.81) occur well coupled to the decreasing MgO as Na-rich plagioclase is more frequent in fractionated samples. However, mineral associations are not always well coupled to the major elements composition. Despite the common presence of apatite in all samples, contents of P_2O_5 are extremely depleted and roughly describe an inverse trend,

ranging from the highest values in CA (0.83-0.33 wt.%) to the lowest in BP (0.78 - 0.1 wt.%); LT (0.15 wt.%) and CB (0.01 wt.%). A weak positive correlation is observed from the depleted MnO contents with respect to MgO. Values range like 0.29-0.06 wt.% in BP, 0.20-0.10 in CA, 0.13 and 0.08 wt.% in LT and CB at given compositions of MgO.

Major element compositions previously described are in most cases all well coupled no matter their stratigraphic and geographic differences. In general, they agree the typical mineral assembly of mafic-intermediate magmas, as the one observed on these samples (Px+Pl±Ol±Spl). In addition, some remarkable features like the peralouminous character and the unusual Ca-enrichment of the set, might a first evidence of processes like anatexis of aluminous metasedimentary rocks in the continental crust (Bergantz, 1989), either melting of subducted sediments (Mori et al., 2007). In agreement with these hypothesis, earlier evidences from the petrography and the mineral chemistry have suggested that magma mixing is plausible in the petrogenesis of these rocks. The calc-alkaline probed character and the required oxidized conditions involving the fractionation of magnetite during the differentiation, also support the thought subducted material influence.

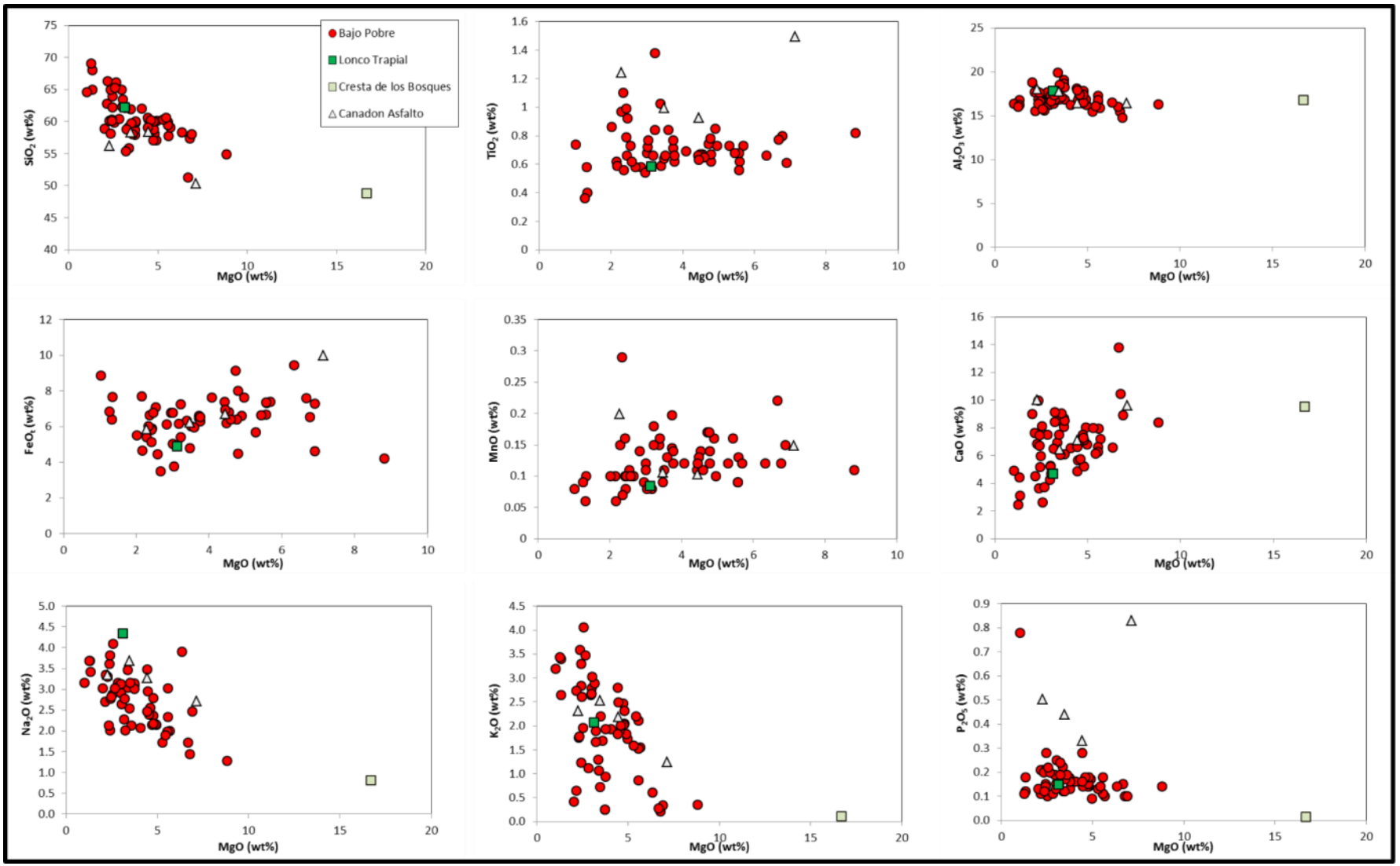

Figure 49. Major elements compositions of mafic rocks from the Patagonian Province with respect to their MgO (wt%) content. Data from Bajo Pobre, Cresta de los Bosques, Cañadon Asfalto and Loncotrapial Formation.

9.1.2 Felsic rocks

Felsic rocks from the Patagonian Province are restricted to Marifil, El Quemado and Chon Aike Formations. They are represented by ignimbritic and lava flows of dacitic and rhyolitic composition. Variations in terms of silica and alkalis range from 78.8 - 63.4wt% and 5.7-10.6wt% in Chon Aike and from 79.0-70.7wt% and 6.2-10.6wt% in Marifil, with a great majority of the samples plotting in the subalkaline field of the TAS diagram (fig 50). Equivalent, according to the regional geology, the only sample from El Quemado Formation (72.6wt%; 8.22wt%) span also the observed compositions of Chon Aike.

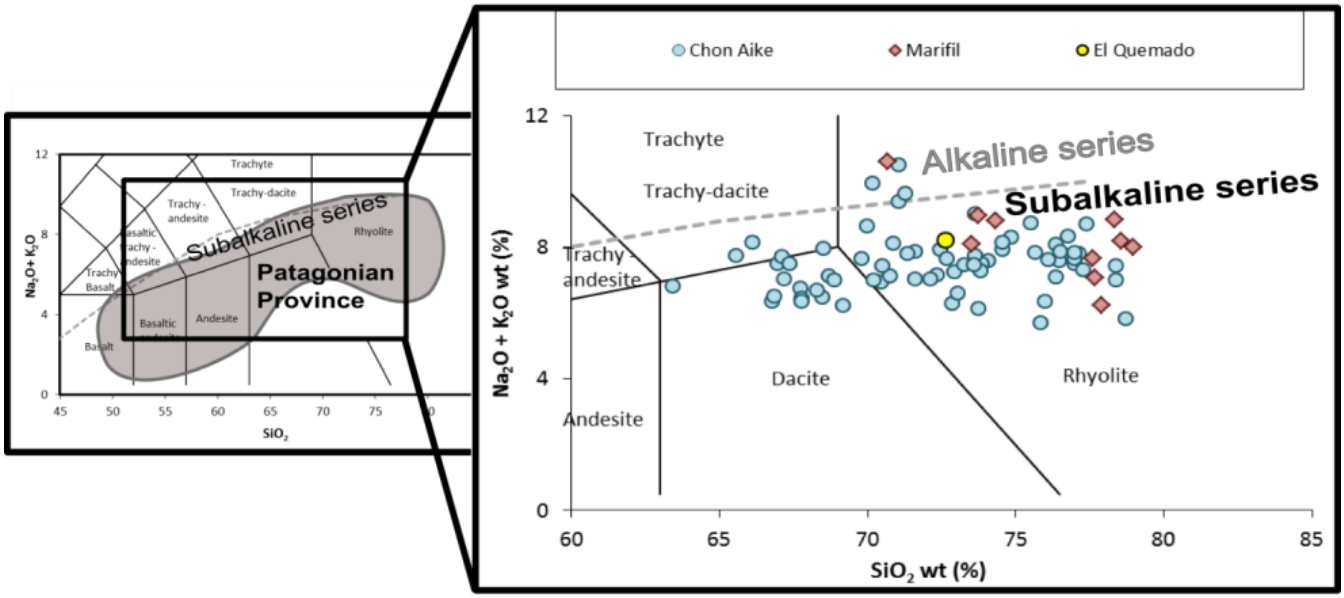

Figure 50. Total alkalis versus silica (TAS) classification diagram of 10 samples from Marifil, 1 from El Quemado and 69 from Chon Aike Formation. Compositional fields are from LeMaitre et al (1989). The dashed line separates the alkaline and subalkaline field, after Irvine & Baragar (1971).

Felsic samples display K_2O contents that vary from 9.86-3.27wt% in Chon Aike, 8.27-2.87wt% in Marifil and 4.59wt% in El Quemado, plotting in the medium and high K calc-alkaline series, (fig. 51). Four more samples display low K and are in the field of the tholeiitic rocks with values of 3.27wt% and 3.20wt% in Chon Aike, 3.20wt% and 2.87wt% in Marifil at similar contents of silica (~77wt%).

MgO, FeO_t, CaO, P_2O_5 and TIO_2 are both negatively correlated with SiO_2 and range from about 3 wt.% and 0.6 wt.% to near-zero in the highest SiO_2 rhyolites. Only one sample from Chon Aike is exceptionally enriched in Na_2O (6.83 wt.%) and highly depleted in K_2O (0.68 wt.%). The rest from this

group range show Na_2O ranging from 4.57-0.15 wt.% whereas those from Marifil vary like 4.79-0.56 wt.% and 3.63 wt.% in El Quemado. Comparable to the mafic rocks, high and almost constant Al_2O_3 compositions at changing SiO_2 are observed (19.7-11.4 wt.%; 15.5-11.2 and 14.7 wt.%) in all samples defining the peraluminous of the Province (fig 52).

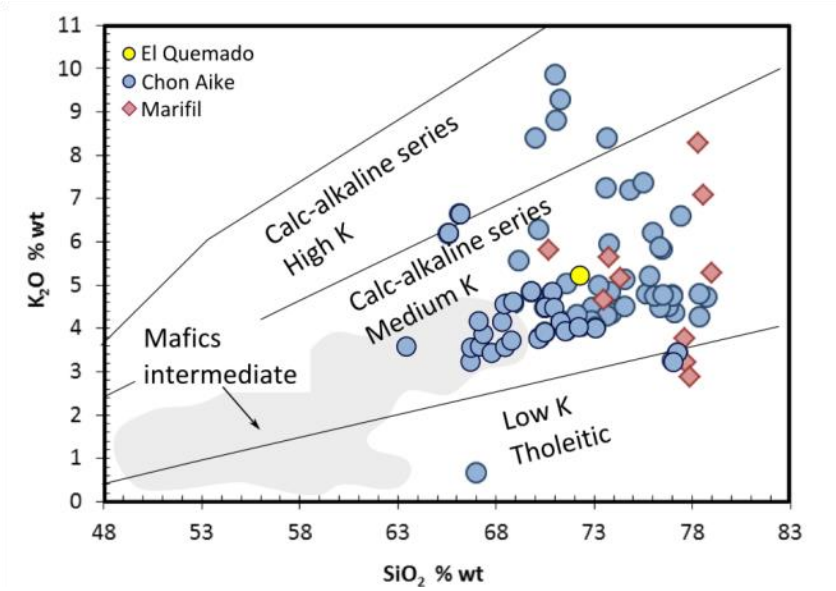

Figure 51. K_2O-SiO_2 classification diagram for samples from Marifil, Chon Aike and El Quemado Formation, after Peccerillo and Taylor (1976).

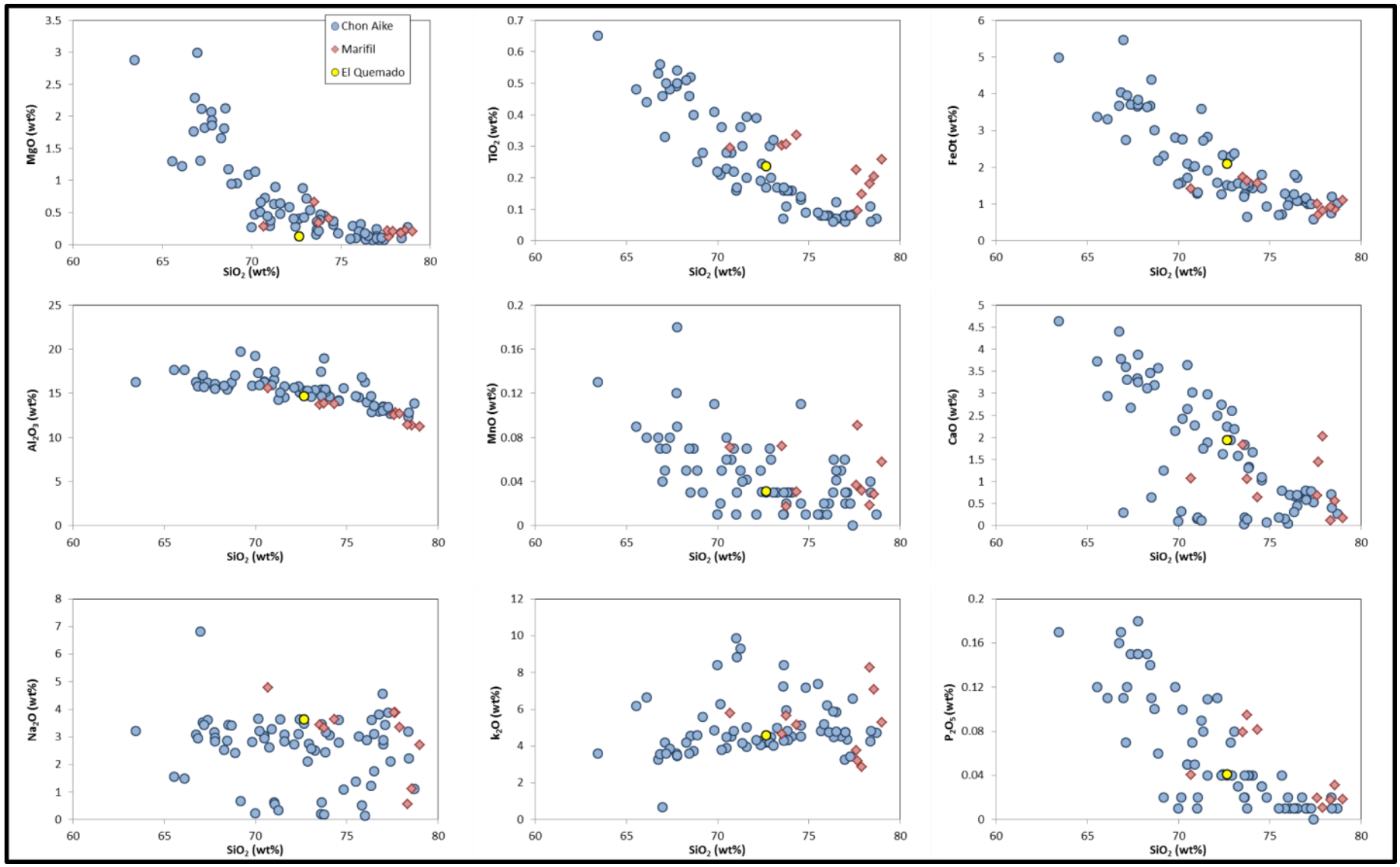

Figure 52. Major elements compositions of the felsic rocks from the Patagonian Province with respect to their SiO_2 (wt%) content.

9.2 Incompatible trace elements compositions

Trace elements composition of 31 samples representative of the whole Province were obtained by inductively coupled plasma mass spectrometry (ICP-MS) in two different analytic sets. Eight rocks of the Marifil, Chon Aike and Bajo Pobre fms. from Northern Patagonia and the Deseado Massif (Prof. Bertrand collection), were measured using an Agilent 7500cs ICP-MS instrument ICPMS-Lab of the Institute of Geosciences, University of Kiel, Germany. Analytical quality control was monitored by estimations of two procedural blanks and the certified international standards BIR-1, BHVO-2; BE-N and W-2. Analysis of further 23 samples from the Chon Aike and Bajo Pobre (Deseado Massif), and from Loncotrapial, Cresta de los Bosques, Cañadón Asfalto, and Marifil, (Northern Chubut Province), were performed at CODES, ARC, University of Tasmania on an Agilent 7700 ICP-MS with a 3rd generation octopole reaction system. Reproducibility of the data is given by the average concentrations of one procedural blank, the certified international standards BHVO-1, BIR-1, GSR-1, RGM-1 and two in-house standards (basalt: TASBAS and granite: TASGRAN). Analytic results are reported in the appendix.

Results

Incompatible trace element compositions of the Patagonian rocks display a prominent enrichment in Large Ion Lithophile Elements (LILE) with respect to High Field Strength (HFS) and Rare Earth Elements (REE) (fig. 53). Fractionated REE patterns with heavy REE (HREE) vs. light REE (LREE) depletion (Yb_N 33-4ppm) are characteristic of little to strongly differentiated rocks (fig 54). However, La/Yb ratios change widely in the felsic rocks (Marifil: 47 - 9.3; Chon Aike: 21-4.9), whereas more restricted ratios are observed in the mafic ones (CA: 18-15; BP: 9.61-7.60 and LT: 13.15) and considerably more depleted in CB (3.47).

The two rock-groups (mafic and felsic) yield incompatible trace element patterns typical of arc magmatism. A positive anomaly of Pb observed in all samples is accompanied by clear troughs of Sr, Nb-Ta, and occasional and less pronounced negative anomalies of Zr-Hf limited to the felsic Marifil and Chon Aike rocks (fig. 53). Large amounts of highly incompatible (Th>2.6ppm; U>1.2) and fluid

mobile trace elements (Rb> 35 ppm; Ba> 500 ppm) are characteristic of the most samples in the two groups. Higher contents of Th and U might be explained by their concentration in accessory phases, like zircon and apatite, more common in the felsic rocks. Its enrichment in the mafics could be indicative of fluid contribution in their genesis. Exceptional depletion of U in a couple of samples from CA (<0.8 ppm) could be related to more oxidized conditions producing loss of this element during re-mobilization within the source or secondary alteration processes.

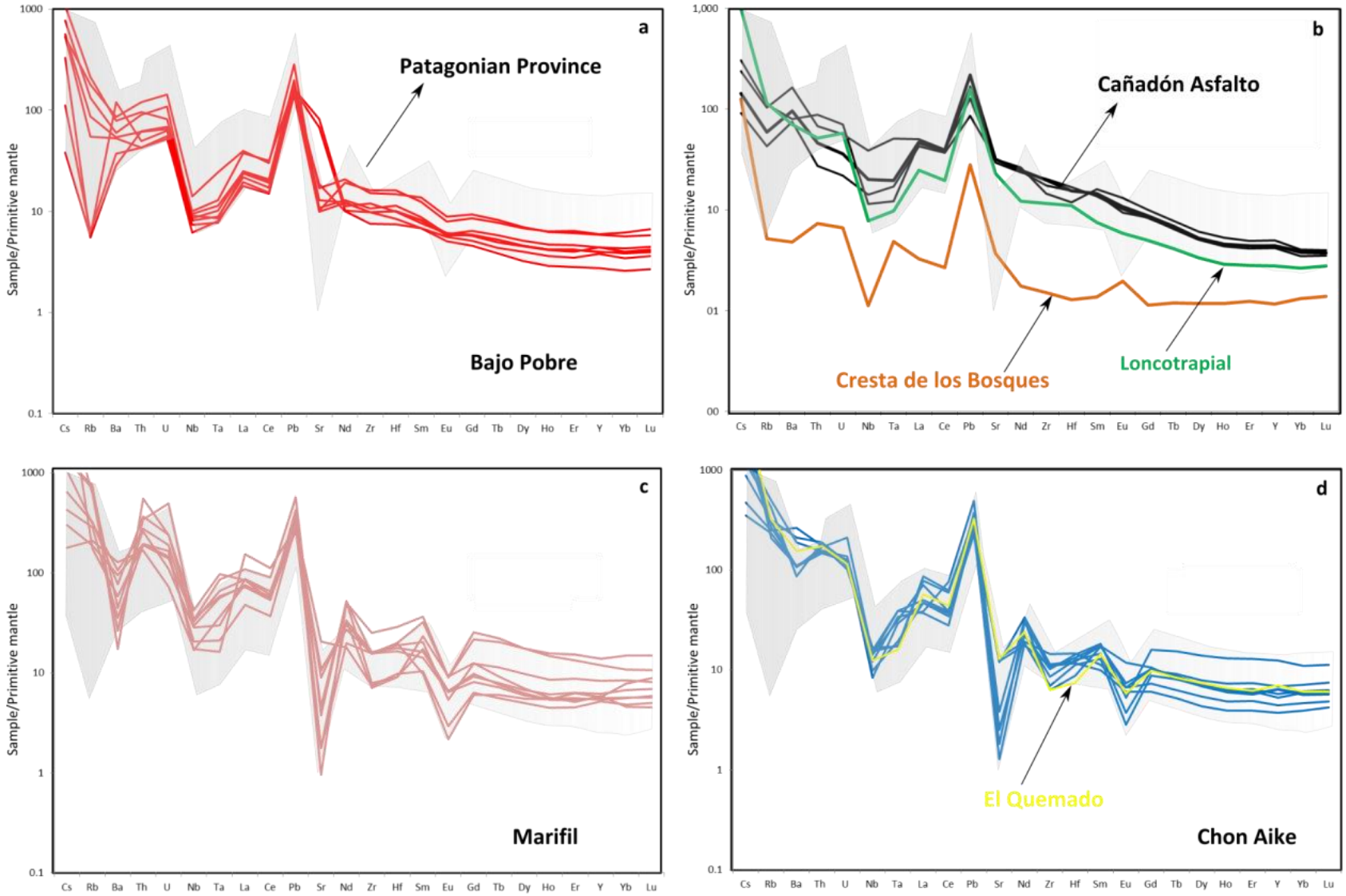

Figure 53. Trace elements composition of Bajo Pobre (a), Cresta de los Bosques, Loncotrapial and Cañadón Asfalto (b), Marifil (c) and Chon Aike Formation (d). Values normalized to primitive mantle from Sun and McDonough (1989). The gray field show trace element composition of the complete set of samples from the Patagonian Province in this work.

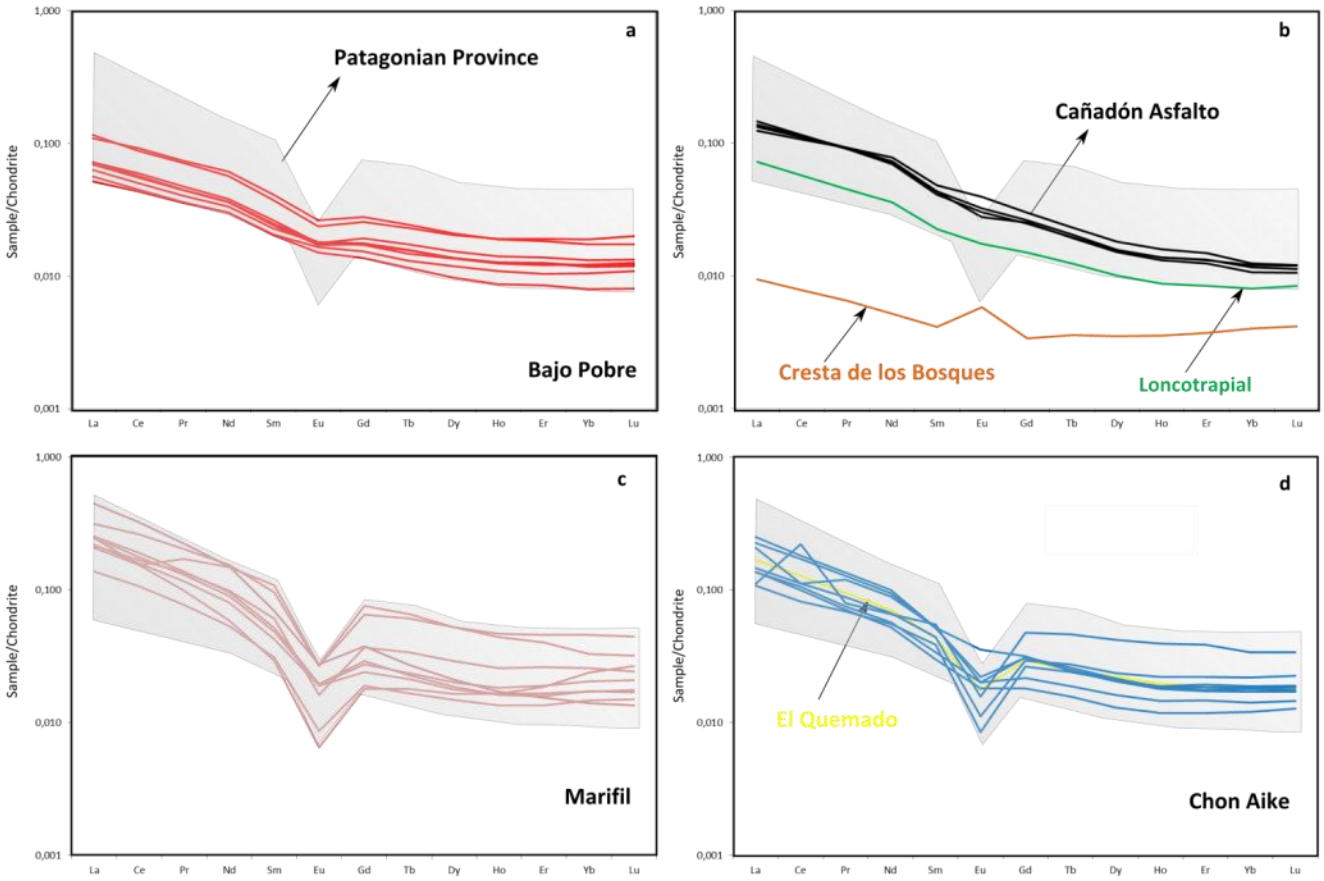

Figure 54. Chondrite normalized rare earth elements (REE) diagram of Bajo Pobre (a), Cresta de los Bosques, Loncotrapial and Cañadón Asfalto (b), Marifil (c) and Chon Aike Formation (d). Chondrite values from McDonough and Sun (1995).

Differences among the two groups are mainly given by the relative increase of trace element contents at rising SiO_2 and the typical anomalies related to the fractionation of mineral phases (ie: plagioclase, leading to low Sr and Eu in evolved rocks). However, it is remarkable that a set of dacites and rhyolites (SiO_2 67-78 wt.%) resemble the patterns of BP and CA. In general, highly incompatible trace elements (Rb, U), Y and REE (La, Yb) are positively correlated with SiO_2 (fig 55). Less obvious correlations are displayed by Hf and Nb vs SiO2, where at given SiO_2, CA and BP yield widely different Hf (CA: 5.2 ppm and BP:3.7 ppm) and Nb (CA:10 and BP:28 ppm) compositions. Opposite to these trends, decreasing contents of Sr occur at higher SiO_2. Exceptionally depleted values of all elements are recognized for the CB sample.

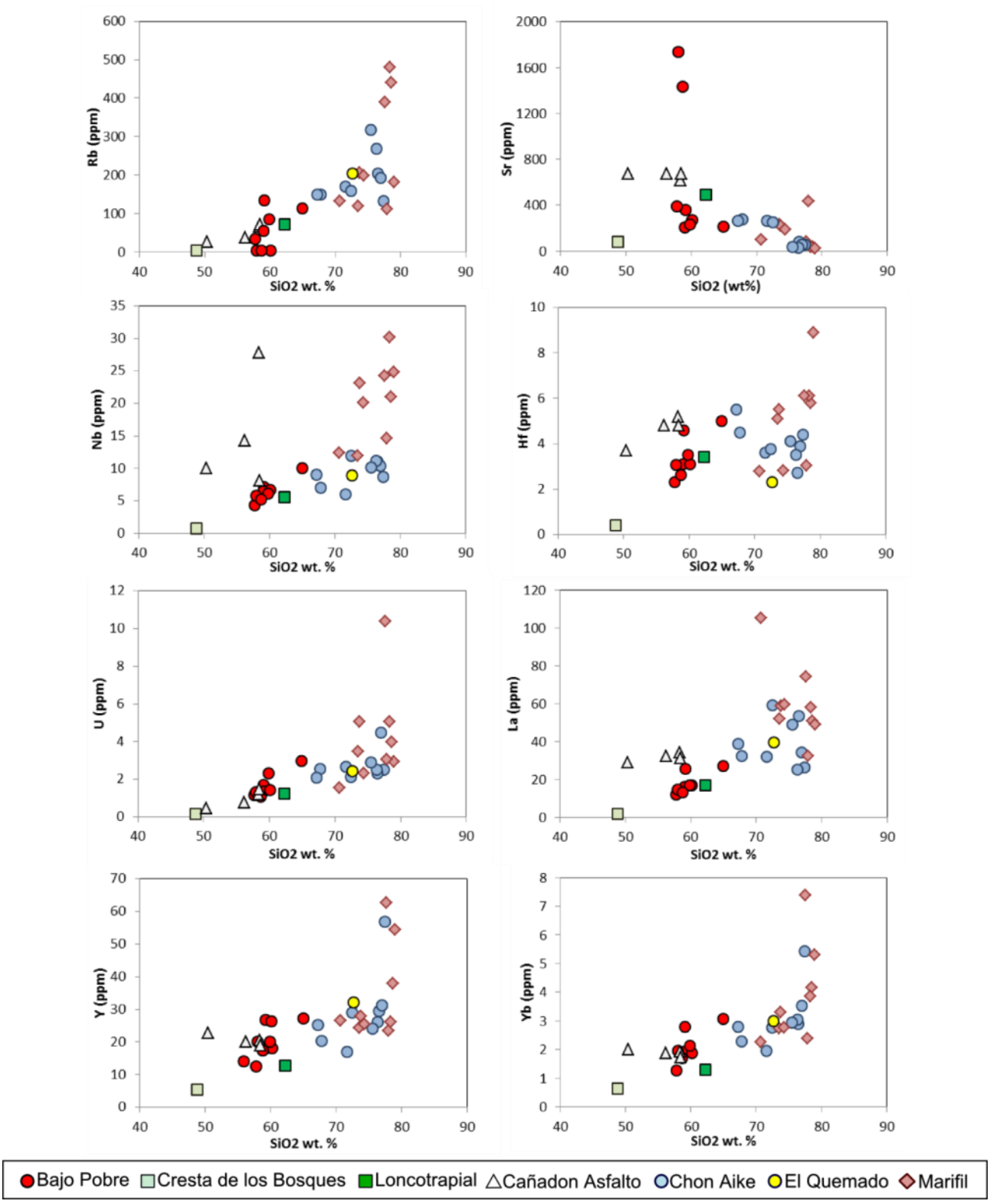

Figure 55. Harker diagrams of incompatible trace elements compositions of Patagonian samples.

Although Sr content is in general moderate, some particularly enriched compositions are recognized in the mafic group. Concentrations in BP rocks vary between 215 ppm and 398 ppm generally, yet with some samples yielding up to 1734 ppm Sr. Also CA and LT rocks are high in Sr (675-620 ppm and 489 ppm, respectively). Enriched Sr abundances (>400ppm) are not accompanied by significant Eu anomaly (Eu/Eu*= 0.95-0.78) or extremely high Al_2O_3 dismissing the possibility that the Sr enrichment could be related to plagioclase accumulation. In contrast, lower Sr compositions (Chon Aike: 278 – 27ppm; Marifil: 436 - 38 ppm) and strong negative Eu anomalies (Eu/Eu* = 0.5-0.2) are restricted to the felsic group. Very depleted Sr (78ppm) and a positive anomaly of Eu (Eu/Eu* = 1.6) are only recognized in CB reflecting the elevated modal plagioclase of this rock. A group composed by four samples from BP, rocks from CA and LT, is defined by high Al_2O_3 (>16 wt.%), Sr enrichment (>400ppm), absence of Eu anomaly, high Sr/Y (86 - 30) and Gd/Yb (3 - 1.8) (fig 56). Similar features are described as typical of *adakitic magmas* formed *by* partial melting of metamorphosed (eclogite, amphibolite) hot and young oceanic crust in subduction settings (Defant y Drummond, 1990). Other petrogenetic processes, like melting of the basaltic lower crust (Condie, 2005; Mori et al., 2007) can partially reproduce this signature.

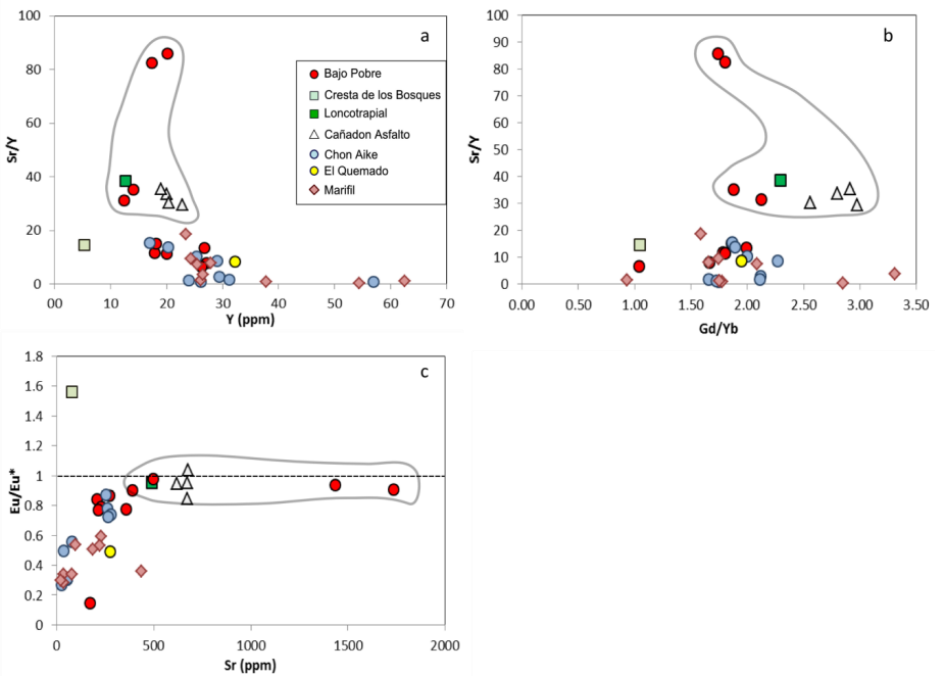

Figure 56. Variation diagrams of incompatible trace elements composition of the Patagonian Province rocks. a) Sr/Y vs Y; b) Sr/Y vs Gd/Yb; c) Eu/Eu* vs Sr. Eu/Eu*= $Eu_N/(Gd_N \cdot Sm_N)^{1/2}$

Pairs of incompatible trace elements with almost identical bulk partition coefficient (Rollinson, 1993), were tested in the Patagonian samples as proxies of extent of melting and/or source characteristics. A bivariate plot between Nb and Ta (not shown) display a positive trend nearly linear in the majority of BP, CA, LT and CB samples. Changes in the slope of correlation defined by higher Ta at lower Nb are observed in most felsic and in one BP sample (Nb/Ta≤10). On the contrary, the majority of mafic rocks and a few felsic ones yield Nb/Ta ≥ 13 (fig. 57). Selective fractionation of Nb and Ta in silicate melts is only caused by rutile fractionation or residual rutile in the source rock (Green, 1995). Experimental studies have shown that rutile is not a likely residual phase in the source of basaltic melts, but appears to be stable during partial melting of hydrous basalts and eclogites (Green and Pearson, 1986; Ryerson and Watson, 1987; Gomez Tuena et al., 2003). High ratios of Gd/Yb (>2), like the ones observed in the enriched group, point out to an eclogite or garnet amphibolite in the source.

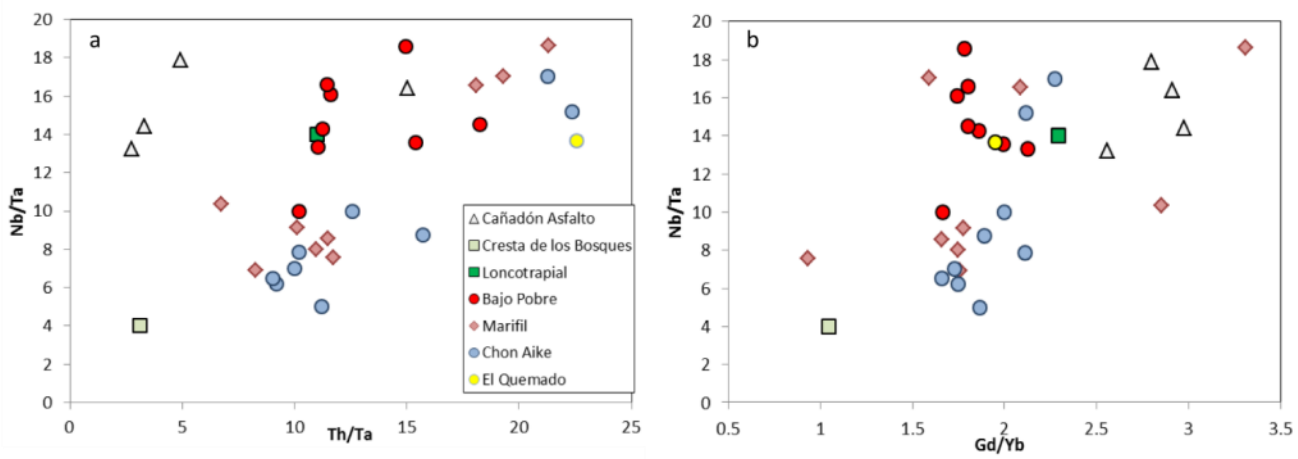

Figure 57. Bivariate ratio plots of incompatible trace elements of Patagonian rocks. A) Nb/Ta vs Th/Ta. B) Nb/Ta vs Gd/Yb.

10. Geochronology

Previous radio-isotopic dating (Rb-Sr, Ar-Ar and U-Pb) available from the literature suggest that the magmatism of the Patagonian Province occurred in a period between 188 Ma and 145 Ma (Rapela and Pankhurst., 1993; Pankhurst et al., 1993; Pankhurst et al., 1995; Alric et al., 1996; Feraud et al., 1999; Pankhurst et al., 2000; Cúneo et al., 2013). Despite the lithological and geochemical affinities displayed by Marifil and Chon Aike Formation, distinct ages on Marifil place this unit as the oldest pulse in the Province (188 Ma – 169 Ma). In contrast, younger dates on Chon Aike (177 Ma- 151 Ma) are mainly spanned by the mafics of Bajo Pobre (164-151 Ma Ma) and Cañadon Asfalto Formation (179-176 Ma). Comparable silicic volcanic rocks from El Quemado (170-145 Ma), interpreted as the Cordilleran equivalent of Chon Aike (Pankhurst et al., 1998),record the latest activity of the Province, up to the Upper Jurassic times (table 1).

10.1 U-Pb dating

In order to further constrain the length of the Patagonian Province and its magmatic pulses, laser ablation ICP-MS (LA ICP-MS) zircon dating was undertaken on three samples: two rhyolites from Marifil (Patvj 39) collected near Florentino Medina and near the Juricó- Valcheta Lake (Patvj 51), in the Somuncura Massif, and one ignimbrite from Chon Aike sampled in the Deseado Massif (Pt113). The analyses were performed Dr. Maya Kamenetsky at the LA ICPM-MS laboratory, University of Tasmania.

Methods

Approximately 100 g of rock was repeatedly sieved and crushed in a Cr-steel ring mill to a grain size <400 micron. Non-magnetic heavy minerals were then separated using a gold pan and a Fe-B-Nd hand magnet. The zircons were hand-picked from the heavy mineral concentrate under the microscope in cross-polarised transmitted light. The selected crystals were placed on double sided sticky tape and epoxy glue was then poured into a 2.5 cm diameter mould on top of the zircons. The mount was dried

for 12 hours and polished using clean sandpaper and a clean polishing lap. The samples were then washed in distilled water in an ultrasonic bath.

The analyses in this study were performed on an Agilent 7500cs quadrupole ICPMS with a 193 nm Coherent Ar-F gas laser and the Resonetics S155 ablation cell at the University of Tasmania in Hobart. The downhole fractionation, instrument drift and mass bias correction factors for Pb/U ratios on zircons were calculated using 2 analyses on the primary (91500 standard of Wiendenbeck et al. 1995) and 1 analysis on each of the secondary standard zircons (Temora standard of Black et al. 2003 & JG1 of Jackson et al. 2004) analysed at the beginning of the session and every 15 unknown zircons (roughly every 1/2 hour) using the same spot size and conditions as used on the samples. Additional secondary standards (The Mud Tank Zircon of Black & Gulson 1978, Penglai zircons of Li et al. 2010, and the Plesovice zircon of Slama et al. 2008) were also analysed. The correction factor for the $^{207}Pb/^{206}Pb$ ratio was calculated using large spots of NIST610 analysed every 30 unknowns and corrected using the values recommended by Baker et al. (2004).

Each analysis on the zircons began with a 30 second blank gas measurement followed by a further 30 seconds of analysis time when the laser was switched on. Zircons were sampled on 32 micron spots using the laser at 5 Hz and a density of approximately 2 J/cm2. A flow of He carrier gas at a rate of 0.35 litres/minute carried particles ablated by the laser out of the chamber to be mixed with Ar gas and carried to the plasma torch. Isotopes measured were ^{49}Ti, ^{56}Fe, ^{90}Zr, ^{178}Hf, ^{202}Hg, ^{204}Pb, ^{206}Pb, ^{207}Pb, ^{208}Pb, ^{232}Th and ^{238}U with each element being measured every 0.16 s with longer counting time on the Pb isotopes compared to the other elements. The data reduction used was based on the method outlined in detail in Meffre et al. 2008 and Sack et al. 2011 similar to that outlined in Black et al. (2004) and Paton et al (2010).

Element abundances on zircons were calculated using the method outlined by Kosler (2001) using Zr as the internal standard element, assuming stoichiometric proportions and using the NIST610 to standard correct for mass bias and drift.

Results

Pure unimodal zircon population where analyzed on the three samples. Only patvj 39 display inclusions of galena, scarce zonation and low U in one of the 15 measured crystals. The full results of the U-Pb zircon dating are presented in the fig. 58 and appendix

Eleven zircon grains on Pt113 (Chon Aike) yielded a Concordia intercept date of 154.4 ±1.4 Ma (mean square of weighted deviates, MSWD = 1.2, fig. 58c). Two older and inherited ages (318.6 Ma and 237.1 Ma) on this sample are coeval to the S and I-type granites from the North Patagonian Massif, respectively (table 10, Appendix). The Paleozoic age S-type granites may be related to a complex setting that comprise subduction, crustal anatexis and the collision between the Deseado and the North Patagonian Massif during the Mid Carboniferous. The early Mesozoic I-type granites are instead related to the delamination of the subducted plate at Permian and Triassic times (Pankhurst et al., 2006).

Two ages of 187.1±1.8 Ma (MSDW= 0.60) and 183.0±1.6 (MSWD = 1.13), were yielded from 12 and 15 analyses on patvj 51 (fig. 58a) and patvj 39 (fig. 58b), respectively (both Marifil). One age of 539 Ma on an inherited zircon from patvj 51 coincides with the I/A-type Cambrian granites of 531±4 Ma(Rapela et al., 2003), belonging to the Brasiliano/Pampean orogenic cycles of South America farther north (Pankhurst et al., 2006).

Geochronology derived from this study is consistent with previous data from the literature, being the oldest age obtained indistinguishable from the previous Rb-Sr (188 ± 1Ma) and Ar-Ar (187.4 ± 1.2 Ma) radio-isotopic dating on Marifil. A first pulse of magmatic activity which probably started at ca. 187 Ma and exclusively represented by this unit is confirmed from these data. Moreover, the younger age here obtained on Chon Aike (154.4 ±1.4 Ma) span the length period known for this unit ca.177- 151 Ma), but also match the late outburst of the Province (ca. 156-144 Ma).

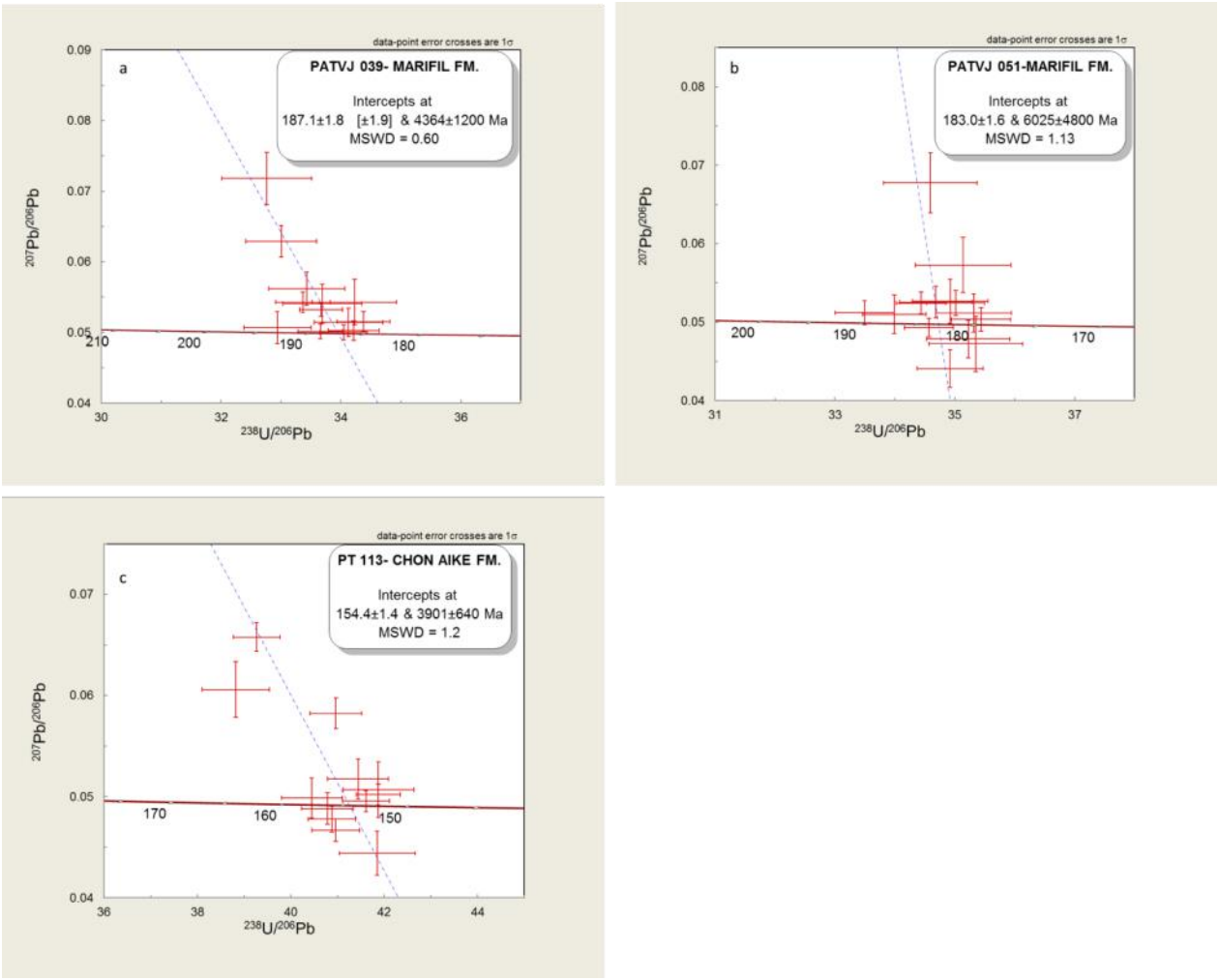

Figure 58. U-Pb laser ablation zircon dating on Marifil (a, b) and Chon Aike Formation (c) displayed in Tera-Wasserburg concordia diagrams. Error crosses were plotted at 1σ level.

ll. Discussion

In the PA, large volumes of felsic rocks occur associated to minor volumes of mafic magma. Probably due to this and the pervasive alteration of the mafics, most of the previous studies have been focused on the felsic rocks. Geochemical analysis derived from these works, have supported a debate about the role of assimilation - fractional crystallization and anatexis in the origin of the PA magmas (see for example Pankhurst et al., 1998). In agreement, a tectonic setting that invoked a generalized extension related to the break-up of Gondwana has been widely accepted together with the influence of the distant plume that formed the Karoo Province (Pankhurst et al., 1995, 1998; Feraud et al., 1999; Pankhurst et al., 2000; Ripley et al., 2001). However, a calc-alkaline affinity and a record of ca. 36 Ma (189-151 Ma) confirmed by this study, are the most typical features of the PA and are not indicative of involvement of a mantle-plume. Notably, a subduction zone acting before and during the PA, has been recognized (Rapela et al., 2005; Seton et al., 2012; Storey et al., 1992, Storey, 1995) but poorly explored in the literature. Its effects added to the complex tectonic setting, seems to be of remarkable meaning in the understanding of the PA magmas.

Petrographic and geochemical evidences of the PA rocks, and particularly of the mafic units, provide some insights into the little evolved melts closest primary melts of a Silicic Large Igneous Province. These data, the derived petrogenetic aspects and the consequences for the previous models are discussed in this chapter.

11.1 The Karoo Province and the PA: A long distance relationship?

The Karoo Large Igneous Province represents a huge volume of continental flood basalts (CFB), preserved as erosional remnants in Southern Africa (Karoo), Antarctica, Australia and New Zealand (Ferrar) (Duncan et al., 1997; Heinonen et al., 2010). It extends over Archean cratons (Kaapvaal-Zimbabwe), Proterozoic belts (Limpopo), and Permian–Jurassic basins as lava flows, sills, and giant radiating dike swarms, covering ca. 3 x 10^6 km^2 (Cox, 1988). Along with the Ferrar CFB, its origin has been related to the early breakup of southern Gondwana and the opening of the Indian Ocean (Ernst and Buchan., 2002; Hawkesworth et al., 1999; Jourdan et al.,2005; 2007; -Heinonen et al., 2010). Compositionally dominated by mafic products, the Karoo event also record a silicic episode that occurs mainly in the Eastern part of the Province (Mwenezi intrusive complex and Lebombo series). Geochronological studies performed by Jourdan et al (2007, 2005 and references therein) constrained the magmatic activity of the Province to a period of 10 Ma, from 184 Ma to 174 Ma, with the main basaltic phase occurred mostly over the first 5 Ma and progressively followed by a more differentiated and less voluminous magmatism over the last 4 Ma (Jourdan et al., 2007).

In terms of age, composition and structure, the Karoo and PA LIPs display clear differences that appeal for other than a common origin derived from a mantle plume.

11.1.1 A matter of timing

The length of the PA is constrained by a set of U-Pb, Rb-Sr and Ar-Ar radio-isotopic dating obtained by Rapela and Pankhurst (1993); Pankhurst et al. (1993); Pankhurst et al. (1995); Alric et al. (1996); Feraud et al. (1999); Pankhurst et al. (1993); Cuneo et al. (2013) and this study. Despite the different methodologies applied, and after recalculating the Ar-Ar ages (after Renne et al., 2010 on Feraud et al (1999) data, since are the only for which the considered age standard was fully detailed), the results are consistent from one method to other (see table 1) and are confirmed by the obtained data from this research (chapter 10). Together, they define a period of at least 38 Ma of magmatic activity in the extra-Andean area, which can be extended to 43 Ma if the Cordilleran magmatism (represented by El

Quemado Fm) is considered (fig. 59). In general, there is a good agreement that the volcanism of PA started with the felsic rocks of the Marifil Formation at ~189 Ma, 5 Ma before the first pulse of the Karoo. However, the occurrences of mafic volcanism in PA, represented by the calc-alkaline basalts from Cañadón Asfalto (~178 Ma – 176 Ma) and basaltic andesites from Bajo Pobre (~166-152Ma) postdate the main phase of Karoo magmatism (~184 Ma -179 Ma).

Moreover, previous geochronological studies and this research, support the fact that overlapping and continuous ages occur along different and geographically distant stratigraphic units during at least 38 Ma. In agreement, it seems more plausible that the Province was formed by a persistent outburst instead of separated pulses (Pankhurst et al 2000). The few and short periods where no volcanism is reported, could be an artifact of the limited sampling given the size and thickness of the Province, more than a gap in the magmatic record.

Figure 59. Probability density plot (Isoplot 4.15, Ludwig, 2012?) for the Jurassic volcanic rocks in the PA. The red line represents the degree of confidence of the data based on error at 1σ. Ages from by Rapela and Pankhurst (1993); Pankhurst et al (1993); Pankhurst et al (1995); Alric et al. (1996); Feraud et al. (1999); Pankhurst et al. (1993); Cuneo et al. (2013) and this study.

Based on the similar ages displayed by the Karoo and the Marifil Fm in PA, Pankhurst et al (2000) and Riley et al. (2001) proposed they could have been formed by the same thermal anomaly that originated the Karoo. Moreover, Ernst and Buchan (2002), supported this hypothesis proposing that 3 or 4 synchronous centers (Lower Limpopo, Lower Zambesi, Dufek and the triple junction of the Weddell Sea; Burke and Dewey, 1973; Windley, 1984; Ernst and Buchan, 1997a; Storey and Kyle, 1997 and Elliot and Fleming, 2000) could gave place to a Karoo-Ferrar-Chon Aike event. In this model, it is considered that a spacing of about 1000 km (Eldhom and Coffin, 2000) between the plume centers was indicative of an underlying mantle upwelling (Storey and Kyle, 1997; Elliot and Fleming, 2000). However, a first and more obvious conflict with this models is derived from the fact that the PA record a long-lasting life of ~ 38Ma whereas the Karoo was formed in a much shorter period of only ~10 Ma (184-174 Ma; Jourdan et al., 2007). In addition, the felsic Marifil formation is 5 Ma older than the main pulse of the dominantly mafic Karoo, opposite to the expected evolution in a traditional plume setting. Moreover, no decreasing ages away from the initial plume centers or neither a trace of migration towards the Marifil Fm have been recognized. In summary, the traditional plume context can be hardly applied to the origin of the PA, and would require either an unconventional diachronic thermal anomaly with an exceptional long life, either different plumes at distances of about 1000 km.

Regional studies have shown that intrusive bodies in northwestern Patagonia display coeval ages to Karoo, and to the less older of Marifil Formation. Granitic and granodioritic rocks from the Sub-Cordillera in Patagonia, display K-Ar (Lizuaín 1981; Spikermann et al., 1988; Haller *et al.,* 1999) and Rb-Sr (Gordon and Ort., 1993) ages in a range from 184 Ma to 177 Ma (with considerable errors up to 10 Ma). However, more recent and precise U-Pb SHIRMP zircon dating yielded ages of 181 ± 2 Ma to 185 ± 2 Ma (Rapela et al., 2005). Comparable to these data, Page and Page (1999) reported Ar-Ar ages on subalkaline gabbros indicating an age interval of 187–178 Ma (not recalibrated due to missing data on the used age monitor). Compositions of these rocks show a signature typical of the I-type granites, that together with the coeval basic rocks, were interpreted by Rapela et al. (2005) as subduction-related cordilleran-type signatures. In addition, the same authors described that this event was compositionally indistinguishable from those of the Andean batholiths (150 Ma - 5 Ma) emplaced in the Pacific margin of South America after Gondwana break-up (Rapela et al., 2005). Despite the

synchrony observed between these data and the beginning of PA, it is in general accepted that different and coeval tectonic settings gave place to the volcanic and plutonic rocks.

MPodozis and Ramos (2008) suggested that the end of the Sub-Cordilleran magmatism (related to a subduction system) occurred at 170 Ma with the beginning of the Chon Aike Province (or PA). They referred that the absence of Jurassic batholiths in Patagonia was indicative of the cease in the subduction regime southward of the North Patagonian Massif. However, it should be considered that intrusive bodies would be hardly exposed on the surface after the emplacement of 235.000 km^3 of volcanic rocks of the PA and the Andean deformation. It is curious that even despite the great efforts on the previous works to solve the tectonic setting, it was not mentioned that the volcanism itself could be expression of an active subduction zone. Thus, from all the geochronological evidence, it seems that there is no need to relate the coeval occurrence of Marifil and the plutons in the Subcordillleran region to different tectonic settings, especially when the plume model does not fully explain all the observed data.

11.1.2 A matter of composition

Despite the large heterogeneities and the mainly felsic character of the PA , all samples share a common signature mainly characterized by the subalkaline character, low Ti, and peraluminous affinity (Al_2O_3 > Na_2O+K_2O+CaO). Although the Karoo Province record some rhyolitic compositions, most of its volcanism is dominantly mafic and tholeiitic. In terms of the trace element compositions, the differences are clear from a multi-element diagram where the Karoo rocks display flatter trends than the PA, accompanied by negative anomalies of Eu, positive of Y and almost absent troughs of Nb-Ta (fig. 60).

Combined with the geochronological evidence previously discussed, the distinct geochemical character of the two Provinces does not support a common origin.

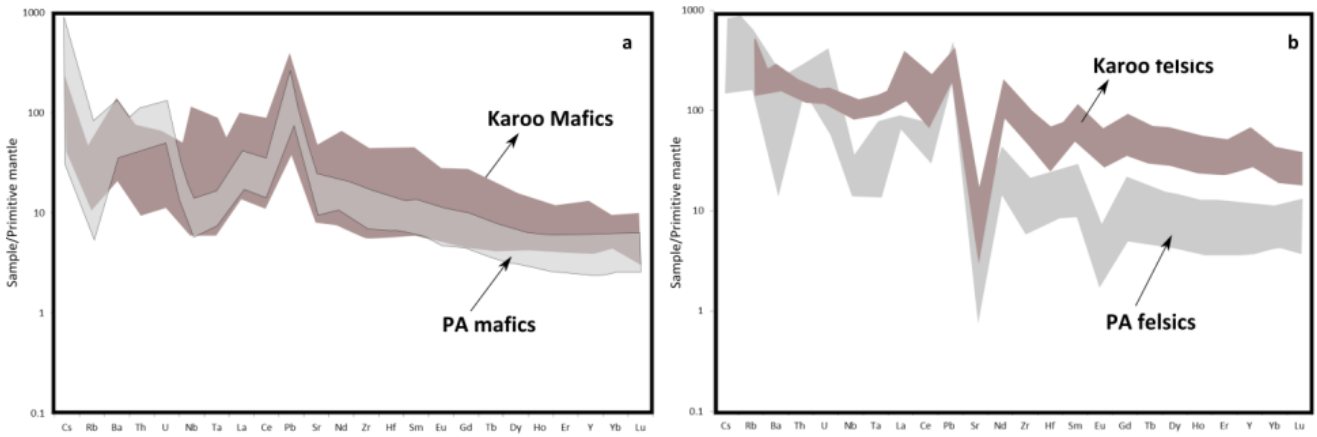

Figure 60. Trace elements composition of mafic (a) and felsic (b) Jurassic volcanic rocks of the PA analyzed in this study and available data from the Karoo Province. Values normalized to primitive mantle from Sun and McDonough (1989). Karoo data from GEOROC database (2008) (http://georoc.mpch-mainz.gwdg.de).

11.2 Petrogenesis of the Patagonia Province

11.2.1 Subduction melts or lower crustal melts?

Geochemically less known than the dominant felsic rocks, the mafic volcanics from PA have compositional features that represent the closest evidence of little evolved mantle-derived melts. A characteristic calc-alkaline affinity combined with high Al_2O_3 (16 wt.% – 20 wt.%), LILE enrichment (Rb >35 ppm; Ba >500 ppm), troughs of Nb-Ta, and positive anomalies of Pb, resemble subduction magmas. A general depletion of Y and slightly of HREE (La/Yb of CA: 18-15; BP: 9.61-7.60 and LT: 13.15) (see chapter 9), is accompanied in a few mafic samples by unusual high contents of Sr and high ratios of Gd/Yb and Sr/Y that akin adakitic rock-types (Deffant and Drummond, 1990) (fig. 61).

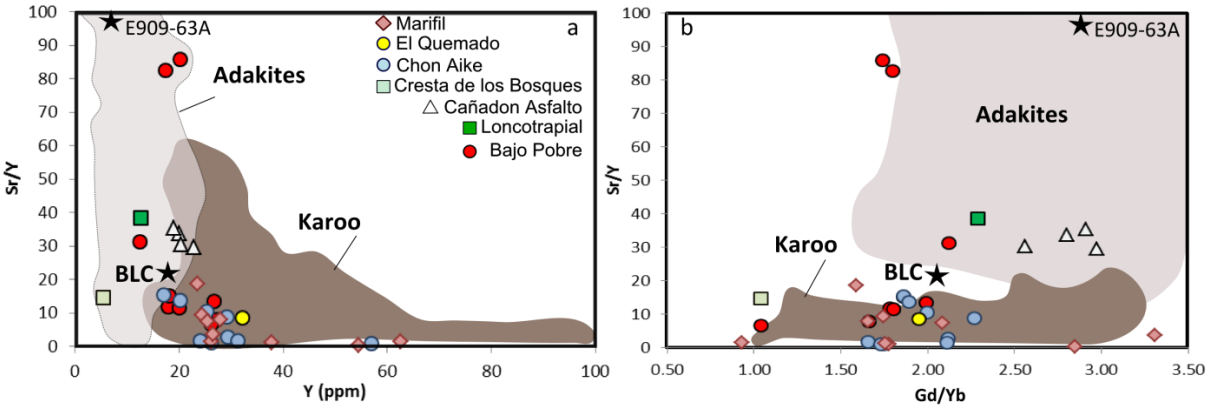

Figure 61. Sr/Y vs Y (a) and Sr/Y vs Gd/Yb ratios on mafic samples from PA and E909-63A (xenolith data reported by Castro et al (2011). Bulk composition of the lower continental crust (BLC) from Rudnick and Gao, 2003).

Analogues to the Archean Tonalite – Trondhjemite – Granodiorite (TTG) (Martin et al., 1999), the adakite compositions of $SiO_2 \geq 56$ wt.%, Y ≤18 ppm, low HREE (Yb ≤ 1.9 ppm), high Sr (rarely < 400 ppm) and $Al_2O_3 \geq 15$ wt.% are explained by the direct melting of a hot and young (<25 Ma) subducted oceanic crust (Deffant and Drummond., 1990). In that setting, the partial melting of a metamorphosed basalt (amphibolite / eclogite) would produce relatively high-Al_2O_3, mostly corundum-normative intermediate-silicic melts. The garnet (or amphibole) rich residue would lead to the HREE and Y depletion, and therefore to the high Sr/Y ratios. Alternatively, comparable compositions have been also explained by melting of a garnet bearing continental crust (Kay and Abbruzzi, 1996; Petford and Atherton, 1996; Xu et al., 2002).

In the Patagonian region, granulite xenoliths enclosed in Paleogene alkali basalts from Paso de Indios in the Cañadón Asfalto Basin, have been reported by Castro et al. (2011). They represent an exceptional evidence of the crustal composition and of Jurassic lithospheric processes of the Province. Composed by orthopyroxene, clinopyroxene and plagioclase, dominantly, these rocks display extremely depleted incompatible trace elements compositions similar to other lower crust mafic granulites. Castro et al. (2011) suggested that the granulites from Paso de Indios represent the residue of a segregated silicic melt by either partial melting of a solid source, or incomplete crystallization of a parental intermediate magma during a complex lithospheric evolution. However, the granulites may alternatively be interpreted as co-genetic cumulates. High ratios of Sr/Y (97.58; 526.72) (fig 61a) and Gd/Yb (2.90; 2.17) (fig 61b) calculated from the reported values on these samples (E909-63A, E909-63B), akin the typical ratios of adakitic rocks. It is thus implicit that melts derived from a rock similar to such granulites would display Eu troughs, and lower ratios of Sr/Y (than the ones described) as result of the high plagioclase content observed therein. Moreover, neither garnet or rutile are residues in such granulites as required to form the adakitic signal. Therefore, it is unlikely that the adakitic signature of the PA samples was formed by melting of a lower crust similar to that of Paso the Indios.

Additional evidence derived from high Gd/Yb (>2) and Nb/Ta ratios, strongly suggest that garnet and/or rutile were residual phases during melting of subducted crust as eclogite or garnet amphibolite. Moreover, Foley et al. (2002) suggested from experimental data that Nb/Ta variations, like those described in the chapter 9, might also occur due to melting different levels of the slab where amphiboles have variable Mg Although none of these hypothesis can be really constrained form the available data, it is clear that a source that involved a residue of rutile or garnet played an important role in the petrogenesis of these magmas. In agreement, experimental results obtained by Rapp and Watson (1995) show that adakitic or TTG compositions can be formed by 5 – 20% of partial melting of garnet amphibolite at 8 – 16 kbar and 1000°C. – 1025°C, analogous to those obtained on PA samples after Putirka (2008).

In order to contribute to decipher the *tectonic environment* involved in the generation of the PA, were performed microprobe analysis on chromium spinel inclusions on the basis that obtained compositions can be used to distinguish the tectonic setting of volcanic, and even altered, mafic rocks. Almost identical compositions were displayed by some of the samples with adakitic signal also belonging to different and geographically far stratigraphic units (BP and CA) (better described in the chapter 8). The analyzed spinels present high Al_2O_3 and moderate TiO_2 contents, differing clearly from the typical compositions described for LIPs and OIBs (low Al_2O_3 and high TiO_2) and instead akin to MORB and back arc compositions reported by (Kamenetsky et al., 2001). However, no other evidence derived from this study or from the literature support the possibility that PA magmas could be caused by a depleted, MORB-like mantle. Although isotope data are not available from this study, initial isotopic ratios of Sr obtained by Pankhurst and Rapela (1995) on Marifil and Chon Aike show uniform $^{87}Sr/^{86}Sr_i$ (0.7067 ± 0.0005) similar to those of Bajo Pobre (0.7067 ± 0.0005). More heterogeneous results from Nd isotopes were observed from Marifil (εNd: -8.2 to -3.9) and the few data from Chon Aike (εNd: - 1.8 and -3.9) and Bajo Pobre (εNd: -3.8 to -4.3), which in general indicate that the continental crust or subducted sediments (or both) contributed to the origin of these magmas. Clearly, a complex interpretation is required to combine the fairly enriched Sr-Nd isotopic compositions and the spinel analyses which point instead to a depleted source. This interpretation will be attempted by considering the possible tectonic context active during the Jurassic in southern South America.

Paleo-tectonic reconstructions presented by Seton et al. (2012) described a convergent margin between the Phoenix plate and the western margin of Gondwana during Jurassic times (fig. 62). Although the age of the Phoenix plate is unknown, it is well defined that the accelerating growth of the Pacific plate was related to the triple junction Phoenix-Farallon-Izanagi at ca. 188- 180 Ma (Handschumacher, 1988; Nakanishi and Winterer, 1998), and that a spreading center in the Pacific was active during those times. Therefore, it is likely that the recently formed oceanic crust (not older than 30 Ma) of the Phoenix plate with a direction motion ENE, inexorably converged and subducted beneath the western margin of Gondwana during Jurassic times.

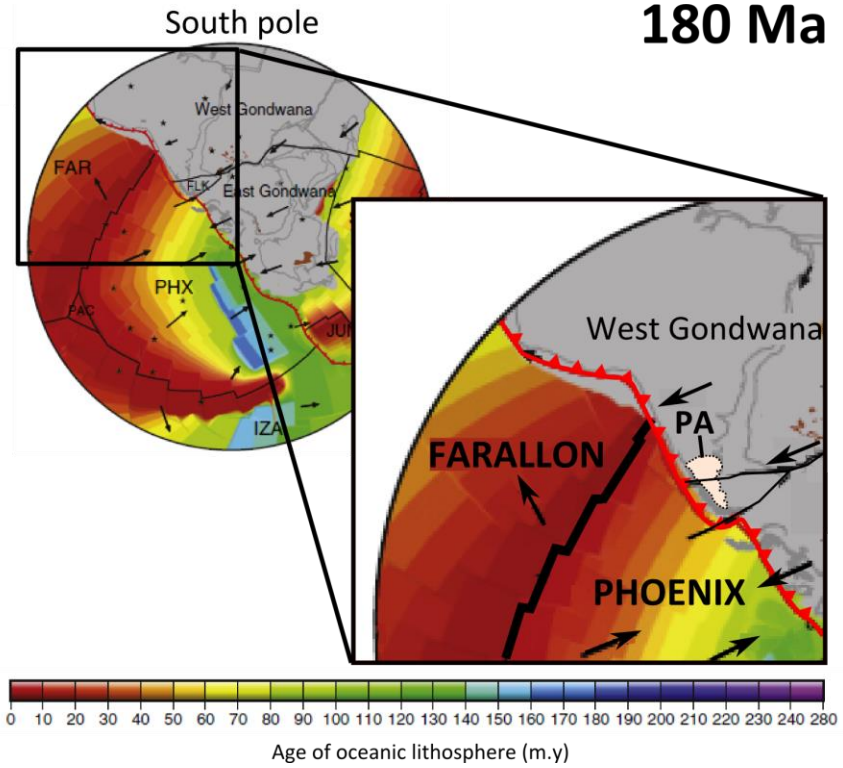

Figure 62. Global plate tectonic reconstruction at 180 Ma. Modified from Seton et al. (2012).The West Gondwana margin, Farallon and Phoenix plates and Patagonia Province (PA) are evidenced. At the base of the figure it is shown the age-area distribution of oceanic lithosphere at the time of formation. Black arrows represent the absolute plate velocity.

MORB-type compositions recorded by the chromium spinel inclusions cannot be explained by crustal melting like previous models predicted for the whole Province. However, an scenario where young oceanic crust formed at the Phoenix-Farallon spreading center converged with evolving continental rifts could produce slab melts and astenospheric flux. The contribution of such processes would be evidenced by the geochemical fingerprint of chromium spinel. Slab melts derived from the subduction of that crust would impart the adakitic signature. However, since the PA rocks with a clear adakite signature are rare, and primitive melts are nearly inexistent, it is possible that slab melt or astenospheric influx (Kay, 1978) were not volumetrically important as much as thermally determinant in the origin of PA. Therefore, the majority of PA rocks, which lack of a dominant adakitic signature were likely influenced by a combination of petrogenetic processes that diluted the this contribution. Supporting such hypothesis, high Rb/Nb ratios in the PA are almost exclusive of the felsic rocks (31.2 – 9.8) whereas more depleted values are typical of the mafics (11.4 - 0.52) (fig. 63). High solubility in aqueous fluids of Rb contrasts with the more immobile character of Nb, even if this element can be

mobile at elevated temperatures (Mori et al., 2007). Therefore, lower ratios of Rb/Nb occur in the slab melts after dehydration of the subducted plate, whereas higher ratios would be related to flux and addition of the derived fluids. A common origin but different components of the subduction seems then to have played an important role in the petrogenesis of the PA. In agreement, most of the samples are slightly corundum-normative but not all of them show the garnet signature. It is possible that lower Gd/Yb ratios reflect higher degrees of partial melting in agreement with a process of adiabatic decompression, also evident from a weak but clear, positive correlation between Nb/Zr and La/Yb. In addition, the peraluminous character of these rocks and the uniform contents of Na_2O (~ 4 – 2.4 wt.%) at variable SiO_2, support the influence of subducted sediments (eg: metagrawackes, pelites), fluid addition or crustal assimilation (Miller, 1981) in the whole sequence.

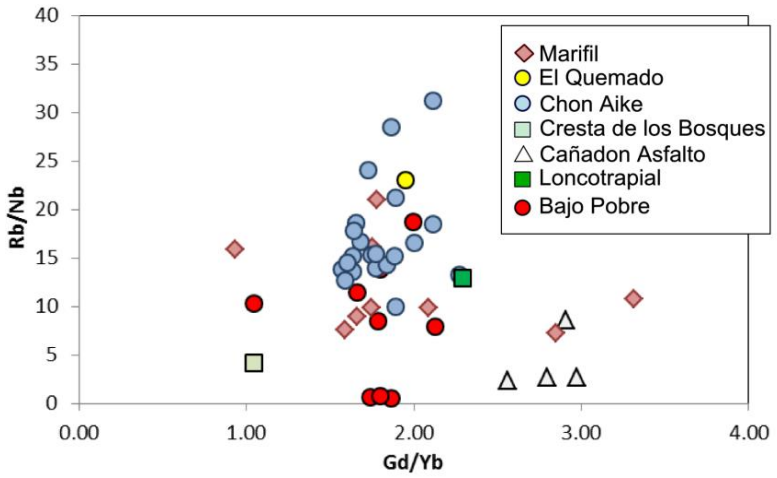

Figure 63. Rb/Nb vs Gd/Yb ratios of Pa rocks.

U-Pb SHRIMP zircon dating on one of the xenoliths from Paso de Indios show a Concordia age of 175.9 ± 4.9 Ma representative of the metamorphic event (Castro et al., 2011) which, within errors, is coeval to the Cañadón Asfalto rocks (~179 – 176 Ma) and the I-type granites of the Sub-cordillera region (187 - 178 Ma). A connection between these events is supported by the similar granitic to granodioritic compositions of the segregated melts associated to the xenoliths (Castro et al., 2011) and the intrusive Sub-cordilleran rocks. In addition, the metamorphic evolution of the residual rocks was apparently dominated by a decompression pattern at starting conditions of > 0.9 GPascal (9kbar) and temperatures of 1000 °C (Castro et al., 2011). Similar data obtained on Bajo Pobre rocks (see chapter

8), indirectly trace a regional process occurring at those conditions along the the Province. Considering that temperatures lower than 1000 °C would be expected for mafic granulite terrains (Harley, 1989), it is possible to suggest that the PA region was suffering an anomalously high heat supply, possibly related to astenospheric flux in response to the combined influence of the hot subducting slab and the extensional regime induced by the break-up of Gondwana.

11.2.2 Fractional crystallization?

Pankhurst and Rapela (1995) interpreted the rhyolites from Marifil and Chon Aike as the products of multistage partial melting and fractionation from an andesitic parental magma, which probably was formed by partial melting of the Grenvillian lower crust. Based on this, Riley et al. (2011) proposed that the heat source that caused the melting, was related to basaltic underplating as a result of the peripheral effects of a mantle plume. Alternatively, and given the evidences of a subduction signature in the PA magmas, the same authors proposed that a hydrous lower crust formed by addition of an amphibolite-rich mafic layer (derived from a subducted plate) could have caused the mafic underplating. Intermediate to felsic magma with uniform isotopic chemistry (Chon Aike: $^{87}Sr/^{86}Sr$= 0.7067 ± 0.0005; εNd=from - 1.8 to -3.9) were then considered as result of a MASH process (melting, assimilation, storage and homogenization). This hypothesis predicts that after MASH, melts would crystallize or fractionate further to re-establish buoyant ascent and geochemical and isotopic variations (Riley et al., 2001; Gomez Tuena et al., 2003). It would be then expected that further fractional crystallization from such homogenized magma occur under the same liquid line of descent. Although no isotope data are available from this study to test if mafic-intermediate magmas display also the uniformity described by the MASH model, it is supposed on the basis of this hypothesis that a close system with fractional crystallization should reflect a consistent trend in the evolution of the major elements compositions in agreement with the observed compositions of PA.

In order to model a closed system where the magmatic differentiation occurred through fractional crystallization it was used MELTS (Ghiorso and Sack, 1995; Asimow and Ghiorso, 1998). The initial composition consisted of an andesitic rock from the Bajo Pobre Formation (pt 116), representing the

parental composition of rhyolitic magmas as described by Pankhurst and Rapela (1995). A pressure of 9 kbar spanning the crystallization pressure range obtained following Putirka (2008) (see chapter 8) was considered, as well as lower pressures of 6 kbar and 3 kbar in agreement with a process of polibaric magma chambers, as is suggested from the literature. Anhydrous and hydrous conditions as well as oxygen fugacity constrained by the Nickel Nickel Oxide (NNO) buffer were the initial parameters considered. Additional trends derived from the composition of the xenolith from Paso de Indios were also included using the same starting conditions.

Liquidus temperatures at 9kbar and anhydrous conditions were about 1370°C. Fractionation of orthopyroxene was followed by low-Ca clinopyroxene and plagioclase (An_{60}) assemblage. Low-Ca and high-Ca clinopyroxene + plagioclase appeared at 1249°C, a temperature much higher than the ones calculated according to Putika (2008) (1011°C and 987°C). Other mineral phases like quartz at 1089°C followed by spinel + oxides and garnet are displayed at 1049°C and 1009 °C, respectively. Similarities in the mineral paragenesis from the model and the real data are evident only during the first parts of the model (opx + low Ca-cpx + pl). A negative correlation observed from the MgO vs SiO_2 diagram is in good agreement with observed PA compositions, being progressively more similar to the PA felsics with decreasing of pressure. However, it is remarkable that for all major elements vs SiO_2, liquid trends of descent are clearly decoupled from the PA rock compositions. Therefore, the closed system fractionation model at anhydrous conditions in general fails describing the evolution from mafic to intermediate and felsic compositions. Results obtained from modeling the evolution from the xenolith composition (data from Castro et al., 2011) show slight changes for SiO_2 and major element trends even more decoupled and completely in disagreement with the whole set of PA (fig 64).

At hydrous conditions and 9 kbar, the liquidus temperature was 1308°C. Fractionation of orthopyroxene started at 1268°C whereas high-Ca clinopyroxene appeared at 1188°C, also above the estimated temperature according to Putika (2008). Garnet and plagioclase (An_{63}) occurred at 1068°C. Except for the fractionation of garnet, the paragenesis is comparable to the mafic and intermediate rocks of the PA. However, the absence of quarts in the model contrast with the modal abundance of this phase in the PA. At difference of the obtained esults at anhydrous conditions, this model is able to reproduce the trend of some elements like TiO_2, CaO and FeO_t vs SiO_2 of PA, particularly at low

pressures (3 kbar). However, decoupled compositions of MgO, Na_2O, K_2O MnO, and P_2O_5 still suggest that even at hydrous conditions a closed system cannot explain the evolution of these rocks (fig. 65). Petrographic evidence described in the chapter 7, suggest magma mixing occurring during the evolution of the PA magmas, also in agreement with the geochemical features previously described. Hence, the hypothesis of a closed system according to the MASH model cannot fully explain the observed compositions in the PA. An open system where recharge, assimilation and mixing occur seems more realistic.

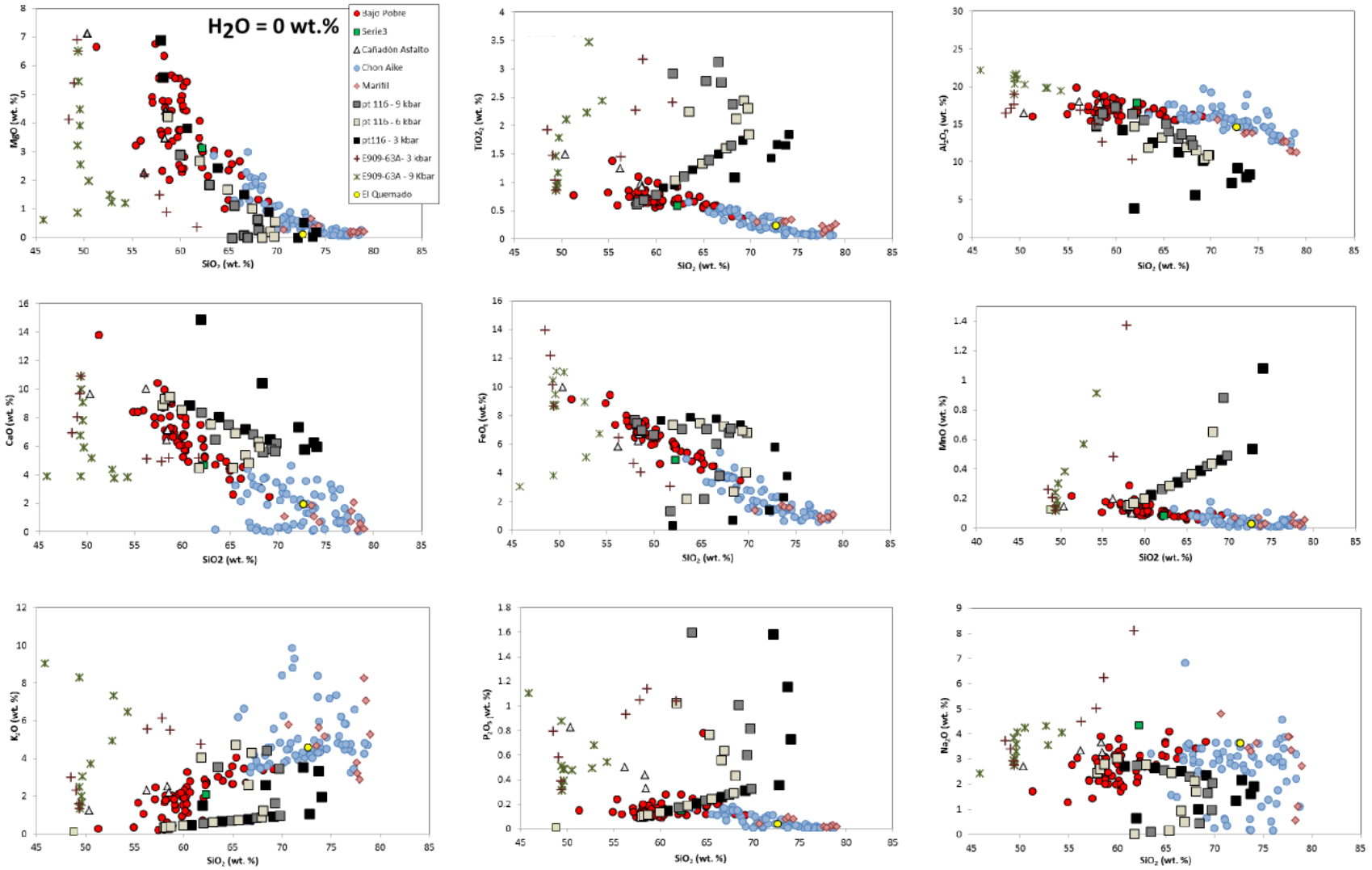

Figure 64. Major elements variations diagrams showing compositions of PA rocks and liquid lines of descent modeled with MELTS at 9 kbar, 6 kbar and 3 kbar at anhydrous conditions. Temperture increaments were set at 40°C. E909-63A and E909-63B correspond to trends modeled from xenoliths reported by Castro et al (2011).

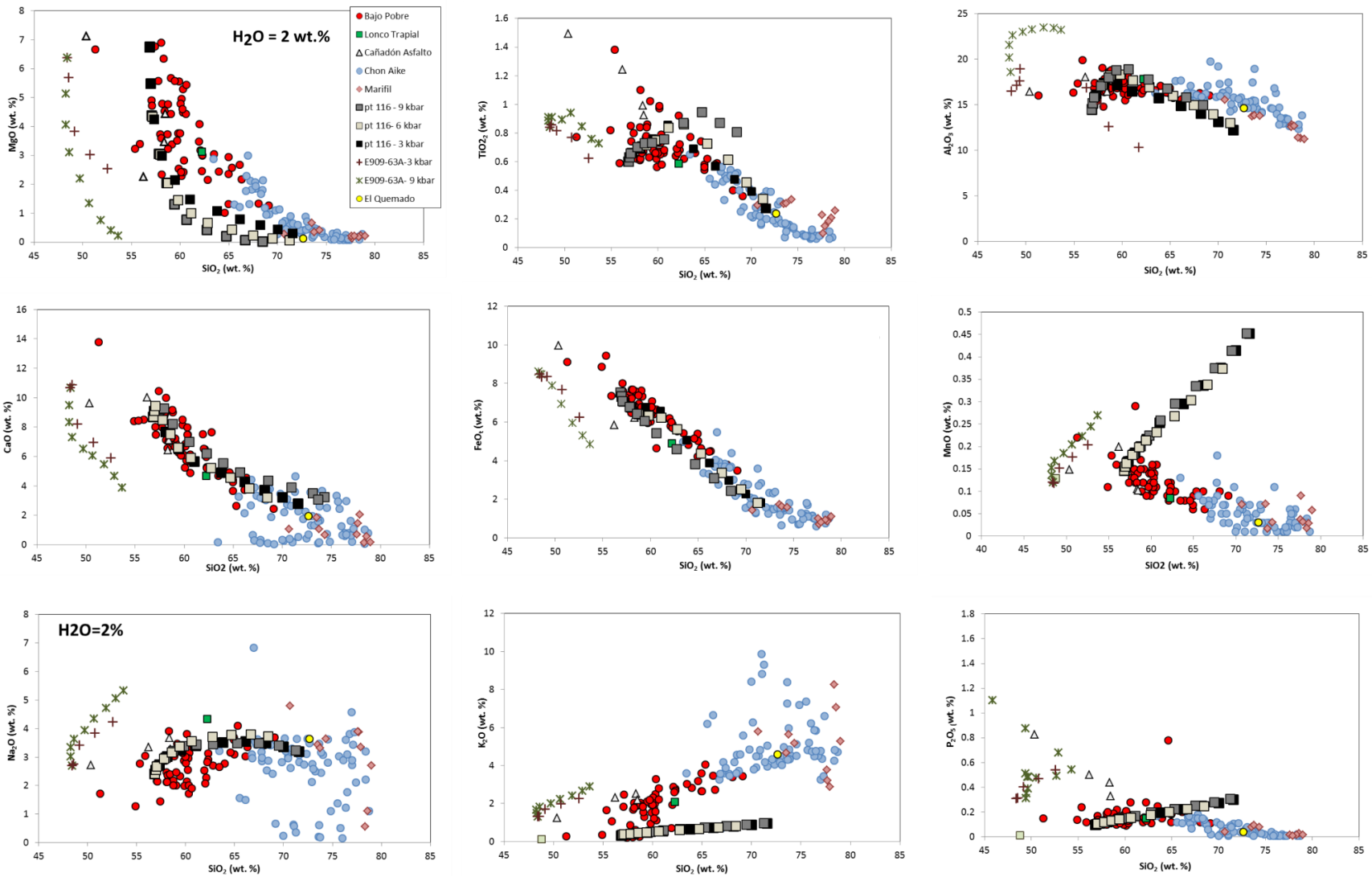

Figure 65. Major elements variations diagrams showing compositions of PA rocks and liquid lines of descent modeled with MELTS at 9 kbar, 6 kbar and 3 kbar at hydrous conditions. Temperture increaments were set at 40°C. E909-63A and E909-63B correspond to trends modeled from xenoliths reported by Castro et al (2011).

11.3 Tectonic considerations

Since the Karoo-plume was an unlikely heat-source for the PA, and considering that a plume activity of 38 Ma duration without a hotspot track is questionable, we explored the possibility that the PA could be derived exclusively from crustal processes related to the breakup of Gondwana. Although the generalized extensional regime could promote crustal thinning and adiabatic decompression, there is a general consensus that the continental crust cannot reach temperatures high enough for fluid absent (or water-deficient) melting without additional heating from a basic source (i.e., underplated or intraplated mantle-derived magma) (Thompson, 1999; Pettford and Gallagher, 2001). A new model based on geochemical evidences derived from this study which akin to the arc magmatism, suggest the contribution of different components of the slab in the origin of the PA magmas. Chromium-spinel compositions comparable to those normally found in MORBs, can be hardly explained in the light of the previous models but are instead consistent with the hypothesis that oceanic crust or an asthenospheric upper mantle was involved in the petrogenesis of the PA magmas. The influence of the continental crust accepted by the earlier studies on the basis of high initial $^{87}Sr/^{86}Sr$ (0.7067 ± 0.0003; Pankhurst and Rapela, 1995), is here alternatively explained as derived from melting of subducted sediments. This hypothesis is supported by enriched ratios of incompatible trace elements tracers of the subduction processes (ie: Rb/Nb).

While the subduction signature could explain the composition of the mafic magmas, the volumetrically dominant acid rocks still require a substantial involvement of the local continental crust, since otherwise enormous volumes of slab melts and very large degrees of fractional crystallization would be needed. However, the geochemical modeling (MELTS) shows that closed system fractional crystallization starting from (BP or CA) mafic magmas cannot explain the generation of the acid magmas, i.e. Chon Aike and Marifil. Therefore, it seems more realistic to propose a model where subduction-derived melts and fluids migrated through and interacted with the continental crust. Examples of similar magmatism and processes are represented by the analogous silicic magmatism of the Sierra Madre Occidental in Mexico (eg: Ferrari et al., 1999, 2007).

According to the regional geology data and tectonic reconstructions, the PA was probably formed during a generalized extensional regime that involved the continental rupture, but also rifting stages and formation of local basins related to the subduction and the opening of the Weddell Sea (Storey, 1992, 1995; MPodozis and Ramos, 2008; Figari, 2005).

Subduction of oceanic crust and sediments followed by metamorphism, dehydration and fluid-induced melting of a mantle wedge, could have caused the formation of andesitic (and adakitic) compositions in agreement with the predictions that andesitic magmas occur at conditions close to water saturation (Grove et al., 2002; 2003; Parman and Grove, 2004). Accordingly, a fast increase of the temperature at the base of the mantle wedge would be expected, as result of spreads melting out by the large temperature lowering at cause of the H_2O released during metamorphic reactions (Grove et al., 2006), as well as a thermal effect promoted by the influx of asthenospheric mantle due the meeting between a convergent and a divergent setting.

It is also possible that due to crustal stretching and plate boundary forces acting at the same time, the crust-mantle boundary (Moho) was at shallower depths promoting the influx of asthenospheric mantle in the Patagonian region. Although the mean Moho depths for continental areas is of about 38 km (Mooney et al., 1998), it is predictable that crustal thinning could be caused by extension of a previously already thinned crust (Panhkhurst et al., 2006; Ramos, 2008; Klemperer, 1989). In such setting, the inflow of the asthenosphere and slab melts migrating to the base of a shallower crust could have triggered partial melting and subsequent crustal assimilation and magma mixing. Supporting this hypothesis, numerical simulations performed by Pettford and Gallagher (2001) and Annen et al (2006), explored the effect of emplacing mafic intrusions in the continental crust. They suggested that silicic melts and different degrees of partial melting (at 0.7 – 1.6 GPa and 900 - 1000°C; Pettford and Gallagher, 2001) can be reached by the influence of periodical basaltic intrusions, and that partial melting of continental crust beneath intrusions may provide means of mixing mantle and crustal components.

Moreover, It may be suggested that the NNW-SSE oriented half grabens described by Feraud et al. (1999) and inherited extensional structures formed during the Triassic and Permian extensional events (Zeil, 1979; Kay et al., 1989; Ramos, 2000; Franzese and Spalletti, 2001), were probably used as

emplacing channels and might determine the mainly fissural eruption-style of this Province (eg: Marquez et al., 2011). Despite this, no migration pattern is observed from the available ages suggesting that either the structures preceded the magmatism or just confirm that the magmatism was continuous and not cyclic by defined pulses.

Finally, a comprehensive view of all available (geochemical, geochronologic, geodynamic) data, point out that the origin of the PA could not obey to a unique process or tectonic setting. It is thus likely that a combination of mechanisms that define the signature and main characteristics of the PA were necessarily driven by two major processes which remained active for the 38 Ma of the PA length: the rupture Gondwana and the subduction of the Phoenix plate.

CONCLUDING REMARKS

The results obtained from this research were achieved in order to contribute to the knowledge of the Patagonian geology and the study of the Large Igneous Provinces. The most remarkable evidences and major interpretations can be summarized as next:

Geochemistry

- The PA magmas display a bimodal composition and a signature typical of arc magmatism characterized by calc-alkaline affinity, Nb-Ta troughs, LILE enrichment, peraluminous character and presence of orthopyroxene
- A group of mafic rocks from the BP, CA and LT show adakitic compositions (Gd/Yb: 3 – 1.8; Sr/Y: 86 – 30)
- Nb/Ta and Gd/Yb ratios suggest residual garnet or rutile in an amphibolitic or eclogitic source (ie: methamorphosed oceanic basalt).
- The typical peraluminous character and LILE enrichment of the PA rocks can be related to melting of metamorphosed pelitic sediments.
- Fractional crystallization in an open system and assimilation of continental crust is deduced from the (not satisfactory) geochemical modeling of a closed system.

Petrography and Mineral chemistry

- Magma mixing is suggested from petrographic evidences
- Calculated crystallization pressure and temperature show conditions of ~9 kbar and ~1000°C for BP (in the Deseado Massif) coinciding with inferred conditions of Jurassic silicic melts in the Cañadón Asfalto Basin (Castro et al., 2011) trace a regional magmatic process occurring at such conditions
- Chromium spinel inclusions in olivine are similar to compositions of Cr-spinel in MORB (Al_2O_3: 22 – 31 wt.% and TiO_2: 1.3 – 1.3 wt.%).

- Almost identical compositions of major, trace elements and Cr-spinel compositions in BP and CA suggest a petrogenetic connection between the two stratigraphic units.

Geochronology

- Ages of 187.4 ± 1.2 Ma and 183 ± 1.6 on Marifil and 154±1.4 Ma on Chon Aike, were obtained by LA-zircon dating in this study confirming that correspond the oldest and youngest units (respectively) of the PA
- A period of magmatic activity of at least 38 Ma with no geographic migration pattern is defined by the new U-Pb ages and available geochronology from the literature
- No geochronological record support the existence of defined pulses in the PA

Tectonic consideration and alternative model for the origin of PA

While the volcanism of the PA was largely continues and the mantle plumes are sporadic and short episodes, an alternative model is appealed to explain the volcanism of the PA as an unavoidable consequence of the plate tectonics.

During Jurassic times, two processes were constant and synchronous to the formation of the PA: The break-up of the Gondwana supercontinent and the subduction of the young and hot Phoenix plate. Melting of an oceanic crust of such characteristics produces adakitic magmas as those reported for some of the PA mafics, while meeting a convergent and divergent setting predict the influx of the asthenospheric mantle. The combination of these processes acted as heat source in a thinned continental crust due to the generalized extensional regime governed by the Gondwana break up. As a consequence, the large volumes of felsic magmas recorded in the PA would be derived from the partial melting, mixing and assimilation processes in the continental crust triggered by a hybrid tectonic setting.

Further considerations for future works

All earlier studies considered the volcanism of the PA as one of the most representative silicic Large Igneous Provinces in the world on the basis of its voluminous outburst formed at three defined periods of magmatic activity during the Jurassic times. The undeniable size of this Province and the felsic domain, are clearly strong arguments to put it in the list of the silicic LIPs. However, some remarkable observations about its origin and length should be considered at the light of the LIP definition. Obtained results from this research supported by a compilation of previous studies, suggest that the intra-plate origin and short pulses of activity described by previous authors are inconsistent. Therefore, if the PA is considered a LIP, it is thus required that the perspective of a new model be included in a revisited definition of silicic Large Igneous Provinces.

BIBLIOGRAPHY

Alibert, C., Michard, A. and Albaréde, F., 1986. Isotope and trace element geochemistry of Colorado Plateau volcanics. Geochimica et Cosmochimica Acta, 50(12): 2735-2750.

Allan, J.F., Batiza, R. Perfit, M., Fornari, D., Scak, R., 1989. Petrology of lavas from the Lamont seamount chain and adjacent East Pacific Rise, 10 N. Journal of Petrology, 30(5): 1245-1298.

Alric, V., Haller, M., Féraud, G., Bertrand, H. and Zubia, M., 1996. Cronología 40Ar/39Ar del vulcanismo jurásico de la Patagonia extraandina, 13 Congreso Geológico Argentino.

Anderson, D.L., 1996. Enriched asthenosphere and depleted plumes. International Geology Review, 38(1): 1-21.

Anderson, D.L., 1998. The scales of mantle convection. Tectonophysics, 284(1): 1-17.

Annen, C., Blundy, J. and Sparks, R., 2006. The genesis of intermediate and silicic magmas in deep crustal hot zones. Journal of Petrology, 47(3): 505-539.

Aragón, E., Rodriguez, A.M.I. and Benialgo, A., 1996. A calderas field at the Marifil Formation, new volcanogenic interpretation, Norpatagonian Massif, Argentina. Journal of South American Earth Sciences, 9(5): 321-328.

Asimow, P.D. and Ghiorso, M.S., 1998. Algorithmic modifications extending MELTS to calculate subsolidus phase relations. American Mineralogist, 83: 1127-1132.

Atherton, M. and Petford, N., 1996. Plutonism and the growth of Andean crust at 9 S from 100 to 3 Ma. Journal of South American Earth Sciences, 9(1): 1-9.

Baker, J., Peate, D., Waight, T. and Meyzen, C., 2004. Pb isotopic analysis of standards and samples using a< sup> 207</sup> Pb–< sup> 204</sup> Pb double spike and thallium to correct for mass bias with a double-focusing MC-ICP-MS. Chemical Geology, 211(3): 275-303.

Ballhaus, C., Berry, R. and Green, D., 1991. High pressure experimental calibration of the olivine-orthopyroxene-spinel oxygen geobarometer: implications for the oxidation state of the upper mantle. Contributions to Mineralogy and Petrology, 107(1): 27-40.

Basei, M., Varela, R., Sato, A., Siga Jr, O. and Llambías, E., 2002. Geocronología sobre rocas del Complejo Yaminué, Macizo Norpatagónico, Río Negro, Argentina, El Calafate, 15th Congreso Geológico Argentino, Actas, pp. 117-122.

Bergantz, G.W., 1989. Underplating and partial melting: implications for melt generation and extraction. Science, 245(4922): 1093-1095.

Bertrand, H., 1991. The Mesozoic tholeiitic province of northwest Africa: a volcano-tectonic record of the early opening of Central Atlantic, Magmatism in Extensional Structural Settings. Springer, pp. 147-188.

Bertrand, H., Fornari, M., Marzoli, A., García-Duarte, R. and Sempere, T., 2013. The Central Atlantic Magmatic Province extends into Bolivia. Lithos.

Bertrand, H., Villeneuve, M., 1989. Témoins de l'ouverture de l'atlantique central au début du jurassique: les dolérites

tholéiitiques continentales de Guinée (Afrique de l'Ouest). CR. Acad. Sci., Paris 308 ((série II),): 93– 98.

Beutel, E.K., 2009. Magmatic rifting of Pangaea linked to onset of South American plate motion. Tectonophysics, 468(1-4): 149-157.

Black, L. and Gulson, B., 1978. The age of the mud tank carbonatite, strangways range, northern territory. BMR Journal of Australian Geology and Geophysics, 3(3): 227-232.

Black, L.P., Kamo, S.L., Allen, C.M., Davis, D.W., Aleinikoff, J.N., Valley, J.W., Mundil, R., Campbell, I.H., Korsch, R.J. and Williams, I.S., 2004. Improved< sup> 206</sup> Pb/< sup> 238</sup> U microprobe geochronology by the monitoring of a trace-element-related matrix effect; SHRIMP, ID–TIMS, ELA–ICP–MS and oxygen isotope documentation for a series of zircon standards. Chemical Geology, 205(1): 115-140.

Bryan, S., 2007. Silicic large igneous provinces. Episodes, 30(1): 20.

Bryan, S.E. and Ernst, R.E., 2008. Revised definition of Large Igneous Provinces (LIPs). Earth-Science Reviews, 86(1-4): 175-202.

Bryan, S.E., Riley, T.R., Jerram, D.A., Stephens, C.J. and Leat, P.T., 2002. Silicic volcanism: an undervalued component of large igneous provinces and volcanic rifted margins. SPECIAL PAPERS-GEOLOGICAL SOCIETY OF AMERICA: 97-118.

Burke, K. and Dewey, J., 1973. Plume-generated triple junctions: key indicators in applying plate tectonics to old rocks. The Journal of Geology: 406-433.

Cabaleri, N. and Armella, C., 1999. Facies lacustres de la Formación Cañadón Asfalto (Caloviano-Oxfordiano), en la quebrada Las Chacritas, Cerro Cóndor, provincia del Chubut. Revista de la Asociación Geológica Argentina, 54(4): 375-388.

Cabaleri, N., Volkheimer, W., Armella, C., Gallego, O., Silva Nieto, D., Páez, M., Cagnoni, M., Ramos, A., Panarello, H. and Koukharsky, M., 2010. Estratigrafía, análisis de facies y paleoambientes de la formación cañadón asfalto en el depocentro jurásico cerro Cóndor, provincia del Chubut. Revista de la Asociación Geológica Argentina, 66(3): 349-367.

Cabaleri, N.G., Benavente, C.A., Monferran, M.D., Narváez, P.L., Volkheimer, W., Gallego, O.F. and Do Campo, M.D., 2013. Sedimentology and palaeontology of the Upper Jurassic Puesto Almada Member (Cañadón Asfalto Formation, Fossati sub-basin), Patagonia Argentina: Palaeoenvironmental and climatic significance. Sedimentary Geology.

Callegaro, S., Marzoli, A., Bertrand, H., Chiaradia, M., Reisberg, L., Meyzen, C., Bellieni, G., Weems, R.E. and Merle, R., 2013. Upper and lower crust recycling in the source of CAMP basaltic dykes from southeastern North America. Earth and Planetary Science Letters, 376: 186-199.

Caminos, R., Llambías, E.J. and Ramos, V., 1984. El basamento cristalino, Congreso Geológico Argentino No, pp. 37-63.

Carlson, R.W. and Hart, W.K., 1987. Crustal genesis on the Oregon Plateau. Journal of Geophysical Research: Solid Earth (1978–2012), 92(B7): 6191-6206.

Caroff, M., Bellon, H., Chauris, L., Carron, J.-P., Chevrier, S., Gardinier, A., Cotten, J., Moan, Y.L. and Neidhart, Y., 1995. Magmatisme fissural triasico-liasique dans l'ouest du Massif armoricain (France): pétrologie, géochimie, âge, et modalités de la mise en place. Canadian Journal of Earth Sciences, 32(11): 1921-1936.

Caroff, M. and Cotten, J., 2004. Geochemical evolution of a 10 m-thick intrusive body: the South Brenterc h diabase dyke, Western Armorican Massif, France. Canadian Journal of Earth Sciences, 41(7): 775-784.

Castro, A., Aragón, E., Díaz-Alvarado, J., Blanco, I., García-Casco, A., Vogt, K. and Liu, D.-Y., 2011. Age and composition of granulite xenoliths from Paso de Indios, Chubut province, Argentina. Journal of South American Earth Sciences, 32(4): 567-574.

Cebriá, J., Lopez-Ruiz, J., Doblas, M., Martins, L. and Munha, J., 2003. Geochemistry of the early Jurassic Messejana–Plasencia dyke (Portugal–Spain); implications on the origin of the Central Atlantic Magmatic Province. Journal of Petrology, 44(3): 547-568.

Chabou, M.C., Bertrand, H. and Sebaï, A., 2010. Geochemistry of the Central Atlantic Magmatic Province (CAMP) in south-western Algeria. Journal of African Earth Sciences, 58(2): 211-219.

Coffin, M.F. and Eldholm, O., 1992. Volcanism and continental break-up: a global compilation of large igneous provinces. Geological Society, London, Special Publications, 68(1): 17-30.

Condie, K.C., 2005. TTGs and adakites: are they both slab melts? Lithos, 80(1-4): 33-44.

Cordani, U., D'Agrella-Filho, M., Brito-Neves, B.d. and Trindade, R., 2003. Tearing up Rodinia: the Neoproterozoic palaeogeography of South American cratonic fragments. Terra Nova, 15(5): 350-359.

Cortés, J., 1981. Estratigrafía cenozoica y estructura al oeste de la Península de Valdés, Chubut. Consideraciones tectónicas y paleogeográficas. Revista de la Asociación Geológica Argentina, 36(4): 424-445.

Cox, K., 1992. Karoo igneous activity, and the early stages of the break-up of Gondwanaland. Geological Society, London, Special Publications, 68(1): 137-148.

Cúneo, R., Ramezani, J., Scasso, R., Pol, D., Escapa, I., Zavattieri, A.M. and Bowring, S.A., 2013. High-precision U–Pb geochronology and a new chronostratigraphy for the Cañadón Asfalto Basin, Chubut, central Patagonia: Implications for terrestrial faunal and floral evolution in Jurassic. Gondwana Research, 24(3-4): 1267-1275.

Dalla Salda, L., Cingolani, C. and Varela, R., 1992. Early Paleozoic orogenic belt of the Andes in southwestern South America: Result of Laurentia-Gondwana collision? Geology, 20(7): 617-620.

Dantas, C., 2007. Caractérisation du manteau supérieur patagonien: les enclaves ultramafiques et mafiques dans les laves alcalines, Université Paul Sabatier-Toulouse III.

Dars, R., 1961. Les formations sédimentaires et les dolérites du Soudan occidental (Afrique de l'Ouest). Editions Technip.

De Boer, J. and Snider, F.G., 1979. Magnetic and chemical variations of Mesozoic diabase dikes from eastern North America: Evidence for a hotspot in the Carolinas? Geological Society of America Bulletin, 90(2): 185-198.

De Min, A., Piccirillo, E.M., Marzoli, A., Bellieni, G., Renne, P.R., Ernesto, M. and Marques, L.S., 2003. The Central Atlantic Magmatic Province (CAMP) in Brazil: petrology, geochemistry, 40Ar/39Ar ages, paleomagnetism and geodynamic implications. Geophysical Monograph Series, 136: 91-128.

Deckart, K., Bertrand, H. and Liégeois, J.-P., 2005. Geochemistry and Sr, Nd, Pb isotopic composition of the Central Atlantic Magmatic Province (CAMP) in Guyana and Guinea. Lithos, 82(3-4): 289-314.

Deckart, K., Féraud, G. and Bertrand, H., 1997. Age of Jurassic continental tholeiites of French Guyana, Surinam and Guinea: implications for the initial opening of the Central Atlantic Ocean. Earth and Planetary Science Letters, 150(3): 205-220.

Defant, M.J. and Drummond, M.S., 1990. Derivation of some modern arc magmas by melting of young subducted lithosphere. Nature, 347(6294): 662-665.

Dostal, J. and Durning, M., 1998. Geochemical constraints on the origin and evolution of early Mesozoic dikes in Atlantic Canada. European journal of mineralogy, 10(1): 79-93.

Duncan, R.A., Hooper, P., Rehacek, J., Marsh, J. and Duncan, A., 1997. The timing and duration of the Karoo igneous event, southern Gondwana. Journal of Geophysical Research: Solid Earth (1978–2012), 102(B8): 18127-18138.

Dupuy, C., Marsh, J., Dostal, J., Michard, A. and Testa, S., 1988. Asthenospheric and lithospheric sources for Mesozoic dolerites from Liberia (Africa): trace element and isotopic evidence. Earth and Planetary Science Letters, 87(1): 100-110.

Elliot, D. and Fleming, T., 2000. Weddell triple junction: The principal focus of Ferrar and Karoo magmatism during initial breakup of Gondwana. Geology, 28(6): 539-542.

Elton, D., Scarfe C. M., 1984. High-pressurep hasee quilibria of a high-magnesiab asalt and the genesis of primary oceanic basalts. American Mineralogist, 69: l-15.

Ernst, R. and Buchan, K., 1997a. Layered mafic intrusions; a model for their feeder systems and relationship with giant dyke swarms and mantle plume centres. South African Journal of Geology, 100(4): 319-334.

Ernst, R.E. and Buchan, K.L., 1997b. Giant radiating dyke swarms: Their use in identifying pre-Mesozoic large igneous provinces and mantle plumes. Large igneous provinces: continental, oceanic, and planetary flood volcanism: 297-333.

Ernst, R.E. and Buchan, K.L., 2002. Maximum size and distribution in time and space of mantle plumes: evidence from large igneous provinces. Journal of Geodynamics, 34(2): 309-342.

Ernst, R.E., Buchan, K.L. and Campbell, I.H., 2005. Frontiers in large igneous province research. Lithos, 79(3-4): 271-297.

Feraud, G., Alric, V., Fornari, M., Bertrand, H. and Haller, M., 1999. 40Ar/39Ar dating of the Jurassic volcanic province of Patagonia: migrating magmatism related to Gondwana break-up and subduction. Earth and Planetary Science Letters, 172(1-2): 83-96.

Ferrari, L., López-Martínez, M., Aguirre-Díaz, G. and Carrasco-Núñez, G., 1999. Space-time patterns of Cenozoic arc volcanism in central Mexico: From the Sierra Madre Occidental to the Mexican Volcanic Belt. Geology, 27(4): 303-306.

Ferrari, L., Valencia-Moreno, M. and Bryan, S., 2007. Magmatism and tectonics of the Sierra Madre Occidental and its relation with the evolution of the western margin of North America. SPECIAL PAPERS-GEOLOGICAL SOCIETY OF AMERICA, 422: 1.

Feruglio, E., 1950. Descripción geológica de la Patagonia, 3. Coni.

Figari, E.G., 2005. Evolución tectónica de la Cuenca de Cañadón Asfalto (Zona del valle medio del Río Chubut), Universidad de Buenos Aires.

Fodor, R., Sial, A., Mukasa, S. and McKee, E., 1990. Petrology, isotope characteristics, and K-Ar ages of the Maranhao, northern Brazil, Mesozoic basalt province. Contributions to Mineralogy and Petrology, 104(5): 555-567.

Foley, S., Tiepolo, M. and Vannucci, R., 2002. Growth of early continental crust controlled by melting of amphibolite in subduction zones. Nature, 417(6891): 837-840.

Franzese, J., Spalletti, L., Pérez, I.G. and Macdonald, D., 2003. Tectonic and paleoenvironmental evolution of Mesozoic sedimentary basins along the Andean foothills of Argentina (32°–54°S). Journal of South American Earth Sciences, 16(1): 81-90.

Franzese, J.R. and Spalletti, L.A., 2001. Late Triassic–early Jurassic continental extension in southwestern Gondwana: tectonic segmentation and pre-break-up rifting. Journal of South American Earth Sciences, 14(3): 257-270.

Gaetani, G.A., 2004. The influence of melt structure on trace element partitioning near the peridotite solidus. Contributions to Mineralogy and Petrology, 147(5): 511-527.

Gaetani, G.A. and Grove, T.L., 1998. The influence of water on melting of mantle peridotite. Contributions to Mineralogy and Petrology, 131(4): 323-346.

Gaetani, G.A., Kent, A.J.R., Grove, T.L., Hutcheon, I.D. and Stolper, E.M., 2003. Mineral/melt partitioning of trace elements during hydrous peridotite partial melting. Contributions to Mineralogy and Petrology, 145(4): 391-405.

Ghiorso, M.S. and Sack, R.O., 1995. Chemical mass transfer in magmatic processes IV. A revised and internally consistent thermodynamic model for the interpolation and extrapolation of liquid-solid equilibria in magmatic systems at elevated temperatures and pressures. Contributions to mineralogy and petrology, 119(2-3): 197-212.

Girard, J.-P., Deynoux, M. and Nahon, D., 1989. Diagenesis of the upper Proterozoic siliciclastic sediments of the Taoudeni Basin (West Africa) and relation to diabase emplacement. Journal of Sedimentary Research, 59(2): 233-248.

Golonka, J., 2007. Late Triassic and Early Jurassic palaeogeography of the world. Palaeogeography, Palaeoclimatology, Palaeoecology, 244(1-4): 297-307.

Gómez-Tuena, A., LaGatta, A.B., Langmuir, C.H., Goldstein, S.L., Ortega-Gutiérrez, F. and Carrasco-Núñez, G., 2003. Temporal control of subduction magmatism in the eastern Trans-Mexican Volcanic Belt: Mantle sources, slab contributions, and crustal contamination. Geochemistry, Geophysics, Geosystems, 4(8): n/a-n/a.

Green, T. and Pearson, N., 1986. Rare-earth element partitioning between sphene and coexisting silicate liquid at high pressure and temperature. Chemical Geology, 55(1): 105-119.

Green, T.H., 1995. Significance of Nb/Ta as an indicator of geochemical processes in the crust-mantle system. Chemical Geology, 120(3): 347-359.

Greenough, J. and Dostal, J., 1992. Cooling history and differentiation of a thick North Mountain Basalt flow (Nova Scotia, Canada). Bulletin of Volcanology, 55(1-2): 63-73.

Greenough, J.D., Jones, L.M. and Mossman, D.J., 1989. Petrochemical and stratigraphic aspects of North Mountain basalt from the north shore of the Bay of Fundy, Nova Scotia, Canada. Canadian Journal of Earth Sciences, 26(12): 2710-2717.

Grove, T., Parman, S., Bowring, S., Price, R. and Baker, M., 2002. The role of an H2O-rich fluid component in the generation of primitive basaltic andesites and andesites from the Mt. Shasta region, N California. Contributions to mineralogy and petrology, 142(4): 375-396.

Grove, T.L., Chatterjee, N., Parman, S.W. and Médard, E., 2006. The influence of H< sub> 2</sub> O on mantle wedge melting. Earth and Planetary Science Letters, 249(1): 74-89.

Grove, T.L., Elkins-Tanton, L.T., Parman, S.W., Chatterjee, N., Müntener, O. and Gaetani, G.A., 2003. Fractional crystallization and mantle-melting controls on calc-alkaline differentiation trends. Contributions to mineralogy and petrology, 145(5): 515-533.

Guido, D., Escayola, M., de Barrio, R., Schalamuk, I. and Franz, G., 2006. La Formación Bajo Pobre (Jurásico) en el este del Macizo del Deseado, Patagonia: vinculación con el Grupo Bahía Laura. Revista de la Asociación Geológica Argentina, 61(2): 187-196.

Guido, D.M., Escayola, M.P. and Schalamuk, I.B., 2004. The basement of the Deseado Massif at Bahía Laura, Patagonia, Argentina: a proposal for its evolution. Journal of South American Earth Sciences, 16(7): 567-577.

Gust, D., Biddle, K., Phelps, D. and Uliana, M., 1985. Associated Middle to Late Jurassic volcanism and extension in southern South America. Tectonophysics, 116(3): 223-253.

Hagstrum, J.T., 2005. Antipodal hotspots and bipolar catastrophes: Were oceanic large-body impacts the cause? Earth and Planetary Science Letters, 236(1): 13-27.

Haller, M.J., Demichelis, A.H., Cabreros, J.B., Pardo, M.I. 1990. Litologia y geoquımica del vulcanismo triasico–jurasico en la Patagonia extraandina y su relacion con el rifting gondwanico. Actas del XI Congreso Geologico Argentino, San Juan (1): 56–59.

Hames, W., Renne, P. and Ruppel, C., 2000. New evidence for geologically instantaneous emplacement of earliest Jurassic Central Atlantic magmatic province basalts on the North American margin. Geology, 28(9): 859-862.

Handschumacher, D.W., Sager, W.W., Hilde, T.W. and Bracey, D.R., 1988. Pre-Cretaceous tectonic evolution of the Pacific plate and extension of the geomagnetic polarity reversal time scale with implications for the origin of the Jurassic “Quiet Zone”. Tectonophysics, 155(1): 365-380.

Harley, S., 1989. The origins of granulites: a metamorphic perspective. Geological Magazine, 126(3): 215-247.

Hart, S.R. and Davis, K.E., 1978. Nickel partitioning between olivine and silicate melt. Earth and Planetary Science Letters, 40(2): 203-219.

Hawkesworth, C., Kelley, S., Turner, S., Le Roex, A. and Storey, B., 1999. Mantle processes during Gondwana break-up and dispersal. Journal of African Earth Sciences, 28(1): 239-261.

Heatherington, A. and Mueller, P., 1991. Geochemical evidence for Triassic rifting in southwestern Florida. Tectonophysics, 188(3): 291-302.

Heatherington, A. and Mueller, P., 1999. Lithospheric sources of North Florida, USA tholeiites and implications for the origin of the Suwannee terrane. Lithos, 46(2): 215-233.

Heinonen, J.S., Carlson, R.W. and Luttinen, A.V., 2010. Isotopic (Sr, Nd, Pb, and Os) composition of highly magnesian dikes of Vestfjella, western Dronning Maud Land, Antarctica: A key to the origins of the Jurassic Karoo large igneous province? Chemical Geology, 277(3): 227-244.

Herzberg, C. and O’hara, M., 2002. Plume-associated ultramafic magmas of Phanerozoic age. Journal of Petrology, 43(10): 1857-1883.

Hill, R.I., 1991. Starting plumes and continental break-up. Earth and Planetary Science Letters, 104(2): 398-416.

Hofmann, A., 2003. Sampling mantle heterogeneity through oceanic basalts: isotopes and trace elements. Treatise on geochemistry, 2: 61-101.

Iglesia Llanos, M.P., Lanza, R., Riccardi, A.C., Geuna, S., Laurenzi, M.A. and Ruffini, R., 2003. Palaeomagnetic study of the El Quemado complex and Marifil formation, Patagonian Jurassic igneous province, Argentina. Geophysical Journal International, 154(3): 599-617.

Ingle, S. and Coffin, M.F., 2004. Impact origin for the greater Ontong Java Plateau? Earth and Planetary Science Letters, 218(1): 123-134.

Jones, A.P., Price, G.D., Price, N.J., DeCarli, P.S. and Clegg, R.A., 2002. Impact induced melting and the development of large igneous provinces. Earth and Planetary Science Letters, 202(3): 551-561.

Jourdan, F., Bertrand, H., Schärer, U., Blichert-Toft, J., Feraud, G. and Kampunzu, A., 2007a. Major and trace element and Sr, Nd, Hf, and Pb isotope compositions of the Karoo large igneous province, Botswana–Zimbabwe: lithosphere vs mantle plume contribution. Journal of Petrology, 48(6): 1043-1077.

Jourdan, F., Féraud, G., Bertrand, H., Kampunzu, A., Tshoso, G., Le Gall, B., Tiercelin, J. and Capiez, P., 2004. The Karoo triple junction questioned: evidence from Jurassic and Proterozoic< sup> 40</sup> Ar/< sup> 39</sup> Ar ages and geochemistry of the giant Okavango dyke swarm (Botswana). Earth and Planetary Science Letters, 222(3): 989-1006.

Jourdan, F., Féraud, G., Bertrand, H., Kampunzu, A.B., Tshoso, G., Watkeys, M.K. and Le Gall, B., 2005. Karoo large igneous province: Brevity, origin, and relation to mass extinction questioned by new 40Ar/39Ar age data. Geology, 33(9): 745-748.

Jourdan, F., Féraud, G., Bertrand, H. and Watkeys, M., 2007b. From flood basalts to the inception of oceanization: Example from the 40Ar/39Ar high-resolution picture of the Karoo large igneous province. Geochemistry, Geophysics, Geosystems, 8(2).

Jourdan, F., Marzoli, A., Bertrand, H., Cirilli, S., Tanner, L.H., Kontak, D.J., McHone, G., Renne, P.R. and Bellieni, G., 2009. 40Ar/39Ar ages of CAMP in North America: Implications for the Triassic–Jurassic boundary and the 40K decay constant bias. Lithos, 110(1-4): 167-180.

Jourdan, F., Marzoli, A., Bertrand, H., Cosca, M. and Fontignie, D., 2003. The northernmost CAMP: 40Ar/39Ar age, petrology and Sr-Nd-Pb isotope geochemistry of the Kerforne dike, Brittany, France. Geophysical Monograph Series, 136: 209-226.

Kamenetsky, V.S., Maas, R., Sushchevskaya, N.M., Norman, M.D., Cartwright, I. and Peyve, A.A., 2001. Remnants of Gondwanan continental lithosphere in oceanic upper mantle: Evidence from the South Atlantic Ridge. Geology, 29(3): 243.

Kay, R., 1978. Aleutian magnesian andesites: melts from subducted Pacific Ocean crust. Journal of Volcanology and Geothermal Research, 4(1): 117-132.

Kay, S.M., Ramos, V.A., Mpodozis, C. and Sruoga, P., 1989. Late Paleozoic to Jurassic silicic magmatism at the Gondwana margin: Analogy to the Middle Proterozoic in North America? Geology, 17(4): 324.

King, S.D. and Anderson, D.L., 1998. Edge-driven convection. Earth and Planetary Science Letters, 160(3): 289-296.

Klemperer, S.L., 1989. Deep seismic reflection profiling and the growth of the continental crust. Tectonophysics, 161(3): 233-244.

Knight, K., Nomade, S., Renne, P., Marzoli, A., Bertrand, H. and Youbi, N., 2004. The Central Atlantic Magmatic Province at the Triassic–Jurassic boundary: paleomagnetic and< sup> 40</sup> Ar/< sup> 39</sup> Ar evidence from Morocco for brief, episodic volcanism. Earth and Planetary Science Letters, 228(1): 143-160.

Kosler, J., 2001. Laser-ablation ICPMS study of metamorphic minerals and processes. In: Sylvester P. J. ed. Laser-ablation-ICPMS in the earth sciences; principles and applications Mineralogical Association of Canada Short Course Handbook, 29: 185-202.

Kosler J., S.P.J., 2003 Present trends and the future of zircon in geochronology; laser ablation ICPMS. . Reviews in Mineralogy and Geochemistry, 53: 243-275.

Lajoinie, J. and Bonifas, M., 1961. Les dolérites du Konkouré et leur altération latéritique (Guinée, Afrique Occidentale). Bull. Bur. Rech. Geol. Minieres (Paris), 2: 1-34.

Le Maitre, R.W., Bateman, P., Dudek, A., Keller, J., Lameyre, J., Le Bas, M., Sabine, P., Schmid, R., Sorensen, H. and Streckeisen, A., 1989. A classification of igneous rocks and glossary of terms: Recommendations of the International Union of Geological Sciences Subcommission on the Systematics of Igneous Rocks, 193. Blackwell Oxford.

Li, C. and Ripley, E.M., 2010. The relative effects of composition and temperature on olivine-liquid Ni partitioning: Statistical deconvolution and implications for petrologic modeling. Chemical Geology, 275(1-2): 99-104.

Li, X.H., Long, W.G., Li, Q.L., Liu, Y., Zheng, Y.F., Yang, Y.H., Chamberlain, K.R., Wan, D.F., Guo, C.H. and Wang, X.C., 2010. Penglai zircon megacrysts: a potential new working reference material for microbeam determination of Hf–O isotopes and U–Pb age. Geostandards and Geoanalytical Research, 34(2): 117-134.

Lizuaín, A., 1981. Características y edad del plutonismo en los alrededores de Lago Puelo, Cordillera Patagónica (provincia de Chubut), Congreso Geológico Argentino, pp. 607-616.

Long, M.D., Till, C.B., Druken, K.A., Carlson, R.W., Wagner, L.S., Fouch, M.J., James, D.E., Grove, T.L., Schmerr, N. and Kincaid, C., 2012. Mantle dynamics beneath the Pacific Northwest and the generation of voluminous back-arc volcanism. Geochemistry, Geophysics, Geosystems, 13(8).

Loske, W., Márquez, M., Giacosa, R., Pezzuchi, H., Fernández, M.I.,, 1999. . U/Pb geochronology of pre-Permian basement rocks in the Macizo del Deseado, Santa Cruz province, Argentine Patagonia. . 15□ Congreso Geológico Argentino (Salta), , Actas 1: 102. Malvicini, L. and Llambías, E., 1974. Geología y génesis del depósito de manganeso Arroyo Verde, provincia de Chubut, Buenos Aires, 5 Congreso Geológico Argentino, pp. 185-202.

Márquez, M.J., Massaferro, G.I. and Fernández, M.I., 2010. El volcanismo del complejo Marifil en Arroyo Verde, vertiente suroriental del Macizo de Somún Cura, Chubut. Revista de la Asociación Geológica Argentina, 66(3): 314-324.

Márquez, M.J., Massaferro, G.I., Fernández, M.I., Menegatti, N. and Navarrete, C.R., 2011. El centro volcánico Sierra Grande: caracterización petrográfica y geoquímica del magmatismo extensional liásico, noroeste de la Patagonia. Revista de la Asociación Geológica Argentina, 68(4): 555-570.

Martin, H., 1999. Adakitic magmas: modern analogues of Archaean granitoids. Lithos, 46(3): 411-429.

Marzoli, A., Bertrand, H., Knight, K.B., Cirilli, S., Buratti, N., Vérati, C., Nomade, S., Renne, P.R., Youbi, N., Martini, R., Allenbach, K., Neuwerth, R., Rapaille, C., Zaninetti, L. and Bellieni, G., 2004. Synchrony of the Central Atlantic magmatic province and the Triassic-Jurassic boundary climatic and biotic crisis. Geology, 32(11): 973.

Marzoli, A., Jourdan, F., Puffer, J.H., Cuppone, T., Tanner, L.H., Weems, R.E., Bertrand, H., Cirilli, S., Bellieni, G. and De Min, A., 2011. Timing and duration of the Central Atlantic magmatic province in the Newark and Culpeper basins, eastern U.S.A. Lithos, 122(3-4): 175-188.

Mauche, R., Faure, G., Jones, L.M. and Hoefs, J., 1989. Anomalous isotopic compositions of Sr, Ar and O in the Mesozoic diabase dikes of Liberia, West Africa. Contributions to Mineralogy and Petrology, 101(1): 12-18.

May, P.R., 1971. Pattern of Triassic-Jurassic diabase dikes around the North Atlantic in the context of predrift position of the continents. Geological Society of America Bulletin, 82(5): 1285-1292.

McDonough, W.F. and Sun, S.-S., 1995. The composition of the Earth. Chemical Geology, 120(3): 223-253.

McHone, J.G., 1996. Broad-terrane Jurassic flood basalts across northeastern North America. Geology, 24(4): 319-322.

McHone, J.G., 2000. Non-plume magmatism and rifting during the opening of the central Atlantic Ocean. Tectonophysics, 316(3): 287-296.

Meffre, S., Large, R.R., Scott, R., Woodhead, J., Chang, Z., Gilbert, S.E., Danyushevsky, L.V., Maslennikov, V. and Hergt, J.M., 2008. Age and pyrite Pb-isotopic composition of the giant Sukhoi Log sediment-hosted gold deposit, Russia. Geochimica et Cosmochimica Acta, 72(9): 2377-2391.

Merle, R., Marzoli, A., Bertrand, H., Reisberg, L., Verati, C., Zimmermann, C., Chiaradia, M., Bellieni, G. and Ernesto, M., 2011. 40Ar/39Ar ages and Sr–Nd–Pb–Os geochemistry of CAMP tholeiites from Western Maranhão basin (NE Brazil). Lithos, 122(3-4): 137-151.

Merle, R., Marzoli, A., Reisberg, L., Bertrand, H., Nemchin, A., Chiaradia, M., Callegaro, S., Jourdan, F., Bellieni, G. and Kontak, D., 2014. Sr, Nd, Pb and Os Isotope Systematics of CAMP Tholeiites from Eastern North America (ENA): Evidence of a Subduction-enriched Mantle Source. Journal of Petrology, 55(1): 133-180.

Merle, R., Marzoli, A., Reisberg, L., Bertrand, H., Nemchin, A., Chiaradia, M., Callegaro, S., Jourdan, F., Bellieni, G., Kontak, D., Puffer, J. and McHone, J.G., 2013. Sr, Nd, Pb and Os Isotope Systematics of CAMP Tholeiites from Eastern North America (ENA): Evidence of a Subduction-enriched Mantle Source. Journal of Petrology, 55(1): 133-180.

Miller, C.F., 1985. Are strongly peraluminous magmas derived from pelitic sedimentary sources? The Journal of Geology: 673-689.

Mooney, W.D., Laske, G. and Masters, T.G., 1998. CRUST 5.1: A global crustal model at 5× 5. Journal of Geophysical Research: Solid Earth (1978–2012), 103(B1): 727-747.

Mori, L., Gómez-Tuena, A., Cai, Y. and Goldstein, S.L., 2007. Effects of prolonged flat subduction on the Miocene magmatic record of the central Trans-Mexican Volcanic Belt. Chemical Geology, 244(3-4): 452-473.

Morimoto, N., 1988. Nomenclature of pyroxenes. Mineralogy and Petrology, 39(1): 55-76.

Mpodozis, C. and Ramos, V.A., 2008. Tectónica jurásica en Argentina y Chile: extensión, subducción oblicua, rifting, deriva y colisiones? Revista de la Asociación Geológica Argentina, 63(4): 481-497.

Nakanishi, M. and Winterer, E.L., 1998. Tectonic history of the Pacific-Farallon-Phoenix triple junction from Late Jurassic to Early Cretaceous: An abandoned Mesozoic spreading system in the Central Pacific Basin. Journal of Geophysical Research: Solid Earth (1978–2012), 103(B6): 12453-12468.

Nomade, S., Knight, K., Beutel, E., Renne, P., Verati, C., Féraud, G., Marzoli, A., Youbi, N. and Bertrand, H., 2007. Chronology of the Central Atlantic Magmatic Province: implications for the Central Atlantic rifting processes and the Triassic–Jurassic biotic crisis. Palaeogeography, Palaeoclimatology, Palaeoecology, 244(1): 326-344.

Nomade, S., Pouclet, A. and Chen, Y., 2002. The French Guyana doleritic dykes: geochemical evidence of three populations and new data for the Jurassic Central Atlantic Magmatic Province. Journal of Geodynamics, 34(5): 595-614.

O'hara, M., 1968a. Are ocean floor basalts primary magma? Nature, 220 683 - 686

Olsen, P.E., 1997. Stratigraphic record of the early Mesozoic breakup of Pangea in the Laurasia-Gondwana rift system. Annual Review of Earth and Planetary Sciences, 25(1): 337-401.

Page, R. and Page, S., 1993. Petrología y significado tectónico del Jurásico Volcánico del Chubut Central. Asociación Geológica Argentina, Revista, 48(1): 41-58.

Page, R.y.P., S. 1994. Petrología y significado tectónico del Jurásico volcánico del Chubut central. . Revista de la Asociación Geológica Argentina 48(1): 41-58.

Page, S., Page, R., 1999. Las diabasas y gabros del Juraisico de la Precordillera del Chubut. I. 29, 489-495. CAMINOS, R. (ed.) Geologfa Argentina. Subsecretaria de Minerfa de la Naci6n, Servicio Geologico Minero Argentino, Instituto de Geologia y Recursos Minerales. , 29: 489-495.

Panjasawatwong, Y., Danyushevsky, L.V., Crawford, A.J. and Harris, K.L., 1995. An experimental study of the effects of melt composition on plagioclase-melt equilibria at 5 and 10 kbar: implications for the origin of magmatic high-An plagioclase. Contributions to Mineralogy and Petrology, 118(4): 420-432.

Pankhurst, R., Leat, P., Sruoga, P., Rapela, C., Márquez, M., Storey, B. and Riley, T., 1998. The Chon Aike province of Patagonia and related rocks in West Antarctica: A silicic large igneous province. Journal of Volcanology and Geothermal Research, 81(1): 113-136.

Pankhurst, R. and Rapela, C., 1995. Production of Jurassic rhyolite by anatexis of the lower crust of Patagonia. Earth and Planetary Science Letters, 134(1): 23-36.

Pankhurst, R., Riley, T., Fanning, C. and Kelley, S., 2000. Episodic silicic volcanism in Patagonia and the Antarctic Peninsula: chronology of magmatism associated with the break-up of Gondwana. Journal of Petrology, 41(5): 605-625.

Pankhurst, R.J. and Rapela, C.W., 1998. The proto-Andean margin of Gondwana: an introduction. Geological Society, London, Special Publications, 142(1): 1-9.

Pankhurst, R.J., Rapela, C.W. and Anonymous, 1993. The Jurassic acidic volcanism of north-east Patagonia; a short-lived event of deep origin. Colloques et Seminaires - Institut de Recherche Scientifique pour le Developpement en Cooperation, 1993: 423-425.

Pankhurst, R.J., Rapela, C.W., Fanning, C.M. and Márquez, M., 2006. Gondwanide continental collision and the origin of Patagonia. Earth-Science Reviews, 76(3-4): 235-257.

Parman, S.W. and Grove, T.L., 2004. Harzburgite melting with and without H2O: Experimental data and predictive modeling. Journal of Geophysical Research, 109(B2): B02201.

Paton, C., Woodhead, J.D., Hellstrom, J.C., Hergt, J.M., Greig, A. and Maas, R., 2010. Improved laser ablation U-Pb zircon geochronology through robust downhole fractionation correction. Geochemistry, Geophysics, Geosystems, 11(3).

Pearce, J.A., Baker, P.E., HARVEY, P.K. and Luff, I.W., 1995. Geochemical evidence for subduction fluxes, mantle melting and fractional crystallization beneath the South Sandwich island arc. Journal of Petrology, 36(4): 1073-1109.

Peccerillo, A. and Taylor, S.R., 1976. Geochemistry of Eocene calc-alkaline volcanic rocks from the Kastamonu area, northern Turkey. Contributions to mineralogy and petrology, 58(1): 63-81.

Pegram, W.J., 1990. Development of continental lithospheric mantle as reflected in the chemistry of the Mesozoic Appalachian tholeiites, USA. Earth and Planetary Science Letters, 97(3): 316-331.

Petford, N. and Atherton, M., 1996. Na-rich partial melts from newly underplated basaltic crust: the Cordillera Blanca Batholith, Peru. Journal of Petrology, 37(6): 1491-1521.

Petford, N. and Gallagher, K., 2001. Partial melting of mafic (amphibolitic) lower crust by periodic influx of basaltic magma. Earth and Planetary Science Letters, 193(3): 483-499.

Poustovetov, A. and Roeder, P., 2001. Numerical modeling of major element distribution between chromian spinel and basaltic melt, with application to chromian spinel in MORBs. Contributions to Mineralogy and Petrology, 142(1): 58-71.

Putirka, K.D., 2008. Thermometers and barometers for volcanic systems. Reviews in Mineralogy and Geochemistry, 69(1): 61-120.

Pysklywec, R.N., Beaumont, C. and Fullsack, P., 2000. Modeling the behavior of the continental mantle lithosphere during plate convergence. Geology, 28(7): 655-658.

Ramos, V.A., 1989. The birth of southern South America. American Scientist, 77(5): 444-450.

Ramos, V.A., 2008. Patagonia: A paleozoic continent adrift? Journal of South American Earth Sciences, 26(3): 235-251.

Ramos, V.A., 2004. . Tectonics of the southernmost Andes: a comparison between the Patagonian and the Fuegian Cordilleras. . Bolletino di Geofisica Teorica ed Applicata, 45((2 supplement)): 1-10.

Rampino, M.R. and Stothers, R.B., 1988. Flood basalt volcanism during the past 250 million years. Science, 241(4866): 663-668.

Rapaille, C., Marzoli, A., Bertrand, H., Féraud, G., Reisberg, L. and Fontignie, D., 2003. Geochemistry and 40Ar/39Ar age of the European part of the Central Atlantic Magmatic Province, EGS-AGU-EUG Joint Assembly, pp. 11791.

Rapela, C. and Caminos, R., 1987. Geochemical characteristics of the Upper Paleozoic magmatism in the eastern sector of Northpatagonian Massif. Revista Brasileira de Geociencias, 17(4): 535-543.

Rapela, C. and Llambias, E., 1985. La secuencia andesítica terciaria de Andacollo, Neuquén, Argentina, Congreso Geológico Chileno, pp. 458-488.

Rapela, C., Pankhurst, R., Fanning, C. and Grecco, L., 2003. Basement evolution of the Sierra de la Ventana Fold Belt: new evidence for Cambrian continental rifting along the southern margin of Gondwana. Journal of the Geological Society, 160(4): 613-628.

Rapela, C., Pankhurst, R., Fanning, C. and Hervé, F., 2005. Pacific subduction coeval with the Karoo mantle plume: the Early Jurassic Subcordilleran Belt of northwestern Patagonia. Geological Society of London.

Renne, P.R., Mundil, R., Balco, G., Min, K. and Ludwig, K.R., 2010. Joint determination of 40K decay constants and 40Ar∗/40K for the Fish Canyon sanidine standard, and improved accuracy for 40Ar/39Ar geochronology. Geochimica et Cosmochimica Acta, 74(18): 5349-5367.

Riley, T.R. and Knight, K.B., 2001. Age of pre-break-up Gondwana magmatism. Antarctic Science, 13(2): 99-110.

Riley, T.R., Leat, P.T., Pankhurst, R.J. and Harris, C., 2001. Origins of large volume rhyolitic volcanism in the Antarctic Peninsula and Patagonia by crustal melting. Journal of Petrology, 42(6): 1043-1065.

Rivers, T. and Corrigan, D., 2000. Convergent margin on southeastern Laurentia during the Mesoproterozoic: tectonic implications. Canadian Journal of Earth Sciences, 37(2-3): 359-383.

Roeder, P. and Emslie, R., 1970. Olivine-liquid equilibrium. Contributions to Mineralogy and Petrology, 29(4): 275-289.

Rollinson, H. and Data, U.G., 1993. Evaluation, Presentation, Interpretation.

Rossi, P., 1982. Lithostratigraphie et cartographie des formations sédimentaires du pourtour du massif du Kaarta, Mali occidental: précambrien terminal, paléozoïque inférieur (?) du sud-ouest du

bassin de Taoudéni, 18. Laboratoire de géologie dynamique, Faculté des sciences et techniques de Saint Jérôme.

Rudnick, R. and Gao, S., 2003. Composition of the continental crust. Treatise on geochemistry, 3: 1-64.

Ryerson, F. and Watson, E., 1987. Rutile saturation in magmas: implications for TiNbTa depletion in island-arc basalts. Earth and Planetary Science Letters, 86(2): 225-239.

Sack, P.J., Berry, R.F., Meffre, S., Falloon, T.J., Gemmell, J.B. and Friedman, R.M., 2011. In situ location and U-Pb dating of small zircon grains in igneous rocks using laser ablation–inductively coupled plasma–quadrupole mass spectrometry. Geochemistry, Geophysics, Geosystems, 12(5).

Salani, F., 2007. Aporte a la edad de la Formación Cañadón Asfalto, Chubut, Argentina, Resúmenes 30 Simposio Argentino del Jurásico.

Santos, J.O.S., Hartmann, L.A., Bossi, J., Campal, N., Schipilov, A., Piñeyro, D. and McNaughton, N.J., 2003. Duration of the Trans-Amazonian Cycle and its correlation within South America based on U-Pb SHRIMP geochronology of the La Plata Craton, Uruguay. International Geology Review, 45(1): 27-48.

Schaltegger, U., Guex, J., Bartolini, A., Schoene, B. and Ovtcharova, M., 2008. Precise U–Pb age constraints for end-Triassic mass extinction, its correlation to volcanism and Hettangian post-extinction recovery. Earth and Planetary Science Letters, 267(1): 266-275.

Schoene, B., Guex, J., Bartolini, A., Schaltegger, U. and Blackburn, T.J., 2010. Correlating the end-Triassic mass extinction and flood basalt volcanism at the 100 ka level. Geology, 38(5): 387-390.

Secretaria de Mineria, D.N.d.S.G.A., 1995. Mapa geologico de la Provincia del Chubut

Secretaria de Mineria, D.N.d.S.G.A., 1994. Mapa geologico de la Provincia de Santa Cruz.

Seton, M., Müller, R.D., Zahirovic, S., Gaina, C., Torsvik, T., Shephard, G., Talsma, A., Gurnis, M., Turner, M., Maus, S. and Chandler, M., 2012. Global continental and ocean basin reconstructions since 200Ma. Earth-Science Reviews, 113(3-4): 212-270.

Sigurdsson, I., Kamenetsky, V., Crawford, A., Eggins, S. and Zlobin, S., 1993. Primitive island arc and oceanic lavas from the Hunter ridge-Hunter fracture zone. Evidence from glass, olivine and spinel compositions. Mineralogy and Petrology, 47(2-4): 149-169.

Simkin, T. and Smith, J., 1970. Minor-element distribution in olivine. The Journal of Geology: 304-325.

Sláma, J., Košler, J., Condon, D.J., Crowley, J.L., Gerdes, A., Hanchar, J.M., Horstwood, M.S., Morris, G.A., Nasdala, L. and Norberg, N., 2008. Plešovice zircon—a new natural reference material for U–Pb and Hf isotopic microanalysis. Chemical Geology, 249(1): 1-35.

Sobolev, A.V., Hofmann, A.W., Kuzmin, D.V., Yaxley, G.M., Arndt, N.T., Chung, S.-L., Danyushevsky, L.V., Elliott, T., Frey, F.A. and Garcia, M.O., 2007. The amount of recycled crust in sources of mantle-derived melts. Science, 316(5823): 412-417.

Spikermann, J.R., Strelin, J., Marshall, P. , 1988. Geologia del area E1 Batolito Aleusco, Departamento de Languifieo, provincia de Chubut. Revista de la Asociaci6n Argentina de Mineralogia, Petrologia y Sedimentologia 19: 39-48.

Sruoga, P. and Anonymous, 1990. Jurassic silicic volcanism in southern Patagonia (47 degrees 30'S latitude). Bulletin - New Mexico Bureau of Geology & Mineral Resources, 131: 252-252.

Sruoga, P. and Palma, M., 1984. La Formación Chon Aike en su área clásica de afloramientos, Actas IX Congreso Geológico Argentino, pp. 171-184.

Stipanicic, P.N., Rodrigo, F., Baulíes, O., Martínez, C., 1968. Las formaciones presenonianas en el dominio del Macizo Nordpatagónico y regiones adyacentes. Revista de la Asociación Geológica Argentina 23: 67-98.

Storey, B., Alabaster, T., Hole, M., Pankhurst, R. and Wever, H., 1992. Role of subduction-plate boundary forces during the initial stages of Gondwana break-up: evidence from the proto-Pacific margin of Antarctica. Geological Society, London, Special Publications, 68(1): 149-163.

Storey, B. and Kyle, P., 1997. An active mantle mechanism for Gondwana breakup. South African Journal of Geology, 100(4): 283-290.

Storey, B.C., 1995. The role of mantle plumes in continental breakup: case histories from Gondwanaland. Nature, 377(6547): 301-308.

Storey, B.C. and Alabaster, T., 1991. Tectonomagmatic controls on Gondwana break-up models: Evidence from the Proto-Pacific Margin of Antarctica. Tectonics, 10(6): 1274-1288.

Suarez, M. and Marquez, M., 2010. A Toarcian retro-arc basin of Central Patagonia (Chubut), Argentina: Middle Jurassic closure, arc migration and tectonic setting. Andean Geology, 34(1).

Suárez, M. and Márquez, M., 2007. A Toarcian retro-arc basin of Central Patagonia (Chubut), Argentina: Middle Jurassic closure,arc migration and tectonic setting. Revista geológica de Chile, 34(1).

Sun, S.s. and McDonough, W.F., 1989. Chemical and isotopic systematics of oceanic basalts: implications for mantle composition and processes. Geological Society, London, Special Publications, 42(1): 313-345.

Tanner, L., Lucas, S. and Chapman, M., 2004. Assessing the record and causes of Late Triassic extinctions. Earth-Science Reviews, 65(1): 103-139.

Thompson, A.B., 1999. Some time-space relationships for crustal melting and granitic intrusion at various depths. Geological Society, London, Special Publications, 168(1): 7-25.

Uliana, M. and Biddle, K., 1987. Permian to Late Cenozoic evolution of northern Patagonia: main tectonic events, magmatic activity, and depositional trends. Geophysical Monograph Series, 40: 271-286.

Uliana, M., Biddle, K., Phelps, D. and Gust, D., 1985. Significado del vulcanismo y extensión mesojurásicos en el extremo meridional de Sudamérica. Revista de la Asociación Geológica Argentina, 40(3-4): 231-253.

Usui, Y., Tarduno, J., Lô, K., Duncan, R., Mason, S., Cottrell, R. and Voronov, J., 2010. The geodynamo at~ 200 Ma: paleosecular variation and paleointensity recorded by Central Atlantic Magmatic Province mafic rocks of Mauritania, AGU Fall Meeting Abstracts, pp. 0949.

Varela, R., Basei, M., Sato, A., Siga Jr, O., Cingolani, C. and Sato, K., 1998. Edades isotópicas Rb/Sr y U/Pb en rocas de Mina Gonzalito y Arroyo Salado, Macizo Norpatagónico Atlántico, Río Negro, Argentina. Buenos Aires, 10 Congreso Latinoamericano de Geología y 6 Congreso Nacional de Geología Económica, pp. 71-76.

Vaughan, A.P.M. and Storey, B.C., 2007. A new supercontinent self-destruct mechanism: evidence from the Late Triassic-Early Jurassic. Journal of the Geological Society, 164(2): 383-392.

Verati, C., Bertrand, H. and Feraud, G., 2005. The farthest record of the Central Atlantic Magmatic Province into West Africa craton: Precise Ar/Ar dating and geochemistry of Taoudenni basin intrusives (northern Mali). Earth and Planetary Science Letters, 235(1-2): 391-407.

Verati, C., Rapaille, C., Féraud, G., Marzoli, A., Bertrand, H. and Youbi, N., 2007. 40Ar/39Ar ages and duration of the Central Atlantic Magmatic Province volcanism in Morocco and Portugal and its relation to the Triassic–Jurassic boundary. Palaeogeography, Palaeoclimatology, Palaeoecology, 244(1-4): 308-325.

Villemur, J.-R., 1967. Reconnaissance géologique et structurale du nord du basin de Taoudenni. Éditions BRGM.

Volkheimer, W., Gallego, O.F., Cabaleri, N.G., Armella, C., Narváez, P.L., Silva Nieto, D.G. and Páez, M.A., 2009. Stratigraphy, palynology, and conchostracans of a Lower Cretaceous sequence at the Cañadón Calcáreo locality, Extra-Andean central Patagonia: age and palaeoenvironmental significance. Cretaceous Research, 30(1): 270-282.

Von Gosen, W., 2002. Polyphase structural evolution in the northeastern segment of the North Patagonian Massif (southern Argentina). Journal of South American Earth Sciences, 15(6): 591-623.

White, R. and McKenzie, D., 1989. Magmatism at rift zones: the generation of volcanic continental margins and flood basalts. Journal of Geophysical Research: Solid Earth (1978–2012), 94(B6): 7685-7729.

White, R. and McKenzie, D., 1995. Mantle plumes and flood basalts. Journal of Geophysical Research, 100(B9): 17543-17,585.

Wiedenbeck, M., Alle, P., Corfu, F., Griffin, W., Meier, M., Oberli, F., Quadt, A.v., Roddick, J. and Spiegel, W., 1995. Three natural zircon standards for U-Th-Pb, Lu-Hf, trace element and REE analyses. Geostandards Newsletter, 19(1): 1-23.

Wilson, M., 1997. Thermal evolution of the Central Atlantic passive margins: continental break-up above a Mesozoic super-plume. Journal of the Geological Society, 154(3): 491-495.

Windley, B.F., 1984. The evolving continents. Chichester, England and New York, John Wiley and Sons, 1984, 416 p., 1.

Wortel, M. and Spakman, W., 2000. Subduction and slab detachment in the Mediterranean-Carpathian region. Science, 290(5498): 1910-1917.

Xu, J.-F., Shinjo, R., Defant, M.J., Wang, Q. and Rapp, R.P., 2002. Origin of Mesozoic adakitic intrusive rocks in the Ningzhen area of east China: Partial melting of delaminated lower continental crust? Geology, 30(12): 1111-1114.

Zeil, W., 1979. The Andes: a geological review. Gebrüder Borntraeger Berlin.

Zindler, A. and Hart, S., 1986. Chemical geodynamics. Annual Review of Earth and Planetary Sciences, 14: 493-571.

ACKNOWLEDGEMENTS

This thesis was developed thanks to a three-year doctoral grant funded by the CARIPARO Foundation. I performed this doctorate in the frame of an academic agreement between the University of Padova, Italy, and the University of Tasmania, Australia.

I would like to express my great gratitude to my supervisors: Prof. Andrea Marzoli and Prof. Dima Kamenetsky, who have encouraged my research with their expertise, understanding and support, and from who I have learned priceless lessons of science, patience and perseverance.

I would like also to express my deepest gratefulness for the invaluable support of the technical, academic and administrative personnel of the Geosciences Department in the University of Padova. Particularly, I thank to Prof. Matteo Massiorni and Manuele Faccenda for the fruitful discussions about tectonics, and to Leonardo Tauro for his handiness in thin section performance.

My special appreciation to Prof. Marcelo Marquez from the Universidad Nacional de la Patagonia, for his guidance in the geology of Patagonia and all help provided during the fieldwork. I also thank to Prof. Chris Ballhaus, for supporting my research stay at the University of Bonn, as well as Prof. Thorsten Nagel and Sascha Sandmann, who assisted the microprobe analysis at the same institution. I Would like to express my great gratitude to Maya Kamenetsky, for her support in sample preparation and U-Pb dating, as well as to Dr. Karsten Goemann and Dr Sandrin Feig for assisting the chromite analysis at UTAS.

I also thank the support of friends who arrived and stay with every season of research: Sara and Laura my magma partners, Anna, Manu, Luca, Vivi, Sabri, Marta, Silvio and Christine in Padova. Renate, Elke and Claudia, sweet friends from Bonn. My multicultural friends in Hobart: Cami, Marc, Dani, Makrina, Victoria, Di + Chris, Marghi and Irma. To all Cariparo friends, who like me, arrived alone and left with friends all over the world. To my Colombian and Mexican people who remain despite the distance: Pedro, Mafe, Uru, Bety, Wil, Domingo, Angie, Maria^2 and Mar. To Victor, who left us before time.

This thesis would not have been possible without the invaluable and unconditional support of my family and Sandro, who I specially thank for brighten these three years of steps.

APPENDIX

1. Hank, Hodh and Kaarta

Table 1. Major elements composition of samples from Hank, Hodh and Kaarta.

	SiO_2 wt.%	$Al2O_3$ wt.%	FeO_t wt.%	MgO wt.%	CaO wt.%	Na_2O wt.%	K2O wt.%	TiO_2 wt.%	P_2O_5 wt.%	MnO wt.%	LOI wt.%	TOTAL
Hank												
HA 38	52.19	14.16	9.88	7.02	10.43	2.33	0.84	1.09	0.12	0.16	0.40	98.2
HA 42	52.21	13.79	9.88	8.01	10.06	1.96	0.72	1.05	0.12	0.17	0.26	98.0
HA 43	52.62	14.13	9.86	7.54	10.30	2.05	0.71	1.07	0.12	0.16	0.27	98.6
HA 45	52.47	14.23	9.79	7.35	10.41	2.01	0.68	1.07	0.12	0.17	0.15	98.3
HA 48	52.73	13.69	11.52	5.63	9.27	2.45	0.91	1.43	0.18	0.19	0.45	98.0
HA 50	52.07	14.88	8.97	7.44	10.79	2.09	0.62	0.92	0.11	0.16	0.57	98.1
HA 52	52.55	14.29	10.20	6.45	10.47	2.31	0.55	1.19	0.14	0.17	0.39	98.3
HA 56	52.06	14.19	9.96	6.89	10.51	2.02	0.62	1.14	0.13	0.21	0.40	97.7
HA 57	52.40	14.26	10.01	6.92	10.51	2.05	0.65	1.15	0.13	0.18	0.36	98.3
HA 58	52.28	14.19	10.14	6.53	10.27	2.06	0.63	1.20	0.14	0.20	0.57	97.6
HA 62	53.06	14.29	10.11	6.45	10.19	2.16	0.85	1.22	0.15	0.18	0.27	98.7
HA 65	52.25	14.19	10.41	6.28	10.10	2.13	0.70	1.24	0.14	0.17	0.87	97.6
HA 68	52.20	14.25	10.21	6.42	10.34	2.07	0.63	1.22	0.14	0.17	0.99	97.7
HA 71	52.19	13.99	10.44	6.40	10.10	2.11	0.76	1.23	0.14	0.17	0.48	97.5
HA 72	52.97	13.38	12.10	5.18	9.23	2.26	0.94	1.56	0.18	0.20	0.53	98.0
HA 76	52.57	14.09	10.42	6.27	9.97	2.20	0.82	1.24	0.15	0.19	0.41	97.9
HA 77	52.41	13.87	11.13	5.96	9.60	2.28	0.93	1.31	0.16	0.21	0.82	97.9
HA 83	52.13	14.28	10.16	6.92	10.37	2.27	0.75	1.20	0.14	0.17	0.40	98.4
HA 85	52.21	14.62	9.74	6.93	10.35	2.21	0.75	1.10	0.13	0.17	0.31	98.2
HA 87	52.09	14.27	10.04	7.00	10.38	2.32	0.60	1.17	0.13	0.17	0.81	98.2
HA 88	52.81	14.06	9.67	8.79	8.47	1.93	1.14	0.80	0.11	0.15	0.67	97.9
HA 93	48.80	16.00	11.16	8.20	11.10	2.05	0.51	0.82	0.07	0.19	0.08	98.9
HA 99	52.15	14.59	9.31	7.33	10.42	2.11	0.75	1.02	0.16	0.16	0.40	98.0

HA 100	52.40	14.62	9.36	7.48	10.39	2.12	0.82	1.01	0.15	0.16	0.46	98.5
HA 102	53.54	14.48	9.38	6.16	9.18	2.65	1.17	0.92	0.13	0.15	0.67	97.8
HA 109	50.09	16.62	7.71	9.97	11.95	1.56	0.35	0.39	0.04	0.15	0.59	98.8
HA 39	48.97	9.52	7.27	14.90	5.61	0.00	0.02	0.32	0.09	0.19	12.91	86.9
Hodd												
HD 7	52.70	14.01	11.03	5.24	8.86	2.64	1.00	1.86	0.26	0.19	1.09	97.8
HD 8	52.35	13.96	10.77	5.28	8.19	2.88	1.65	1.82	0.25	0.18	1.41	97.3
HD 9	51.98	13.90	10.90	5.66	8.68	3.04	1.20	1.75	0.21	0.20	0.72	97.5
HD 20	52.91	14.44	10.03	6.30	10.01	2.24	0.68	1.22	0.16	0.17	0.75	98.2
HD 22	51.96	15.23	7.77	9.26	12.35	1.83	0.43	0.79	0.07	0.15	0.02	99.8
HD 29	52.39	13.99	10.85	5.36	8.16	2.88	1.38	1.83	0.25	0.18	1.26	97.3
HD 30	52.65	14.07	10.91	5.56	8.44	3.16	1.15	1.83	0.25	0.20	1.11	98.2
HD 36	56.86	12.51	12.43	2.04	4.96	3.33	2.66	2.22	0.41	0.21	0.86	97.6
HD 38	53.99	13.27	11.89	3.78	6.69	3.02	2.24	2.08	0.24	0.18	1.00	97.4
HD 39	52.46	14.71	9.41	6.81	10.40	2.41	0.93	1.30	0.14	0.16	0.29	98.7
HD 41	53.19	13.23	12.44	4.09	7.04	2.91	1.54	2.23	0.32	0.21	1.16	97.2
HD 44	50.62	14.77	9.83	8.16	11.49	1.94	0.57	0.99	0.10	0.23	0.68	98.7
HD 45	50.61	14.77	9.83	8.25	11.81	2.01	0.43	0.98	0.09	0.19	0.66	99.0
HD 48	51.79	13.71	7.07	2.69	10.53	2.23	1.06	0.95	0.15	0.15	8.40	90.3
HD 49	52.36	14.59	9.67	6.93	10.63	2.06	0.78	1.09	0.15	0.17	0.89	98.4
HD 50	46.56	15.60	7.74	1.93	13.11	2.45	0.81	1.13	0.17	0.13	8.98	89.6
Kaarta												
MO 1	51.10	13.90	11.87	6.98	8.41	2.22	1.29	1.61	0.19	0.29	1.25	97.9
MO 2	52.3	13.65	11	7.44	10.45	2.1	0.94	1.24	0.14	0.17	0.3	99.4
MO 3	50.25	13	15.89	4.65	9.16	2.17	0.96	1.94	0.14	0.2	1.1	98.4
MO 5	53.35	13.95	11.88	5.96	9.55	2.5	0.93	1.26	0.18	0.17	0.19	99.7
MO 6	52.6	14	11.51	7.53	10.28	2.06	0.74	1.17	0.12	0.17	0.18	100.2
MO 7	51.35	14.7	11	7.7	11.64	1.95	0.45	0.95	0.09	0.17	0.26	100.0
MO 8	51.6	14.85	11.36	7.13	10.2	2.14	0.85	1.05	0.16	0.17	0.61	99.5
MO 9	50.2	13.75	11.46	8.66	9.44	1.7	0.99	1.09	0.11	0.18	1.56	97.6
MO 10	51.35	12.35	11.38	10.16	9.9	1.92	0.81	1.07	0.11	0.17	0.23	99.2
MO 11	51.5	13.6	13.29	5.82	9.61	2.33	0.96	1.33	0.19	0.16	0.78	98.8
MO 12	50.35	14.55	10.91	7.89	11.67	1.93	0.51	0.95	0.1	0.16	0.21	99.0

MO 13	52.5	13.75	10.52	6.73	10.1	2.45	0.97	1.26	0.14	0.16	0.73	98.6
MO 14	51.75	13.7	11.18	6.95	10.09	2.27	0.98	1.32	0.15	0.17	0.49	98.6
MO 15	52.3	14.2	11.02	6.76	10.2	2.37	0.94	1.25	0.14	0.16	0.6	99.3
MO16	52.35	14.65	10.64	7.24	10.13	2.08	0.9	0.95	0.14	0.2	0.78	99.3
MO 17	52.25	14.5	11.31	6.58	10.25	2.09	0.99	1	0.16	0.21	0.5	99.3
MO 18	52.1	14.65	10.49	7.22	9.98	2.1	0.87	0.93	0.15	0.2	0.54	98.7
MO 19	51.5	14.5	10.8	7.29	10.36	2.07	0.89	0.96	0.16	0.2	0.56	98.7
MO 20	52.75	13.65	10.95	6.96	10.13	2.21	0.98	1.28	0.15	0.21	0.16	99.3
MO 21	52.4	13.75	12.32	6.53	9.63	2.27	1.18	1.33	0.14	0.22	0.55	99.8
MO 22	53.3	14.1	12.53	6.31	9.63	2.26	1.01	1.37	0.16	0.21	-0.35	100.9
MO 24	52.45	13.7	10.62	7.69	10.3	2.15	0.84	1.16	0.13	0.2	0.33	99.2
MO 25	50.7	12.45	10.8	11.3	10.96	1.66	0.61	0.86	0.09	0.2	0.39	99.6
MO 26	50.5	12.7	10.13	12.22	11.62	1.58	0.44	0.63	0.06	0.19	0.33	100.1
MO 27	52.35	13.85	12.1	6.32	9.41	2.82	1.08	1.33	0.16	0.21	0.66	99.6
MO 31a	51.9	13.9	11.15	6.31	9.38	3.68	1.08	1.31	0.15	0.2	0.55	99.1
MO 31b	51.4	13.65	12.27	6.51	9.31	3.22	1.32	1.41	0.16	0.2	0.63	99.5
MO 32	51.9	13.75	10.62	7.4	10.46	2.42	0.93	1.18	0.12	0.16	0.43	98.9

Tabla 2. Trace elements composition (ppm) of Hank and Kaarta rocks.

	HA 38	HA 45	HA 48	HA 50	HA 52	HA 56	HA 58	HA 68	HA 71	HA 72	HA 83	HA 87
	Hank	Hank	Hank	Hank	Hank	Hank	Hank	Hank	Hank	Hank	Hank	Hank
Sc	37.5	35.6	38.1	35.6	38.1	37.3	37.1	37.4	36.7	38.1	36.9	37.7
V	272	254	317	233	285	270	277	280	279	323	272	277
Cr	266	269	31	205	201	274	167	171	156	21.9	212	229
Co	45.7	44.9	45.4	41.8	46.3	44.3	44.3	44.4	43.4	44.6	42.2	43.1
Ni	79.9	86.1	54.4	85.3	68.1	73.4	64.9	61.7	60.9	37.8	74.8	81.0
Cu	111	104	139	85	118	109	114	118	117	150	111	111
Zn	74.7	69.7	90.0	62.0	81.8	75.1	79.1	81.5	79.8	94.5	72.9	80.9
Ga	16.4	15.7	17.7	15.4	17.1	16.5	16.7	17.0	16.7	18.1	16.1	16.1
Li	19.5	15.5	21.6	15.5	14.2	7.6	8.4	9.2	14.4	13.3	16.5	30.0
Rb	25.0	21.4	27.8	18.6	20.7	18.9	18.4	18.3	25.0	29.7	23.4	19.2
Sr	190	175	193	192	200	195	205	212	193	195	198	189
Ba	363	766	254	199	459	153	234	303	898	562	178	199
Cs	0.98	1.14	1.03	1.69	1.22	0.68	0.95	0.99	1.65	2.20	1.03	2.05
Zr	103	102	138	88	72	106	111	110	111	144	102	98
Hf	2.68	2.72	3.56	2.33	2.13	2.74	2.92	2.87	2.91	3.73	2.73	2.61
Nb	7.3	7.2	10.2	6.3	7.8	7.4	7.5	7.9	7.6	9.9	7.0	7.1
Y	23.9	23.2	34.7	20.6	25.5	24.3	24.9	24.9	25.4	31.8	23.8	24.0
Pb	3.9	3.8	5.4	2.7	4.0	3.9	4.1	10.2	4.7	5.3	3.9	4.3
Th	2.4	2.5	3.1	2.1	2.5	2.4	2.5	2.5	2.5	3.2	2.3	2.2
U	0.6	0.6	0.7	0.5	0.5	0.5	0.6	0.5	0.5	0.7	0.5	0.5
Ta	0.48	0.47	0.59	0.39	0.48	0.45	0.47	0.48	0.45	0.62	0.44	0.45
La	10.8	10.6	15.6	9.8	12.0	11.3	11.8	11.9	11.7	15.4	11.2	11.2
Ce	24	26	38	22	30	27	29	30	29	38	27	27
Pr	3.12	3.09	4.48	2.80	3.49	3.27	3.44	3.45	3.43	4.45	3.26	3.29
Nd	13.6	13.5	19.1	12.1	15.2	14.5	15.2	15.3	15.4	19.8	14.7	14.7
Sm	3.47	3.42	4.72	3.05	3.83	3.59	3.78	3.85	3.93	4.95	3.69	3.65
Eu	1.10	1.02	1.44	1.00	1.19	1.15	1.21	1.20	1.14	1.48	1.17	1.19
Gd	4.02	3.95	5.17	3.43	4.36	4.16	4.34	4.31	4.35	5.43	4.14	4.19
Tb	0.67	0.66	0.87	0.59	0.72	0.70	0.73	0.74	0.73	0.93	0.70	0.69
Dy	4.14	4.12	5.40	3.63	4.50	4.33	4.48	4.50	4.59	5.73	4.29	4.25
Ho	0.87	0.87	1.13	0.76	0.93	0.89	0.94	0.93	0.94	1.19	0.89	0.89
Er	2.43	2.42	3.16	2.12	2.61	2.57	2.62	2.62	2.63	3.30	2.53	2.51
Tm												
Yb	2.23	2.26	2.91	2.02	2.37	2.34	2.44	2.43	2.45	3.09	2.36	2.31
Lu	0.33	0.33	0.42	0.29	0.34	0.34	0.35	0.35	0.36	0.44	0.34	0.33

	MO 2 Kaarta	MO 5 Kaarta	MO 6 Kaarta	MO 12 Kaarta	MO 14 Kaarta	MO 18 Kaarta	MO 22 Kaarta	MO 25 Kaarta	MO 26 Kaarta	MO 31a Kaarta
Sc	36.4	35.8	36.6	39.3	34.6	35.4	34.4	34.3	33.3	33.6
V	272	289	277	270	266	231	275	221	196	269
Cr	407	77.8	280	238	307	266	192	891	993	202
Co	45.3	43.7	45.7	43.8	42.8	41.8	43.2	55.2	54.3	41.1
Ni	100	66.9	84.0	94.7	84.1	75.9	73.1	209	226	72.8
Cu	111	115	115	110	111	87.9	125	65.9	44.6	61.3
Zn	73.0	79.9	73.4	67.0	72.3	68.0	81.6	58.4	50.7	54.3
Ga	17.2	18.0	16.9	15.5	17.1	15.9	18.3	13.3	11.9	17.4
Li	9.4	13.6	14.6	9.8	11.1	12.9	10.4	10.6	6.4	11.8
Rb	30.7	27.4	21.9	13.6	31.1	28.6	34.7	18.3	12.3	33.4
Sr	234	243	187	172	215	202	225	182	172	378
Ba	205.8	238.9	165.3	141	202	206	218	127.1	89.3	230
Cs	1.26	0.94	1.09	0.55	1.36	1.23	1.55	0.84	0.52	2.37
Zr	127	124	106	77	127	97	147	74	44	125
Hf	3.32	3.30	2.80	2.07	3.41	2.49	3.75	1.95	1.44	3.23
Nb	12.4	7.7	6.4	4.9	13.3	11.2	14.4	7.9	5.1	13.8
Y	27.8	26.8	24.5	21.0	25.9	21.8	28.2	17.8	13.3	27.2
Pb	4.5	4.5	3.6	2.2	4.7	3.8	5.4	3.0	2.1	2.1
Th	3.6	2.6	2.2	1.3	3.9	2.8	4.2	2.4	1.5	4.1
U	0.8	0.6	0.5	0.3	0.9	0.6	1.0	0.5	0.3	0.9
Ta	0.83	0.49	0.42	0.30	0.87	0.71	0.91	0.54	0.34	0.88
La	15.7	13.5	10.5	7.4	16	13	17	9.67	6.50	16.65
Ce	36.6	33.7	26.1	17.0	37.4	30.8	41.3	20.7	14.3	40.08
Pr	4.23	4.02	3.25	2.33	4.34	3.47	4.69	2.67	1.82	4.59
Nd	18.4	17.6	14.6	10.5	18.6	14.6	20.1	11.7	8.1	19.8
Sm	4.42	4.29	3.79	2.75	4.52	3.39	4.88	2.91	2.08	4.76
Eu	1.38	1.36	1.20	0.97	1.40	1.06	1.47	0.94	0.75	1.44
Gd	4.92	4.73	4.35	3.44	4.89	3.67	5.22	3.18	2.37	5.10
Tb	0.79	0.78	0.73	0.59	0.81	0.61	0.84	0.53	0.39	0.83
Dy	4.83	4.87	4.52	3.72	4.78	3.86	5.13	3.26	2.39	4.98
Ho	0.98	1.01	0.92	0.78	0.99	0.81	1.05	0.66	0.49	1.02
Er	2.70	2.79	2.55	2.19	2.73	2.29	2.90	1.85	1.39	2.75
Tm										
Yb	2.42	2.58	2.31	2.04	2.42	2.14	2.58	1.62	1.25	2.49
Lu	0.35	0.38	0.33	0.30	0.34	0.30	0.36	0.23	0.18	0.36

Table 3. Sr-Nd-Pb isotope ratios. Initial ratios recalculated to 201 Ma.

Sample	$(^{87}Sr/^{86}Sr)_{meas.}$	± 1 σ	$(^{87}Sr/^{86}Sr)_{ini}$	$(^{143}Nd/^{144}Nd)_{meas.}$	± 1 σ	$(^{143}Nd/^{144}Nd)_{ini}$	$(^{206}Pb/^{204}Pb)_{meas.}$	± 1 σ	$(^{206}Pb/^{204}Pb)_{ini}$	$(^{207}Pb/^{204}Pb)_{meas.}$	± 1 σ	$(^{207}Pb/^{204}Pb)_{ini}$	$(^{208}Pb/^{204}Pb)_{meas.}$	± 1 σ	$(^{208}Pb/^{204}Pb)_{ini}$
MO2	0.707068	0.000003	0.705984	0.512597	0.000002	0.512407	18.802	0.0031	18.440	15.665	0.0025	15.647	39.023	0.0063	38.502
MO6	0.707217	0.000003	0.706249	0.512534	0.000002	0.512327	18.504	0.0018	18.224	15.639	0.0014	15.625	38.619	0.0033	38.221
MO8	0.707376	0.000002	0.706724	0.512473	0.000002		18.690	0.0002	18.690	15.681	0.0002	15.681	38.798	0.0005	38.798
MO12	0.706547	0.000003	0.705895	0.512588	0.000002	0.512380	18.330	0.0020	18.061	15.631	0.0016	15.617	38.445	0.0039	38.078
MO22	0.707003	0.000002	0.705728	0.512593	0.000002	0.512399	18.786	0.0007	18.429	15.662	0.0006	15.644	38.981	0.0014	38.467
MO25	0.706932	0.000003	0.706100	0.512585	0.000002	0.512385	18.749	0.0040	18.397	15.666	0.0033	15.648	38.937	0.0082	38.425
MO26	0.706420	0.000003	0.705830	0.512598	0.000003	0.512394	18.742	0.0035	18.405	15.653	0.0029	15.636	38.912	0.0072	38.425
MO31	0.707766	0.000002	0.707035	0.512595	0.000002	0.512401	19.703	0.0032	18.790	15.718	0.0026	15.672	39.616	0.0064	38.310
MO18	0.708317	0.000002	0.707146	0.512465	0.000002	0.512278	18.735	0.0013	18.412	15.684	0.0011	15.668	38.869	0.0026	38.387
HD22	0.706221	0.000003		0.512604	0.000003		18.564	0.0062	18.564	15.648	0.0050	15.648	38.710	0.0124	38.710
HA45	0.708283	0.000003	0.707272	0.512497	0.000002	0.512293	18.651	0.0039	18.350	15.699	0.0034	15.684	38.868	0.0085	38.442
HA50	0.708758	0.000003	0.707954	0.512444	0.000002	0.512243	18.697	0.0051	18.349	15.667	0.0042	15.649	38.795	0.0106	38.289
HA52	0.707946	0.000003	0.707093	0.512481	0.000002	0.512282	18.499	0.0025	18.244	15.639	0.0020	15.626	38.638	0.0050	38.242
HA56	0.707738	0.000003	0.706935	0.512467	0.000002	0.512268	18.533	0.0037	18.268	15.668	0.0030	15.655	38.696	0.0077	38.303
HA58	0.707705	0.000003	0.706962	0.512471	0.000002	0.512272	18.536	0.0039	18.268	15.665	0.0033	15.651	38.688	0.0079	38.294
HA68	0.708020	0.000003	0.707306	0.512474	0.000002	0.512273	18.545	0.0034	18.446	15.662	0.0027	15.657	38.685	0.0067	38.527
HA83	0.710821	0.000003	0.709841	0.512458	0.000002	0.512256	18.503	0.0031	18.247	15.659	0.0025	15.646	38.652	0.0064	38.270

Table 4. Summary of Ar-Ar ages data and relative abundances of Ar isotopes.

Step	Heating	Sample	Material	Location	$^{39}Ar_{(k)}$ (%)	K/Ca	± 2s	$^{40}Ar^*/^{39}Ar$	± 2s	Age (Ma)	± 2s
3M30352D	64 °C	MD3	Plg	Laser	0.06	0.0261	± 0.1102	399.15485	± 74.45342	1579.85	± 196.50
3M30353D	66 °C	MD3	Plg	Laser	2.18	0.0312	± 0.0054	101.33548	± 5.04820	548.48	± 23.57
3M30354D	67 °C	MD3	Plg	Laser	2.70	0.0213	± 0.0029	46.46979	± 1.72272	272.27	± 9.37
3M30356D	68 °C	MD3	Plg	Laser	4.32	0.0192	± 0.0023	41.76699	± 0.94497	246.50	± 5.21
3M30357D	69 °C	MD3	Plg	Laser	3.99	0.0178	± 0.0020	33.94325	± 0.87066	202.82	± 4.92
3M30358D	69 °C	MD3	Plg	Laser	10.49	0.0200	± 0.0021	36.95768	± 0.55086	219.77	± 3.08
3M30359D	70 °C	MD3	Plg	Laser	11.12	0.0203	± 0.0022	32.57921	± 0.52005	195.09	± 2.95
3M30363D	71 °C	MD3	Plg	Laser	5.22	0.0183	± 0.0021	32.64179	± 0.64426	195.44	± 3.66
3M30364D	71 °C	MD3	Plg	Laser	13.89	0.0208	± 0.0022	32.34157	± 0.50546	193.74	± 2.87
3M30365D	72 °C	MD3	Plg	Laser	8.72	0.0169	± 0.0018	32.98495	± 0.49295	197.39	± 2.79
3M30367D	80 °C	MD3	Plg	Laser	10.25	0.0168	± 0.0018	44.46333	± 0.67266	261.32	± 3.68
3M30368D	81 °C	MD3	Plg	Laser	14.17	0.0166	± 0.0017	36.15140	± 0.50730	215.25	± 2.85
3M30369D	82 °C	MD3	Plg	Laser	12.90	0.0171	± 0.0018	41.75966	± 0.61307	246.46	± 3.38

Table 5. Procedural blanks of Ar-Ar step heating dating.

Procedure Blanks		36Ar [V]	1s	37Ar [V]	1s	38Ar [V]	1s	39Ar [V]	1s	40Ar [V]	1s
3M30352D	64 °C	0.0000233	0.0000052	0.0003128	0.0000167	0.0000080	0.0000033	0.0000163	0.0000056	0.0039137	0.0000357
3M30353D	66 °C	0.0000233	0.0000052	0.0003128	0.0000167	0.0000080	0.0000033	0.0000163	0.0000056	0.0039137	0.0000357
3M30354D	67 °C	0.0000233	0.0000052	0.0003128	0.0000167	0.0000080	0.0000033	0.0000163	0.0000056	0.0039137	0.0000357
3M30356D	68 °C	0.0000233	0.0000052	0.0003128	0.0000167	0.0000080	0.0000033	0.0000163	0.0000056	0.0039137	0.0000357
3M30357D	69 °C	0.0000233	0.0000052	0.0003128	0.0000167	0.0000080	0.0000033	0.0000163	0.0000056	0.0039137	0.0000357
3M30358D	69 °C	0.0000233	0.0000052	0.0003128	0.0000167	0.0000080	0.0000033	0.0000163	0.0000056	0.0039137	0.0000357
3M30359D	70 °C	0.0000202	0.0000053	0.0003158	0.0000190	0.0000072	0.0000037	0.0000203	0.0000035	0.0039369	0.0000376
3M30363D	71 °C	0.0000273	0.0000027	0.0002900	0.0000228	0.0000048	0.0000035	0.0000121	0.0000032	0.0037811	0.0000192
3M30364D	71 °C	0.0000273	0.0000027	0.0002900	0.0000228	0.0000048	0.0000035	0.0000121	0.0000032	0.0037811	0.0000192
3M30365D	72 °C	0.0000273	0.0000027	0.0002900	0.0000228	0.0000048	0.0000035	0.0000121	0.0000032	0.0037811	0.0000192
3M30367D	80 °C	0.0000273	0.0000027	0.0002900	0.0000228	0.0000048	0.0000035	0.0000121	0.0000032	0.0037811	0.0000192
3M30368D	81 °C	0.0000273	0.0000027	0.0002900	0.0000228	0.0000048	0.0000035	0.0000121	0.0000032	0.0037811	0.0000192
3M30369D	82 °C	0.0000273	0.0000027	0.0002900	0.0000228	0.0000048	0.0000035	0.0000121	0.0000032	0.0037811	0.0000192

12. Patagonia

Table 4. Major element compositions (wt%) of analyzed olivine in Cañadon Asfalto Formation (patvj 027) and Cresta de los Bosques Formation (patvj 005).

sample	SiO_2 wt%	FeO wt%	MnO wt%	MgO wt%	CaO wt%	NiO wt%	ZnO wt%	TOTAL	Fo %
patvj 027_m2 rim	36.57	32.83	0.65	31.31	0.20	0.02	0.14	101.7	63.0
patvj 027_m2 core	36.96	33.02	0.58	31.37	0.22	0.01	0.11	102.3	62.9
patvj 027_m4 rim	37.27	32.60	0.70	31.84	0.23	0.07	0.09	102.8	63.5
patvj 027_m4b core	36.77	32.05	0.55	31.76	0.23	0.03	0.00	101.4	63.9
patvj 027_m6 rim	37.78	26.75	0.52	36.02	0.28	0.09	0.09	101.5	70.6
patvj 027_m6b core	37.81	27.35	0.44	36.00	0.23	0.06	0.06	102.0	70.1
patvj 027_m8 core	36.88	32.12	0.58	31.66	0.24	0.03	0.03	101.5	63.7
patvj 027_m10 core	37.52	28.03	0.38	35.54	0.26	0.07	0.00	101.8	69.3
patvj 027-82 core	38.67	17.92	0.28	42.49	0.18	0.21	*n.m*	99.7	80.9
patvj 027-22 core	38.43	18.44	0.26	42.01	0.20	0.18	*n.m*	99.5	80.2
patvj 027-106 core	38.75	16.04	0.21	44.05	0.18	0.20	*n.m*	99.4	83.0
patvj 027-60 core	38.57	16.53	0.23	44.10	0.18	0.18	*n.m*	99.8	82.6
patvj 027-112 core	38.94	15.89	0.23	44.16	0.18	0.22	*n.m*	99.6	83.2
patvj 027-63 core	38.29	16.43	0.23	43.73	0.18	0.21	*n.m*	99.1	82.6
patvj 027-42 core	37.66	21.64	0.35	39.67	0.22	0.16	*n.m*	99.7	76.6
patvj 027-131 core	38.33	16.63	0.25	43.62	0.19	0.21	*n.m*	99.2	82.4
patvj 027-44 core	38.42	18.03	0.22	42.46	0.18	0.12	*n.m*	99.4	80.8
patvj 027-88 core	37.90	22.16	0.29	39.43	0.14	0.15	*n.m*	100.1	76.0
patvj 027-129 core	38.36	16.00	0.22	43.73	0.19	0.20	*n.m*	98.7	83.0
patvj 027-72 core	37.95	22.27	0.32	39.43	0.21	0.12	*n.m*	100.3	75.9
patvj 027-69 core	38.57	18.01	0.25	42.55	0.18	0.21	*n.m*	99.8	80.8
patvj 027-73 core	38.99	16.21	0.24	44.03	0.15	0.19	*n.m*	99.8	82.9
patvj 027-96 core	38.34	17.95	0.23	42.49	0.18	0.20	*n.m*	99.4	80.8
patvj 027-6 core	38.45	16.03	0.21	44.22	0.18	0.21	*n.m*	99.3	83.1
patvj 027-86 core	38.30	16.83	0.26	43.19	0.18	0.20	*n.m*	99.0	82.1
patvj 027-78 core	38.72	17.31	0.23	43.14	0.19	0.20	*n.m*	99.8	81.6
patvj 027-21 core	37.35	22.32	0.34	38.81	0.23	0.12	*n.m*	99.2	75.6
patvj 027-49 core	38.83	16.41	0.21	43.50	0.18	0.22	*n.m*	99.4	82.5
patvj 027-104 core	38.12	18.39	0.25	42.55	0.19	0.18	*n.m*	99.7	80.5
patvj 027-50 core	38.72	17.21	0.24	43.28	0.18	0.21	*n.m*	99.8	81.8
patvj 027-17 core	37.35	22.78	0.34	38.50	0.21	0.12	*n.m*	99.3	75.1
patvj 027-85 core	38.46	15.99	0.25	43.69	0.18	0.21	*n.m*	98.8	83.0
patvj 027-95 core	37.97	18.98	0.29	41.99	0.19	0.20	*n.m*	99.6	79.8
patvj 027-30 core	37.85	20.01	0.29	40.97	0.19	0.16	*n.m*	99.5	78.5

patvj 027-32 core	38.72	16.96	0.22	43.53	0.18	0.20	*n.m*	99.8	82.1
patvj 027-8 core	38.54	17.55	0.21	43.10	0.18	0.18	*n.m*	99.8	81.4
patvj 027-133 core	37.47	20.92	0.30	39.98	0.19	0.14	*n.m*	99.0	77.3
patvj 027-74 core	38.56	18.45	0.27	42.10	0.19	0.17	*n.m*	99.8	80.3
patvj 027-23 core	37.99	18.86	0.25	41.91	0.20	0.19	*n.m*	99.4	79.8
PTvj005_1 core	39.13	20.42	0.31	41.28	0.12	0.15	0.00	101.4	78.3
PTvj005_3 core	39.38	20.05	0.23	41.69	0.12	0.17	0.00	101.6	78.8
PTvj005_4 core	39.11	20.92	0.31	41.67	0.09	0.11	0.00	102.2	78.0
PTvj005_8 core	39.06	19.55	0.30	41.49	0.08	0.13	0.00	100.6	79.1
PTvj005_9 core	39.23	19.81	0.33	41.86	0.14	0.15	0.06	101.6	79.0
PTvj005_12 core	39.12	20.80	0.31	40.78	0.07	0.14	0.00	101.2	77.8
PTvj005_14 core	39.53	17.74	0.28	43.54	0.05	0.16	0.00	101.3	81.4
PTvj005_17 core	39.26	19.27	0.31	42.28	0.08	0.19	0.00	101.4	79.6
PTvj005_18 core	39.38	18.53	0.30	42.80	0.16	0.13	0.00	101.3	80.5
PTvj005_24 core	39.40	18.48	0.22	42.82	0.07	0.08	0.03	101.1	80.5
PTvj005_25 core	39.42	18.53	0.29	43.25	0.09	0.17	0.06	101.8	80.6
PTvj005_27 core	39.12	19.74	0.30	41.60	0.08	0.17	0.05	101.1	79.0
PTvj005_28 core	39.05	20.16	0.23	41.69	0.10	0.09	0.03	101.3	78.7
PTvj005_31 core	38.48	22.57	0.34	39.62	0.09	0.16	0.00	101.3	75.8
PTvj005_32 core	38.63	22.31	0.39	39.91	0.18	0.20	0.03	101.6	76.1
PTvj005_33 core	38.38	22.29	0.25	39.82	0.08	0.12	0.00	100.9	76.1
PTvj005_35 core	38.47	22.04	0.35	40.33	0.10	0.19	0.00	101.5	76.5

nm: not measured. Analysis on patvj 027 were performed at the University of Tasmania. Data of patvj 005 obtained at the University of Bonn.

Table 5. Measured composition of spinel inclusions in samples from Bajo Pobre and Cañadon Asfalto Formation.

Sample	Host	SiO_2 wt.%	TiO_2 wt.%	Al_2O_3 wt.%	Cr_2O_3 wt.%	FeO_{tot} wt.%	MnO wt.%	MgO wt.%	NiO wt.%	ZnO wt.%	SUM	Mg#	Cr#
Bajo Pobre													
PT40_CHR7	res. Ol	0.10	1.30	26.80	24.42	34.52	0.35	10.24	0.16	0.22	98.10	46.68	37.94
PT40_CHR7	res. Ol	0.11	1.31	26.75	24.62	34.62	0.26	10.20	0.17	0.20	98.25	46.31	38.18
PT40_CHR8	res. Ol	0.07	1.36	26.40	24.91	35.61	0.27	9.89	0.17	0.19	98.88	44.83	38.76
PT40_CHR9	res. Ol	0.10	1.30	26.02	24.33	36.19	0.25	9.64	0.20	0.17	98.21	44.06	38.54
PT40_CHR25	res. Ol	0.08	1.44	27.41	25.48	32.38	0.27	11.19	0.19	0.14	98.58	50.09	38.41
PT40_CHR25	res. Ol	0.10	1.29	28.36	25.19	31.55	0.25	11.73	0.19	0.08	98.74	52.14	37.34
PT40_CHR10	res. Ol	0.13	1.50	24.66	24.01	37.42	0.30	9.13	0.16	0.18	97.49	42.11	39.52
PT40_CHR11	res. Ol	0.14	1.53	24.72	23.75	37.47	0.30	9.09	0.18	0.16	97.34	41.95	39.19
PT40_CHR21	res. Ol	0.09	1.46	25.63	24.24	36.84	0.32	9.28	0.16	0.21	98.23	42.48	38.82
PT40_CHR22	res. Ol	0.13	1.33	25.86	24.28	35.71	0.28	9.77	0.18	0.19	97.71	44.79	38.64
PT40_CHR23	res. Ol	0.17	1.35	25.32	24.69	36.31	0.38	9.51	0.14	0.20	98.06	43.65	39.54
PT40_CHR25	res. Ol	0.07	1.25	26.04	24.51	36.23	0.30	9.61	0.18	0.19	98.38	44.00	38.71
PT40_CHR25	res. Ol	0.09	1.40	26.08	24.35	36.97	0.29	8.89	0.15	0.22	98.45	40.69	38.51
PT40_CHR16	res. Ol	0.11	1.58	24.67	24.37	38.28	0.32	8.75	0.17	0.18	98.44	40.16	39.86
PT40_CHR25	res. Ol	0.09	1.49	26.34	24.61	36.43	0.30	8.92	0.18	0.24	98.60	40.71	38.53
PT40_CHR12	res. Ol	0.12	1.74	24.26	23.68	39.30	0.36	8.04	0.13	0.20	97.82	37.17	39.56
PT40_CHR15	res. Ol	0.07	1.72	23.92	24.35	38.87	0.30	8.55	0.16	0.14	98.08	39.34	40.58
PT40_CHR17	res. Ol	0.08	1.72	23.31	24.27	39.97	0.32	8.36	0.14	0.13	98.29	38.52	41.12
PT40_CHR18	res. Ol	0.19	1.44	19.22	21.15	42.24	0.39	7.36	0.11	0.27	92.37	36.79	42.47
PT40_CHR20	res. Ol	0.10	1.67	23.33	23.70	40.76	0.35	7.77	0.15	0.16	97.99	36.10	40.52
PT40_CHR24	res. Ol	0.08	1.64	23.20	23.48	40.65	0.31	8.22	0.16	0.21	97.95	38.17	40.44
PT40_CHR19	res. Ol	0.10	2.81	19.62	22.95	43.46	0.33	8.10	0.18	0.14	97.69	37.17	43.96
PT40_CHR25	res. Ol	0.08	2.94	19.22	23.77	43.59	0.36	8.20	0.19	0.16	98.53	37.37	45.34
PT40_CHR13	res. Ol	0.10	1.90	20.89	22.60	45.20	0.32	6.30	0.10	0.19	97.60	29.74	42.06
PT40_CHR14	res. Ol	0.14	1.49	17.47	23.44	48.47	0.39	5.23	0.09	0.19	96.92	25.60	47.38
GEO8 chr	res. Ol	0.08	7.51	10.41	9.83	61.32	0.29	4.32	0.14	0.03	93.93	19.35	38.77
GEO8 chr	res. Ol	0.06	2.49	10.99	21.48	55.14	0.29	5.62	0.16	0.12	96.35	27.55	56.75
GEO8 chr	res. Ol	0.05	1.19	9.18	29.08	51.27	0.29	5.25	0.12	0.14	96.59	26.89	67.99
GEO8 chr	res. Ol	0.14	1.08	8.46	24.40	55.46	0.28	4.40	0.15	0.11	94.48	23.15	65.93

GEO8 chr	res. Ol	0.11	6.58	6.45	7.15	68.76	0.32	3.54	0.11	0.06	93.09	16.58	42.66
GEO8 chr	res. Ol	0.13	4.75	8.31	11.41	63.52	0.30	3.72	0.14	0.10	92.39	18.23	47.96
GEO8 chr	res. Ol	0.24	6.54	7.72	6.44	67.21	0.33	3.34	0.14	0.09	92.05	15.71	35.86
GEO8 chr	res. Ol	0.11	7.21	6.15	11.10	65.79	0.45	2.41	0.12	0.09	93.45	11.27	54.76
GEO8 chr	res. Ol	0.11	9.23	5.61	6.70	68.29	0.73	2.57	0.09	0.11	93.44	11.57	44.49
PT101_Chr	res. Ol	0.13	1.62	17.58	23.68	47.68	0.32	3.02	0.06	0.30	94.38	15.31	47.47
PT101_Chr	res. Ol	0.07	1.04	20.56	30.43	39.25	0.28	3.90	0.03	0.30	95.86	19.51	49.83
PT101_Chr	res. Ol	0.10	5.59	4.01	29.13	50.37	0.46	2.07	0.08	0.17	91.97	10.41	82.98
PT101_Chr	res. Ol	0.14	8.39	7.75	19.75	53.48	0.33	2.66	0.08	0.16	92.74	12.09	63.10
PT101_Chr	res. Ol	0.05	9.91	6.69	25.68	47.46	0.34	3.66	0.05	0.28	94.12	16.01	72.02
PT101_Chr	res. Ol	0.14	8.39	7.75	19.75	53.48	0.33	2.66	0.08	0.16	92.74	12.09	63.10
Cañadon Asfalto													
PATVJ020	Opx	0.11	6.23	7.16	15.44	60.47	0.35	2.67	0.06	0.18	92.67	12.78	59.13
PATVJ020	Opx	0.30	4.25	13.63	19.47	51.48	0.38	4.09	0.14	0.26	94.00	19.60	48.93
PATVJ020	Opx	0.22	4.45	9.47	16.79	56.92	0.38	2.34	0.13	0.20	90.89	11.83	54.33
PATVJ020	Opx	0.15	2.42	10.45	16.42	60.04	0.33	2.05	0.09	0.22	92.16	10.75	51.33
PATVJ020	Opx	0.08	4.44	15.89	18.30	50.57	0.32	3.95	0.15	0.19	93.88	18.78	43.59
PATVJ020	Opx	0.05	4.26	12.00	20.38	52.62	0.40	3.94	0.07	0.15	93.88	19.13	53.25
PATVJ020	Opx	0.11	1.87	6.98	14.84	64.82	0.27	2.68	0.07	0.19	91.83	14.38	58.77
PATVJ020	Opx	0.07	3.66	7.77	15.95	61.55	0.38	1.20	0.08	0.40	91.06	6.31	57.94
PATVJ020	Opx	0.08	1.54	8.98	15.63	64.29	0.38	1.31	0.07	0.23	92.50	7.08	53.87
PATVJ020	Opx	0.05	2.07	7.37	15.38	65.42	0.34	1.21	0.05	0.16	92.03	6.51	58.34
PATVJ020	Opx	0.13	8.38	7.28	15.91	58.12	0.42	2.13	0.08	0.18	92.64	9.79	59.46
PATVJ020	Opx	0.24	5.03	9.75	16.44	57.86	0.42	1.57	0.05	0.23	91.59	7.81	53.08
PATVJ027_CHR2	Ol	0.08	1.33	13.33	30.99	43.26	0.36	6.54	0.14	0.16	96.20	32.72	60.93
PATVJ027_CHR5	Ol	0.10	0.42	11.01	46.09	32.20	0.36	6.87	0.05	0.18	97.28	35.20	73.74
PATVJ027_CHR6	Ol	0.12	0.59	10.55	47.88	31.77	0.38	6.34	0.10	0.20	97.92	32.42	75.27
PATVJ027_CHR7	Ol	0.05	1.03	9.00	50.05	31.47	0.41	6.19	0.04	0.18	98.43	31.49	78.86
PATVJ027_CHR7	Ol	0.09	0.73	10.27	46.82	33.25	0.32	5.76	0.09	0.17	97.50	29.58	75.35
PATVJ027_CHR7	Ol	0.09	1.07	9.93	46.36	34.28	0.38	5.52	0.10	0.12	97.86	28.12	75.79
PATVJ027_CHR1	Ol	0.09	3.23	11.93	23.70	51.13	0.37	5.89	0.13	0.09	96.56	28.20	57.13
PATVJ027_CHR7	Ol	0.09	4.72	6.46	38.48	41.88	0.38	4.28	0.07	0.15	96.51	20.57	79.98
PATVJ027_CHR7	Ol	0.06	6.54	6.65	31.90	46.10	0.37	4.42	0.13	0.17	96.34	20.38	76.29

27-82 c	Ol*	0.05	1.59	26.10	25.64	33.35	0.19	11.23	0.16	0.15	98.45	50.31	39.73
27-106 c	Ol*	0.06	1.39	27.37	24.99	31.84	0.23	11.44	0.20	0.17	97.70	51.63	37.98
27-60 c	Ol*	0.06	1.44	25.55	24.76	34.09	0.21	10.44	0.18	0.14	96.86	47.92	39.39
27-112 c	Ol*	0.06	1.41	26.80	25.88	32.11	0.22	11.34	0.21	0.15	98.18	51.06	39.31
27-63 c	Ol*	0.06	1.36	25.99	25.53	32.95	0.22	10.95	0.20	0.13	97.39	49.92	39.73
27-131 c	Ol*	0.06	1.46	25.45	25.47	34.32	0.23	10.51	0.22	0.13	97.86	47.89	40.17
27-44 c	Ol*	0.06	2.33	22.11	22.57	40.65	0.22	9.49	0.10	0.10	97.62	43.05	40.64
27-88 c	Ol*	0.06	1.63	26.44	25.41	33.56	0.24	10.33	0.16	0.12	97.95	46.66	39.20
27-129 c	Ol*	0.06	1.72	26.78	25.62	31.70	0.22	11.26	0.19	0.14	97.68	50.54	39.08
27-69 c	Ol*	0.07	1.41	26.01	24.61	34.54	0.23	10.18	0.18	0.18	97.40	46.56	38.83
27-73 c	Ol*	0.07	1.34	30.96	21.51	32.59	0.23	11.25	0.18	0.13	98.24	49.84	31.79
27-96 c	Ol*	0.07	1.35	26.77	25.13	32.96	0.19	10.82	0.19	0.15	97.64	49.06	38.64
27-6 c	Ol*	0.07	1.47	26.21	25.38	33.11	0.23	10.96	0.18	0.15	97.76	49.64	39.38
27-86 c	Ol*	0.07	1.47	25.27	25.36	34.17	0.22	10.32	0.22	0.20	97.32	47.36	40.24
27-78 c	Ol*	0.07	1.62	23.47	24.27	37.91	0.26	9.10	0.15	0.22	97.08	42.26	40.96
27-49 c	Ol*	0.08	1.36	26.78	25.00	33.12	0.21	10.96	0.20	0.19	97.90	49.62	38.51
27-104 c	Ol*	0.08	1.75	27.10	25.04	33.55	0.23	10.23	0.18	0.21	98.37	45.93	38.27
27-50 c	Ol*	0.08	1.44	25.62	25.10	34.64	0.22	10.51	0.19	0.15	97.95	47.76	39.66
27-85 c	Ol*	0.08	1.40	27.04	24.96	32.46	0.22	11.16	0.19	0.16	97.67	50.42	38.25
27-95 c	Ol*	0.08	1.43	24.99	24.79	36.48	0.25	9.45	0.16	0.20	97.82	43.44	39.96
27-32 c	Ol*	0.08	1.39	26.64	25.12	32.85	0.21	10.92	0.19	0.15	97.55	49.53	38.74
27-8 c	Ol*	0.09	1.35	25.88	24.51	34.39	0.22	10.52	0.17	0.19	97.32	48.09	38.84
27-133 c	Ol*	0.10	1.44	25.71	25.23	34.85	0.24	9.94	0.16	0.16	97.82	45.35	39.70
27-74 c	Ol*	0.11	1.42	26.02	24.79	35.22	0.27	9.96	0.16	0.16	98.11	45.33	39.00
27-42 c	Ol*	0.06	1.66	23.13	24.17	40.19	0.27	7.96	0.14	0.18	97.77	37.03	41.21
27-72 c	Ol*	0.07	1.63	21.15	23.67	42.14	0.26	7.49	0.13	0.19	96.72	35.55	42.88
27-22 c	Ol*	0.05	2.30	19.16	24.35	42.50	0.23	8.36	0.21	0.15	97.30	38.93	46.02
27-21 c	Ol*	0.08	6.83	7.71	17.83	57.85	0.32	4.51	0.14	0.20	95.47	20.58	60.81
27-17 c	Ol*	0.08	1.60	21.08	23.89	42.05	0.27	7.74	0.12	0.21	97.03	36.59	43.19
27-30 c	Ol*	0.08	1.34	22.62	23.88	39.64	0.25	8.23	0.16	0.25	96.44	39.06	41.47

*Ol: Olivine in grain mounts. Res. Ol: Resorbed olivine. Mg# (Mg# [100*Mg/(Mg+Fe)]). Cr# [100*Cr/(Cr+Al)].

Table 6. Major element compositions of pyroxene cores from Bajo Pobre (BP), Cañadón Asfalto (CA), Lago la Plata (LP), Cresta de los Bosques (CB) and Chon Aike Formation.

sample	Fm	SiO_2 wt.%	TiO_2 wt.%	Al_2O_3 wt.%%	FeO wt.%	MnO wt.%	MgO wt.%	CaO wt.%	Na_2O wt.%	Cr_2O_3 wt.%	TOTAL	Wo wt.%	En wt.%	Fs wt.%	Js Wt.%	Mg#
geo8_m9	BP	50.0	0.7	4.8	7.8	0.3	15.3	20.2	0.3	0.3	99.7	42.0	44.2	12.6	1.1	77.8
geo8_m7	BP	52.4	0.3	4.4	15.1	0.3	26.6	1.8	0.0	0.1	100.9	3.5	73.1	23.3	0.1	75.9
geo2_m1	BP	52.7	0.2	1.3	18.3	0.5	24.9	1.5	0.0	0.0	99.5	3.1	68.6	28.3	0.1	70.8
geo8_m9	BP	50.0	0.7	4.8	7.8	0.3	15.3	20.2	0.3	0.3	99.7	42.0	44.2	12.6	1.1	77.8
geo8_m7	BP	52.4	0.3	4.4	15.1	0.3	26.6	1.8	0.0	0.1	100.9	3.5	73.1	23.3	0.1	75.9
geo2_m1	BP	52.7	0.2	1.3	18.3	0.5	24.9	1.5	0.0	0.0	99.5	3.1	68.6	28.3	0.1	70.8
geo2_m2	BP	49.3	0.7	4.0	10.7	0.3	13.9	19.3	0.4	0.0	98.7	40.3	40.6	17.5	1.7	69.9
geo2_m2b	BP	49.0	0.7	3.9	11.4	0.3	14.4	18.1	0.4	0.0	98.4	37.7	41.9	18.7	1.7	69.2
geo2_m2	BP	49.3	0.7	4.0	10.7	0.3	13.9	19.3	0.4	0.0	98.7	40.3	40.6	17.5	1.7	69.9
geo2_m2b	BP	49.0	0.7	3.9	11.4	0.3	14.4	18.1	0.4	0.0	98.4	37.7	41.9	18.7	1.7	69.2
PT170_m1	BP	51.1	0.3	1.3	10.4	0.5	13.7	21.0	0.3	0.0	98.6	43.0	39.2	16.6	1.1	70.2
PT170_m1	BP	51.1	0.3	1.3	10.4	0.5	13.7	21.0	0.3	0.0	98.6	43.0	39.2	16.6	1.1	70.2
PT182_m5	BP	51.8	0.3	1.0	24.4	0.8	20.4	1.5	0.0	0.0	100.2	3.2	57.9	38.8	0.1	59.9
PT182_m1	BP	51.0	0.6	2.1	10.6	0.4	16.1	18.1	0.2	0.0	99.2	36.9	45.7	16.8	0.6	73.0
PT182_m2	BP	51.4	0.5	2.0	9.1	0.2	15.9	19.6	0.2	0.0	98.8	39.8	45.1	14.4	0.7	75.8
PT182_m3	BP	51.2	0.3	1.4	11.7	0.5	14.0	20.1	0.3	0.0	99.5	40.7	39.5	18.6	1.2	68.0
PT182_m6	BP	51.0	0.4	1.4	12.2	0.4	13.4	20.2	0.3	0.0	99.2	41.4	38.1	19.4	1.1	66.2
PT182_m5	BP	51.8	0.3	1.0	24.4	0.8	20.4	1.5	0.0	0.0	100.2	3.2	57.9	38.8	0.1	59.9
PT182_m1	BP	51.0	0.6	2.1	10.6	0.4	16.1	18.1	0.2	0.0	99.2	36.9	45.7	16.8	0.6	73.0
PT182_m2	BP	51.4	0.5	2.0	9.1	0.2	15.9	19.6	0.2	0.0	98.8	39.8	45.1	14.4	0.7	75.8
PT182_m3	BP	51.2	0.3	1.4	11.7	0.5	14.0	20.1	0.3	0.0	99.5	40.7	39.5	18.6	1.2	68.0
PT182_m6	BP	51.0	0.4	1.4	12.2	0.4	13.4	20.2	0.3	0.0	99.2	41.4	38.1	19.4	1.1	66.2
PT42_m1	BP	52.1	0.2	2.4	7.7	0.2	15.6	20.8	0.2	0.1	99.4	42.5	44.4	12.3	0.8	78.3
PT42_m2	BP	51.1	0.5	2.4	10.4	0.3	14.5	19.7	0.3	0.0	99.2	40.6	41.7	16.7	1.1	71.4
PT42_m5	BP	50.4	0.6	4.0	9.1	0.2	14.2	20.1	0.4	0.0	99.0	42.2	41.5	14.9	1.5	73.6
PT42_m6	BP	51.2	0.6	2.8	11.3	0.3	13.9	19.6	0.4	0.0	100.1	40.5	39.8	18.2	1.5	68.7
PT42_m7	BP	51.3	0.5	2.7	10.8	0.3	14.0	19.7	0.3	0.0	99.8	40.9	40.4	17.5	1.2	69.8
PT42_m8	BP	52.0	0.3	2.6	8.6	0.2	15.9	19.7	0.3	0.1	99.6	40.2	45.0	13.7	1.0	76.6
PT42_m9	BP	51.9	0.4	3.1	9.2	0.2	15.2	19.9	0.2	0.1	100.2	40.9	43.5	14.7	0.9	74.7
PT42_m10	BP	51.7	0.3	2.7	8.7	0.2	15.3	20.4	0.2	0.0	99.6	41.7	43.6	13.9	0.8	75.8
PT42_m11	BP	51.9	0.4	3.0	7.0	0.2	15.9	21.1	0.3	0.2	99.9	42.9	44.8	11.0	1.3	80.3
PT42_m12	BP	51.8	0.3	3.2	7.2	0.2	15.7	21.0	0.3	0.1	99.9	43.0	44.6	11.4	1.0	79.6
PT42_m13	BP	52.2	0.3	2.7	6.5	0.1	16.1	21.3	0.3	0.3	99.7	43.3	45.4	10.3	1.0	81.5
PT42_m14	BP	50.2	0.4	4.4	8.2	0.2	14.6	21.0	0.2	0.1	99.1	43.7	42.2	13.3	0.8	76.0
PT42_m15	BP	52.7	0.2	2.4	6.3	0.2	16.4	21.2	0.2	0.2	99.8	43.0	46.3	10.1	0.6	82.2

PT42_m16	BP	50.8	0.6	3.0	10.9	0.3	14.0	19.9	0.4	0.0	99.8	41.1	40.0	17.5	1.5	69.6
PT42_m17	BP	52.0	0.4	2.2	10.2	0.3	14.7	20.0	0.3	0.0	100.0	40.8	41.7	16.3	1.1	71.9
PT42_m18	BP	49.2	0.5	4.2	8.3	0.2	14.9	21.0	0.2	0.1	98.5	43.2	42.7	13.3	0.9	76.3
PT42_m19	BP	49.4	0.4	4.3	8.0	0.2	14.7	21.1	0.3	0.1	98.5	43.7	42.4	12.8	1.0	76.8
PT42_m20	BP	49.7	0.4	4.4	8.3	0.1	14.8	21.1	0.3	0.0	99.0	43.2	42.2	13.3	1.3	76.0
PT42_m21	BP	49.9	0.5	4.4	8.1	0.1	14.5	21.2	0.3	0.0	99.1	44.0	41.8	13.2	1.0	76.1
PT42_m1	BP	52.1	0.2	2.4	7.7	0.2	15.6	20.8	0.2	0.1	99.4	42.5	44.4	12.3	0.8	78.3
PT42_m2	BP	51.1	0.5	2.4	10.4	0.3	14.5	19.7	0.3	0.0	99.2	40.6	41.7	16.7	1.1	71.4
PT42_m5	BP	50.4	0.6	4.0	9.1	0.2	14.2	20.1	0.4	0.0	99.0	42.2	41.5	14.9	1.5	73.6
PT42_m6	BP	51.2	0.6	2.8	11.3	0.3	13.9	19.6	0.4	0.0	100.1	40.5	39.8	18.2	1.5	68.7
PT42_m7	BP	51.3	0.5	2.7	10.8	0.3	14.0	19.7	0.3	0.0	99.8	40.9	40.4	17.5	1.2	69.8
PT42_m8	BP	52.0	0.3	2.6	8.6	0.2	15.9	19.7	0.3	0.1	99.6	40.2	45.0	13.7	1.0	76.6
PT42_m9	BP	51.9	0.4	3.1	9.2	0.2	15.2	19.9	0.2	0.1	100.2	40.9	43.5	14.7	0.9	74.7
PT42_m10	BP	51.7	0.3	2.7	8.7	0.2	15.3	20.4	0.2	0.0	99.6	41.7	43.6	13.9	0.8	75.8
PT42_m11	BP	51.9	0.4	3.0	7.0	0.2	15.9	21.1	0.3	0.2	99.9	42.9	44.8	11.0	1.3	80.3
PT42_m12	BP	51.8	0.3	3.2	7.2	0.2	15.7	21.0	0.3	0.1	99.9	43.0	44.6	11.4	1.0	79.6
PT42_m13	BP	52.2	0.3	2.7	6.5	0.1	16.1	21.3	0.3	0.3	99.7	43.3	45.4	10.3	1.0	81.5
PT42_m14	BP	50.2	0.4	4.4	8.2	0.2	14.6	21.0	0.2	0.1	99.1	43.7	42.2	13.3	0.8	76.0
PT42_m15	BP	52.7	0.2	2.4	6.3	0.2	16.4	21.2	0.2	0.2	99.8	43.0	46.3	10.1	0.6	82.2
PT42_m16	BP	50.8	0.6	3.0	10.9	0.3	14.0	19.9	0.4	0.0	99.8	41.1	40.0	17.5	1.5	69.6
PT42_m17	BP	52.0	0.4	2.2	10.2	0.3	14.7	20.0	0.3	0.0	100.0	40.8	41.7	16.3	1.1	71.9
PT42_m18	BP	49.2	0.5	4.2	8.3	0.2	14.9	21.0	0.2	0.1	98.5	43.2	42.7	13.3	0.9	76.3
PT42_m19	BP	49.4	0.4	4.3	8.0	0.2	14.7	21.1	0.3	0.1	98.5	43.7	42.4	12.8	1.0	76.8
PT42_m20	BP	49.7	0.4	4.4	8.3	0.1	14.8	21.1	0.3	0.0	99.0	43.2	42.2	13.3	1.3	76.0
PT42_m21	BP	49.9	0.5	4.4	8.1	0.1	14.5	21.2	0.3	0.0	99.1	44.0	41.8	13.2	1.0	76.1
PT15_m1	BP	51.9	1.1	1.0	17.8	0.3	17.4	10.6	0.3	0.0	100.4	21.5	49.3	28.2	1.0	63.6
PT100_m1	BP	51.8	0.1	1.8	11.4	0.4	14.1	19.7	0.3	0.0	99.5	40.4	40.4	18.3	0.9	68.9
PT100_m2	BP	51.2	0.3	1.8	11.2	0.3	13.7	20.3	0.2	0.1	99.2	41.8	39.3	18.1	0.8	68.5
PT100_m3	BP	51.5	0.5	1.7	11.7	0.4	13.9	19.8	0.3	0.0	99.7	40.6	39.7	18.7	1.0	67.9
PT100_m5	BP	51.1	0.6	2.8	9.8	0.3	14.8	20.3	0.3	0.1	100.1	41.5	41.9	15.7	1.0	72.8
PT100_3	BP	51.9	0.4	1.4	12.2	0.4	13.5	19.8	0.2	0.1	99.8	40.9	38.6	19.7	0.8	66.3
PT100_4	BP	50.8	0.5	2.5	11.6	0.4	13.4	19.8	0.2	0.2	99.5	41.2	39.0	18.9	0.9	67.3
PT100_9	BP	52.2	0.6	2.5	10.0	0.3	15.1	20.2	0.2	0.1	101.1	41.0	42.5	15.8	0.7	73.0
PT100_10	BP	51.4	0.7	2.9	10.8	0.3	15.0	19.7	0.2	0.0	101.1	40.0	42.2	17.1	0.8	71.2
PT100_14	BP	51.4	0.6	2.3	9.7	0.3	14.9	20.2	0.2	0.1	99.8	41.4	42.3	15.5	0.9	73.2
PT100_m1	BP	51.8	0.1	1.8	11.4	0.4	14.1	19.7	0.3	0.0	99.5	40.4	40.4	18.3	0.9	68.9
PT100_m2	BP	51.2	0.3	1.8	11.2	0.3	13.7	20.3	0.2	0.1	99.2	41.8	39.3	18.1	0.8	68.5
PT100_m3	BP	51.5	0.5	1.7	11.7	0.4	13.9	19.8	0.3	0.0	99.7	40.6	39.7	18.7	1.0	67.9
PT100_m5	BP	51.1	0.6	2.8	9.8	0.3	14.8	20.3	0.3	0.1	100.1	41.5	41.9	15.7	1.0	72.8
PT100_3	BP	51.9	0.4	1.4	12.2	0.4	13.5	19.8	0.2	0.1	99.8	40.9	38.6	19.7	0.8	66.3

PT100_4	BP	50.8	0.5	2.5	11.6	0.4	13.4	19.8	0.2	0.2	99.5	41.2	39.0	18.9	0.9	67.3
PT100_9	BP	52.2	0.6	2.5	10.0	0.3	15.1	20.2	0.2	0.1	101.1	41.0	42.5	15.8	0.7	73.0
PT100_10	BP	51.4	0.7	2.9	10.8	0.3	15.0	19.7	0.2	0.0	101.1	40.0	42.2	17.1	0.8	71.2
PT100_14	BP	51.4	0.6	2.3	9.7	0.3	14.9	20.2	0.2	0.1	99.8	41.4	42.3	15.5	0.9	73.2
PT24_m1	BP	51.5	0.3	1.4	10.6	0.3	14.0	20.9	0.3	0.0	99.4	42.4	39.6	16.8	1.2	70.2
PT24_m2	BP	51.6	0.3	0.9	25.0	0.6	19.7	1.6	0.1	0.0	99.7	3.2	56.3	40.2	0.2	58.3
PT24_m4	BP	51.4	0.1	0.7	26.5	0.6	19.2	1.1	0.0	0.0	99.8	2.3	55.1	42.5	0.1	56.4
PT24_m1	BP	51.5	0.3	1.4	10.6	0.3	14.0	20.9	0.3	0.0	99.4	42.4	39.6	16.8	1.2	70.2
PT24_m2	BP	51.6	0.3	0.9	25.0	0.6	19.7	1.6	0.1	0.0	99.7	3.2	56.3	40.2	0.2	58.3
PT24_m4	BP	51.4	0.1	0.7	26.5	0.6	19.2	1.1	0.0	0.0	99.8	2.3	55.1	42.5	0.1	56.4
PTvj005_2	CB	55.5	0.1	1.1	11.4	0.3	29.6	2.3	0.0	0.1	100.5	4.4	78.5	17.0	0.1	82.2
PTvj005_10	CB	55.9	0.1	1.1	10.3	0.2	30.6	2.4	0.0	0.2	100.8	4.5	80.2	15.2	0.2	84.1
PTvj005_20	CB	56.0	0.1	0.9	10.1	0.2	30.7	2.4	0.0	0.1	100.6	4.5	80.6	14.9	0.0	84.4
PTvj005_26	CB	56.0	0.1	1.0	9.4	0.2	30.8	2.3	0.0	0.2	100.1	4.3	81.6	14.0	0.1	85.4
PTvj005_34	CB	54.1	0.6	1.1	13.8	0.3	27.9	2.0	0.1	0.0	99.7	3.8	75.2	20.8	0.2	78.3
PTvj005_5	CB	52.9	0.4	1.8	6.0	0.2	18.4	19.5	0.1	0.0	99.3	38.9	51.2	9.4	0.5	84.5
PTvj005_21	CB	53.5	0.2	1.5	6.9	0.2	20.1	16.9	0.3	0.2	99.7	33.3	55.2	10.6	0.9	83.9
PT 39	BP	52.4	0.3	1.7	9.2	0.4	14.9	21.3	0.3		100.4	42.8	41.8	14.4	1.0	74.3
PT 39	BP	50.8	0.6	2.9	10.9	0.5	13.7	19.8	0.3		99.3	41.5	39.7	17.7	1.1	69.1
PT 39	BP	52.5	0.1	1.5	20.0	0.4	23.3	1.4	0.0	0.1	99.4	2.8	65.5	31.5	0.1	67.5
PT 39	BP	52.3	0.2	1.8	20.4	0.6	23.0	1.4	0.1		99.7	2.8	64.8	32.2	0.2	66.8
PT 39	BP	52.4	0.2	1.4	19.4	0.6	24.2	1.2	0.0	0.0	99.4	2.3	67.2	30.4	0.1	68.9
PT 39	BP	51.7	0.2	3.1	20.4	0.6	22.9	1.3	0.0		100.2	2.6	64.9	32.4	0.0	66.7
PT 39	BP	54.0	0.2	0.8	18.9	0.7	24.5	1.4			100.5	2.8	67.8	29.3	0.0	69.8
PT 39	BP	53.8	0.2	0.7	18.4	0.6	24.9	1.4	0.0		99.9	2.7	68.6	28.5	0.1	70.6
PT 39	BP	53.9	0.2	0.6	19.3	0.7	24.2	1.6	0.0		100.4	3.2	66.8	29.9	0.1	69.0
PT 40	BP	51.1	0.5	2.1	11.3	0.3	13.8	20.0	0.2	0.0	99.3	41.4	39.6	18.2	0.8	68.6
PT 40	BP	51.4	0.5	1.9	11.3	0.4	13.5	20.4	0.3		99.6	42.0	38.7	18.1	1.2	68.1
PT 40	BP	52.2	0.2	1.1	22.9	0.7	21.2	1.5			99.7	3.0	60.4	36.6	0.0	62.3
PT 40	BP	52.2	0.2	0.9	22.8	0.7	21.6	1.4	0.0		99.9	2.8	61.0	36.1	0.1	62.8
PT 40	BP	51.7	0.2	1.3	22.8	0.5	21.3	1.4	0.0	0.1	99.4	2.9	60.7	36.4	0.0	62.5
PT 40	BP	51.7	0.2	1.0	23.2	0.6	21.7	1.3	0.0		99.7	2.7	60.9	36.4	0.0	62.6
PT 40	BP	54.0	0.2	0.9	16.8	0.4	25.9	1.7	0.0		100.0	3.4	70.8	25.8	0.0	73.3
PT 40	BP	52.6	0.2	2.0	16.6	0.4	25.8	1.4	0.0	0.1	99.1	2.8	71.4	25.8	0.0	73.5
PT 40	BP	51.8	0.2	1.0	22.1	0.6	21.7	1.3	0.0		98.8	2.6	61.9	35.4	0.1	63.6
PT 40	BP	51.9	0.2	1.2	21.4	0.6	22.3	1.4	0.0		99.0	2.9	63.0	33.9	0.1	65.0
PT 40	BP	52.5	0.3	1.5	20.0	0.6	22.7	1.6	0.0		99.2	3.3	64.6	32.0	0.1	66.9
PT 43	BP	50.3	0.5	2.6	14.3	0.3	12.9	18.2	0.4		99.6	37.9	37.4	23.3	1.4	61.6
PT 43	BP	50.3	0.6	2.6	14.2	0.3	12.9	18.3	0.4	0.0	99.5	38.0	37.3	23.1	1.5	61.7
PT 43	BP	51.8	0.4	1.8	11.1	0.3	13.8	20.2	0.3	0.1	99.6	41.6	39.4	17.9	1.0	68.8

PT 43	BP	52.1	0.5	2.1	8.1	0.2	15.8	20.1	0.2	0.0	99.2	41.2	45.1	13.0	0.7	77.6
PT 43	BP	49.6	0.7	4.5	9.4	0.3	14.7	19.8	0.2	0.1	99.1	41.3	42.7	15.3	0.7	73.6
PT 43	BP	52.8	0.2	1.5	19.6	0.5	23.6	1.5	0.0	0.0	99.7	3.0	66.1	30.8	0.1	68.2
PT 43	BP	51.3	0.3	1.7	23.1	0.6	20.7	1.5			99.2	3.2	59.5	37.3	0.0	61.5
PT 43	BP	53.4	0.1	1.4	19.0	0.5	24.2	1.6	0.0	0.0	100.1	3.2	67.2	29.5	0.1	69.5
PT 43	BP	53.0	0.2	1.5	18.9	0.4	23.8	1.7	0.0	0.0	99.7	3.3	66.7	29.8	0.1	69.2
PT 43	BP	51.9	0.3	1.8	20.1	0.4	22.7	1.8		0.1	98.9	3.6	64.4	32.0	0.0	66.8
PT 101	BP	54.4	0.1	2.6	12.5	0.3	28.5	1.7	0.0	0.2	100.3	3.2	77.6	19.1	0.1	80.3
PT 101	BP	53.8	0.2	3.1	13.2	0.3	28.2	1.7	0.0	0.3	100.7	3.4	76.4	20.1	0.1	79.1
PT 101	BP	51.9	0.2	0.7	23.9	0.4	20.6	1.3	0.0		99.0	2.7	58.9	38.4	0.0	60.5
PT 101	BP	52.3	0.2	0.6	24.1	0.5	20.2	1.3		0.0	99.4	2.7	58.3	39.0	0.0	59.9
PT 101	BP	55.3	0.1	1.7	10.4	0.2	31.3	1.5	0.0	0.4	100.9	2.8	81.8	15.3	0.1	84.3
PT 101	BP	52.2	0.3	2.2	22.8	0.4	19.9	1.9	0.2	0.0	100.0	4.0	58.0	37.4	0.6	60.8
PT 115	BP	51.9	0.4	1.4	10.3	0.2	14.0	20.4	0.2	0.2	99.0	42.2	40.3	16.7	0.8	70.7
PT 115	BP	50.4	0.7	2.4	11.1	0.2	13.1	19.8	0.3	0.6	98.5	42.1	38.5	18.4	1.0	67.7
PT 115	BP	55.1	0.1	2.1	10.3	0.2	30.4	1.3	0.0	0.6	100.1	2.5	81.9	15.6	0.1	84.0
PT 115	BP	55.7	0.1	2.0	10.1	0.1	30.5	1.6	0.0	0.4	100.4	3.0	81.7	15.2	0.1	84.3
PT 115	BP	51.8	0.2	3.0	18.5	0.3	23.9	1.3	0.0	0.1	99.1	2.7	67.8	29.4	0.1	69.7
PT 115	BP	55.7	0.1	1.7	8.8	0.2	31.7	1.4	0.0	0.5	100.1	2.7	84.1	13.1	0.0	86.5
PT 115	BP	55.4	0.1	2.0	9.3	0.2	31.2	1.9	0.1	0.6	100.7	3.5	82.5	13.8	0.2	85.7
PT 115	BP	52.5	0.2	0.5	24.5	0.5	20.5	1.4			100.3	2.9	58.1	39.0	0.0	59.9
PT 84	BP	51.6	0.5	2.0	9.6	0.4	14.6	20.8	0.2		99.8	42.5	41.3	15.3	0.9	73.0
PT 84	BP	51.3	0.5	2.2	11.0	0.4	14.2	20.7	0.2		100.6	41.9	40.0	17.3	0.7	69.8
PT 84	BP	51.7	0.5	1.7	10.2	0.4	14.7	20.5	0.2		99.8	41.6	41.5	16.2	0.7	71.9
PT 84	BP	51.8	0.4	1.7	10.5	0.5	14.6	20.2	0.2		100.1	41.1	41.4	16.7	0.8	71.2
PT 84	BP	51.6	0.2	0.4	14.9	0.5	11.0	20.4	0.3	0.0	99.3	42.6	32.0	24.3	1.0	56.8
PT 14	BP	50.8	1.3	3.3	7.6	0.1	14.8	21.5	0.4	0.2	100.0	44.1	42.3	12.2	1.4	77.6
PT 14	BP	49.4	1.7	3.7	8.7	0.2	14.0	20.8	0.4	0.1	99.1	43.5	40.8	14.2	1.6	74.2
PT 14	BP	50.7	1.6	2.9	8.5	0.2	14.1	21.7	0.5		100.2	44.5	40.3	13.5	1.7	74.9
PT 14	BP	50.3	1.6	3.3	8.5	0.2	14.3	22.0	0.4	0.0	100.4	44.6	40.4	13.4	1.5	75.1
PT 14	BP	46.4	2.3	6.2	8.0	0.1	13.0	22.1	0.5		98.6	46.8	38.1	13.3	1.8	74.2
PT 150	BP	51.9	0.6	2.2	11.0	0.3	13.9	20.9	0.2	0.0	100.9	42.4	39.3	17.4	0.9	69.3
PT 150	BP	52.3	0.3	1.2	12.1	0.4	13.8	21.0	0.2		101.5	41.9	38.3	18.9	0.9	67.0
PT 150	BP	52.6	0.5	1.7	12.3	0.4	13.6	20.9	0.2		102.2	42.0	37.9	19.2	0.9	66.4
PT 150	BP	51.7	0.4	1.3	12.1	0.4	13.4	20.6	0.2	0.1	100.3	42.0	38.0	19.2	0.9	66.4
PT 151	BP	51.5	0.5	2.0	12.0	0.3	13.4	20.4	0.3		100.4	41.6	38.0	19.2	1.1	66.5
PT 151	BP	51.9	0.6	2.1	10.1	0.3	15.7	19.4	0.2		100.3	39.2	44.1	15.9	0.7	73.5
PT 151	BP	51.0	0.3	1.8	24.2	0.7	19.8	1.7	0.0		99.5	3.6	57.1	39.2	0.1	59.3
PT 153	BP	52.1	0.3	1.2	14.4	0.5	12.5	20.2	0.3	0.0	101.4	40.9	35.3	22.9	0.9	60.7
PT 153	BP	51.5	0.5	1.9	12.1	0.4	13.6	20.9	0.3		101.2	42.0	38.0	19.0	0.9	66.7

PT 153	BP	52.4	0.2	0.9	24.7	0.8	20.4	1.5	0.0		100.9	3.1	57.6	39.1	0.1	59.6
PT 153	BP	52.8	0.2	0.7	24.5	0.7	20.8	1.5	0.0	0.0	101.2	3.1	58.3	38.5	0.1	60.2
PT 153	BP	51.5	0.3	0.7	26.5	0.8	18.8	1.6			100.2	3.3	54.0	42.7	0.0	55.9
PT 180	BP	52.6	0.6	2.3	9.8	0.4	15.7	20.6	0.2	0.0	102.2	40.8	43.3	15.2	0.8	74.1
PT 180	BP	49.2	1.0	4.9	8.6	0.2	14.3	21.8	0.2	0.1	100.5	44.7	40.7	13.7	0.9	74.7
PT 180	BP	49.6	1.0	4.1	9.9	0.2	14.7	21.7	0.2	0.1	101.6	43.2	40.5	15.4	0.8	72.4
PT 180	BP	47.7	1.2	5.0	9.0	0.2	13.8	21.5	0.2		98.7	44.7	39.9	14.6	0.9	73.3
PT 180	BP	46.4	2.1	5.6	11.3	0.5	12.7	20.3	0.3		99.1	43.0	37.4	18.6	1.0	66.8
PT 183	BP	52.3	0.4	1.8	10.7	0.3	14.9	20.5	0.2	0.0	101.1	41.0	41.4	16.8	0.8	71.2
PT 183	BP	51.9	0.5	1.7	10.9	0.4	14.4	20.3	0.2	0.0	100.2	41.4	40.7	17.3	0.7	70.2
PT 183	BP	51.9	0.4	1.6	11.1	0.4	14.3	20.5	0.2	0.0	100.5	41.5	40.2	17.5	0.7	69.7
PTvj004_1	LP	51.5	0.5	1.7	10.4	0.3	15.2	19.4	0.3	0.0	99.3	39.5	42.9	16.5	1.2	72.2
PTvj004_2	LP	50.4	0.7	2.3	10.6	0.3	14.8	19.9	0.3	0.0	99.4	40.4	41.6	16.7	1.2	71.3
PTvj004_8	LP	51.0	0.7	2.2	10.7	0.3	15.0	19.1	0.3	0.0	99.3	39.0	42.7	17.1	1.1	71.4
PTvj004_9	LP	51.3	0.6	1.8	10.8	0.5	14.7	19.4	0.3	0.0	99.5	39.8	41.8	17.3	1.2	70.7
PTvj004_11	LP	51.0	0.7	2.1	11.0	0.4	15.0	19.2	0.4	0.0	99.8	38.9	42.4	17.4	1.3	70.9
PTvj004_12	LP	51.2	0.8	2.3	10.4	0.4	15.1	19.3	0.4	0.0	99.9	39.2	42.8	16.6	1.4	72.1
PTvj004_13	LP	50.9	0.6	2.1	11.1	0.4	14.9	19.3	0.4	0.0	99.7	39.1	41.9	17.6	1.3	70.4
PTvj004_16	LP	50.8	0.8	2.3	10.8	0.4	14.6	19.8	0.4	0.0	99.9	40.2	41.2	17.1	1.5	70.7
PTvj004_17	LP	51.2	0.6	2.0	10.4	0.4	15.1	19.3	0.3	0.0	99.2	39.4	42.9	16.6	1.1	72.1
PTvj004_18	LP	50.9	0.6	2.1	10.7	0.3	14.9	19.7	0.3	0.0	99.6	39.8	42.1	16.8	1.2	71.4
PTvj004_19	LP	51.4	0.5	1.9	9.8	0.4	15.3	19.6	0.3	0.0	99.3	39.9	43.5	15.5	1.1	73.7
PTvj004_20	LP	50.7	0.7	2.4	9.9	0.3	15.2	19.5	0.3	0.0	99.0	39.9	43.1	15.8	1.1	73.2
PTvj004_21	LP	51.1	0.8	1.5	13.7	0.5	14.6	16.8	0.3	0.0	99.3	34.8	42.0	22.2	1.0	65.4
PT vj 033_1	CA	53.6	0.3	1.5	14.7	0.4	27.6	1.8	0.0	0.2	100.1	3.5	74.3	22.1	0.1	77.0
PT vj 033_2	CA	53.5	0.2	1.1	15.8	0.3	26.3	1.7	0.0	0.0	98.9	3.4	72.1	24.3	0.2	74.8
PT vj 033_3	CA	53.4	0.3	1.4	14.9	0.3	26.9	1.7	0.0	0.1	99.2	3.4	73.7	22.9	0.1	76.3
PT vj 033_9	CA	53.3	0.3	1.4	15.5	0.4	26.9	1.8	0.0	0.1	99.8	3.4	72.9	23.6	0.1	75.6
PT vj 033_10	CA	53.7	0.4	1.0	15.5	0.3	26.8	1.9	0.0	0.0	99.6	3.6	72.7	23.5	0.1	75.5
PT vj 033_11	CA	53.4	0.3	1.4	15.9	0.4	27.0	1.8	0.0	0.1	100.3	3.4	72.6	24.0	0.0	75.2
PT vj 033_13	CA	53.4	0.3	1.2	16.5	0.3	26.5	1.8	0.0	0.0	100.1	3.5	71.5	24.9	0.0	74.2
PT vj 033_14	CA	53.1	0.4	1.3	16.3	0.3	26.6	1.8	0.0	0.0	99.9	3.6	71.7	24.6	0.1	74.4
PT vj 033_19	CA	53.8	0.3	1.3	16.5	0.4	26.2	1.8	0.1	0.0	100.4	3.5	71.1	25.2	0.2	73.9
PT vj 033_20	CA	53.4	0.3	1.5	16.0	0.4	26.8	1.8	0.1	0.1	100.3	3.5	72.2	24.1	0.3	75.0
PT vj 033_21	CA	52.9	0.5	0.9	19.6	0.5	23.8	2.1	0.0	0.0	100.4	4.1	65.5	30.2	0.2	68.4
PT vj 033_22	CA	52.7	0.4	0.8	19.9	0.4	23.5	2.6	0.0	0.0	100.3	5.2	64.3	30.5	0.0	67.9
patvj024_4	CA	50.3	0.6	4.6	7.8	0.2	16.2	19.2	0.3	0.5	99.7	39.7	46.6	12.6	1.1	78.7
patvj024_2	CA	54.2	0.2	2.0	12.7	0.3	28.6	1.5	0.1	0.3	99.9	3.0	77.4	19.3	0.2	80.0

Mg# (Mg# [100*Mg/(Mg+Fe)]).

Tabla 7 . Major elements composition of plagioclase cores from Cresta de los Bosques (CB); Cañadon Asfalto (CA); Bajo Pobre (BP) and Chon Aike (C:Aike) Formation.

Sample	Formation	SiO_2 wt.%	TiO_2 wt.%	Al_2O_3 wt.%	FeO wt.%	CaO wt.%	Na_2O wt.%	K_2O wt.%	TOTAL	An	Ab	Or	#Ca
PTvj005_7	CB	45.8	0.03	33.8	0.49	18.1	1.33	0.08	99.6	87.9	11.7	0.46	93.8
PTvj005_19	CB	45.8	0.00	34.0	0.32	18.0	1.23	0.07	99.4	88.6	11.0	0.38	94.2
PTvj005_6	CB	46.6	0.01	33.5	0.29	17.2	1.74	0.09	99.4	84.1	15.4	0.53	91.6
PTvj005_13	CB	46.7	0.07	33.3	0.26	17.0	1.77	0.12	99.1	83.6	15.7	0.69	91.4
PTvj005_16	CB	45.8	0.03	33.6	0.24	17.7	1.40	0.10	98.9	87.0	12.4	0.58	93.3
PTvj005_22	CB	45.8	0.06	33.7	0.38	17.8	1.22	0.10	99.0	88.5	11.0	0.57	94.2
PTvj005_23	CB	45.4	0.0	34.3	0.34	17.9	1.38	0.06	99.4	87.5	12.2	0.35	93.5
PT vj 033_4	CA	54.1	0.1	27.0	1.52	10.6	5.44	0.49	99.2	50.5	46.7	2.79	68.4
PT vj 033_7	CA	50.5	0.1	29.9	0.67	13.8	3.70	0.23	98.8	66.4	32.3	1.30	80.4
PT vj 033_8	CA	65.6	0.6	18.2	1.67	2.1	5.78	4.12	98.0	11.9	60.0	28.2	28.3
PT vj033_12	CA	67.2	0.5	17.6	1.50	2.5	5.68	3.68	98.7	14.4	60.0	25.6	32.5
PT vj033_16	CA	50.7	0.1	30.1	0.79	13.6	3.82	0.25	99.3	65.3	33.3	1.41	79.7
PT vj033_17	CA	52.1	0.0	29.1	0.75	12.7	4.62	0.30	99.5	59.2	39.1	1.69	75.2
PT vj033_18	CA	50.1	0.0	29.6	1.64	13.6	3.37	0.23	98.5	68.0	30.6	1.39	81.7
PT vj033_23	CA	51.6	0.05	29.2	0.78	13.0	3.97	0.28	98.8	63.4	35.0	1.62	78.3
PT vj033_24	CA	50.1	0.06	30.3	0.95	14.2	3.26	0.23	99.1	69.6	29.0	1.35	82.7
PT vj033_25	CA	56.1	0.08	26.4	0.78	9.37	5.93	0.59	99.3	45.0	51.6	3.39	63.6
PT24_m3	BP	46.4	0.03	35.1	0.63	17.2	1.64	0.09	101.1	84.8	14.6	0.54	92.1
PT42_m3	BP	49.2	0.00	32.6	0.87	15.0	3.03	0.08	100.8	72.9	26.7	0.4	84.5
PT100_1	BP	67.4	0.04	19.9	0.12	0.35	12.3	0.06	100.2	1.53	98.2	0.30	3.03
PT100_17	BP	67.8	0.01	19.9	0.06	0.34	12.3	0.06	100.4	1.52	98.2	0.32	3.01
PT100_18	BP	47.4	0.07	32.6	0.57	16.5	2.09	0.07	99.3	81.0	18.6	0.42	89.7
PT100_20	BP	46.4	0.03	33.2	0.50	17.0	1.93	0.06	99.1	82.7	17.0	0.35	90.7
PT100_21	BP	66.8	0.01	20.1	0.07	0.8	11.7	0.05	99.6	3.5	96.2	0.28	6.8
PT100_22	BP	46.8	0.04	33.1	0.52	16.4	2.37	0.08	99.3	78.9	20.6	0.45	88.5
PT100_m6	BP	47.9	0.02	33.6	0.71	16.3	2.18	0.06	100.7	80.3	19.4	0.33	89.2
PT100_11	BP	46.5	0.03	33.4	0.50	17.4	1.74	0.04	99.6	84.5	15.3	0.24	91.7
PT 39	BP	46.5		34.3	0.51	17.5	1.54	0.04	100.4	86.0	13.7	0.23	92.6
PT 39	BP	51.4	0.02	30.6	0.48	13.3	3.85	0.17	99.8	64.9	34.1	0.99	79.2
PT 39	BP	50.9	0.04	30.8	0.51	13.5	3.71	0.11	99.6	66.4	33.0	0.64	80.1
PT 39	BP	47.9		33.0	0.54	16.1	2.28	0.07	99.9	79.2	20.4	0.41	88.6
PT 40	BP	48.7		32.6	0.49	15.5	2.55	0.17	100.0	76.3	22.7	1.00	87.1
PT 40	BP	47.0	0.05	33.6	0.57	16.7	1.88	0.06	99.8	82.8	16.8	0.35	90.8
PT 40	BP	47.7		33.4	0.71	16.4	2.11	0.07	100.4	80.8	18.8	0.41	89.6
PT 40	BP	47.5	0.04	33.5	0.60	16.6	2.04	0.05	100.3	81.5	18.2	0.29	90.0
PT 40	BP	48.5		32.8	0.73	15.7	2.48	0.10	100.3	77.3	22.1	0.59	87.5

PT 43	BP	46.0	0.01	34.4	0.55	17.7	1.39	0.02	100.1	87.4	12.4	0.12	93.4
PT 43	BP	51.2	0.04	30.8	0.68	13.5	3.71	0.20	100.2	66.0	32.8	1.16	80.1
PT 43	BP	51.7	0.05	30.2	0.72	12.8	4.01	0.22	99.7	63.1	35.6	1.29	78.0
PT 43	BP	47.8	0.02	32.9	0.74	16.0	2.24	0.11	99.9	79.3	20.1	0.65	88.8
PT 43	BP	52.2	0.08	29.9	0.83	12.5	4.23	0.24	100.0	61.1	37.5	1.40	76.5
PT 101	BP	52.0	0.08	30.6	0.42	13.1	3.92	0.31	100.3	63.7	34.5	1.80	78.7
PT 101	BP	53.1		29.8	0.3	12.2	4.4	0.4	100.2	59.2	38.6	2.1	75.4
PT 101	BP	51.1	0.05	31.1	0.41	13.7	3.56	0.26	100.3	67.1	31.4	1.51	81.0
PT 101	BP	50.8	0.06	31.1	0.32	13.8	3.49	0.23	99.8	67.7	30.9	1.34	81.4
PT 101	BP	48.5		32.7	0.36	15.7	2.49	0.09	99.8	77.3	22.2	0.53	87.5
PT 115	BP	50.8	0.0	31.3	0.42	14.0	3.42	0.25	100.1	68.3	30.3	1.46	81.9
PT 115	BP	53.2	0.1	29.8	0.45	12.2	4.43	0.37	100.4	59.0	38.9	2.14	75.2
PT 115	BP	49.9	0.0	32.1	0.48	14.8	3.00	0.19	100.5	72.4	26.5	1.11	84.5
PT 115	BP	52.6		30.2	0.36	12.7	4.18	0.32	100.4	61.4	36.7	1.85	77.0
PT 115	BP	49.0	0.03	32.3	0.43	15.2	2.70	0.19	100.0	74.9	24.0	1.11	86.2
PT 30	BP	55.8		27.7	0.23	9.9	5.69	0.43	99.7	47.7	49.8	2.48	65.7
PT 30	BP	55.3		27.9	0.41	10.1	5.51	0.39	99.6	49.3	48.5	2.26	67.0
PT 30	BP	55.2		28.1	0.30	10.3	5.51	0.29	99.7	49.9	48.4	1.68	67.4
PT 30	BP	54.9		28.3	0.30	10.5	5.25	0.50	99.8	51.0	46.1	2.89	68.9
PT 84	BP	42.9	0.01	36.4	0.39	19.3	0.75	0.04	99.7	93.2	6.6	0.23	96.6
PT 84	BP	43.0		36.5	0.51	19.5	0.59	0.03	100.1	94.6	5.2	0.17	97.3
PT 84	BP	52.5	0.06	30.0	0.77	12.5	4.29	0.18	100.3	61.1	37.9	1.05	76.3
PT 150	BP	53.7	0.02	29.3	0.33	11.6	4.72	0.35	100.0	56.5	41.5	2.00	73.1
PT 150	BP	51.7	0.06	30.2	0.49	12.9	4.00	0.24	99.6	63.1	35.5	1.42	78.1
PT 150	BP	53.0	0.01	29.7	0.4	12.1	4.42	0.35	100.0	59.1	38.9	2.01	75.2
PT 150	BP	52.2	0.01	30.2	0.39	12.8	4.04	0.36	100.0	62.2	35.7	2.09	77.7
PT 151	BP	53.9	0.04	28.7	0.42	11.1	4.90	0.43	99.5	54.2	43.3	2.51	71.5
PT 151	BP	54.9	0.02	28.4	0.41	10.6	5.21	0.48	100.0	51.5	45.7	2.77	69.3
PT 151	BP	50.8	0.01	31.2	0.51	13.9	3.49	0.22	100.0	67.8	30.9	1.29	81.4
PT 151	BP	50.7	0.05	31.3	0.44	14.0	3.41	0.24	100.0	68.4	30.2	1.38	81.9
PT 151	BP	48.2	0.02	32.8	0.64	15.8	2.38	0.15	100.0	77.9	21.2	0.85	88.0
PT 153	BP	49.1	0.02	32.3	0.46	15.2	2.75	0.17	100.0	74.6	24.4	1.01	85.9
PT 153	BP	50.5	0.02	31.7	0.50	14.4	3.25	0.22	100.5	70.0	28.7	1.30	83.0
PT 153	BP	52.8	0.00	30.2	0.35	12.6	4.25	0.28	100.5	61.1	37.3	1.60	76.6
PT 153	BP	53.2	0.05	29.5	0.42	11.9	4.55	0.33	100.0	58.0	40.1	1.89	74.3
PT 153	BP	52.5	0.07	29.9	0.59	12.4	4.29	0.27	100.0	60.5	37.9	1.58	76.2
PT 180	BP	48.5	0.02	32.4	0.86	15.4	2.54	0.19	100.0	76.2	22.7	1.09	87.0
PT 180	BP	48.9	0.02	32.5	0.90	15.4	2.61	0.18	100.5	75.7	23.2	1.06	86.7
PT 180	BP	49.6	0.05	31.9	0.96	14.8	2.94	0.23	100.5	72.5	26.1	1.34	84.7
PT 180	BP	59.6	0.00	25.6	0.18	7.2	6.88	1.11	100.5	34.3	59.4	6.31	53.6

PT 180	BP	57.2	0.00	26.9	0.25	8.8	6.05	0.81	100.0	42.6	52.8	4.65	61.7
PT 183	BP	45.0	0.00	35.5	0.43	18.8	0.80	0.02	100.5	92.7	7.14	0.13	96.3
PT 183	BP	44.5	0.02	35.5	0.35	18.9	0.66	0.03	100.0	93.9	5.93	0.16	96.9
PT 36	C. Aike	65.6		18.7	0.03	0.16	3.84	11.2	99.6	0.8	34.0	65.2	4.40
PT 36	C. Aike	63.1	0.02	22.8	0.12	4.08	8.73	0.96	99.8	19.4	75.2	5.44	34.1
PT 36	C. Aike	62.9	0.01	23.0	0.11	4.33	8.62	0.92	99.9	20.6	74.2	5.21	35.7
PT 51	C. Aike	62.4		23.4	0.10	4.72	8.35	0.98	99.9	22.5	72.0	5.56	38.5
PT 51	C. Aike	62.3		23.3	0.09	4.70	8.30	1.04	99.7	22.4	71.7	5.91	38.5
PT 51	C. Aike	62.9		22.7	0.10	4.06	8.56	1.16	99.5	19.4	74.0	6.60	34.4
PT 51	C. Aike	62.6	0.04	23.1	0.12	4.41	8.43	1.09	99.8	21.0	72.8	6.19	36.6
PT 107	C. Aike	61.7	0.02	23.9	0.16	5.34	8.02	0.96	100.2	25.4	69.1	5.44	42.4
PT 107	C. Aike	62.8		23.0	0.13	4.35	8.41	1.20	99.9	20.7	72.5	6.80	36.4
PT 107	C. Aike	65.8		18.9	0.05	0.23	4.76	9.85	99.6	1.12	41.9	57.0	5.07
PT 107	C. Aike	65.8		19.0	0.06	0.29	4.89	9.60	99.6	1.41	43.0	55.6	6.15
PT 107	C. Aike	62.2		23.3	0.15	4.66	8.37	0.94	99.6	22.3	72.4	5.3	38.1
PT 107	C. Aike	63.2		22.8	0.06	4.08	8.61	1.14	99.9	19.4	74.1	6.5	34.4
PT 107	C. Aike	65.6	0.02	18.9	0.10	0.26	4.52	10.1	99.5	1.27	39.9	58.9	5.98
PT 107	C. Aike	65.6		18.9	0.06	0.32	4.50	10.14	99.6	1.56	39.7	58.8	7.29
PT 37	C. Aike	63.0		22.9	0.08	4.14	8.62	1.06	99.8	19.7	74.3	6.0	34.7
PT 37	C. Aike	62.8	0.01	22.9	0.15	4.28	8.55	1.03	99.8	20.4	73.8	5.8	35.6
PT 37	C. Aike	65.7		18.9	0.15	0.26	4.30	10.5	99.9	1.27	37.9	60.9	6.3
PT 37	C. Aike	65.8		18.9	0.08	0.27	4.55	10.1	99.7	1.31	40.0	58.7	6.2
PT 37	C. Aike	62.4		23.1	0.15	4.48	8.48	0.9	99.6	21.4	73.3	5.29	36.9
PT 37	C. Aike	62.5		23.1	0.03	4.49	8.51	0.9	99.6	21.4	73.5	5.11	36.8
PT 37	C. Aike	65.8		19.0	0.10	0.34	4.90	9.6	99.8	1.65	43.0	55.3	7.1
PT 17	C. Aike	65.5		18.7	0.18	0.17	3.27	12.1	99.9	0.83	29.0	70.2	5.4
PT 17	C. Aike	65.5		18.8	0.16	0.21	3.42	11.8	99.9	1.03	30.2	68.7	6.4
PT 17	C. Aike	57.3		26.7	0.17	8.60	6.33	0.55	99.6	41.5	55.3	3.16	60.0
PT 17	C. Aike	57.5	0.02	26.5	0.18	8.45	6.43	0.54	99.7	40.8	56.1	3.10	59.2
PT 33	C. Aike	55.1	0.03	28.4	0.22	10.53	5.34	0.40	100.0	50.9	46.8	2.30	68.5
PT 33	C. Aike	56.7	0.01	27.5	0.17	9.50	5.95	0.45	100.3	45.7	51.8	2.58	63.8
PT 33	C. Aike	57.9		26.8	0.19	8.60	6.46	0.51	100.5	41.2	55.9	2.91	59.5
PT 33	C. Aike	57.9	0.05	26.7	0.22	8.53	6.43	0.59	100.4	40.9	55.8	3.37	59.5
PT 130	C. Aike	57.9	0.01	26.5	0.15	8.36	6.49	0.58	99.9	40.2	56.5	3.32	58.7
PT 130	C. Aike	59.0	0.01	25.7	0.16	7.44	7.00	0.62	99.9	35.7	60.8	3.54	54.0
PT 130	C. Aike	56.5	0.03	27.1	0.18	9.19	5.99	0.52	99.5	44.5	52.5	3.00	62.9
PT 130	C. Aike	57.9		26.4	0.22	8.26	6.47	0.67	99.9	39.8	56.4	3.84	58.5
PT 93	C. Aike	57.9		26.2	0.19	8.09	6.56	0.65	99.6	39.0	57.3	3.73	57.7
PT 93	C. Aike	57.9		26.2	0.24	8.09	6.66	0.49	99.6	39.0	58.2	2.82	57.3
PT 93	C. Aike	57.4	0.02	27.1	0.25	8.95	6.26	0.48	100.4	42.9	54.3	2.74	61.2

PT 93	C. Aike	57.7		26.3	0.17	8.23	6.58	0.49	99.5	39.7	57.5	2.82	58.0
PT 47	C. Aike	58.0	0.01	26.2	0.10	8.03	6.74	0.43	99.5	38.7	58.8	2.47	56.8
PT 47	C. Aike	60.3		24.6	0.07	6.25	7.59	0.72	99.5	30.0	65.9	4.11	47.6
PT 47	C. Aike	65.4	0.04	18.8	0.10	0.24	3.78	11.2	99.5	1.17	33.5	65.3	6.6
PT 47	C. Aike	65.6		18.9	0.07	0.30	4.12	10.7	99.7	1.46	36.4	62.2	7.4
PT 47	C. Aike	58.5		25.8	0.20	7.65	6.88	0.54	99.5	36.9	60.0	3.10	55.1
PT 47	C. Aike	59.8	0.01	24.9	0.19	6.56	7.44	0.66	99.6	31.5	64.7	3.78	49.4
PT 96	C. Aike	60.0	0.01	24.8	0.18	6.45	7.47	0.71	99.6	31.0	64.9	4.06	48.8
PT 96	C. Aike	60.6		24.5	0.19	6.04	7.71	0.74	99.7	28.9	66.8	4.22	46.4
PT 96	C. Aike	61.4		23.8	0.23	5.28	8.06	0.85	99.6	25.3	69.9	4.85	42.0
PT 96	C. Aike	61.0		24.2	0.20	5.73	7.96	0.64	99.7	27.4	68.9	3.65	44.3
PT 106	C. Aike	57.6	0.03	26.4	0.17	8.32	6.56	0.43	99.5	40.2	57.3	2.47	58.4
PT 106	C. Aike	61.0	0.04	24.0	0.16	5.56	7.88	0.86	99.5	26.7	68.4	4.91	43.8
PT 106	C. Aike	56.9		26.9	0.17	8.90	6.20	0.47	99.5	43.0	54.3	2.71	61.3
PT 106	C. Aike	60.9	0.0	24.3	0.15	5.80	7.82	0.79	99.7	27.8	67.7	4.50	45.0
PT 5	C. Aike	65.5		18.8	0.07	0.19	3.63	11.5	99.7	0.93	32.1	67.0	5.47
PT 5	C. Aike	65.4		18.7	0.10	0.19	3.63	11.5	99.6	0.93	32.2	66.9	5.47
PT 5	C. Aike	65.5		18.7	0.08	0.17	3.63	11.5	99.6	0.83	32.2	67.0	4.92
PT 5	C. Aike	65.4		18.7	0.16	0.18	3.67	11.4	99.6	0.88	32.5	66.6	5.14
PT 117	C. Aike	65.6		18.8	0.04	0.18	3.52	11.7	99.8	0.88	31.1	68.0	5.35
PT 117	C. Aike	65.8		18.8	0.12	0.18	4.04	11.0	100.0	0.88	35.6	63.6	4.69
PT 117	C. Aike	65.5	0.01	18.8	0.07	0.20	3.81	11.2	99.5	1.0	33.7	65.3	5.5
PT 117	C. Aike	65.6		18.8	0.05	0.16	4.04	10.9	99.5	0.8	35.7	63.5	4.2
PT 129	C. Aike	58.4		25.8	0.20	7.61	6.76	0.75	99.5	36.7	59.0	4.31	55.4
PT 129	C. Aike	58.9	0.05	25.4	0.23	7.25	6.94	0.79	99.6	34.9	60.5	4.53	53.6
PT 129	C. Aike	59.2		25.3	0.23	7.09	7.10	0.71	99.6	34.1	61.8	4.07	52.5
PT 129	C. Aike	59.4	0.04	25.6	0.21	7.27	7.07	0.71	100.3	34.8	61.2	4.04	53.2
PT 111	C. Aike	55.2		28.0	0.26	10.2	5.53	0.33	99.5	49.5	48.6	1.91	67.1
PT 111	C. Aike	57.1		27.3	0.28	9.21	6.12	0.47	100.5	44.2	53.1	2.68	62.5
PT 111	C. Aike	53.3	0.0	29.5	0.3	11.9	4.6	0.28	99.9	57.9	40.5	1.62	74.1
PT 111	C. Aike	54.6		29.0	0.33	11.2	5.07	0.28	100.5	54.1	44.3	1.61	71.0
PT 91	C. Aike	55.9	0.03	28.2	0.21	10.2	5.58	0.42	100.5	49.0	48.6	2.40	66.9
PT 91	C. Aike	58.8		26.1	0.27	7.79	6.84	0.63	100.5	37.2	59.2	3.6	55.7
PT 91	C. Aike	57.6		26.4	0.20	8.30	6.45	0.61	99.5	40.1	56.4	3.51	58.7
PT 91	C. Aike	59.0	0.03	26.0	0.20	7.68	6.93	0.60	100.5	36.7	59.9	3.41	55.1
PT 91	C. Aike	57.5		27.0	0.20	8.86	6.31	0.50	100.4	42.4	54.7	2.85	60.8
PT 91	C. Aike	58.3	0.03	26.0	0.18	7.83	6.81	0.52	99.7	37.7	59.3	2.98	56.0
PT 91	C. Aike	65.1	0.03	18.7	0.14	0.20	2.83	12.6	99.6	0.98	25.2	73.8	7.25
PT 91	C. Aike	65.1		18.7	0.09	0.21	2.71	12.8	99.6	1.03	24.1	74.9	7.89

Anorthite, An ($CaAl_2Si_2O_8$)= 100×Ca/(Ca+Na+K), Albite, Ab ($NaAlSi_3O_8$)=100×Na/(Ca+Na+K) and Orthoclase, Or ($KAlSi_3O_8$)= 100×K/(Ca+Na+K))

Table 8. Geochemistry of major elements of the Patagonia Province

Sample	Fm	Latitude	Longitude	SiO_2 wt.%	TiO_2 wt.%	Al_2O_3 wt.%	Fe_2O_3 wt.%	FeO wt.%	FeOt* wt.%	MnO wt.%	MgO wt.%	CaO wt.%	Na_2O wt.%	K_2O wt.%	P_2O_5 wt.%	L.O.I.	TOT
Patvj020	[1]CA	-42.4071	-68.8060	52.8	1.17	16.9	6.11			0.19	2.14	9.42	3.14	2.17	0.47	4.97	99.49
Patvj027	[1]CA	-43.5169	-69.1394	49.2	1.46	16.1	10.81			0.15	6.97	9.41	2.65	1.21	0.81	1.37	100.06
Patvj030	[1]CA	-43.8923	-68.3880	57.0	0.97	17.4	6.75			0.10	3.40	6.29	3.60	2.47	0.43	1.90	100.32
Patvj033	[1]CA	-43.8305	-67.8985	57.1	0.90	16.0	7.27			0.10	4.34	6.96	3.20	2.13	0.32	2.11	100.44
Patvj005	[1]CB	-47.9114	-69.2953	48.1	0.14	16.5	7.68			0.13	16.5	9.41	0.80	0.11	0.01	1.07	100.48
Patvj023	[1]LT	-47.8994	-69.7203	60.3	0.57	17.3	5.28			0.08	3.03	4.53	4.21	2.01	0.14	2.36	99.83
Pt 182	[1]BP	-47.6633	-70.1925	58.1	1.00	16.8	7.99			0.15	3.31	6.79	3.40	1.28	0.22	1.29	100.27
Pat 4	[1]BP			49.4	1.35	16.4	9.89			0.12	4.66	9.58	2.74	2.78	0.81	2.17	99.91
Geo 2	[2]BP			56.06	0.69	18.43	6.96			0.14	3.61	8.40	2.78	0.23	0.14	2.18	99.59
Geo 8	[2]BP			56.62	0.74	18.01	6.77			0.19	3.60	7.81	2.99	0.24	0.17	2.45	99.59
Pt 40	[3]BP	-47.9386	-68.5472	57.75	0.62	16.57	1.51	6.04	7.40	0.13	5.58	7.96	3.02	0.86	0.11	1.48	100.00
Pt 101	[3]BP	-48.1283	-69.8575	59.07	0.73	15.91	2.02	5.82	7.64	0.12	5.68	7.21	2.00	1.54	0.10	1.48	100.00
Pt 115-A	[3]BP	-48.1300	-69.8522	60.14	0.73	16.23	2.16	5.13	7.07	0.10	4.96	6.81	2.14	1.73	0.09	3.29	100.00
Pt 25	[3]BP	-47.9100	-69.7194	59.84	0.73	17.30	2.32	4.31	6.40	0.11	2.54	8.14	2.88	1.96	0.10	2.67	100.00
Pt 30	[3]BP	-47.8919	-69.7381	64.95	0.58	16.75	3.87	1.92	5.40	0.06	1.32	4.43	3.69	2.64	0.18	2.89	100.00
Pt 152	[3]BP	-47.6589	-70.1847	60.13	0.97	17.74	4.11	2.92	6.62	0.15	2.29	6.84	3.30	1.75	0.21	3.16	100.00
Pt 39	[3]BP	-47.8653	-68.6211	55.89	0.59	19.88	2.84	4.70	7.36	0.16	3.39	8.50	3.04	1.07	0.12	1.47	100.00
Pt 41	[3]BP	-47.9489	-69.5408	59.90	0.56	17.27	6.03	0.55	6.30	0.09	5.56	6.63	1.99	1.52	0.18	5.34	100.00
Pt 42	[3]BP	-47.9553	-68.5508	59.81	0.62	16.85	3.35	2.82	6.11	0.14	3.76	8.50	3.14	0.94	0.13	4.66	100.00
Pt 43	[3]BP	-48.0125	-68.4544	60.38	0.58	17.67	0.88	5.59	6.53	0.14	2.83	7.49	3.15	1.12	0.11	2.32	100.00
Pt 114	[3]BP	-48.1300	-69.8522	57.39	0.80	15.45	1.88	5.11	7.28	0.12	6.77	10.44	1.44	0.21	0.10	7.03	100.00
Pt 116	[3]BP	-48.1325	-69.8453	58.05	0.61	14.80	1.99	5.45	7.69	0.15	6.90	8.90	2.46	0.34	0.10	6.23	100.00
Pt 24	[3]BP	-47.9058	-69.7208	62.81	0.62	17.70	0.91	4.46	5.51	0.10	2.15	7.65	2.70	0.65	0.11	4.32	100.00
Pt 26	[3]BP	-47.8956	-69.7489	58.86	0.86	18.80	1.51	5.18	6.79	0.10	2.02	8.99	3.03	0.42	0.13	3.78	100.00
Pt 29	[3]BP	-47.8900	-69.7361	64.97	0.54	16.23	4.51	0.81	5.02	0.09	2.95	4.26	3.10	2.65	0.19	3.07	100.00
Pt 31	[3]BP	-47.9178	-69.7992	62.30	0.68	16.69	2.48	3.43	5.89	0.12	3.00	5.26	3.13	2.78	0.15	4.01	100.00
Pt 32	[3]BP	-47.9181	-69.7992	63.97	0.66	17.09	2.27	2.58	4.81	0.08	2.44	5.19	2.77	2.84	0.15	3.04	100.00
Pt 44	[3]BP	-47.9058	-69.7208	61.92	0.64	16.82	2.49	3.75	6.17	0.09	3.47	7.51	2.54	0.72	0.12	5.09	100.00

Pt 80	^{3}BP	-47.9361	-69.7869	62.10	0.66	16.39	1.81	3.90	5.81	0.08	3.17	6.48	2.28	2.88	0.15	5.47	100.00
Pt 81	^{3}BP	-47.9369	-69.7775	60.33	0.79	16.78	2.14	4.40	6.67	0.10	2.42	7.47	2.01	3.29	0.14	4.51	100.00
Pt 82	^{3}BP	-47.9347	-69.7817	59.44	0.68	16.81	3.13	3.49	6.59	0.09	5.57	6.27	2.33	2.11	0.11	3.64	100.00
Pt 83	^{3}BP	-47.9167	-69.9033	57.07	0.85	16.83	2.95	5.07	8.01	0.16	4.90	8.02	2.16	1.83	0.17	5.19	100.00
Pt 84	^{3}BP	-47.9275	-69.9122	58.14	0.62	17.85	1.55	5.08	6.81	0.12	4.79	7.12	2.36	2.05	0.14	3.91	100.00
Pt 85	^{3}BP	-47.9325	-69.9186	58.41	0.67	17.20	1.75	5.74	7.60	0.14	4.54	7.01	2.39	1.89	0.15	3.99	100.00
Pt 86	^{3}BP	-47.9117	-69.9461	51.28	0.77	16.01	3.56	5.57	9.12	0.22	6.67	13.79	1.72	0.27	0.15	11.10	100.00
Pt 108	^{3}BP	-47.9808	-69.8236	57.12	0.74	17.39	2.78	4.35	7.62	0.17	4.72	7.49	2.14	2.46	0.14	5.93	100.00
Pt 126	^{3}BP	-47.9622	-69.8928	62.01	0.69	16.22	1.56	4.44	6.19	0.12	4.08	6.52	2.07	1.94	0.16	2.90	100.00
Pt 127	^{3}BP	-47.9622	-69.8928	60.30	0.67	16.77	2.22	4.21	6.39	0.13	4.48	5.68	2.95	2.49	0.14	4.14	100.00
Pt 128	^{3}BP	-47.9606	-69.8906	58.75	0.78	16.50	2.50	4.85	7.39	0.17	4.77	7.28	2.18	2.03	0.15	4.20	100.00
Pt 1	^{3}BP	-47.9022	-69.2697	60.61	0.66	18.09	3.23	1.56	4.65	0.11	4.43	4.89	3.48	2.80	0.28	3.24	100.00
Pt 172	^{3}BP	-47.8906	-69.7367	66.33	0.59	15.53	3.25	0.74	4.49	0.06	2.17	4.53	3.35	2.74	0.21	3.23	100.00
Pt 97	^{3}BP	-48.7861	-69.6336	60.05	0.67	17.43	2.19	4.24	6.41	0.14	4.79	5.23	2.79	2.31	0.18	3.32	100.00
Pt 98	^{3}BP	-48.7903	-69.6228	60.23	0.65	17.38	3.48	3.21	6.55	0.11	4.60	5.74	2.55	2.01	0.18	3.01	100.00
Pt 99	^{3}BP	-48.7914	-69.6183	59.99	0.66	18.25	3.09	3.06	6.02	0.12	3.76	6.09	3.01	1.94	0.16	2.78	100.00
Pt 100	^{3}BP	-48.7931	-69.6136	59.70	0.66	18.50	3.18	2.92	5.94	0.11	3.51	6.06	3.15	2.20	0.17	3.38	100.00
Pt 159	^{3}BP	-47.9258	-69.9008	58.05	0.84	17.10	4.54	2.92	7.24	0.13	3.59	9.04	2.13	1.69	0.19	5.37	100.00
Pt 160	^{3}BP	-47.9258	-69.9008	58.77	0.84	16.81	4.08	2.92	6.95	0.15	3.23	9.15	2.01	1.90	0.19	5.12	100.00
Pt 183	^{3}BP	-47.9356	-69.9078	59.04	0.63	17.90	3.92	2.92	6.78	0.12	4.44	6.64	2.46	1.83	0.16	3.83	100.00
Pt 184	^{3}BP	-47.9489	-69.9167	62.31	0.72	17.26	2.84	2.92	5.69	0.11	3.01	5.20	2.90	2.67	0.13	5.38	100.00
Pt 185	^{3}BP	-47.9122	-69.9172	60.31	0.73	15.48	3.77	2.92	6.65	0.12	5.29	7.98	1.72	1.59	0.13	5.43	100.00
Pt 186	^{3}BP	-47.9700	-69.9083	60.64	0.68	16.06	3.75	2.92	6.64	0.16	5.44	6.13	1.90	2.21	0.14	4.49	100.00
Pt 187	^{3}BP	-47.9603	-69.9539	64.95	0.56	16.88	1.24	2.92	4.22	0.07	2.36	3.64	3.61	3.59	0.12	4.95	100.00
Pt 188	^{3}BP	-47.9408	-69.9333	54.90	0.82	16.33	6.14	2.92	8.86	0.11	8.82	8.39	1.28	0.35	0.14	8.19	100.00
Pt 150	^{3}BP	-47.6472	-70.1669	64.60	0.74	16.36	2.04	2.92	5.15	0.08	1.02	4.91	3.16	3.20	0.78	2.07	100.00
Pt 151	^{3}BP	-47.6544	-70.1711	60.12	0.99	17.59	4.13	2.92	6.77	0.16	2.42	6.70	3.81	1.23	0.21	2.06	100.00
Pt 153	^{3}BP	-47.6656	-70.2603	62.22	0.92	16.62	3.30	2.92	6.01	0.10	2.46	5.96	2.82	2.61	0.28	2.53	100.00
Pt 177	^{3}BP	-47.6664	-70.2400	58.13	1.10	16.39	5.07	2.92	7.67	0.29	2.34	9.97	2.13	1.78	0.20	6.30	100.00
Pt 178	^{3}BP	-47.6656	-70.2394	68.06	0.40	16.26	0.71	2.92	3.78	0.10	1.34	3.13	3.42	3.39	0.12	3.77	100.00
Pt 179	^{3}BP	-47.6506	-70.2603	63.46	0.77	16.62	2.56	2.92	5.42	0.08	3.04	4.69	2.65	3.02	0.25	3.08	100.00

Pt 180 a	[3]BP	-47.6422	-70.2586	55.35	1.38	17.35	6.92	2.92	9.43	0.18	3.22	8.42	2.77	1.66	0.24	2.41	100.00
Pt 189	[3]BP	-47.9408	-69.9333	58.29	0.66	16.50	4.20	2.92	6.86	0.12	6.34	6.57	3.91	0.61	0.14	5.38	100.00
Pt 181	[3]BP	-47.6589	-70.2717	69.10	0.36	16.01	0.44	2.92	3.49	0.09	1.26	2.45	3.69	3.44	0.11	3.00	100.00
Pt 169	[3]BP	-47.9400	-69.5456	66.14	0.58	15.61	1.58	2.92	4.47	0.10	2.67	3.73	3.03	3.47	0.20	3.17	100.00
Pt 170	[3]BP	-47.9450	-69.5467	65.31	0.62	15.76	1.75	2.92	4.64	0.10	2.58	2.62	4.10	4.05	0.22	2.59	100.00
Patvj037	[3]MA	-43.6971	-66.4287	72.7	0.09	12.0	0.72			0.09	0.11	1.35	3.63	3.00	<0.01	6.37	100.10
Patvj040	[3]MA			72.3	0.30	13.5	1.89			0.07	0.65	1.80	3.38	4.59	0.08	1.17	99.76
Patvj042	[3]MA	-41.6357	-65.3695	77.3	0.20	11.2	0.93			0.03	0.22	0.55	1.09	6.96	0.03	1.44	99.92
Patvj044	[3]MA	-41.6214	-65.3538	77.0	0.18	11.2	1.00			0.02	0.18	0.12	0.55	8.13	0.02	1.40	99.83
Patvj046	[3]MA	-44.1324	-65.4359	77.9	0.25	11.1	1.21			0.06	0.20	0.17	2.67	5.21	0.02	0.82	99.61
Patvj052	[3]MA	-40.6118	-65.8342	73.5	0.21	11.9	1.06			0.04	0.20	0.65	3.68	3.58	0.02	5.00	99.83
M2	[3]MA			72.8	0.30	13.7	1.79			0.02	0.34	1.05	3.27	5.57	0.09	0.61	99.49
Pat 34	[3]MA			73.10	0.33	13.58	1.72			0.03	0.40	0.63	3.57	5.08	0.08	1.02	99.54
Pat 32	[3]MA			69.60	0.29	15.31	1.55			0.07	0.28	1.05	4.72	5.71	0.04	1.19	99.81
Pat 55	[3]MA			74.27	0.14	12.05	0.86			0.03	0.20	1.93	3.19	2.74	0.01	4.38	99.80
Pat 104	[2]Que.			70.41	0.23	14.20	2.26			0.03	0.13	1.88	3.52	4.45	0.04	2.41	99.56
Pat 89	[1]C.Aik			76.1	0.08	12.4	0.65			<0.01	0.07	0.52	2.07	6.48	<0.01	1.47	99.87
Pt 156	[3]C.Aik	-47.6961	-70.1019	70.7	0.39	14.4	3.10			0.04	0.47	2.93	3.03	3.90	0.11	1.22	100.25
Pt 111	[3]C.Aik	-48.0767	-69.9161	74.52	0.12	13.14	1.85			0.04	0.10	0.43	1.72	5.69	0.01	1.85	99.47
Pat 48	[2]C.Aik			70.87	0.24	14.75	2.53			0.03	0.28	1.59	3.56	4.20	0.04	1.62	99.71
Pt 51	[3]C.Aik	-47.8433	-69.7489	76.97	0.08	12.99	0.37	0.78	1.16	0.06	0.10	0.79	4.57	3.27	0.01	4.31	100.00
Pt 117	[3]C.Aik	-47.6375	-69.6514	76.34	0.06	14.71	0.80	0.51	1.26	0.03	0.18	0.31	1.23	5.87	0.01	2.60	100.00
Pt 129	[3]C.Aik	-47.8808	-69.9303	67.78	0.54	15.50	2.14	1.83	3.83	0.09	1.86	3.87	2.85	3.50	0.18	2.09	100.00
Pt 113	[3]C.Aik	-48.0519	-69.8725	67.19	0.50	15.70	3.44	0.77	3.95	0.07	2.12	3.31	3.44	3.60	0.12	2.23	100.00
Pt 119	[3]C.Aik	-47.6561	-69.7344	75.50	0.09	14.66	0.48	0.27	0.71	0.01	0.09	0.18	1.37	7.38	0.01	1.67	100.00
Pt 2	[3]C.Aik	-47.8292	-69.2858	74.84	0.09	15.55	0.67	0.32	0.94	0.01	0.18	0.08	1.10	7.19	0.02	1.55	100.00
Pt 4	[3]C.Aik	-47.9092	-69.2853	73.63	0.16	15.47	0.83	0.50	1.27	0.01	0.23	0.19	0.62	8.40	0.02	1.90	100.00
Pt 5	[3]C.Aik	-47.9114	-69.2953	71.03	0.16	16.56	0.90	0.46	1.29	0.01	0.29	0.16	0.63	9.86	0.01	1.57	100.00
Pt 8	[3]C.Aik	-47.9139	-69.3531	71.05	0.17	17.45	0.93	0.46	1.32	0.03	0.38	0.19	0.57	8.82	0.02	1.86	100.00
Pt 6	[3]C.Aik	-47.9264	-69.2469	77.11	0.08	13.12	0.04	0.92	1.00	0.03	0.07	0.78	3.43	4.37	0.01	4.79	100.00
Pt 7	[3]C.Aik	-47.9283	-69.2439	78.71	0.07	13.82	0.86	0.20	1.01	0.01	0.27	0.27	1.11	4.72	0.01	3.46	100.00

Pt 16	^{3}C.Aik	-47.9681	-69.3972	70.15	0.21	17.30	1.23	0.44	1.58	0.02	0.47	0.32	3.65	6.28	0.02	1.95	100.00
Pt 22	^{3}C.Aik	-47.9722	-69.4733	69.98	0.22	19.21	1.39	0.27	1.55	0.01	0.27	0.10	0.24	8.41	0.01	2.03	100.00
Pt 9	^{3}C.Aik	-47.8200	-69.3658	68.51	0.52	15.70	3.49	1.13	4.38	0.03	2.13	0.64	3.43	4.55	0.11	2.66	100.00
Pt 12	^{3}C.Aik	-47.8525	-69.4403	66.97	0.46	16.15	3.41	2.25	5.47	0.04	2.99	0.30	6.83	0.68	0.11	2.76	100.00
Pt 27	^{3}C.Aik	-47.8956	-69.7606	67.12	0.33	17.06	1.92	0.95	2.75	0.05	1.31	3.60	3.53	4.18	0.07	2.66	100.00
Pt 3	^{3}C.Aik	-47.8361	-69.3208	71.26	0.36	14.25	3.25	0.60	3.59	0.05	0.63	0.12	0.35	9.30	0.09	1.81	100.00
Pt 17	^{3}C.Aik	-47.9311	-69.5283	67.73	0.49	15.69	2.25	1.56	3.66	0.12	2.07	3.33	3.18	3.58	0.15	2.21	100.00
Pt 18	^{3}C.Aik	-47.9214	-69.6161	67.38	0.48	16.23	2.03	1.79	3.70	0.08	1.82	2.67	3.62	3.87	0.15	2.17	100.00
Pt 33	^{3}C.Aik	-47.8564	-69.6967	66.76	0.53	16.26	1.83	1.93	3.68	0.08	1.77	4.40	3.09	3.27	0.16	2.81	100.00
Pt 89	^{3}C.Aik	-47.9347	-69.7817	66.83	0.56	15.75	3.18	1.08	4.04	0.07	2.29	3.78	2.95	3.56	0.17	2.46	100.00
Pt 121	^{3}C.Aik	-47.6867	-69.6233	68.69	0.40	16.23	1.47	1.59	3.00	0.07	1.18	3.19	3.42	3.72	0.10	2.87	100.00
Pt 93	^{3}C.Aik	-47.7500	-69.6772	67.78	0.50	16.06	3.31	0.64	3.70	0.18	1.94	3.25	2.97	3.47	0.15	2.31	100.00
Pt 94	^{3}C.Aik	-47.7422	-69.6536	65.55	0.48	17.62	1.84	1.57	3.37	0.09	1.30	3.73	1.56	6.18	0.12	4.34	100.00
Pt 95	^{3}C.Aik	-47.7442	-69.6647	68.46	0.46	15.45	2.15	1.66	3.68	0.07	1.81	3.46	2.87	3.60	0.14	2.24	100.00
Pt 130	^{3}C.Aik	-47.8031	-69.5750	69.81	0.41	15.84	1.76	1.17	2.81	0.11	1.09	2.15	2.82	4.84	0.12	2.00	100.00
Pt 131	^{3}C.Aik	-47.7778	-69.5517	66.12	0.44	17.65	1.74	1.62	3.30	0.08	1.22	2.94	1.49	6.65	0.11	3.70	100.00
Pt 35	^{3}C.Aik	-47.8439	-69.7442	75.66	0.08	14.57	0.37	0.37	0.72	0.01	0.29	0.80	3.02	4.81	0.04	2.08	100.00
Pt 36	^{3}C.Aik	-47.8439	-69.7442	76.76	0.07	12.94	0.45	0.66	1.10	0.05	0.07	0.66	3.81	4.52	0.02	3.69	100.00
Pt 37	^{3}C.Aik	-47.8439	-69.7442	76.99	0.08	13.49	0.67	0.42	1.05	0.02	0.24	0.63	2.72	4.77	0.01	2.34	100.00
Pt 48	^{3}C.Aik	-47.7872	-70.0050	76.99	0.06	13.42	0.50	0.66	1.13	0.03	0.13	0.58	2.89	4.76	0.01	1.60	100.00
Pt 49	^{3}C.Aik	-47.7872	-70.0050	76.37	0.07	12.85	1.34	0.53	1.80	0.06	0.08	0.67	3.61	4.48	0.01	3.58	100.00
Pt 50	^{3}C.Aik	-47.8839	-69.7914	76.11	0.08	13.97	0.88	0.33	1.15	0.02	0.32	0.70	2.89	4.75	0.01	2.41	100.00
Pt 107	^{3}C.Aik	-47.7542	-69.7469	76.50	0.07	13.57	0.59	0.55	1.09	0.05	0.14	0.69	3.10	4.78	0.01	1.05	100.00
Pt 45	^{3}C.Aik	-47.8153	-69.9403	72.66	0.17	15.28	0.87	0.70	1.51	0.03	0.41	2.24	3.48	4.18	0.04	1.73	100.00
Pt 46	^{3}C.Aik	-47.7881	-69.9725	72.34	0.19	15.81	0.69	0.61	1.26	0.05	0.41	2.74	3.11	4.05	0.04	2.47	100.00
Pt 47	^{3}C.Aik	-47.7872	-70.0050	70.47	0.23	16.36	0.79	0.96	1.72	0.08	0.51	3.64	3.03	3.91	0.05	3.11	100.00
Pt 96	^{3}C.Aik	-47.7939	-69.8994	74.05	0.16	14.59	1.02	0.50	1.44	0.03	0.45	1.66	3.07	4.51	0.04	1.67	100.00
Pt 102	^{3}C.Aik	-48.0103	-69.8447	73.85	0.16	15.13	0.99	0.59	1.50	0.03	0.47	1.33	3.16	4.33	0.04	1.48	100.00
Pt 103	^{3}C.Aik	-47.7731	-69.9114	72.92	0.20	15.04	1.01	0.53	1.48	0.06	0.42	2.60	2.76	4.48	0.04	2.55	100.00
Pt 106	^{3}C.Aik	-47.7486	-69.7664	73.81	0.16	15.41	1.25	0.40	1.56	0.03	0.39	1.31	2.45	4.84	0.04	2.35	100.00
Pt 109	^{3}C.Aik	-48.0472	-69.9633	73.25	0.17	15.35	0.62	0.97	1.57	0.03	0.54	1.58	2.50	4.98	0.03	2.84	100.00

Pt 110	[3]C.Aik	-47.9578	-70.0522	73.63	0.17	14.66	1.22	0.40	1.52	0.03	0.36	1.83	3.46	4.30	0.04	1.38	100.00
Pt 19	[3]C.Aik	-47.9381	-69.6400	73.59	0.07	17.46	0.29	0.92	1.20	0.01	0.16	0.03	0.20	7.26	0.02	1.96	100.00
Pt 20	[3]C.Aik	-47.9622	-69.6697	69.17	0.28	19.73	1.00	1.33	2.32	0.03	0.96	1.25	0.67	5.57	0.02	4.23	100.00
Pt 21	[3]C.Aik	-47.9369	-69.6653	76.00	0.08	16.29	0.50	0.50	0.97	0.01	0.21	0.05	0.15	6.22	0.02	1.96	100.00
Pt 34	[3]C.Aik	-47.8644	-69.6911	78.37	0.11	12.35	0.58	0.23	0.76	0.04	0.19	0.71	3.19	4.26	0.02	0.97	100.00
Pt 38	[3]C.Aik	-47.8439	-69.7442	74.55	0.13	14.20	1.38	0.52	1.80	0.02	0.31	1.03	2.80	5.13	0.03	2.21	100.00
Pt 118	[3]C.Aik	-47.6344	-69.6456	78.38	0.06	12.80	0.86	0.41	1.20	0.03	0.10	0.40	2.21	4.81	0.01	1.73	100.00
Pt 87	[3]C.Aik	-47.9008	-69.9622	70.74	0.28	15.96	1.66	0.47	2.02	0.06	0.73	3.02	2.61	4.51	0.07	2.91	100.00
Pt 88	[3]C.Aik	-47.8949	-69.9084	68.29	0.51	15.88	2.72	1.10	3.64	0.05	1.66	3.11	2.53	4.18	0.15	2.61	100.00
Pt 122	[3]C.Aik	-47.9503	-69.8211	70.49	0.28	16.29	0.75	1.36	2.09	0.06	0.66	2.64	2.96	4.48	0.05	2.66	100.00
Pt 123	[3]C.Aik	-47.9583	-69.7964	70.87	0.22	15.94	0.83	1.23	2.03	0.07	0.44	2.27	3.29	4.82	0.05	2.81	100.00
Pt 124	[3]C.Aik	-47.9625	-69.7497	71.60	0.20	15.78	1.22	0.76	1.91	0.07	0.64	1.89	2.83	5.04	0.04	2.75	100.00
Pt 125	[3]C.Aik	-47.9689	-69.8639	68.88	0.25	17.06	1.16	1.05	2.18	0.05	0.95	3.57	2.41	4.59	0.06	4.15	100.00
Pt 90	[3]C.Aik	-47.7761	-69.6914	72.87	0.30	15.27	2.05	0.36	2.30	0.07	0.88	1.94	2.12	4.18	0.07	4.11	100.00
Pt 91	[3]C.Aik	-47.7669	-69.7006	73.05	0.32	14.62	1.82	0.69	2.38	0.03	0.72	2.19	2.58	4.03	0.08	2.31	100.00
Pt 92	[3]C.Aik	-47.7511	-69.6789	70.21	0.36	15.95	2.31	0.62	2.76	0.05	1.14	2.42	3.22	3.79	0.10	2.18	100.00
Pt 104	[3]C.Aik	-47.7736	-69.8556	75.83	0.08	16.80	0.95	0.40	1.29	0.02	0.10	0.16	0.51	5.20	0.01	3.08	100.00
Pt 105	[3]C.Aik	-47.7775	-69.8358	73.75	0.11	18.95	0.08	0.56	0.65	0.02	0.22	0.15	0.18	5.96	0.01	2.58	100.00
Pt 111	[3]C.Aik	-48.0767	-69.9161	63.44	0.65	16.30	3.37	1.80	4.98	0.13	2.88	4.63	3.22	3.60	0.17	2.96	100.00
Pt 112	[3]C.Aik	-48.0611	-69.8767	71.34	0.30	15.07	2.35	0.56	2.72	0.04	0.90	1.74	3.64	4.17	0.08	1.66	100.00
Pt 120	[3]C.Aik	-47.6389	-69.7458	72.11	0.39	15.67	1.40	0.29	1.58	0.01	0.59	2.49	2.73	4.32	0.11	2.21	100.00
Pt 23	[3]C.Aik	-47.8994	-69.7203	74.55	0.14	14.12	0.97	0.55	1.44	0.11	0.37	1.10	3.62	4.52	0.03	1.29	100.00
Pt 28	[3]C.Aik	-47.8900	-69.7664	77.26	0.08	13.43	0.53	0.47	1.00	0.02	0.11	0.78	3.88	3.43	0.01	5.72	100.00

The superscript numbers identify the laboratories where the samples were analyzed: 1: CODES, University of Tasmania; 2: Steinman Institute, University of Bonn; 3: Geosciences Department, University of Padova.

Table 9 . Trace elements composition (ppm) of Patagonia samples.

	1	1	1	1	1	1	1
Sample	Patvj020	Patvj 027	Patvj030	Patvj033	Patvj005	Patvj023	Pt 182
Formation	CA	CA	CA	CA	CB	LT	BP
Latitude	-42.4071	-43.5169	-43.8923	-43.8305	-47.9114	-47.8994	-47.6633
Longitude	-68.8060	-69.1394	-68.3880	-67.8985	-69.2953	-69.7203	-70.1925
Li	27.9	10.5	9.03	18.8	16.3	22.5	12.9
Sc	18.6	28.8	17.7	19.8	19.4	12.0	22.6
Ti	6708	8666	5668	5353	840	3300	6000
V	187	253	133	166	110	96.7	169
Cr	72.7	245	74.1	149	487	73	20
Mn	1476	1124	802.8	767	990	630	1100
Co	43.0	58.0	41.6	46.8	78	34.6	67.5
Ni	38.5	93.5	34.8	56.1	354	20.7	6.32
Cu	32.5	35.8	21.9	36.8	77.8	20.4	16.0
Zn	78.6	93.0	75.1	78.9	45.9	68.1	87.1
Ga	18.7	18.5	19.4	19.1	9.70	19.2	20.0
As	0.0 < x < 3.0	0.0 < x < 3.0	0.0 < x < 3.0	8.40	0.0 < x < 3.0	5.9	16
Rb	37.7	27.2	65.6	70.8	3.30	72.4	135
Sr	674	675	620	674	78.1	489	359
Y	20.0	22.8	20.4	19.0	5.34	12.7	26.7
Zr	223	163.2	228	196	17.0	130	170
Nb	14.3	10.1	27.8	8.20	0.80	5.6	7.2
Mo	0.70	1.50	1.80	1.10	0.10	0.50	0.86
Ag	8.3	0.0 < x < 0.3	0.30	0.30	0.0 < x < 0.3	0.28	.011 < x < 0.2
Cd	0.0 < x < 0.3	0.0 < x < 0.3	0.0 < x < 0.3	0.0 < x < 0.3	0.0 < x < 0.3	).001 < x < 0.2	.001 < x < 0.2
Sn	1.6	1.30	1.80	2.00	0.20	1.1	1.8
Sb	0.1	0.000	0.10	0.10	0.00	0.15	0.13
Te	0.0 < x < 0.1	0.0 < x < 0.1	0.00	0.0 < x < 0.1	0.00	).004 < x < 0.2	0.01
Cs	1.14	0.72	1.88	2.41	1.00	7.84	8.54
Ba	673	521.4	1150	557	33.6	490	550
La	32.6	29.4	34.6	31.4	2.25	17.1	25.8
Ce	69.6	65.5	70.7	68.2	4.77	35.0	56.3
Pr	8.6	8.57	8.43	8.43	0.60	4.19	6.89
Nd	33.5	35.8	31.8	32.7	2.38	16.5	28.1
Sm	6.44	7.14	6.07	6.36	0.61	3.35	6.12
Eu	1.82	2.22	1.70	1.57	0.33	0.988	1.49
Gd	5.23	5.95	4.97	5.03	0.68	2.98	5.58
Tb	0.741	0.839	0.707	0.701	0.130	0.448	0.885
Dy	3.89	4.47	3.80	3.72	0.87	2.48	5.15
Ho	0.76	0.87	0.75	0.72	0.20	0.476	1.03
Er	2.12	2.37	2.10	1.99	0.60	1.35	2.95
Tm	0.30	0.33	0.30	0.28	0.10	0.199	0.428
Yb	1.87	2.00	1.94	1.73	0.65	1.30	2.80
Lu	0.28	0.30	0.30	0.26	0.10	0.207	0.429
Hf	4.80	3.70	5.20	4.80	0.40	3.4	4.6
Ta	0.80	0.70	2.10	0.50	0.20	0.40	0.53
W	114.0	183	176	189.5	158.7	182	371
Tl	0.132	0.08	0.24	0.23	0.10	0.425	1.68
Pb	15.5	6.09	9.13	12.01	1.99	11.2	12.3
Bi	0.00	0.00	0.00	0.10	0.00	0.03	0.03
Th	3.95	2.33	5.78	7.52	0.62	4.41	8.17
U	0.76	0.46	1.19	1.48	0.14	1.22	1.71

	1	1	1	1	1	1	1
Sample	Pt 40	Pt 101	Pt 115-A	Pt 25	Pt 30	Pat 4	Pt 152
Formation	BP	BP	BP	BP	BP	BP	BP
Latitude	-47.9386	-48.1283	-48.1300	-47.9100	-47.8919		-47.6589
Longitude	-68.5472	-69.8575	-69.8522	-69.7194	-69.7381		-70.1847
Li	19.7	21.2	45.6	10.8	23.7	002 < x < 0.0(	11.738
Sc	24.2	24.0	22.2	20.4	13.0	26.2	2.464
Ti	3600	4000	4100	4300	3600	8047	492.8
V	167	146	130	149	62.5	268	0.892
Cr	240	300	260	42	11	93.1	2.6
Mn	1100	850	820	820	420	921	621
Co	68.4	47.8	46.5	41.0	26.9	49.8	35.6
Ni	82.9	54.3	51.5	17.7	4.09	48.0	1.37
Cu	42.9	28.7	27.2	23.3	8.71	44.1	4.03
Zn	75.9	74.0	82.4	67.2	70.6	94.8	58.3
Ga	17.6	16.8	17.3	17.3	18.2	21.1	17.1
As	0.006 < x < 3	0.006 < x < 3	3.9	3.7	5.2	4.7	0.0 < x < 3.0
Rb	34.7	55.0	3.51	84.3	114	73.7	180
Sr	392	209	272	230	215	1106	171
Y	12.5	17.9	18.1	20.0	27.2	23.5	26.2
Zr	85	110	110	120	180	198	107
Nb	4.4	6.5	6.7	6.1	10	6.90	17.5
Mo	0.79	0.45	1.6	0.72	0.60	0.60	3.60
Ag	.011 < x < 0.2	.011 < x < 0.2	.011 < x < 0.2	.011 < x < 0.2	.011 < x < 0.2	0.0 < x < 0.3	0.0 < x < 0.3
Cd	).001 < x < 0.2	9.001 < x < 0.2	9.001 < x < 0.2	9.001 < x < 0.2	9.001 < x < 0.2	0.0 < x < 0.3	0.0 < x < 0.3
Sn	1.1	1.5	1.7	1.8	3.1	1.60	3.50
Sb	0.22	0.32	0.92	0.30	0.33	0.00	0.10
Te	).004 < x < 0.2	9.004 < x < 0.2	9.004 < x < 0.2	9.004 < x < 0.2	9.004 < x < 0.2	0.00	0.0 < x < 0.0
Cs	4.23	4.46	2.61	6.11	4.18	3.07	62.2
Ba	370	380	200	420	600	913.7	44.2
La	12.3	16.4	17.0	17.1	27.4	51.7	24.7
Ce	26.7	34.0	34.9	36.6	53.7	106.1	49.0
Pr	3.32	4.11	4.18	4.40	6.64	13.4	4.97
Nd	13.7	16.5	16.7	17.5	26.0	54.3	15.8
Sm	3.02	3.60	3.67	3.89	5.52	10.6	3.43
Eu	0.850	0.972	1.02	0.999	1.34	2.85	0.16
Gd	2.72	3.46	3.52	3.82	5.09	8.17	3.32
Tb	0.416	0.566	0.569	0.629	0.837	1.04	0.620
Dy	2.39	3.38	3.37	3.77	5.03	5.06	4.05
Ho	0.477	0.692	0.687	0.770	1.04	0.90	0.89
Er	1.36	2.02	2.00	2.22	3.07	2.34	2.89
Tm	0.196	0.292	0.291	0.327	0.463	0.31	0.46
Yb	1.28	1.94	1.89	2.12	3.06	1.84	3.19
Lu	0.198	0.302	0.293	0.329	0.492	0.26	0.500
Hf	2.3	3.1	3.1	3.5	5.0	4.60	5.10
Ta	0.33	0.35	0.47	0.42	1.0	0.50	1.50
W	304	136	184	161	161	147.0	265.2
Tl	0.561	0.251	0.059	0.339	0.500	0.17	1.62
Pb	10.1	10.2	11.5	14.1	20.1	8.55	38.61
Bi	0.12	0.04	0.06	0.05	0.10	0.00	0.30
Th	3.64	5.23	5.28	7.66	10.2	6.39	21.13
U	1.16	1.37	1.44	2.30	2.99	1.44	4.34

	2	2	1	1	1	1	1
Sample	Geo 2	Geo 8	Patvj 040	Patvj 042	Patvj 044	Patvj 046	Patvj 052
Formation	BP	BP	MA	MA	MA	MA	MA
Latitude				-41.6357	-41.6214	-44.1324	-40.6118
Longitude				-65.3695	-65.3538	-65.4359	-65.8342
Li	15.3	13.27	23.3	40.0	19.8	28.3	13.4
Sc	16.8	17.74	4.22	2.86	3.13	3.18	2.13
Ti			1781.1	1129	1043	1500	1222
V	140	151	22.5	16	31	7	12
Cr	57.3	34.5	3.0	2.7	2.3	2.5	2.3
Mn			511.1	191	110	380	218
Co	18.5	21.1	57.97	52.6	69.912	53.407	41.939
Ni	22.1	17.6	2.18	1.99	2.09	5.99	1.59
Cu	23.5	26.2	3.46	5.48	2.74	2.15	5.04
Zn	86.3	86.1	34.3	21.7	31.3	82.7	30.5
Ga	19.9	20.0	15.4	14.1	16.3	17.6	18.3
As			0.0 < x < 3.0	6.6	4.70	7.70	5.30
Rb	3.68	4.0	119	441	480	181	390
Sr	1734	1433	229.5	37.6	37.1	20.2	79.0
Y	20.2	17.3	24.4	37.9	26.1	54.4	62.6
Zr	134	110	175.5	180.0	174.5	282.2	172.8
Nb	5.82	5.2	12.0	21.0	30.2	24.8	24.2
Mo	0.40	0.58	0.60	0.2	1.2	0.6	4.3
Ag			0.30	0.0 < x < 0.3	0.0 < x < 0.3	0.0 < x < 0.3	0.0 < x < 0.3
Cd	0.14	0.14	0.0 < x < 0.3	0.0 < x < 0.3	0.0 < x < 0.3	0.0 < x < 0.3	0.0 < x < 0.3
Sn	1.47	1.26	2.20	2.70	2.70	4.80	6.00
Sb	0.35	0.20	0.10	1.40	0.60	0.40	0.20
Te			0.0 < x < 0.0	0.0 < x < 0.0	0.0 < x < 0.0	0.0 < x < 0.0	0.0 < x < 0.0
Cs	0.30	0.88	2.4	10.5	10.6	3.4	40.6
Ba	842.7	261.1	659.6	311.4	121	248	185
La	14.94	13.4	52.2	51.1	58.4	49.3	74.4
Ce	30.69	27.4	97.4	102.8	94.8	94.8	161
Pr	3.74	3.35	10.8	12.5	9.2	16.0	18.8
Nd	15.3	13.8	36.7	45.0	26.9	68.1	70.7
Sm	3.39	3.05	6.31	9.0	4.4	16.1	14.2
Eu	1.01	0.94	1.07	0.9	0.4	1.5	1.5
Gd	3.42	3.05	4.80	7.4	3.6	15.1	12.9
Tb	0.534	0.47	0.77	1.23	0.65	2.39	2.19
Dy	3.34	2.93	4.37	7.2	4.1	12.9	12.9
Ho	0.68	0.59	0.90	1.4	0.9	2.4	2.6
Er	1.93	1.67	2.66	4.2	3.0	6.4	7.4
Tm	0.29	0.25	0.41	0.6	0.5	0.9	1.1
Yb	1.97	1.69	2.75	4.1	3.9	5.3	7.4
Lu	0.31	0.27	0.43	0.60	0.66	0.79	1.10
Hf	3.06	2.61	5.10	5.8	6.1	8.9	6.1
Ta	0.36	0.32	1.50	2.3	4.0	2.4	3.5
W	0.71	0.81	502.9	489.2	674.1	538.8	359.3
Tl	0.026	0.017	0.644	2.393	2.952	0.813	3.491
Pb	11.5	11.2	19.2	19.8	27.2	30.3	40.3
Bi			0.10	0.00	0.00	0.20	0.80
Th	4.20	3.62	16.5	23.3	46.9	16.1	29.0
U	1.32	1.09	3.47	4.0	5.1	2.9	10.4

	1	2	2	2	2	2	2
Sample	M2	Pat 34	Pat 32	Pat 55	Pat 104	Pat 111	Pt 156
Formation	MA	MA	MA	MA	Que	C.Aike	C.Aike
Latitude						-48.0767	-47.6961
Longitude						-69.9161	-70.1019
Li	23.1	45.6	15.1	14.3	143.0	40.4	29.5
Sc	3.73	5.54	4.61	2.82	7.70	7.30	7.00
Ti	1830						2233
V	67	64	13	4	16	2	38
Cr	3.0	5.82	2.80	0.80	2.02	0.36	7.4
Mn	107						293.4
Co	62.0	1.350	< 0.5	< 0.5	1.569	< 0.5	74.661
Ni	3.20	< 0.5	< 0.5	< 0.5	< 0.5	< 0.5	3.95
Cu	4.31	2.59	1.83	2.61	3.74	2.33	5.61
Zn	28.4	39.3	46.8	32.5	43.6	32.7	47.0
Ga	16.9	18.1	19.6	16.5	19.6	16.7	14.7
As	6.30						4.80
Rb	206	199	133	111	205	204	171
Sr	221.6	188.1	96.7	435.8	274.7	80.6	261.1
Y	27.9	25.4	26.6	23.5	32.2	29.4	17.0
Zr	178.7	78.7	88.0	83.3	70.7	70.7	123
Nb	23.1	20.1	12.4	14.6	8.90	11.0	6.00
Mo	0.5	0.9	0.27	1.32	0.33	0.31	1.20
Ag	0.0 < x < 0.3						0.4
Cd	0.0 < x < 0.3	0.15	0.14	0.13	0.20	0.09	0.0 < x < 0.3
Sn	3.00	2.92	1.74	2.00	3.29	1.61	1.80
Sb	0.10	0.10	0.07	0.09	2.48	1.18	0.70
Te	0.0 < x < 0.0						0.0 < x < 0.0
Cs	5.1	8.4	1.4	61.4	30.0	7.0	13.1
Ba	533	737	893	410	1091	1485	768
La	58.9	59.7	106	32.8	39.7	53.6	32.4
Ce	108	116	198	65.5	78.2	105	61.3
Pr	12.0	12.76	20.7	7.18	8.84	11.81	6.60
Nd	40.9	44.1	68.9	24.4	32.5	43.0	24.1
Sm	7.2	7.65	10.4	4.59	6.43	7.63	4.42
Eu	1.1	1.10	1.54	0.49	0.99	1.24	1.02
Gd	5.5	5.79	7.45	3.78	5.86	6.11	3.62
Tb	0.86	0.82	0.98	0.60	0.90	0.89	0.57
Dy	4.9	4.58	5.17	3.66	5.46	5.17	3.20
Ho	1.0	0.88	0.93	0.74	1.08	1.00	0.65
Er	3.0	2.54	2.47	2.17	3.00	2.82	1.89
Tm	0.5	0.41	0.34	0.34	0.45	0.43	0.30
Yb	3.3	2.78	2.25	2.38	3.00	2.89	1.94
Lu	0.51	0.42	0.33	0.37	0.45	0.43	0.31
Hf	5.5	2.81	2.78	3.02	2.31	2.72	3.60
Ta	2.7	1.22	0.66	0.86	0.65	0.73	1.20
W	466.8	0.85	0.57	0.45	3.19	2	606
Tl	0.985	0.92	0.61	0.44	1.11	0.75	0.65
Pb	18.8	23.4	20.7	20.8	23.1	24.0	19.9
Bi	0.20						0.1
Th	31.1	22.0	14.2	16.6	14.7	16.2	13.4
U	5.1	2.30	1.53	3.06	2.43	2.30	2.67

	1	1	1	1	1	1	1
Sample	Pat 89	Pat 48	Pt 51	Pt 117	Pt 129	Pt 113	Pt 119
Formation	C.Aike	C.Aike	C.Aike	C.Aike	C.Aike	C.Aike	C.Aike
Latitude			-47.8433	-47.6375	-47.8808	-48.0519	-47.6561
Longitude			-69.7489	-69.6514	-69.9303	-69.8725	-69.7344
Li	10.6	35.6	13.4	62.5	34.4	69.3	41.8
Sc	7.83	9.47	4.64	4.34	9.28	12.74	3.76
Ti	489		399	299	2511	2714	450
V	8	10	1	3	48	59	4
Cr	2.3	1.33	2.9	2.6	6.7	14.6	2.4
Mn	33.8		344	158	700	485	30
Co	47.442	< 0.5	68.6	42.8	31.7	25.6	45.2
Ni	2.05	< 0.5	2.47	1.61	3.80	5.52	2.67
Cu	2.12	3.63	2.57	3.49	6.06	8.01	2.18
Zn	85.4	54.7	42.3	35.3	51.0	58.6	17.5
Ga	16.2	19.5	14.7	12.9	15.3	17.1	12.9
As	55.80		12.0	22.8	3.40	6.10	13.7
Rb	133	158	194	269	149	149	318
Sr	52.7	253	54.2	27.0	278	264	38
Y	56.9	29.1	31.2	26.1	20.3	25.3	24.0
Zr	114	128	96.3	78.1	161.7	201.1	116.9
Nb	8.70	11.9	10.4	11.2	7.0	9.0	10.2
Mo	0.40	0.86	1.50	0.80	0.40	0.60	0.20
Ag	0.0 < x < 0.3		0.0 < x < 0.3	0.0 < x < 0.3	0.3	0.3	0.0 < x < 0.3
Cd	0.0 < x < 0.3	0.18	0.0 < x < 0.3	0.0 < x < 0.3	0.0 < x < 0.3	0.0 < x < 0.3	0.0 < x < 0.3
Sn	4.80	2.35	4.10	3.80	2.20	2.80	2.40
Sb	0.30	0.33	2.70	2.80	0.30	0.60	4.30
Te	0.0 < x < 0.0		0.0 < x < 0.0	0.0 < x < 0.0	0.0 < x < 0.0	0.0 < x < 0.0	0.0 < x < 0.0
Cs	22.6	3.7	18.3	9.3	2.8	5.1	11.7
Ba	775	1853	752	607	761	765	1330
La	26.5	59.3	34.6	25.6	32.5	39.0	49.1
Ce	136	111	68.3	49.9	64.9	77.9	68.5
Pr	7.37	12.59	8.20	6.41	7.00	9.16	11.06
Nd	30.1	45.7	30.6	25.2	26.2	34.2	40.7
Sm	8.16	7.72	6.53	5.71	5.00	6.56	7.79
Eu	0.88	1.99	0.63	0.48	1.13	1.43	1.13
Gd	9.50	6.28	5.85	5.25	4.33	5.59	6.19
Tb	1.67	0.89	0.99	0.87	0.68	0.87	0.94
Dy	10.34	5.06	5.84	5.15	4.00	5.09	5.29
Ho	2.16	0.98	1.21	1.03	0.80	1.00	1.01
Er	6.19	2.75	3.54	3.09	2.35	2.91	2.94
Tm	0.88	0.41	0.54	0.46	0.35	0.43	0.44
Yb	5.43	2.77	3.53	3.04	2.29	2.79	2.93
Lu	0.83	0.42	0.55	0.47	0.36	0.43	0.46
Hf	4.40	3.78	3.90	3.50	4.50	5.50	4.10
Ta	1.40	0.70	1.60	1.60	0.80	0.90	1.30
W	394	1	556	433	256	175	394
Tl	1.14	0.79	1.68	1.28	0.69	0.66	1.92
Pb	34.9	23.0	26.6	19.6	16.3	22.0	17.0
Bi	0.0		0.5	0.3	0.1	0.2	0.0
Th	12.8	14.9	14.4	16.0	12.6	11.3	13.2
U	2.50	2.13	4.47	2.52	2.57	2.07	2.88

The numbers at the top of the table identify the laboratories where the analysis were performed: 1: CODES, University of Tasmania; 2: Institute of Geosciences, University of Kiel, Germany. BP: Bajo Pobre, CA: Canadon Asfalto, MA: Marifil, LT: Lonco Trapial; C.Aike: Chon Aike.

Table 10. U-Pb zircon dating of Patagonia samples

	Isotopic ratios and 1 s errors (%)						Ages and 1s absolute errors (Ma)						Reported age	
Sample	$^{206}Pb/^{238}U$	+/-1 RSE	$^{208}Pb/^{232}Th$	+/-1 RSE	$^{207}Pb/^{206}Pb$	+/-1 RSE	$^{206}Pb/^{238}U$	+/-1 ster	$^{208}Pb/^{232}Th$	+/-1 ster	$^{207}Pb/^{206}Pb$	+/-1 ster	Age (Ma)	+/-1 ster
PT-113	0.0239	1.8%	0.0073	2.6%	0.0507	5.4%	152	3	147	4	227	125	151.8	2.8
PT-113	0.0239	1.1%	0.0072	1.5%	0.0502	2.1%	152	2	145	2	204	48	151.9	1.7
PT-113	0.0239	1.9%	0.0074	2.9%	0.0444	4.9%	152	3	150	4	-89	120	152.2	3.0
PT-113	0.0240	1.2%	0.0074	1.5%	0.0496	2.1%	153	2	150	2	175	49	153.0	1.8
PT-113	0.0241	1.6%	0.0075	2.6%	0.0517	3.9%	154	2	151	4	274	89	153.2	2.4
PT-113	0.0244	1.4%	0.0081	1.9%	0.0582	2.6%	155	2	163	3	539	57	153.7	2.1
PT-113	0.0244	1.2%	0.0075	1.5%	0.0467	2.4%	155	2	150	2	33	58	155.5	1.9
PT-113	0.0245	1.2%	0.0074	1.6%	0.0478	2.7%	156	2	149	2	88	63	155.8	1.9
PT-113	0.0245	1.3%	0.0078	1.9%	0.0488	3.2%	156	2	157	3	139	75	156.1	2.1
PT-113	0.0247	1.6%	0.0077	2.2%	0.0499	4.0%	157	3	156	3	190	92	157.3	2.5
PT-113	0.0255	1.3%	0.0095	1.8%	0.0658	2.2%	162	2	192	3	799	46	158.8	2.0
PT-113	0.0258	1.9%	0.0094	3.0%	0.0606	4.6%	164	3	188	6	624	98	161.7	3.0
PT-113	0.0379	1.6%	0.0112	2.9%	0.0598	3.2%	240	4	225	7	595	69	237.1	3.8
PT-113	0.0508	1.3%	0.0218	1.5%	0.0549	2.0%	319	4	436	7	410	44	318.6	4.0
Patvj 39	0.0288	1.3%	0.0088	1.6%	0.0695	3.4%	183	2	176	3	914	70	178.6	2.3
Patvj 39	0.0291	1.3%	0.0095	1.4%	0.0515	2.8%	185	2	190	3	264	63	184.5	2.4
Patvj 39	0.0292	2.1%	0.0088	1.9%	0.0543	5.9%	186	4	178	3	383	133	184.6	3.8
Patvj 39	0.0292	1.2%	0.0090	1.3%	0.0503	2.8%	186	2	181	2	207	65	185.6	2.3
Patvj 39	0.0293	1.7%	0.0093	2.0%	0.0514	3.9%	186	3	187	4	260	89	185.8	3.1
Patvj 39	0.0294	1.2%	0.0092	1.3%	0.0500	2.2%	187	2	185	2	196	51	186.6	2.2
Patvj 39	0.0297	2.0%	0.0097	2.1%	0.0541	5.1%	189	4	194	4	373	115	187.6	3.7
Patvj 39	0.0297	1.1%	0.0093	1.3%	0.0532	1.9%	189	2	187	2	338	42	187.9	2.0
Patvj 39	0.0299	1.9%	0.0093	2.1%	0.0562	4.2%	190	4	188	4	460	93	188.5	3.6
Patvj 39	0.0305	2.3%	0.0102	2.5%	0.0718	5.1%	194	4	205	5	981	105	188.6	4.4
Patvj 39	0.0297	1.1%	0.0093	1.3%	0.0501	2.1%	189	2	186	2	200	49	188.7	2.1
Patvj 39	0.0303	1.8%	0.0096	1.9%	0.0629	3.6%	192	3	193	4	705	76	189.3	3.4
Patvj 39	0.0300	1.4%	0.0092	1.3%	0.0543	2.7%	190	3	185	2	383	60	189.3	2.6
Patvj 39	0.0304	1.7%	0.0097	1.6%	0.0507	4.5%	193	3	194	3	226	105	192.6	3.3
Patvj-51	0.0306	3.9%	0.0097	3.3%	0.0453	12.1%	194	8	195	6	-37	294	194.2	7.6
Patvj-51	0.0285	2.3%	0.0090	3.3%	0.0573	6.1%	181	4	181	6	502	135	179.2	4.1

Patvj-51	0.0282	1.4%	0.0089	1.7%	0.0503	2.9%	179	2	179	3	211	68	179.2	2.5
Patvj-51	0.0289	2.3%	0.0102	3.3%	0.0678	5.6%	184	4	205	7	861	117	179.6	4.1
Patvj-51	0.0283	1.8%	0.0090	3.2%	0.0512	4.8%	180	3	181	6	248	110	179.7	3.2
Patvj-51	0.0283	2.2%	0.0094	3.2%	0.0472	7.4%	180	4	190	6	60	177	179.8	4.0
Patvj-51	0.0284	2.0%	0.0085	1.9%	0.0478	5.0%	180	4	171	3	91	118	180.5	3.6
Patvj-51	0.0286	1.4%	0.0087	1.9%	0.0524	3.0%	182	2	176	3	305	69	180.9	2.5
Patvj-51	0.0286	1.8%	0.0087	3.1%	0.0527	5.3%	182	3	175	5	315	121	181.3	3.3
Patvj-51	0.0286	1.6%	0.0087	2.7%	0.0441	5.4%	182	3	175	5	-106	134	182.0	2.9
Patvj-51	0.0288	1.7%	0.0093	2.1%	0.0525	3.9%	183	3	187	4	309	88	182.6	3.2
Patvj-51	0.0289	1.2%	0.0090	1.7%	0.0493	2.3%	184	2	182	3	162	55	183.8	2.2
Patvj-51	0.0290	1.2%	0.0091	1.9%	0.0524	2.7%	185	2	183	3	304	61	183.9	2.2
Patvj-51	0.0294	1.6%	0.0089	2.9%	0.0510	4.8%	187	3	180	5	240	111	186.6	2.9
Patvj-51	0.0299	1.5%	0.0095	2.7%	0.0512	3.0%	190	3	190	5	250	69	189.3	2.8
Patvj-51	0.0873	1.0%	0.0259	1.9%	0.0578	1.5%	539	6	517	10	521	34	539.3	5.4